Attrition-resistant membranes for hydrogen separation in fluidized-bed membrane reactors

Document status and date:
Published: 22/10/2018

Document Version:
Publisher's PDF, also known as Version of Record (includes final page, issue and volume numbers)

Please check the document version of this publication:

• A submitted manuscript is the version of the article upon submission and before peer-review. There can be important differences between the submitted version and the official published version of record. People interested in the research are advised to contact the author for the final version of the publication, or visit the DOI to the publisher's website.
• The final author version and the galley proof are versions of the publication after peer review.
• The final published version features the final layout of the paper including the volume, issue and page numbers.

Link to publication

Attrition–resistant membranes for hydrogen separation in fluidized–bed membrane reactors

Alba Arratibel Plazaola
Attrition-resistant membranes for hydrogen separation in fluidized-bed membrane reactors
Eindhoven University of Technology

Attrition-resistant membranes for hydrogen separation in fluidized-bed membrane reactors

PROEFSCHRIFT

ter verkrijging van de graad van doctor aan de Technische Universiteit Eindhoven,
op gezag van de rector magnificus prof.dr.ir. F.P.T. Baaijens,
voor een commissie aangewezen door het College voor Promoties,
in het openbaar te verdedigen op
maandag 22 oktober 2018 om 16:00 uur

door

Alba Arratibel Plazaola
geboren te Donostia-San Sebastian, Spanje

Dit proefschrift is goedgekeurd door de promotoren en de samenstelling van de promotiecommissie is als volgt:

voorzitter:	prof.dr.ir. K. Nijmeijer
1^e promotor:	prof.dr.ir. M. Van Sint Annaland
copromotor(en):	prof.dr. F. Gallucci
	dr. D.A. Pacheco Tanaka (Tecnalia)
leden:	prof.dr. K .Li (Imperial College London)
	prof.Dr. A. Mendes (Universidade de Porto)
	dr. Z. Borneman
	prof.dr.ir. N. E. Benes (UT)

Het onderzoek of ontwerp dat in dit proefschrift wordt beschreven is uitgevoerd in overeenstemming met de TU/e Gedragscode Wetenschapsbeoefening.

To my little king,
Poker.

Index

Summary

Hydrogen production is attracting increasing attention, not only for large-scale applications such as refineries, but also for small-scale applications like heat and power (micro) cogeneration systems. More and more research projects focus on the production and separation of hydrogen using various carbon feedstocks (methane, methanol and ethanol) by steam reforming or autothermal reforming. To further increase the efficiency of reforming systems and decrease the required volumes of reactors/separators, research efforts are being invested in the development of novel membrane reactors, where reaction and hydrogen separation and purification (often through Pd-based membranes) are integrated in a single process unit. The resulting increase in the reaction equilibrium conversion via Le Châtelier's principle also enables operation of the reactors at milder conditions, thus improving the overall process efficiency.

Fluidized-bed membrane reactors can offer very good mass and heat transfer characteristics, while also allowing sufficient freedom to tune the installed membrane area and required catalyst volume in comparison with packed-bed membrane reactors. One important concern that may adversely affect the performance of fluidized bed membrane reactors (FBMR) is possible erosion or damage of the membrane surface by the scouring action of the moving and colliding fluidized particles.

Hydrogen selective membranes must present a high hydrogen flux and purity in order to surpass US DOE (Unite States Department of Energy) targets. To achieve this, the thickness of the hydrogen selective layer must be as thin as possible. The development of supported ultra-thin Pd-based membranes is therefore required. Selection of adequate porous supports and optimal materials is crucial for the preparation of pinhole-free ultra-thin layers. Several deposition techniques are usually employed to deposit the selective layer onto the porous support, viz. electroless plating (ELP), electroplating (EP), physical vapor deposition (PVD) and chemical vapor deposition (CVD). In this thesis, the electroless plating technique has

been used because of the simplicity of the required equipment, its low cost and capacity to cover samples with different geometries. The main objective of the research described in this thesis is the development and investigation of attrition-resistant membranes for hydrogen separation. Two types of membranes have been studied: pore-filled membranes and double-skin membranes. These membranes differ from conventional thin-film supported membranes in that a mesoporous ceramic layer is deposited on top of the H_2 selective layer (Pd or Pd-based alloy) to avoid direct contact of the catalyst with H_2 selective material. The preparation and operational properties of the membranes have been studied in detail.

First, the preparation of the mesoporous ceramic layer (mixtures of nano-size γ-Al_2O_3 and YSZ) has been studied in order to obtain a defect-free porous layer, which does not induce substantial mass transfer limitations. Mesoporous layers have been deposited by a vacuum-assisted dip-coating technique. This technique has been chosen due to its simplicity and ability to provide complete coverage of supports with challenging geometries. The effect of several operating parameters on the thickness of the deposited layers has been studied (viz. concentration of ceramic particles in the solution, concentration of polymer, deposition time, application of vacuum or not). A complete physico-chemical characterization of different YSZ/γ-Al_2O_3 mixtures calcined at different temperatures has been performed by BET nitrogen adsorption, X-ray diffraction (XRD), scanning electron microscopy (SEM) and transmission electron microscopy (TEM). The diffusion mechanisms of N_2, He and CO_2 in these layers have been studied in detail. Mesoporous layers with a different amount of YSZ (ranging from 50 to 90 wt%) has been studied in the temperature range from 50 to 400 °C at 30-100 KPa of pressure difference. Depending on the composition of the mesoporous layer and the operating temperature, different diffusion mechanisms are rate-determining, mainly viscous or Poiseuille and Knudsen diffusion. Layers with a high content in γ-Al_2O_3 showed also a contribution of surface diffusion in the presence of CO_2.

Subsequently, so-called pore-filled type membranes have been prepared. The Pd (or a Pd-based alloy) is encapsulated in the pores of the mesoporous layer, while another mesoporous layer is added on top of this layer to avoid that Pd is exposed at the surface of the membrane. Nano-palladium particles deposited in the first mesoporous layer are forced to grow inside the pores using a vacuum-assisted electroless plating technique (VA-ELP). Another advantage of these membranes is the small amount of palladium used per membrane in comparison with conventional supported palladium-based membranes.

Different tubular ceramic asymmetric porous supports have been employed for the preparation of pore-filled membranes, like α-Al_2O_3 and ZrO_2 and with a different pore size of the top layer. The composition of the mesoporous layers depends on the employed support, where a low YSZ content for α-Al_2O_3 supports is preferred and a high YSZ content for ZrO_2 supports. Several membranes have been tested and it has been found that these membranes

did not reach the required properties in terms of H_2 permeance (> $1 \cdot 10^{-6}$ mol m^{-2} s^{-1} Pa^{-1}) and ideal H_2/N_2 perm-selectivity (>1000). It has been confirmed by TEM, that the nano-palladium located inside the pores does not form a percolated network across the mesoporous layers, explaining why the measured hydrogen fluxes are so low for the prepared pore-filled membranes.

Another membrane concept was developed, the so-called double-skin (DS) membrane, where a conventional supported Pd-based membrane deposited by an electroless plating (ELP) technique is protected with a mesoporous ceramic layer using a dip-coating technique. DS-membranes have been prepared onto ceramic and metallic porous supports. Mesoporous layers with a high content in γ-Al$_2$O$_3$ have been employed for the preparation of double-skin membranes because of their small and narrow pore size and high surface area.

Ceramic supported membranes have been studied under fluidization conditions in the presence of two types of particles (glass beads and Rh reforming catalyst supported on promoted alumina) and different gas mixtures. Prepared membranes (1-2 µm thick) showed a remarkably high hydrogen permeance (1-5$\cdot 10^{-6}$ mol m^{-2} s^{-1} Pa^{-1}) and ideal perm-selectivity even up to 25000 at 400 °C. Mass transfer limitations towards the membrane (concentration polarization) were observed during tests with binary mixtures at 400 °C due to the large hydrogen permeance of the membranes. An improvement in the hydrogen flux was observed when particles (glass beads) were integrated in the membrane reactor and/or when the total feed flow rate was increased with a consequent decrease in the recovered hydrogen at the permeate. It has also been demonstrated that the sealing of the membrane (graphite gasket) needs to be further improved. An increase in the leakage through the fittings has been observed after several hours of operation; especially at higher temperatures, the leakage level increased faster.

The metallic supported membranes provide a much higher mechanical strength and are relatively easily integrated in the reactor in comparison with ceramic-supported membranes that require a graphite-based sealing for their integration into the reactor. A comparison between conventional and double-skin membranes tested for more than 600 hours under fluidization showed similar hydrogen permeances during the test at 400-500 °C, where the double-skin membrane maintained the high permeance and perm-selectivity during the test, whereas the nitrogen leakage through the conventional membrane increased with time with a corresponding decrease in the perm-selectivity from 10000 to 1000. The addition of a porous protective layer on a metallic supported Pd-based membrane has thus enabled stable performance of the membranes under fluidization conditions, even when fluidizing with catalyst particles that have shown before to chemically interact with Pd (TiO$_2$-based catalyst), thus paving the way for their application in fluidized-bed membrane reactors, while their H_2 permeance is not compromised with an ideal H_2/N_2 perm-selectivity that is virtually infinite.

Results obtained in this thesis with double-skin membranes demonstrates that the hydrogen purity needed for its use in fuel cells can be achieved with the double-skin membranes, which could promote the further development of membrane reactors for small-scale hydrogen production.

Chapter 1

Introduction

This chapter introduces the main motivation for the development of attrition resistant membranes for their integration in fluidized bed membranes reactor (FBMR) for hydrogen production. Hydrogen production is attracting increasing attention, not only for large-scale applications such as refineries, but also for small-scale applications like heat and power (micro) cogeneration systems. Integration of membranes into a FBMR results in higher conversions compared to the equilibrium conversion of a conventional system due to Le Châtelier's principle, which also enables operation of the reactors at milder conditions, thus improving the overall process efficiency. The advantages that fluidized-bed membrane reactors offer in comparison with packed-beds are discussed. One important concern that may adversely affect the performance of a membrane under fluidization conditions is possible erosion or damage of the membrane surface by the scouring action of the moving and colliding fluidized particles. This thesis reports on the research that was carried out to develop membranes that are resistant towards particle fluidization.

"Chapter one, the end".
Dame Sally Markham (Little Britain).

1.1. Introduction: Hydrogen production

Hydrogen is the most abundant and lightest element in the universe which, however, does not exist on Earth in its pure gaseous state. It has the higher energy content by weight amongst common fuels (3 times that of gasoline). Hydrogen offers an elegant solution for the capping of greenhouse gas emissions, since it can be converted to electricity by a fuel cell and the only by product would be water.

More than 50 million tons of hydrogen are produced each year, mainly via steam reforming of natural gas (see Figure 1.1 left) [1]. Hydrogen is also produced from electrolysis of water, which is a more energy-intensive method. For the case of hydrogen production from steam reforming of natural gas, the reaction is performed at 850-950 °C and high pressures (20-30 bar). The reaction between methane and steam to produce CO and H_2 ($CH_4 + H_2O \leftrightarrow CO + 3\ H_2$) is favoured at low pressures, however high-pressure operation is always preferred because of economic reasons. In this reaction, excess of steam is employed which react with carbon monoxide producing more hydrogen and CO_2 through the water gas shift reaction ($CO + H_2O \leftrightarrow CO_2 + H_2$) occurring at lower temperatures (200-450 °C).

The hydrogen produced nowadays is mainly used in the chemical industry for ammonia, methanol and fertilizers production. Is it also used in the refining industry as a petrochemical for hydrocracking and desulphuration reactions. Other uses of hydrogen are for applications in the metal production, food processing and electronics sectors, and account for up to 10% of the hydrogen market (see Figure 1.1 right).
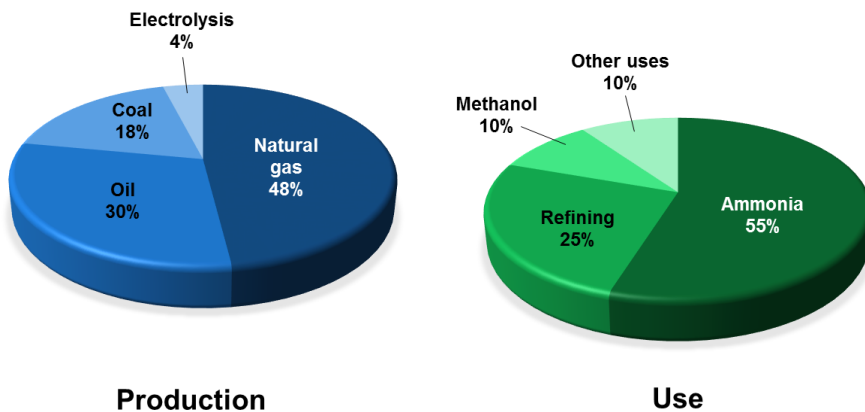

Figure 1.1. Estimated world hydrogen production and use [1].

Recent advances in Polymer Electrolyte Membrane Fuel Cells (PEMFC) for small or medium scale applications make the production of ultra-pure hydrogen an increasingly hot topic in

the energy conversion landscape. The traditional SRM process (at industrial scale) consists of different process steps such as feed gas preheating and pre-treatment (for example hydrodesulphurisation), primary and secondary reformers (often top-fired or wall-fired multi-tubular fixed-bed reactors) and high and low temperature shift converters, CO_2 removal and methanation units. Often a PSA (Pressure Swing Adsorption) unit is used to achieve the desired hydrogen purity. In view of thermodynamic limitations and the high endothermicity of steam reforming, heat transfer at high temperatures (850-950 °C) is required, where excess steam is used to avoid carbon deposition (with typical feed H_2O/CH_4 molar ratios of 2-5) [2]. For the production of ultra-pure hydrogen for small-scale applications, this route is not preferred because of the large number of process units with complex heat integration and the associated uneconomic downscaling. However, a high degree of process integration and process intensification can be accomplished by integrating hydrogen perm-selective membranes in the steam reformer, such that all reaction steps and separation steps are integrated in a single system [3,4].

1.2.   Membrane reactors for hydrogen production and separation

Integration of hydrogen perm-selective membranes into a catalytic reactor where hydrogen is produced by steam reforming or authothermal reforming of different feedstocks (methane, methanol, ethanol among other hydrocarbons), allows elimination of hydrogen purification units downstream of the reformer together with a reduction in the total reactor volume [5]. Another positive aspect of the membrane reactor concept is related to the decrease in the total capital cost, associated with the milder operating conditions that are required to achieve similar conversions as conventional systems due to the *in-situ* hydrogen extraction through the membranes, resulting in shifting of the reaction equilibria towards the products according to Le Châtelier's principle [4,6,7]. Pd-based membranes are considered as the best candidate due to the high hydrogen permeability and catalytic activity to hydrogen dissociation. Supported membranes are preferred due to the higher permeance which depends on the inverse of the thickness, allowing to decrease the required membrane area.

When using a membrane reactor, the practical configurations can be either a packed (fixed) bed (Figure 1.2 left) or a fluidized bed (Figure 1.2 right), where the catalyst is free to move around the membranes. At smaller scales, also micro-structured reactors have been demonstrated [8–10]. The advantages of packed-beds lie in its simplicity in construction and well-established and validated models for its design and scale-up. Additionally, the catalyst is kept in a fixed position, thus any damage of the membranes due to erosion is circumvented, while scratches on the thin membrane surface can also happen during loading and unloading of the catalyst to/from the reactor. On the other hand, the main disadvantage of this reactor type is the unavoidable temperature gradients that the reactor (and thus the membrane) is experiencing in both endothermic (steam reforming like) or exothermic (autothermal

reforming) reactions [11]. More importantly, as thinner membranes are nowadays produced with much higher fluxes, concentration polarization (or better the bed-to-membrane mass transfer limitations) prevailing in packed beds will be extremely detrimental for the hydrogen recovery and thus for the overall performance of the membrane reactor [11,12].
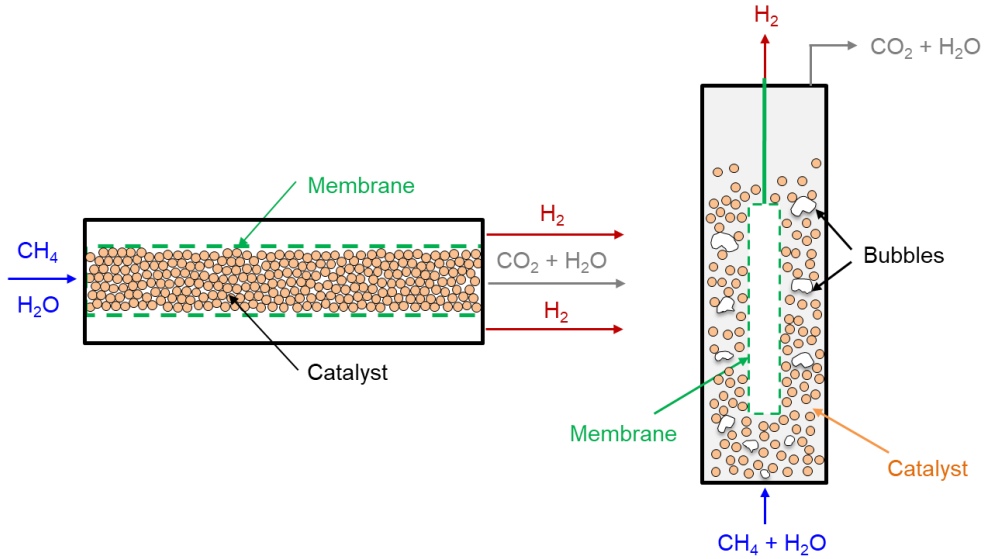
Figure 1.2. Schematic representation of packed-bed (left) and fluidized-bed (right) membrane reactors.

On the other hand, fluidized-bed membrane-reactors (FBMR), have much better heat and mass transfer rates [13], so that the membranes always experience a uniform temperature and the highest hydrogen partial pressure (when avoiding excessive gas back-mixing), thus maximizing both membrane flux and lifetime. Additionally, smaller particles can be used in fluidized beds because of the limited pressure drop, while simultaneously circumventing any possible intraparticle mass transfer limitations. On the other hand, problems with membrane erosion and bubble-to-emulsion mass transfer limitations can adversely affect the performance of the FBMR and the lifetime of the membranes [14]. An alternative to avoid direct contact between particles in constant motion with the membrane surface, is to cover the surface with a porous layer with a porosity and pore size sufficiently large to avoid additional mass transfer limitations and small enough to avoid particles entering the pores. The porous structure can be a separate structure but physically attached to the membrane, or it can be part of the membrane itself. The second option can be achieved by using "pore-filled" membranes prepared with a very thin and porous ceramic layer covering the palladium deposited onto nanopores. Nevertheless, this kind of membranes were not yet tested inside a fluidized bed reactor. It should also be reminded that to protect the membrane the thin Pd layer cannot be deposited on the inner surface of a porous support (as one might

immediately propose), because the large pressure difference used between the reaction zone (the fluidized bed) and the permeation zone (inside the tube) would result in fast delamination of the Pd layer with consequent loss in perm-selectivity.

The application of extremely permeable membranes in FBMRs could lead to formation of densified zones close to the membrane walls in case mild fluidization of small particles [15,16]. It was inferred that it may preferable to work at higher fluidization velocities and with somewhat larger particles (in the order of few hundreds of microns), which results in putting stronger targets on the membrane's resistance against erosion.

A recent paper by Fernandez et al. shows that the integration of membranes in membrane reactors can be also hampered by chemical interaction between the membrane itself and (some component of) the catalyst used in the reactor [17]. For instance, the results have shown that, by using a catalyst bed containing TiO_2, a strong chemical interaction between this component and the membrane surface decreased the permeation flux by a factor of 14 within a few hours of experimentation under fluidization conditions. Other tests with the same material and powder in a packed-bed configuration showed the same effect with an even higher decrease up to a 25 times lower flux (unpublished results).

Different combinations of supports, membrane materials and alloys have been investigated with the aim of developing high-flux membranes showing long-term stability at industrially relevant conditions. The early investigations were based on self-supported thick membranes which presented a very high selectivity (required for niche applications such as nuclear), but low permeation rates and extremely high costs. As the USA Department Of Energy (US DOE) targets for palladium membranes (used as reference in many countries, including Europe) are getting more demanding every 5 years [18], more efforts have been made toward the development of supported thin films due to the improvements in mechanical stability while maintaining high hydrogen permeation rates. As explained previously, thinner membranes allow increasing the H_2 permeance, while reducing the membrane costs, as the amount of employed palladium is lower as well as the required membrane area. Alloying palladium other metals such as silver and copper further increase the H_2 permeability (and stability), while further reducing the membrane cost.

1.3.   This thesis

The main objective of the research described in this thesis is the development and investigation of attrition-resistant membranes for hydrogen separation. Two types of membranes have been studied: pore-filled membranes and double-skinned membranes. These membranes differ from conventional thin-film supported membranes in that a mesoporous ceramic layer is deposited on top of the H_2 selective layer (Pd or Pd-based alloy)

to avoid direct contact of the catalyst with the H$_2$ selective material. The preparation and operational properties of the membranes have been studied in detail.

First the state-of-art on Pd-based membranes for hydrogen separation is presented in **Chapter 2**, were the most employed/suitable materials for membrane (with high H$_2$ flux) production and their preparation techniques in the last decades are reported; special attention has been paid to attrition resistant membranes. In this thesis, two type of attrition resistant membranes have been studied: pore-filled and double-skinned membranes where a mesoporous ceramic layer protects the H$_2$ selective material. First, in **Chapter 3**, the preparation of the mesoporous ceramic layer has been studied in order to obtain a defect-free porous layer, which does not induce substantial mass transfer limitations. The diffusion mechanisms in these layers have been studied in detail. Subsequently, the so-called pore-filled type membranes have been prepared, as described in **Chapter 4**. The Pd (or a Pd-based alloy) is encapsulated in the pores of the mesoporous layer, while another mesoporous layer is added on top to avoid that Pd is exposed at the surface of the membrane. Different tubular ceramic asymmetric porous supports have been employed for their preparation. It has been demonstrated that it is very difficult to form a percolated interconnected structure of Pd, which limits the hydrogen flux and makes these membranes less attractive than previously anticipated. To solve the problem of the low flux, while maintaining the protective characteristics of the porous layer, another membrane concept was developed (and patented), the so-called double-skinned (DS) membrane, where a conventional supported Pd-based membrane is protected with a mesoporous ceramic layer. DS-membranes have been prepared onto ceramic (**Chapter 5**) and metallic porous supports (**Chapter 6**). The performance of these membranes under fluidization conditions has been studied and reported, showing an unprecedented combination of high flux, high selectivity and high stability in fluidized bed reactors. Finally, the main conclusions obtained with the two types of membranes are summarized in **Chapter 7**. The use of double-skinned membranes in the presence of catalyst that can interact chemically with the Pd-layer is also addressed in **Chapter 7**, as well as some guidelines for further development of membrane preparation for their use in FBMRs.

Bibliography

[1]   P. Zakkour, G. Cook, CCS Roadmap for Industry: High-purity CO2 sources, (2010) 13–22. http://hub.globalccsinstitute.com/sites/default/files/publications/15686/ccs-roadmap-industry-high-purity-co2-sources-sectoral-assessment.pdf.

[2]   J.R. Rostrup-Nielsen, New aspects of syngas production and use, Catal. Today. 63 (2000) 159–164.

[3]   A.M. Adris, S.S.E.H. Elnashaie, R. Hughes, Fluidized bed membrane reactor for the steam reforming of methane, Can. J. Chem. Eng. 69 (1991) 1061–1070.

[4]   E.K. Ikuchi, S.K. Awabe, M.M. Atsukata, Steam Reforming of Methanol on Ni/Al2O3 Catalyst in a Pd-membrane Reactor, J. Japan Pet. Inst. 46 (2003) 93–98.

[5]   G. Barbieri, A. Brunetti, G. Tricoli, E. Drioli, An innovative configuration of a Pd-based membrane reactor for the production of pure hydrogen. Experimental analysis of water gas shift, J. Power Sources. 182 (2008) 160–167.

[6]   F. Gallucci, L. Paturzo, A. Basile, A simulation study of the steam reforming of methane in a dense tubular membrane reactor, Int. J. Hydrogen Energy. 29 (2004) 611–617.

[7]   C.S. Patil, M. van Sint Annaland, J.A.M. Kuipers, Fluidised bed membrane reactor for ultrapure hydrogen production via methane steam reforming: Experimental demonstration and model validation, Chem. Eng. Sci. 62 (2007) 2989–3007.

[8]   T. Boeltken, A. Wunsch, T. Gietzelt, P. Pfeifer, R. Dittmeyer, Ultra-compact microstructured methane steam reformer with integrated Palladium membrane for on-site production of pure hydrogen: Experimental demonstration, Int. J. Hydrogen Energy. (n.d.). doi:http://dx.doi.org/10.1016/j.ijhydene.2014.06.091.

[9]   R. Dittmeyer, T. Boeltken, P. Piermartini, M. Selinsek, M. Loewert, F. Dallmann, H. Kreuder, M. Cholewa, A. Wunsch, M. Belimov, S. Farsi, P. Pfeifer, Micro and micro membrane reactors for advanced applications in chemical energy conversion, Curr. Opin. Chem. Eng. 17 (2017) 108–125. doi:10.1016/j.coche.2017.08.001.

[10]   T. Boeltken, M. Belimov, P. Pfeifer, T.A. Peters, R. Bredesen, R. Dittmeyer, Fabrication and testing of a planar microstructured concept module with integrated palladium membranes, Chem. Eng. Process. Process Intensif. 67 (2013) 136–147.

[11]   F. Gallucci, M. van Sint Annaland, J.A.M. Kuipers, Theoretical comparison of packed bed and fluidized bed membrane reactors for methane reforming, Int. J. Hydrogen Energy. 35 (2010) 7142–7150.

[12]   A.L. Mejdell, T.A. Peters, M. Stange, H.J. Venvik, R. Bredesen, Performance and application of thin Pd-alloy hydrogen separation membranes in different configurations, J. Taiwan Inst. Chem. Eng. 40 (2009) 253–259.

[13]   S.A.R.K. Deshmukh, M. van Sint Annaland, J.A.M. Kuipers, Gas back-mixing studies in membrane assisted bubbling fluidized beds, Chem. Eng. Sci. 62 (2007) 4095–4111.

[14]   L. Roses, F. Gallucci, G. Manzolini, S. Campanari, M. Van Sint Annaland, Comparison between fixed bed and fluidized bed membrane reactor configurations for PEM based micro-cogeneration systems, Chem. Eng. J. 171 (2011) 1415–1427. doi:10.1016/j.cej.2011.05.061.

[15]   N.T.Y. Dang, F. Gallucci, M. van Sint Annaland, Micro-structured fluidized bed membrane reactors: Solids circulation and densified zones distribution, Chem. Eng. J. 239 (2014) 42–52.

[16]   N.T.Y. Dang, F. Gallucci, M. Van Sint Annaland, Influence of reactor and particle scale on the hydrodynamics of microstructured fluidized bed membrane reactors, Ind. Eng. Chem. Res. 52 (2013) 18192–18205.

[17]   E. Fernandez, A. Helmi, K. Coenen, J. Melendez, J.L. Viviente, D.A. Pacheco Tanaka, M. van Sint Annaland, F. Gallucci, Development of thin Pd–Ag supported membranes for fluidized bed membrane reactors including WGS related gases, Int. J. Hydrogen Energy. 40 (2015) 3506–3519.

[18]   Energy Efficiency and Renewable Energy Report of the DOE Workshop on Hydrogen Separations and Purification, Arlinton, VA, USA, 2004.

Chapter 2

Pd-based membranes: State-of-art

Palladium-based membranes for hydrogen separation have been studied by several research groups over the last 40 years. Much effort has been dedicated to improving the hydrogen flux of these membranes employing different alloys, supports, deposition/production techniques, etc. High flux and cheap membranes, yet stable at different operating conditions are required for their exploitation at industrial scale. The integration of membranes in multifunctional reactors (membrane reactors) poses additional demands on the membranes as interactions at different levels between the catalyst and the membrane surface can occur. Particularly, when employing the membranes in fluidized bed reactors, the selective layer should be resistant to (or protected against) erosion. A novel kind of membranes, the pore-filled type membranes prepared by Pacheco Tanaka and co-workers represent a possible solution to integrate thin selective membranes into membrane reactors while protecting the selective layer. This chapter is particularly focused on recent advances on metallic supports, materials used as an intermetallic diffusion layer when metallic supports are used and the most recent advances on Pd-based composite membranes.

"The science of today is the technology of tomorrow".
Edward Teller.

2.1. Characteristics and properties of membranes for hydrogen separation

As already reported in Chapter 1, the targets for H_2 membranes are generally taken from the targets set by the US DOE (United States Department of Energy). Some targets set for 2005, 2010 and 2015 have been summarized in Table 2.1. Some of these targets are within reach thanks to the yearly increasing number of research groups devoted to the further development and improvement of hydrogen selective membranes [1]. The target set for the hydrogen flux for 2015 was 1.135 mol m^{-2} s^{-1} with a hydrogen purity of 99.99%, which can be achieved with an ideal H_2 perm-selectivity in the order of 10000 (in gas mixture conditions).

Table 2.1. US DOE 2015 targets for hydrogen separation membranes [1].

Performance criteria	2005 Target	2010 Target	2015 Target
Flux (mol m^{-2} s^{-1})	0.378 (100 Scfh ft^{-2})	0.567 (200 Scfh ft^{-2})	1.135 (300 Scfh ft^{-2})
Membrane Cost (\$ m^{-2})	17600 (2000 \$ ft^{-2})	8800 (1000 \$ ft^{-2})	< 4400 (< 500 \$ ft^{-2})
Durability (years)	1	3	>5
H_2 recovery (%)	> 70	> 80	90
Hydrogen purity (%)	> 99.9	> 99.95	99.99

However, all these criteria are set for membranes working in the presence of impurities like sulfur compounds and CO, which can be challenging for Pd-based membranes (especially the sulfur). The flux target is set for a hydrogen differential partial pressure of 20 psi (=138 kPa) with a minimum value for the pressure at the permeate side of 15 psi (=103 kPa), and at 400 °C. The cost per square meter of membrane area seems to be achievable for supported membranes. To surpass the high flux DOE 2015 target, very thin (but dense) membranes are required. The required thickness of the membrane to achieve a certain flux can be estimated from Sieverts' law [2,3]:

$$J_{H_2} = \frac{Pe_{H_2}}{t}\left(p_{H_2,ret}^{0.5} - p_{H_2,perm}^{0.5}\right)$$
(Eq. 2.1)

where J_{H_2} is the permeated hydrogen flux, Pe_{H_2} the hydrogen permeability, t membrane thickness, $p_{H_2,ret}$ and $p_{H_2,perm}$ are the partial pressures of hydrogen in the retentate and permeate sides, respectively [2,3]. To surpass the DOE target, the permeance, defined as the hydrogen flux divided by the driving force, and thus equal to Pe_{H_2}/t, should exceed $3 \cdot 10^{-3}$ mol m^{-2} s^{-1} Pa$^{-0.5}$, or $1 \cdot 10^{-5}$ mol m^{-2} s^{-1} Pa^{-1} in units that are often used in literature for ease of comparison. With a relatively high permeability of $1 \cdot 10^{-12}$ mol m^{-1} s^{-1} Pa^{-1} the required membrane thickness to reach the DOE target is in the order of 0.1 μm, clearly indicating the necessity to develop ultra-thin Pd membranes or layers on supported membranes.

2.1.1. Supported membranes for high H$_2$ flux

2.1.1.1. Selection of porous support

For the preparation of very thin and pinhole-free supported membranes the choice of the porous substrate (support) is crucial. Different support configurations and materials are commercially available; however, asymmetric tubular supports are preferred because of their larger surface/volume ratio compared with disk shape substrates. The characteristics of the support determine the required selective layer thickness in order to obtain a defect-free thin layer. Both ceramic and metallic supports have been extensively used. On the one hand, ceramic supports are very interesting because of their suitable surface properties and chemical compatibility with Pd-layers. However, their integration in a membrane reactor is more complex and they are mechanically weaker than metallic supports. On the other hand, the thermal expansion of ceramic supports is smaller than metallic supports and is closer to the thermal expansion of Pd and its alloys. The thermal expansion coefficients of some materials used for the preparation of composite membranes have been listed in Table 2.2. The most widely used support is alumina, which has a smaller thermal expansion coefficient than Pd, which could cause failures in the membranes when used at higher temperatures. This problem can be reduced by using ZrO$_2$ or YSZ (yttria stabilized zirconia), which both have a thermal expansion coefficient closer to that of Pd.

Table 2.2. Thermal expansion coefficients of some materials used for the preparation of hydrogen selective membranes [4–6].

Material	Thermal expansion coefficient (10^{-6} °C^{-1})
Al$_2$O$_3$	6.5-7.6
YSZ	10
ZrO$_2$	10
CeO$_2$	11.0
TiO$_2$	9.2
316L	16.0
Pd	11.8
Ag	18.9-19.7
Au	14.2
Cu	16.5-17.0
Ni	11.8-13.3

The most important characteristics of porous supports for the deposition of very thin pinhole-free selective layers are: a) small pore size, b) smooth surface c) thermal and chemical stability.

Supports with a small pore size are required for thin membranes without defects. Thus, the pore size of the support determines the minimum amount of material required to completely

cover them and form a continuous layer. Mardilovich et al. [7] have proven that the thickness required to obtain a dense layer is three times the diameter of the largest pore in the support. The minimum thickness of palladium required to deposit a dense layer on top of a porous support with different pore sizes was found to be much larger, as reported by Uemiya [8] (see Table 2.3).

Table 2.3. Required Pd-layer thickness to cover supports with different pore sizes [8].

Media grade of support (μm)	Thickness of deposited Pd layer (μm)
$5 \cdot 10^{-3}$	0.8
0.1	2.2
0.2	4.5
0.3	13

Another property of the porous supports will influence the required layer thickness: the surface roughness. High surface quality (low roughness) and controlled porosity can be more easily obtained in ceramic supports. High surface quality can also be obtained by depositing a meso-porous layer onto porous supports [9–11], which could however reduce the hydrogen permeation because of the induced mass transfer resistance of the additional layer. Additionally, the adhesion between the Pd layer and the additional meso-porous layer could be a problem, which would result in weak Pd membrane. McCool and co-workers [9] improved the surface quality of commercial α-Al_2O_3 by deposition of a 5 μm thick γ-Al_2O_3 layer using a slip-casting technique of boehmite. The initial average pore size of the porous support was reduced from 200 nm to 4 nm, with a final porosity around 40%. Very thin PdAg layers (163-525 nm) with a different silver content were deposited by DC sputtering. The best permeation results were obtained for a 117 nm thick $Pd_{82.6}Ag_{17.6}$ layer, for which the measured H_2/He selectivity and H_2 permeance at 300 °C were ~3800 and $7.69 \cdot 10^{-8}$ mol m^{-2} s^{-1} Pa^{-1}, respectively.

Thoen et al. [11] used commercial asymmetric α-Al_2O_3 tubes coated with ZrO_2 from Pall Corporation with a pore size of 20 nm. A 1.3 μm thick $Pd_{95}Cu_5$ layer was deposited by sequential electroless plating without the presence of EDTA as complexing agent. The permeated hydrogen flux at 365 °C with a feed pressure of ~ 435kPa (~ 63 psig) was 1.5 mol m^{-2} s^{-1}. Checchetto et al. [12] deposited a SiO_2 nanolayer (100 nm) on top of an Al_2O_3 porous disk with nominal pore size of 200 nm followed by deposition of 150 nm of PdAg by pulsed laser deposition, which was not completely defect free since the selectivity observed at 300 °C was around 600-900 at a pressure difference of 1 bar with a permeance of $1.4 \cdot 10^{-6}$ mol m^{-2} s^{-1} Pa^{-1}. Pan et al. [13] modified α-Al_2O_3 hollow fibres with an initial pore size of 200 nm with 1 μm thick γ-Al_2O_3 by dip-coating and finally 2-3 μm of Pd were coated by ELP with a final selectivity exceeding 1000 at 400 °C and a permeance of $1.1 \cdot 10^{-6}$ mol m^{-2} s^{-1} Pa^{-1}, which is one order of magnitude smaller than the original support (2.1-$2.5 \cdot 10^{-5}$ mol m^{-2} s^{-1} Pa^{-1}). Wu

et al. [14] and Li et al. [15] modified α-Al$_2$O$_3$ (0.1 µm pore size) and Al$_2$O$_3$-ZrO$_2$ (0.2 µm pore size) supports, respectively, with TiO$_2$ followed by photo-catalytic deposition of Pd thin layers of 100 nm and 400 nm, respectively. The observed permeance and selectivity are presented in Table 2.4, which can be compared with other layers deposited onto modified Al$_2$O$_3$, and ZrO$_2$ supports.

Table 2.4. Comparison of the hydrogen permeation for various composite membranes.

Membrane/support	Thickness (µm)	Permeance (mol m^{-2} s^{-1} Pa^{-1})	Temp. (°C)	Selectivity H$_2$/N$_2$	Ref.
Pd-Ag/γ-Al$_2$O$_3$/α-Al$_2$O$_3$	0.117	7.7·10^{-8}	300	~ 3800*	[9]
Pd$_{95}$Cu$_5$/ZrO$_2$/α-Al$_2$O$_3$	1.3	4.5·10^{-6}	365	127	[11]
Pd-Ag/SiO$_2$/Al$_2$O$_3$	0.15	1.4·10^{-6}	300	600-900	[12]
Pd/γ-Al$_2$O$_3$/α-Al$_2$O$_3$ (HF)	2-3	1.1·10^{-6}	400	> 1000	[13]
Pd/TiO$_2$/α-Al$_2$O$_3$	0.1	3.3·10^{-6}	450	4.7	[14]
Pd/TiO$_2$/Al$_2$O$_3$-ZrO$_2$	0.4	4.8·10^{-6}	430	83-130	[15]

* H$_2$/He selectivity.

Pacheco Tanaka et al. [10] modified tubular α-Al$_2$O$_3$ substrates with an average pore size of 150 nm by deposition of a meso-porous γ-Al$_2$O$_3$ layer by vacuum assisted dip-coating followed by a slow drying process at 40 °C and final calcination at 550 °C. These porous supports were also modified with YSZ/γ-Al$_2$O$_3$ mixtures, which were calcined at different temperatures (500-1000 °C) [16]. The nitrogen permeance of the supports calcined at 1000 °C was close to twice the permeance of those calcined at 600 °C. During the calcination the pore radius decreased, causing larger pore size distributions at higher temperatures (2-9 nm) and a smaller distribution and size at 600 °C (1-4 nm). Both modified supports [10,16] were used for the preparation of pore-filled type membranes (which will be discussed in more detail in the section 2.1.5.2 *Pore-filled type membranes*).

In addition to the pore size (distribution) and surface roughness, the stability of the support material under reductive environments at high temperatures and possible interactions with the material of the selective layer (in particular Pd) are two very important aspects to be considered in the preparation of supported membranes. Thermal stability of alumina supports in the presence of hydrogen at different temperatures was evaluated by Okazaki et al. [17]. The authors found that alumina interacts with hydrogen at temperatures above 650 °C producing aluminium. This diffuses through the Pd layer forming an alloy at the interface as revealed by EDX analysis. In their experiments the hydrogen flux was diminished by a factor two after 50 h. This phenomenon proceeds even faster at higher temperatures, as the hydrogen permeation was totally suppressed after 2-3 hours at 850 °C.

Paglieri et al. [18] observed a similar decrease in the permeated hydrogen flux at 750 °C, where Pd was deposited onto alumina porous supports, with a complete and irreversible flux decay that could not be recovered even after thermal treatment in air or hydrogen.

Huang et al. [19] detected diffusion between Pd and TiO_2 used as interdiffusion barrier. In membranes used for 23 days at 600 °C in the presence of pure hydrogen the authors found diffusion of components of the support (and interdiffusion barrier layer) at a depth of 2-3 µm along the interface. Diffusion was not observed when using ZrO_2 and YSZ interdiffusion barriers. Stability under reductive and oxidative atmospheres is obtained with cubic phase YSZ. Okazaki et al. [17] found that YSZ represents the best choice for high temperature environments, such as for membrane assisted reactors for autothermal reforming. The authors tested a Pd/YSZ membrane during 336 h at 650 °C in pure hydrogen observing 10% reduction in the hydrogen flux during the first 50 h, as shown in Figure 2.1. After this period, the hydrogen flux reached a *plateau* without presence of nitrogen leaks. The tested membrane was analysed by cross-section SEM images and it was found that the selective layer did not show presence of Y and/or Zr. However, when using Pd/Al_2O_3 composite membranes, the hydrogen permeation flux was completely lost after ~125 h.
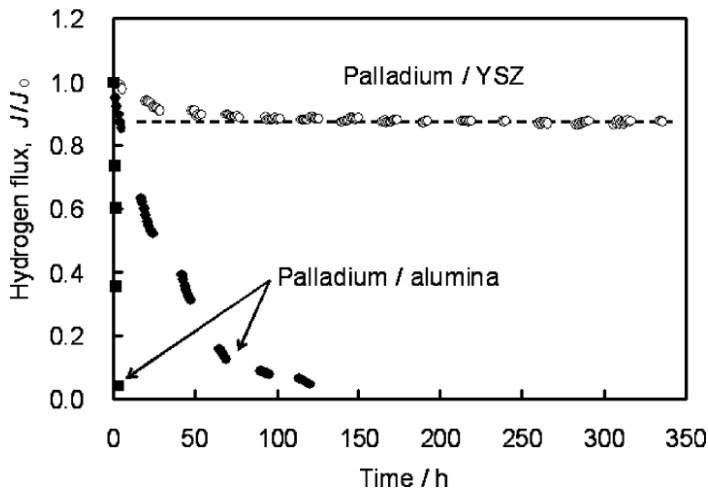
Figure 2.1. Hydrogen flux measured at 650 °C for Pd-YSZ and $Pd-Al_2O_3$ membranes at 100 kPa of pressure difference [17].

As far as metal supports are concerned, most of the papers published in the last few years have used porous supports made of stainless steel, followed by nickel substrates for higher temperatures. Metallic supports employed in the most recent studies have been summarized in Table 2.5 including some characteristic parameters of the supports and techniques used for the deposition of the ceramic barriers. Stainless steel porous supports with different pore sizes from Mott Metallurgical Corporation are commonly used, where smaller pore size are

preferred due to their smoother surface [20–25]. Commercially available PSS supports are made of stainless steel 316L with different pore size, also called media grade. Typical media grades used are 0.1 µm and 0.2 µm, corresponding to an average pore size of 2-5 µm and 10 µm, respectively (measured by mercury intrusion). Larger media grades, 0.5 µm, are less used due to their larger average pore size (10-20 µm) which requires thicker Pd or interdiffusion barriers to reach complete surface coverage. Porous stainless steel substrates from Pall corporation were used with a pore size of 2 µm [26], while YSZ modified PSS from Pall have also been used for membrane preparation [27–29]. Some research groups prepared in-house metallic porous supports. A PSS tubular support was prepared by Straczewski using powder from GKN Sinter Metals [30].

On the other hand, nickel porous support were prepared by sintering commercial nickel powder supplied by Vale Inco Pacific Ltd [5,31]. For high temperature applications (> 550 °C), Hastelloy X (Ni-based) from Mott Corporation is another option [32,33]. Except for the YSZ modified PSS from Pall, all other metallic supports require an interdiffusion barrier, as discussed in the next section.

Table 2.5. Recently reported studies employing porous metal supports: materials and suppliers.

Material	Supplier	Media grade (µm)*	Pore size (µm)	Reference
Stainless steel	Mott Metallurgical Corporation	0.1	2-5	[21–23]
		0.2	10	[20,21]
		0.5	20	[24,25]
	Pall Corporation	0.1	2	[26]
	Pall Corporation (30µm YSZ)	-	-	[27–29]
	GKN Sinter Metal **	-	-	[30]
Nickel	Vale Inco Pacific Ltd. **	-	-	[5,31]
Hastelloy X	Mott Corporation	0.2	-	[32,33]

* Particle retention size. 95% rejection of particles with a size greater than the grade is guaranteed.
** Powder provided by GKN and Vale Inco. Authors manufactured the porous supports.

Mechanical failure of supported thin films due to the difference in thermal expansion coefficients between the selective layer and the porous supports can be avoided by deposition of an interdiffusion barrier with a similar expansion coefficient of the dense selective layer. Another possibility was reported by Zhao et al. [34], who prepared a membrane with a modified electroless plating bath mixing a solution containing Pd (II) with a γ-Al$_2$O$_3$ (boehmite) sol. The porous substrate was coated with this solution in the presence of small amounts of polyvinyl alcohol (PVA) and polyethyleneglycol (PEG). Before calcination at 600 °C, the coated layer was dried during two days at low temperature (5 °C) and 65% relative humidity. Before electroless plating, the membrane was exposed to hydrogen at 500 °C to reduce the palladium. Finally, a 1 µm thick Pd layer was deposited by ELP as the support was

activated. The permeated hydrogen flux of the supported membrane was 0.108 mol m^{-2} s^{-1} at 450 °C, but the corresponding ideal H$_2$/N$_2$ selectivity was very low: 20.

The development of a thin membrane with high permeation and selectivity is therefore not always possible due to the factors discussed before such as support pore size, roughness, etc. In many of the studies presented in this period either a high flux or a high selectivity was achieved. However, Bredesen and co-workers (SINTEF) reported the preparation of Pd-Ag membranes with both very high permeation and selectivity [26]. A 2.8 µm thick Pd$_{77}$Ag$_{23}$ layer was deposited by magnetron sputtering onto a silicon wafer, which was removed and rolled onto a 316L stainless steel tubular porous support. The measured hydrogen flux at 400 °C and 26 bar of feed pressure was 8.64 mol m^{-2} s^{-1} with a H$_2$/N$_2$ selectivity of 1600. These results were even improved after thermal treatment in air at 400 °C for three days. The hydrogen flux and selectivity measured under the same conditions reported before thermal treatment in air were 18.43 mol m^{-2} s^{-1} and 2900, respectively. The initial hydrogen permeance, 6.48·10^{-3} mol m^{-2} s^{-1} Pa$^{-0.5}$, was enhanced one order of magnitude after thermal treatment in air with a measured permeance of 1.46·10^{-2} mol m^{-2} s^{-1} Pa$^{-0.5}$. A long-term test was performed at temperatures below 375 °C during 85 days in the presence of a 50% H$_2$/50% N$_2$ feed gas revealing great stability for the first 40 days. However, the nitrogen flux increased from 4.46·10^{-3} to 6.32·10^{-3} mol m^{-2} s^{-1} at 10 bar feed pressure, while the hydrogen flux was maintained at around 8.78 mol m^{-2} s^{-1}. The corresponding H$_2$/N$_2$ ideal selectivity was 1400. Pinholes of about 0.1-0.3 µm in diameter were observed by SEM on the membrane surface exposed to hydrogen after long-term experiments.

A short air treatment allows activation (or perhaps cleaning) of the membrane and increases the flux of H$_2$. It was suggested by Roa and Way [35] that exposure to air resulted in surface cleaning and enhancement in the surface area for "as prepared" (not totally clean) membranes. This effect depends on the exposure time and temperature. However, this effect is not representative for all Pd-alloyed membranes as Zhang et al. [36] reported in their study where Pd$_{75}$Ag$_{25}$ and Pd$_{90}$Au$_{10}$ membranes were "activated" under air treatment at 300 °C. The measured hydrogen flux before and after air treatment for the PdAu layer were practically the same, while the authors observed an increase in the flux for the PdAg membrane ranging between ~80% at a transmembrane pressure difference of 55 Pa$^{0.5}$, and ~50% at a pressure difference of 180 Pa$^{0.5}$.

2.1.1.2. *Selection of the interdiffusion layer*

The undesired diffusion of components from the porous stainless-steel support such as Fe, Cr and Ni to the Pd selective layer at high temperatures is a well-known phenomenon. After diffusion, an alloy with Pd is formed that decreases the hydrogen permeance of the membrane due to the reduction of the solubility and diffusivity of hydrogen into the Pd-alloy

lattice; Pd and Fe from the support start forming a solid solution at 500 °C in the presence of hydrogen after 20 h [37]. The amount of iron in the Pd layer interface increases from 2 wt% to 59 wt% upon a thermal treatment with a temperature increase from 500 °C to 800 °C. In contrast, silver does not form a solid solution with iron at these temperatures.

In order to avoid the diffusion of elements between the metallic support and the dense selective layer during operation at high temperatures, the deposition of a ceramic barrier is performed on top of the metallic porous support. Moreover, metallic supports having an adequate pore size and roughness for thin Pd membranes are difficult to fabricate. Therefore, the deposition of the ceramic layer also improves the surface quality of the original support allowing the deposition of thinner selective layers.

The selection of the ceramic material for the interdiffusion barrier layer is a critical point to take into account, since an asymmetric membrane composed of materials with different thermal expansion coefficients could result in a total failure of the membrane during operation especially at high temperatures. Ceramics used as interdiffusion barrier need to have as similar thermal expansion coefficient as the selective metallic layer and support. The most common barrier material, alumina [38–41], has a low thermal expansion coefficient compared with ZrO_2 [21,42–45] or YSZ [22,25,27–30], which both have larger thermal expansion coefficients and closer to Pd and its alloys (see Table 2.2). Other ceramic layers used as barrier are TiO_2 [30] or CeO_2 [5,46] which both possess a large thermal expansion coefficient and close to the thermal expansion coefficient of Pd. Oxidation of porous stainless-steel supports provides a chromium oxide (Cr_2O_3) layer, which can act as an interdiffusion barrier. The thickness of the Cr_2O_3 layer is controlled by the oxidation temperature and time [25] or by the electrodeposition of Cr followed by oxidation treatment in air [47]. Nickel porous supports are generally modified by the deposition of thin ceramic layers of Al_2O_3, ZrO_2 and CeO_2. By physical vapour deposition, 0.2 μm thick alumina and zirconia layers were deposited [31], while CeO_2 (0.5 μm) was obtained by dip-coating after modification of the Ni-support by wetness impregnation with alumina [5]. The composite membranes based on metallic porous supports modified with interdiffusion barriers have been summarized in Table 2.6.

The large pore size of commercial PSS supports can be reduced before deposition of ceramic layers by a pre-treatment based on polishing and then etching with an acid solution (HNO_3 and HCl) as Li et al. have suggested [40]. The initial roughness of PSS supports with media grade of 0.2 μm was reduced from 20 μm to 5 μm by polishing. However, most of the pores were completely closed, decreasing the initial H_2 permeation rate more than 99%. Acid etching of the polished surface removed more than 15 μm of material, opening pores and, as a result, the permeance of the support was enhanced 15% more than with the initial support without polishing. The remaining roughness was reduced by deposition of a 2 μm thick

alumina layer using particles of around 2.5 μm. The surface roughness was decreased from 5 μm to 2 μm after deposition of the first layer, which did not cover the metallic substrate completely and the permeation rate was reduced by 40%. Subsequently, the metallic support was completely covered by deposition of a second layer (~ 1 μm) with a particle size of 0.3 μm. The measured separation factor H_2/N_2 was less than 3.74 (Knudsen diffusion), suggesting still a contribution of viscous flow. A defect-free Pd layer (5 μm) was deposited by ELP exhibiting a permeance of $3.39 \cdot 10^{-3}$ mol m^{-2} s^{-1} Pa$^{-0.5}$ at 550 °C and a pressure difference of 340 kPa.

A similar method for the deposition of alumina was reported by Chi et al. [41] without pre-treatment for supports with the same characteristics as used by Li et al. [40]. The particle sizes of the deposited layers were about 10 μm and 1 μm. The authors did not report the thickness of the layers, but suggested that the first layer blocked the large pores of the metallic support, while the second layer covered the surface completely [41]. The measured helium flux was reduced 7.36% and 21.3% after deposition of the two layers, respectively. The deposited dense Pd-layer by ELP onto the original support and the modified support with two layers was reduced from 31.5 μm to 4.4 μm. The permeance of the thinner membrane at 500 °C and a pressure difference of 800 kPa was $2.94 \cdot 10^{-3}$ mol m^{-2} s^{-1} Pa$^{-0.5}$, with an ideal selectivity H_2/He of 1124. Additionally, the hydrogen flux through unmodified PSS with a 31.5 μm thick Pd layer was decreasing during the experiment due to diffusion of metal elements from the support to the Pd layer.

Broglia et al. [39] reduced the original roughness of PSS with a nominal pore size of 0.1 μm with γ-Al$_2$O$_3$ by dip coating followed by the deposition of a second layer obtained by hydrolysis of metal-organic alumina. They found that the mesoporous alumina (3-4 μm) layer covered the support completely. However, part of this ceramic layer was dissolved by the Pd-activation solution due to the acidity of the solution. A pinhole-free 11 μm thick Pd layer was deposited by ELP with total coverage of the modified support. Unfortunately, the authors did not report permeation experiments.

Tong et al. introduced a cerium hydroxide solution into a Mott PSS tubular support (particle retention size of 0.2 μm) applying vacuum in the inner side of tube [46]. Two layers of 6 μm and 10 μm of Pd were deposited by ELP, resulting in a H_2/Ar selectivity of 108 for the thicker layer, while the separation factor of the 6 μm layer was lower (only 14). The defects of this last membrane were repaired by chemical vapor deposition (CVD) sublimating Pd (II) hexafluoroacetylacetonate. After 3 CVD treatments the overall thickness of Pd was around 6.4 μm and the selectivity was improved to 565 with a hydrogen permeation flux of 0.235 mol m^{-2} s^{-1} at 500 °C and a pressure difference of 100 kPa.

Straczewski deposited YSZ and TiO_2 onto an in-house PSS substrate produced using powder from GKN Sinter Metals [30]. A smoother surface was obtained before deposition of the interdiffusion layer by wet powder spraying of fine particles, followed by deposition of <100 μm thick YSZ layer by atmospheric plasma spraying (APS) or thinner (<15 μm thick) TiO_2 by wet powder spraying (WPS). The thinner TiO_2 layers presented a larger surface quality (small pore size, large porosity and smooth surface) than the YSZ layers. Furthermore, the measured nitrogen permeance for the TiO_2 layers was ~$1.8 \cdot 10^{-5}$ mol m^{-2} s^{-1} Pa^{-1}, one order of magnitude higher than for the thicker YSZ layer, ~$3.2 \cdot 10^{-6}$ mol m^{-2} s^{-1} Pa^{-1}. No significant changes were observed on the permeated N_2 flux through the YSZ layer after nine thermal-cycling tests at 700 °C with different heating rates. On the other hand, the N_2 flux was reduced every cycle for TiO_2 till 10% of the initial N_2 flux. Thicker Pd layers were required and were deposited onto YSZ (24.8-30 μm) than on TiO_2 (8.3-14.9 μm) due to the better surface quality of the last one. A slight increase in the N_2 flux was measured for the Pd-YSZ-PSS composite after a thermal treatment at 700 °C. Meanwhile, the N_2 flux decreased for the Pd-TiO_2 system when the heating rate was increased, suggesting sintering of the particles of the intermediate layer. The properties of the intermediate and selective layers are reflected in the hydrogen permeation flux. The thicker Pd(25.3μm)-YSZ-PSS membranes permeated 0.14 mol m^{-2} s^{-1} of H_2 at 600 °C and a transmembrane pressure of 2 bar, in terms of permeance ($5.7 \cdot 10^{-4}$ mol m^{-2} s^{-1} $Pa^{-0.5}$) one order of magnitude smaller than for the Pd(14.3 μm)-TiO_2-PSS composite ($2.6 \cdot 10^{-3}$ mol m^{-2} s^{-1} $Pa^{-0.5}$). The calculated ideal H_2/N_2 selectivity was similar and close to 200 for both membranes.

Huang et al. [19] compared three different ceramic barriers (ZrO_2, YSZ and TiO_2) deposited onto 310L porous supports by different deposition techniques. Very thin (2 μm) ZrO_2 layers were obtained by magnetron sputtering resulting in incomplete coverage of the porous support, which resulted in intermetallic diffusion at points where the Pd-layer was in contact with stainless steel. Thicker (10-70 μm) and rougher YSZ layers were obtained by APS, where the largest pore size (1.9 μm) of the original support was reduced to 0.78 μm. However, the nitrogen flux was reduced to 15% of the flux through the original support. In contrast, the nitrogen flux of the deposited TiO_2 by WPS with a large thickness (40-60 μm) was still 77% of the initial value having a smaller pore diameter (0.22 μm). Nevertheless, adherence of the TiO_2 layer was compromised at higher temperatures. The required thicknesses of Pd to obtain complete coverage via ELP were 9 μm, 14 μm and 23 μm for TiO_2, ZrO_2 and YSZ, respectively. Permeance values of the composite membranes at 500 °C and a pressure difference of 0.5 bar are reported in Table 2.6, where the best results were obtained for a Pd/TiO_2/PSS with $1.91 \cdot 10^{-3}$ mol m^{-2} s^{-1} $Pa^{-0.5}$ with an ideal H_2/N_2 selectivity of ~800. Other composites showed a lower permeance related to the thicker Pd layers, however, the selectivity of both was around ~200.

Tardini et al. [21] compared the effect of ZrO_2 and Al_2O_3 as an interdiffusion barrier layer on top of PSS, requiring at least a 10 μm thick selective layer ($Pd_{92}Au_8$) for the ZrO_2 modified porous stainless steel support, while a double thickness was required to deposit a defect-free membrane on top of an Al_2O_3 modified porous support. Moreover, 4-5 % Fe was detected in the PdAu layer deposited on top of an Al_2O_3 modified composite due to interdiffusion of elements from the metallic support, because the ceramic layer was too thin and did not cover the metallic support adequately. In terms of permeation rates, KIER (Korea Institute of Energy Research) reported that ZrO_2 deposited by sputtering was preferred as interdiffusion barrier layer on top of porous nickel supports (PNS), since the measured nitrogen flux was 1.5 times higher when compared with Al_2O_3 interdiffusion barrier layers. Larger pore sizes were observed by SEM on the ZrO_2 supported surface [31]. Chotirach and co-workers [43] reported that a 0.5 μm thick ZrO_2 (used as a barrier) deposited by DC magnetron sputtering and oxidized in air, reduced the diffusion of elements from the support to the selective layer. The same authors also deposited ZrN, however larger hydrogen permeation rates were obtained with ZrO_2.

Wang et al. [44] used a colloidal zirconium oxide (colloid size around 3 media grade at a pH 7.6) solution into PSS with media grade of 0.2 μm. The deposition was repeated five times until a constant separation factor between He/Ar was obtained. A pinhole-free Pd layer of 10 μm was deposited by ELP exhibiting $6.86 \cdot 10^{-4}$ mol mol m^{-2} s^{-1} Pa$^{-0.5}$ as permeance at 550 °C and a pressure difference of 100 kPa. Argon was detected during the heating process indicating the formation of defects.

Gao and co-workers [45] deposited Pd-doped zirconia sol by dip coating onto PSS substrates (0.2 μm media grade) followed by co-deposition of pinhole-free $Pd_{84}Cu_{15}$ layers of 5 μm by electroless plating. The thicknesses of the ZrO_2 layers were not reported. Homogeneity of the selective layer was confirmed by XPS analysis after a thermal treatment at 480 °C in H_2 for 5 h. The measured hydrogen flux at 480 °C and a pressure difference between the retentate and permeated side of 250 kPa was 0.6 mol m^{-2} s^{-1} corresponding to a permeance of $2.19 \cdot 10^{-3}$ mol m^{-2} s^{-1} Pa$^{-0.5}$.

To select the powder that provides smaller surface roughness, the research group from URJC (Universidad Rey Juan Carlos) [22] studied and reported the porosity and roughness of the intermediate layer of different commercial YSZ particles obtained by atmospheric plasma spraying (APS) on top of PSS with media grade of 0.1 μm. The initial porosity of the support (20%) was reduced to 2% by the intermediate YSZ layer made by Nanox s4007 and AMDRY 6600. The selected YSZ powder was Nanox s4007 since the deposited 100 μm thick layer presented the smallest average roughness (Ra = 2.89 μm) compared to the value measured with AMDRY 6600 (Ra = 4.73 μm) and original supports (Ra = 5.87 μm). The differences in surface quality of the original porous support and YSZ-modified with Nanox s4007 are

shown in Figure 2.2. It is clear from the pictures that the layer completely covered the support and at the same time a reduction in pore size was achieved. A 13.6 μm thick Pd-membrane was deposited by ELP onto YSZ/PSS. No nitrogen leaks were detected during single gas tests of the Pd-composite membrane, where the best hydrogen flux measured at 400 °C and a trans-membrane pressure of 2.5 bar was 0.062 mol m^{-2} s^{-1}. This flux dramatically decreased in the presence of CO and CO_2 during gas mixture tests with 70 mol% H_2. The initial H_2 flux was, however, recovered after removing all gas mixtures, thus the reduction is attributed to the very well-known CO poisoning of the membrane surface [48].
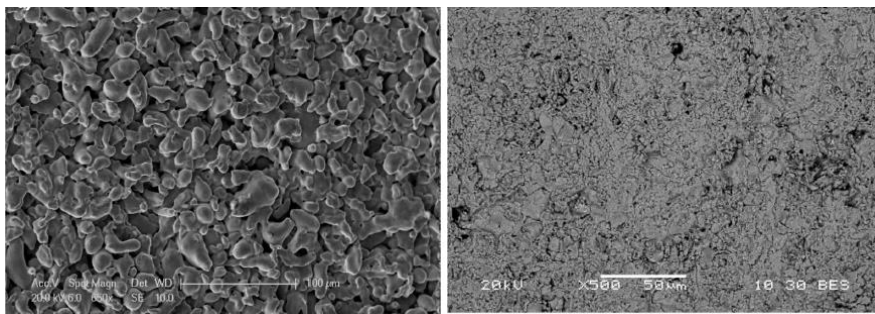

Figure 2.2. SEM images of original PSS support surface (left) and YSZ intermediate layer obtained with Nanox s4007 (right) [22].

Zhang et al. [25] pre-treated PSS (316L) disks with large media grade (0.5 μm) by polishing with #3000 carborundum sandpaper followed by oxidation at 800 °C during 8 h. The measured nitrogen permeance at room temperature was 3.13·10^{-6} mol m^{-2} s^{-1} Pa^{-1}, which was two orders of magnitude smaller than for the original support. A larger N_2 permeance was obtained (1.21·10^{-5} mol m^{-2} s^{-1} Pa^{-1}) with thick YSZ layers of 2.5-3 μm deposited directly onto the supports by dip-coating. Diffusion of components from the porous support was suppressed only with YSZ at 700 °C. An 11 μm thick Pd layer was deposited onto an YSZ/PSS substrate by ELP technique. The hydrogen permeance of the composite was 1.05·10^{-3} mol m^{-2} s^{-1} Pa$^{-0.5}$ at 650 °C and a pressure difference of ~220 kPa. The ideal H_2/N_2 selectivity was not reported, however N_2 was observed at room temperature and 100 kPa of pressure difference (10^{-10} mol m^{-2} s^{-1} Pa^{-1}). On the other hand, a thicker Pd layer (25 μm) was deposited onto oxidized PSS, which suffered from intermetallic diffusion at 650 °C, since the hydrogen flux started decreasing after a few hours. The authors suggested high atomic vibrations of elements from stainless steel and palladium, since they were exposed to temperatures above their Tamman temperature (316L, 560 °C; Pd, 640 °C). The hydrogen permeance was measured at 600 °C and the same pressure difference as for the thinner membrane resulting in one order of magnitude smaller permeance (1·10^{-4} mol m^{-2} s^{-1} Pa$^{-0.5}$) at the same temperature.

Interdiffusion barriers of mixed Al_2O_3-YSZ were deposited on top of Hastelloy X (0.2 μm media grade) by APS and powder suspension deposition (dip-coating) [32]. The roughnesses for layers deposited by APS were found to be larger than by dip-coating. A 4-5 μm thick PdAg layer was deposited by ELP on top of a modified support with a ceramic interdiffusion layer deposited by dip-coating, and the measured hydrogen permeance was $7.69 \cdot 10^{-4}$ mol m^{-2} s^{-1} Pa$^{-0.5}$ at 400 °C and 100 kPa pressure difference. The measured H_2/N_2 perm-selectivity was over 200000. A long-term test with this membrane was performed by Medrano et al. [33] during 800 h in the temperature range of 500-600 °C. The ideal perm-selectivity was maintained above 200000 for 795 hours. Nonetheless, defects started forming at high operating temperatures (600 °C) and the ideal perm-selectivity dropped to 2650.

Oxidation of metallic supports allows growth of a Fe-Cr oxide (Cr_2O_3) layer in order to prevent diffusion of support elements to the selective layer. Gharibi et al. [20] oxidized a porous stainless steel 316L disk (nominal particle retention size of 0.2 μm) in air at 800 °C for 12 h before the depositing a $Pd_{90.2}Ag_{3.6}Cu_{6.2}$ layer by electroless plating. A very thick selective layer, 40 μm, was required to avoid the presence of defects. The thickness and pore size of the grown oxide was not reported. However, it can be expected to be of the order of nanometers with a small reduction of the initial pore size of the supports.

Deposition of a 4 times thinner Pd layer (10.2 μm) by electroless plating was achieved by Sanz et al. [23] as the retention size of the used PSS was 0.1 μm. Since the initial pore size of supports is small, the required thickness for the creation of a defect-free dense layer is decreased. Fe-Cr oxide was obtained at lower temperatures (650 °C) also for 12 h. Again, the thickness of the Fe-Cr oxide was not reported. The membrane was first tested with pure hydrogen before being used with syngas in a packed-bed membrane reactor. The best permeation results were obtained in pure hydrogen at 400 °C and a pressure difference between retentate and permeate sides of 2.5 bar, obtaining a hydrogen flux of 0.054 mol m^{-2} s^{-1} with an infinite ideal perm-selectivity (H_2/N_2), which indicates that the membrane was completely dense and defect-free.

However, it has also been reported that the generated oxide layer by oxidation in air on top of PSS substrates could not completely suppress intermetallic diffusion, as Samingprai and co-workers found [47]. The authors compared oxidized PSS in air at 450 °C for 6 h with Cr_2O_3 layers of different thickness obtained by electrodeposition of Cr followed by oxidation at 700 °C for 6 h in air. Intermetallic diffusion was suppressed for a 2 μm thick Cr_2O_3 layer on top of substrates with an average pore size of 0.1 μm. The authors deposited Pd onto the modified supports by ELP until a dense film was achieved. A defect-free layer was obtained with a 32 μm thick layer which exhibited a low permeance due to the large thickness, $5.84 \cdot 10^{-5}$ mol m^{-2} s^{-1} Pa$^{-0.5}$ at 500 °C and a pressure difference of 100 kPa.

Summarizing, smooth surfaces are required to deposit a very thin selective layer without compromising the permeation rate. Also, it is well established that the mechanical stability of thin films is improved as they are supported. Chemical compatibility (avoiding interdiffusion of elements from metallic supports) and closer thermal expansion coefficients between the materials is necessary for long-term stability of the membranes.

Table 2.6. Pd-based layers deposited onto modified metallic supports with different interdiffusion barriers.

Interdiffusion barrier		Selective layer			Membrane performance						Ref.
Material	Deposition method	Thickness (µm)	Material	Method	Thickness (µm)	T (°C)	Pressure difference (kPa)	n	H_2 permeance (mol m^{-2} s^{-1} Pa^{-n})	H_2/N_2 Selectivity	
Membranes prepared onto porous stainless–steel supports											
γ-Al_2O_3	Dip-coating sol-gel	3-4	Pd	ELP	11	-	-	-	-	-	[39]
Al_2O_3	2 step dip-coating	~3	Pd	ELP	5	550	340	0.5	$3.39\cdot10^{-3}$	-	[40]
α-Al_2O_3	2 step dip-coating	-	Pd	ELP	4.4	500	800	0.5	$2.94\cdot10^{-3}$	1124*	[41]
Al_2O_3	Vacuum assisted dip-coating	<1	$Pd_{92}Au_8$	ELP	24	400	100	0.5	$3.25\cdot10^{-4}$	>10000	[21]
ZrO_2	Vacuum assisted dip-coating	<1	$Pd_{92}Au_8$	ELP	12	400	100	0.5	$1.07\cdot10^{-3}$	>10000	[21]
ZrO_2	PVD-MS	2.0	Pd	ELP	14	500	50	0.5	$8.93\cdot10^{-4}$	~180	[19]
ZrO_2	Vacuum assisted dip-coating	~5	Pd	ELP	7.5	600	500	0.5	$2.53\cdot10^{-3}$	685	[24]
ZrO_2	Vacuum assisted dip-coating	-	$Pd_{78}Ag_9Au_{13}$	ELP	~14	450	50	0.5	$1.15\cdot10^{-3}$	-	[42]
ZrO_2	Vacuum assisted dip-coating	-	$Pd_{90}Ag_{10}$	ELP	~14	450	50	0.5	$1.46\cdot10^{-3}$	-	[42]
ZrO_2	Coating by sucking	-	Pd	ELP	10	550	100	0.5	$6.86\cdot10^{-4}$	-	[44]
Pd-ZrO_2	Dip-coating	-	$Pd_{84}Cu_{16}$	ELP	5	480	250	0.5	$2.19\cdot10^{-3}$	-	[45]
YSZ	-	~30	$Pd_{77}Au_{23}$	ELP	5.7	400	~590	0.5	$2.19\cdot10^{-3}$	690	[27]
YSZ	-	~30	$Pd_{67}Ag_{13}Au_{20}$	ELP	9.3	400	~590	0.5	$1.44\cdot10^{-3}$	2200	[27]
YSZ	-	~30	$Pd_{95}Au_5$	ELP	2.3	400	75	0.6	$1.35\cdot10^{-3}$	82000	[28]
YSZ	-	~30		ELP	4.9	550	50	0.5	$2.39\cdot10^{-3}$	1750	[29]
YSZ	-	~30	$Pd_{73}Pt_{27}$	ELP	4.4	550	50	0.5	$8.82\cdot10^{-4}$	626	[29]
YSZ	-	~30	$Pd_{99.7}Ru_{0.3}$	ELP	6	550	50	0.5	$2.10\cdot10^{-3}$	1860	[29]
YSZ	APS	~100	Pd	ELP	13.6	400	250	0.5	$2.88\cdot10^{-4}$	∞	[22]
YSZ	APS	80-100	Pd	ELP	25.3	600	200	0.5	$5.70\cdot10^{-4}$	~225	[30]
YSZ	APS	10-70	Pd	ELP	23	500	50	0.5	$8.43\cdot10^{-4}$	~200	[19]
YSZ	Dip-coating	2.5-3	Pd	ELP	11	650	~220	0.5	$1.05\cdot10^{-3}$	-	[25]
Cr_2O_3	Oxidation in air at 800 °C, 12h	-	$Pd_{90.2}Ag_{3.6}Cu_{6.2}$	ELP	40	280	90	0.5	$4.32\cdot10^{-4}$	700	[20]
Cr_2O_3	Oxidation at 650 °C, 12h	-	Pd	ELP	10.2	400	250	0.5	$3.30\cdot10^{-4}$	∞	[23]
Cr_2O_3	Oxidation at 800 °C	-	Pd	ELP	25	600	~220	0.5	$1\cdot10^{-4}$	-	[25]
Cr_2O_3	Oxidation at 700 °C, 6h and	2-10	Pd	ELP	32	500	100	0.5	$5.84\cdot10^{-5}$	-	[47]

electrodeposition

TiO_2	WPS	<15	Pd	ELP	14.4	600	200	0.5	$2.6 \cdot 10^{-3}$	~160	[30]
TiO_2	WPS	40-60	Pd	ELP	9	500	50	0.5	$1.91 \cdot 10^{-3}$	~800	[19]
CeO_2	Suction of $Ce(OH)_4$ sol	-	Pd	ELP	10	500	100	0.5	$1.36 \cdot 10^{-3}$	108**	[46]
CeO_2	Suction of $Ce(OH)_4$ sol	-	Pd	ELP+CVD	6.4	500	100	0.5	$1.79 \cdot 10^{-3}$	565**	[46]
Membranes prepared onto porous nickel supports											
Al_2O_3	Sputtering	~0.2	$Pd_{97}Au_3$	PVD	-	-	-	-	-	-	[31]
ZrO_2	Sputtering	~0.2	$Pd_{97}Au_3$	PVD	3.05	450	2000	0.83	$1.52 \cdot 10^{-6}$	2000	[31]
CeO_2	Dip-coating	~0.5	$Pd_{93}Cu_7$	PVD	7	500	400	0.5	$7 \cdot 10^{-4}$	50000	[5]
Al_2O_3-YSZ	Dip-coating	1	PdAg	ELP	4-5	400	100	0.5	$7.69 \cdot 10^{-4}$	200000	[32]

* H_2/He selectivity; ** H_2/Ar selectivity.

2.1.2. Embrittlement and sulfur resistant membranes

Hydrogen selective membranes are often made of Pd-alloys. The metals used to alloy the palladium help in decreasing the challenges that can be detrimental for the hydrogen flux and hydrogen purity. The first challenge affecting Pd membranes is the hydrogen embrittlement occurring below 298 °C and 2 MPa of pressure. Below these critical conditions, the so-called α–β transition occurs. The α-phase appears at low concentrations of hydrogen (solid solution), and the β-phase is formed at high concentrations of hydrogen (metal hydride). Transformation to the β-phase results in crystal expansion with an increased lattice parameter, and may cause membrane failure. Characteristic lattice parameters and Pd/H ratio of both phases and pure palladium are shown in Table 2.7 [49,50].

Table 2.7. Characteristics of PdH phases and pure Pd [49,50].

Phase	Pd/H	Lattice parameter (Å)
α	≤1/0.015	3.889-3.894
β	≥1/0.6	≥4.025
Pd-metal	-	3.889

This problem can be diminished by alloying Pd with elements such as silver. For instance, it has been proven that the durability of Pd membranes alloyed with 20% of silver is improved and H_2 embrittlement was not observed after cycling hydrogenation/dehydrogenation even at temperatures as low as 100 °C [51]. Additionally, it has been proven that the hydrogen permeance is improved by 70% when the silver content reaches 23% in comparison with pure palladium [52]. McCool et al. [9] investigated the effect of the silver content on membrane embrittlement. Membranes with a lower content of silver (4 wt%) delaminated at 200 °C in the presence of hydrogen, whereas membranes with a larger amount of silver (7.8-12.3 wt%) delaminated at lower temperatures (150 °C). The same authors did not observe peel-off of the membranes at 150 °C when using higher contents of silver.

Furthermore, alloying palladium with other noble and non-noble metals could enhance the permeation rate, reduce the temperature of phase transition and improve sulfur resistance [53]. The largest permeance improvement has been reported when alloying Pd with yttrium in a weight content from 6.6% to 10%, exhibiting a hydrogen flux 350-375% larger than for pure palladium [52].

When integrating the membranes in membrane reactors for steam reforming of different feedstocks (CH_4, CH_3OH, C_2H_5OH), the membrane surface may be exposed surface to gases like H_2S and CO which react with palladium and/or other metals, poisoning the membrane and decreasing the permeation rate.

As far as the CO poisoning is concerned, it has been demonstrated that CO adsorbs on the palladium surface occupying the same sites where hydrogen adsorbs before splitting [48]. The poisoning of the membrane occurs at very low concentrations of CO, and when the surface coverage reaches a certain value, the additional CO in the mixture only contributes to the dilution of the hydrogen. The effect of CO is well studied, and it is evident that this poisoning decrease with temperature (as the adsorption is decreased at higher temperatures). Moreover, the membrane can be completely regenerated by removing the CO, and the CO poisoning effect can be easily taken into account in models by modifying Sieverts' equation with a Langmuir type sorption term [54]. On the other hand, poisoning with H_2S is a more serious problem for Pd-based membranes. First of all, the poisoning with H_2S occurs at much lower concentrations (at ppm levels). Secondly, the poisoning occurs via a reaction and a palladium sulfide layer is produced at the membrane surface that in many cases cannot be removed, so that the poisoning is not completely reversible. Alloying Pd with other metals can also help in decreasing the poisoning effects of the contaminant. Pd membranes alloyed with Ag have been shown to be more resistant to hydrogen inhibition by CO [55,56]. Resistance to H_2S poisoning is improved by alloying palladium with noble metals. The most common alloys which present poisoning resistance are Pd-Cu [57] and Pd-Au [27] alloys. Presence of gold reduces embrittlement problems associated with the hydride phase transformation and improves resistance to sulfur poisoning due to the large heat of formation of Au_2S (+230.5 kJ mol^{-1}) compared with other elements of the periodic table, which possess a negative value of heat formation [53].

2.1.3. Thermal stability at high temperature

For Pd-based membranes, one can distinguish "low" (below 450 °C) and "high" (above 450 °C) temperature applications. Many industrially relevant applications fall in the "low" temperature class, including high-temperature water-gas-shift. Other applications, such as methane steam reforming, would be more efficient when operated at higher temperatures (in the range of 600 °C). At these temperatures a good balance between membrane flux, reaction kinetics and thermodynamic constraints can be found. For these "high" temperature applications, the main issue for the membrane is their thermal stability and sealing.

For Pd thin films it was observed that the high-temperature resistance is somewhat limited due to pinholes/defects formation. As the temperature increases, not only the hydrogen diffusion through the membrane lattice is improved, but also Pd diffusion itself is increased, which could result in the formation of micro-holes, which are responsible for the loss of selectivity. Strategies to increase the thermal stability are based on employment of: i) different synthesis techniques; ii) alloying the metal with different dopants; and iii) thermal treatments. It was recently observed by Abu El Hawa and co-workers [29] that alloying Pd with Pt or Ru improves the stability of thin films deposited by ELP. This phenomenon is

related to the higher melting points of both alloying elements reducing the diffusivity of each atom along the thin film for membranes with a thickness lower than 5 μm. Experiments performed at 500-600 °C showed that the N_2 leaks increased faster for Pd than for alloys with 27 wt% Pt or 0.3 wt% Ru. An increase in the nitrogen leakage was measured at 600 °C for every membrane, but the increase in the N_2 leakage was one order of magnitude larger for the pure Pd membrane. In terms of hydrogen flux and selectivity, the Pd-Pt alloy represented the best choice, since the hydrogen flux was extremely stable after 850 h, while pinhole formation was very low.

In a recent study of the same authors [58], the stability of a 5 μm thick Pd-Ru membrane (0.3 wt%) was investigated at 580 °C in a membrane reactor for methane steam reforming for 1000 h. After the experiments, the membrane was cooled down to room temperature to check for leakages at the membrane by submerging the membrane in water and pressurizing the membrane from the lumen side with nitrogen to 1 barg. Small bubbles were observed emerging from the membrane surface suggesting the formation of defects during the long-term test. The addition of Ru decreased the Pd grain growth, so that the grain size did not reach the selective layer thickness. Addition of ruthenium in small quantities did not only improve the mechanical properties of the alloy, but also the permeability increased [59]. However, due to their immiscibility, alloys of Pd and Ru with higher amounts than 1 wt% cannot be obtained at temperatures below 600 °C [60]. It was recently reported by Didenko and co-workers [61] that the properties of a Pd-In-Ru alloy (93.5;6;0.5 wt%) showed an almost three times larger hydrogen flux than $Pd_{77}Ag_{23}$.

Applications of membranes for high-temperature processes such as methane steam reforming, which are often also operated at elevated pressures, need supports with higher mechanical stability. While metallic supported membranes are mechanically more stable than ceramic supported membranes, high-temperature applications require metals that are more stable than stainless steel. This is why often Inconel and Hastelloy supports are being investigated. Porous nickel supports (PNS) represents another possibility, however, all metallic supports still require surface modification to avoid interdiffusion.

2.1.4. Non-palladium membranes

Palladium and its alloys are not the only materials proposed for the preparation of hydrogen perm-selective membranes. BCC metals with a high hydrogen diffusion rate and lower thermal expansion (closer to alumina, $7.6 \cdot 10^{-6}$ °C^{-1}) for hydrogen separation and purification have been studied and fully characterized already more than 20 years ago. Elements from group V such as Nb, V and Ta possess higher permeation rates than FCC metals and alloys [62] and their permeation rate increases as the temperature decreases, as shown in Figure 2.3 [63].
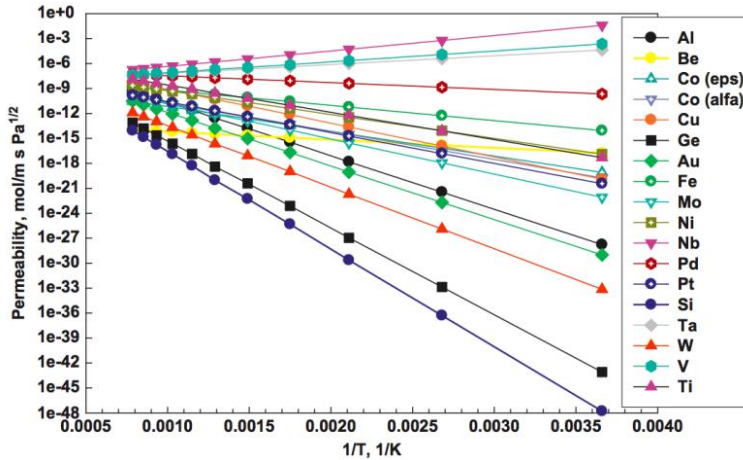
Figure 2.3. Hydrogen permeability as a function of temperature for different interesting metals [63].

This phenomenon is based on the number and size of octahedral and tetrahedral interstices. The number of tetrahedral interstices per atom in FCC and BCC structures is 2 and 6 respectively, which have a relative size to metallic atom radius of 0.225 and 0.291, respectively. In case of octahedral sites, the FCC structure gives three times more sites than the BCC structure with larger size, but the tetrahedral sites represent the main path for transport of hydrogen through the crystal structure. Despite the higher permeation rates, the main disadvantage of these metals is the low resistance to embrittlement, which leads to membrane failure after only few hours of operation [64]. Moreover, their surface activation is much larger than for palladium and the surface is easily oxidized in the presence of low oxygen content, even at very low temperatures (~100 °C) [65]. Their susceptibility to oxidation and their low catalytic activity for hydrogen dissociation/recombination can be solved by covering their surface with other materials which acts as oxygen barrier and as catalysts for hydrogen. Often the membranes based on these metals were prepared by depositing a very thin layer of palladium on both sides of the membrane [66]. However, the embrittlement problem is not solved and remains a key issue for these membranes. Resistance against embrittlement is enhanced by alloying with metals which can reduce the hydrogen solubility. As suggested by Kim et al. [67], addition of Fe to vanadium decreases the hydrogen solubility and the ductility of the alloy. Additionally, the introduction of aluminium to V-Fe alloys increases the embrittlement resistance, but the hydrogen solubility is dramatically decreased. A V-Fe-Al ternary alloy was prepared by arc melting and 400 μm-thick disk cut by electrical discharge. In order to promote hydrogen dissociation, palladium was sputtered in both sides (150 nm). The best result was obtained with a ternary alloy $V_{0.9}Fe_{0.05}Al_{0.05}$ at 500 °C with a permeance of $3 \cdot 10^{-4}$ m^{-2} s^{-1} $Pa^{-0.5}$, while the embrittlement resistance was enhanced since (under cooling tests) the membrane only failed when operated close to 175 °C. Better results were obtained by Alimov and co-workers [66] with a Pd(2 μm)-

V(100 μm)-Pd(2 μm) composite membrane obtained by depositing palladium by electroless plating onto a vanadium disc. At 400 °C the hydrogen permeance was $1.8 \cdot 10^{-3}$ mol m^{-2} s^{-1} Pa$^{-0.5}$. In order to minimize the cost of the membrane, Viano et al. [68] replaced the Pd layer at the permeate side with nickel. The flux of the asymmetric membrane composed by Pd (500nm)-V(200 μm)-Ni (150 nm) was 65% of that of a Pd-V-Pd symmetric membrane. On the other hand, Oh et al. [69] showed that addition of yttrium (0.2 at%) to a $V_{85}Ni_{15}$ 500 μm thick layer enhanced the stability of the membrane at 480 °C. The permeability of the $V_{85}Ni_{15}$ layer decreased from $2.4 \cdot 10^{-7}$ to $1.4 \cdot 10^{-7}$ mol m^{-1} s^{-1} Pa$^{-0.5}$ after 290 h, while the doped layer with yttrium showed a smaller decline, from $2.0 \cdot 10^{-7}$ to $1.65 \cdot 10^{-7}$ mol m^{-1} s^{-1} Pa$^{-0.5}$.

Watanabe and co-workers improved the embrittlement resistance as well as the hydrogen permeation flux of niobium by alloying it with 5 mol% of W or Ru [70]. Paglieri et al. prepared a ternary (Ni-Nb-Zr) and quaternary (Ni-Nb-Zr-Ta) alloy membranes by planar flow casting, which were coated with 500 nm of palladium by PVD [71]. The thickness of the disk-shaped membranes was around 50-90 μm. Those membranes were tested employing porous stainless steel with 0.5 μm grade as mechanical support. The authors found that increasing the amount of zirconium enhanced the hydrogen permeation flux, while the embrittlement resistance was reduced as well as the thermal stability. When tantalum is added, the thermal stability was improved at the expense of a decrease in permeability. The higher permeability ($1.4 \cdot 10^{-8}$ mol m^{-1} s^{-1} Pa$^{-0.5}$) was obtained for $(Ni_{0.6}Nb_{0.4})_{0.7}Zr_{0.3}$ alloy at 450 °C.

2.1.5. Attrition resistant membrane

The durability of the membranes in membrane reactors could be compromised by their contact with catalyst particles. This could even be more stringent when the membranes are integrated in a fluidized bed membrane reactor, as the surface of the selective layer is directly exposed to particles in continuous movement. While very long-term tests should be carried out to assure the stability of the membranes under such conditions, a possible solution to circumvent or decrease erosion problems is to reduce the exposed surface of the membrane. An option for minimization of the membrane area exposed to the fluidized suspension is the use of Cermet membranes, since the exposed area is about 50% of conventional thin-film membranes. Another possibility to protect the surface from contact with catalyst particles is by covering it with a nanoporous ceramic layer, such as in the pore-filled type membranes prepared by Pacheco Tanaka et al. [10]. A comparison of the permeation characteristics of conventional, cermet and pore-filled membranes are reported in Table 2.8.

2.1.5.1. Dual-phase ceramic-metallic membranes (cermet)

Ceramic-metallic composite membranes or more commonly called Cermet membranes for hydrogen separation are increasingly attracting the interest of researchers. In 1994 Iwahara et al. [72] reported proton conductivity of $BaCeO_{3-\delta}$ layers and suggested the possibility to be

used as hydrogen selective membranes, since these layers exhibit the highest reported proton conductivity reported so far [73]. However, their electronic conductivity is insufficient for achieving high hydrogen permeation rates without applying voltage, as reported by Guan et al. [74], because the measured electronic conductivity of $BaCe_{0.95}Y_{0.05}O_{3-\delta}$ (BCY) at 700 °C was $2.1 \cdot 10^{-3}$ Ω^{-1} m^{-1}, which is 3 times smaller than the protonic conductivity. The same authors found that $SrCeO_{3-\delta}$ has a lower conductivity than the $BaCeO_{3-\delta}$ material [75]. Although the conductivity was improved by doping it with larger contents of yttrium, they found that the electronic conductivity was too low for real applications as a hydrogen separation system. Some years later, they increased the electronic conductivity of $BaCe_{0.8}Y_{0.2}O_{3-\delta}$ (BCY) by dispersing a metallic powder in a ceramic matrix, creating a novel metallic-ceramic matrix [76]. The authors suggested that the dispersion of metal helps the hydrogen permeability by creating an additional transport path for hydrogen. When 40% of the hydrogen transport metal was dispersed in the ceramic (BCY) matrix, the hydrogen permeation flux was enhanced. However, higher permeation rates were obtained when the perovskite structure was replaced with Al_2O_3 or ZrO_2. A 40 µm-thick membrane consisting of a mechanically stable ceramic mixed with 50 vol% of a hydrogen transport metal (the authors did not specify the employed materials), exhibited a hydrogen flux of 0.108 mol m^{-2} s^{-1} at 900 °C [77]. The same permeation rate was obtained with a 22 µm thick Pd (50 vol%)-YSZ at 900 °C in the presence of pure hydrogen at atmospheric pressure [78]. The interconnected ceramic/metal networks (see Figure 2.4) were prepared by pressing powders into a disc-shape membrane with different thicknesses (22-200 µm). The authors observed an inverse linearity of the hydrogen flux with the membrane thickness, which suggests that bulk diffusion was the limiting step for the membrane permeation.
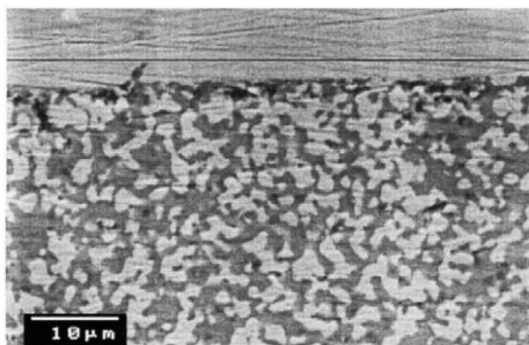
Figure 2.4. Cross section SEM image of Pd-YSZ membrane after exposure to H_2S at 600 °C [78].

In 2011 Hoon Park et al. [79] employed Ta (60 vol%) as metallic phase dispersed in YSZ since tantalum is cheaper than noble metals like Ag, Au, Pd or Pt and exhibit higher permeation rates. However, a critical point of this metal is its instability under oxygen and hydrogen containing atmospheres, which react at low temperatures with the membrane decreasing its permeation properties. Tantalum hydride was formed during permeation tests

resulting in membrane failure. Before failure, the measured hydrogen flux was $8.93 \cdot 10^{-3}$ mol $m^{-2} s^{-1}$ at 500 °C in the presence of pure hydrogen (feed pressure 2 bar) for a membrane with a thickness of 500 μm.

In 2011 other research groups reported the preparation of cermet membranes dispersing Pd in fluorite type GDC [80], where GCD stands for Gd-doped ceria and is also known as GCO (gadolinium cerium oxide) and perovskite type $CaZr_{0.9}Y_{0.1}O_{3-\delta}$ (CZY) [81]. Proton conducting CZY was chosen, since it is thermodynamically stable in CO_2-containing atmospheres and mixed with electron and hydrogen conducting palladium powder. The highest hydrogen flux, 0.017 mol $m^{-2} s^{-1}$, was obtained for a 500 μm thick 50 vol% Pd-50 vol% CZY membrane at 900 °C using a feed gas with 80% hydrogen. This value is higher than cermet membranes based on Al_2O_3 and YSZ as these showed lower hydrogen fluxes at the same operating conditions. The hydrogen flux for Pd/Al_2O_3 and Pd/YSZ membranes were $1.41 \cdot 10^{-2}$ and $8.18 \cdot 10^{-3}$ mol $m^{-2} s^{-1}$, respectively. In 2013 the same authors prepared a thinner (218 μm) Pd/YSZ membranes for water splitting [82], showing a higher hydrogen flux (0.024 mol $m^{-2} s^{-1}$) from H_2-H_2O mixture with a steam partial pressure below 1 atm. Although the thermal stability is enhanced and the YSZ does not form the corresponding oxysulfide in H_2S environment, the Pd metal reacts easily in the presence of 300 ppm H_2S forming Pd_4S and decreasing the hydrogen permeation flux. Luckily, when introducing steam (even as sweep gas), it reacts with Pd_4S producing SO_2, which "regenerates" the Pd so that the permeation flux can be recovered.

Results obtained with Pd/CZY membranes [81] where improved when the perovskite phase was replaced by GDC ($Ce_{0.8}Gd_{0.2}O_{2-\delta}$) [80]. Pd/GDC operating under the same conditions as Pd/CZY presented a hydrogen flux of 0.041 mol $m^{-2} s^{-1}$.

As was explained before, the proton conductivity of BCY is one of the highest reported. Nevertheless, degradation of this material occurs in the presence of CO_2 and H_2O forming cerium oxide and barium carbonate [83], as well as $BaCeO_3$ peroskite [84]. The chemical stability of yttrium-doped barium zirconate is larger than BCY, but their electron conductivity is lower due to the presence of zirconium [85]. An increase in the electron conduction rate is achieved by dispersing 40 vol% nickel in the BZCY ($Ba(Zr_{0.1}Ce_{0.7}Y_{0.2})O_{3-\delta}$) phase [86,87]. A low hydrogen permeation ($4.2 \cdot 10^{-4}$ mol $m^{-2} s^{-1}$) was achieved at 900 °C for a 1 mm thick Ni-BZCY membrane [86]. For a thinner membrane (266 μm) the hydrogen flux was increased up to $6.0 \cdot 10^{-3}$ mol $m^{-2} s^{-1}$ at 900 °C when 100% H_2 was fed [87]. The hydrogen flux decreases in the presence of CO_2. In particular, when using mixtures containing 10-30% of CO_2 and 40% of hydrogen, an initial decrease in the hydrogen flux was observed followed by a constant flux for the remaining 80 h. However, once the CO_2 is removed from the feed gas, the initial hydrogen flux is recovered for Ni-BCZY. In contrast, unstable Ni-BCY presented a continuous decrease in the flux in the presence of 20-30% CO_2 [88]. The

advantage of doping Ni-BCZ with rare earth metals such as erbium and samarium was reported in 2015 [89]. The chemical stability against CO_2 was improved when erbium was used as a dopant. The chemical stability in the presence of a pure CO_2 atmosphere of several perosvkites based on $BaCeO_3$ is shown in Figure 2.5. The decomposition of $BaCeO_3$ is promoted at higher temperatures, while substitution of Ce with samarium and erbium enhances the chemical stability. On the other hand, introduction of zirconium to $BaCeO_3$, $BaCe_{0.8}Er_{0.2}O_{3-\delta}$ and $BaCe_{0.8}Sm_{0.2}O_{3-\delta}$, increases the stability for all cases, since the temperature at which barium carbonate started to be formed was increased to 550 °C. As shown in Figure 2.5, the chemical stability of $Ni-BaCe_{0.5}Zr_{0.3}M_{0.2}O_{3-\delta}$ (M = Sm, Er) in the range of 550-670 °C is better than Ni-BCZ, and these cermets can be applied for hydrogen separation from methane steam reforming.
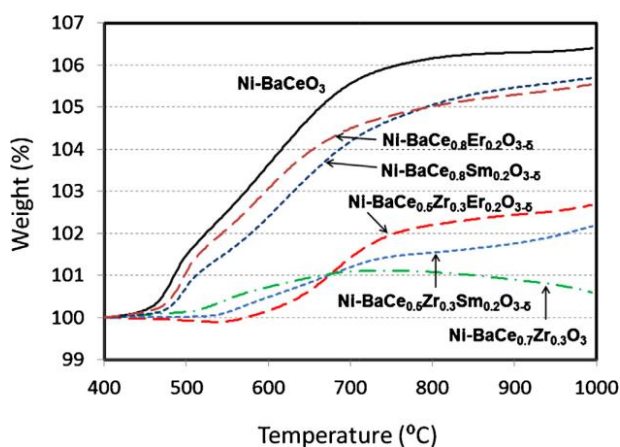

Figure 2.5. Weight change of reduced $Ni-BaCeO_3$, $Ni-BaCe_{0.7}Zr_{0.3}O_3$, $Ni-BaCe_{0.8}M_{0.2}O_{3-\delta}$ and $Ni-BaCe_{0.5}Zr_{0.3}M_{0.2}O_{3-\delta}$ (M=Sm, Er) cermet powders with increasing temperature in pure CO_2 atmosphere [89].

As the hydrogen flux is increased by preparing thin membranes on asymmetric supports, Zhu et al. [90] prepared a 30 µm Ni-BZCY on top of a porous support made of $BZCY(Ba(Zr_{0.1}Ce_{0.7}Y_{0.2})O_{3-\delta})$. However, the obtained result was not as good as expected. At 900 °C with 80% of hydrogen in the feed gas, the permeation flux was only $2.5 \cdot 10^{-3}$ mol s^{-1} m^{-2}, which is one order of magnitude smaller than for Pd/GDC reported by Jeon et al. [80]. Suggested reasons for the observed low flux are: i) surface exchange becomes the rate limiting step as the thickness of the membrane decreases and ii) too low porosity of the porous substrate. Self-supported cermet with a similar composition (50 wt% Ni-50 wt% $BaCe_{0.9}Y_{0.1}O_{3-\delta}$) was studied by Kim et al. [91], who found for a thicker membrane (230 µm) a higher hydrogen permeation flux ($5.88 \cdot 10^{-3}$ mol s^{-1} m^{-2}) than supported Ni-BZCY even at a lower temperature (800 °C) when feeding pure hydrogen. In 2013, a supported Ni-BZCYYb $(BaZr_{0.1}Ce_{0.7}Y_{0.1}Yb_{0.1}O_{3-\delta})$ was developed by Mingfei Liu et al. [92]. Incorporation of Yb enhances the ionic conductivity while maintaining the thermal and chemical stability. The

highest hydrogen permeation flux, $8.33 \cdot 10^{-3}$ mol m^{-2} s^{-1}, was measured at 900 °C when pure hydrogen and nitrogen were used on the feed and permeate side, respectively. During 2014 and 2015, many research groups investigated other types of cermets such as Ni-BZPY [93], Ni-BCTZ [94] and Ni-LCD [95], which showed stability in the presence of CO_2 and H_2O, while the hydrogen fluxes were below $2 \cdot 10^{-3}$ mol m^{-2} s^{-1} at 800 °C.

In 2014, a supported 18 µm thick 60 vol% Pd/YSZ cermet membrane supported on an alumina porous substrate was reported by Balachandran et al. [96]. The dense cermet layer was supported on a porous disk made by the paste-painting method (see Figure 2.6). The permeated hydrogen flux increased from 0.193 mol m^{-2} s^{-1} at 400 °C to 0.387 mol m^{-2} s^{-1} at 900 °C for a feed gas containing 90% H_2 (in helium) at ambient pressure and nitrogen as sweep gas. Bulk diffusion is the rate limiting step for this thin dense membrane. A long-term test was carried out for four months for a thicker membrane (25 µm) in the temperature range of 500-600 °C. The hydrogen flux was stable as the same hydrogen flux was measured at 500 °C initially and at the end of test (0.07 mol m^{-2} s^{-1}). Moreover, the Pd/YSZ cermet membrane was chemically stable in the presence of syngas at high pressure. The resistance to H_2S was also determined for an even thicker membrane (200 µm) at 900 °C in the presence of 400 ppm H_2S and 79.8% H_2. In the first hours a decrease in the hydrogen flux was observed, however, the permeated flux reached a plateau that was maintained for more than 120 h. This underlines that the Pd/YSZ cermet membrane is an interesting membrane for hydrogen production systems.
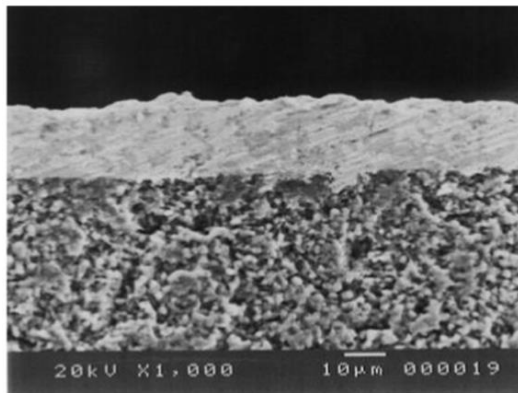
Figure 2.6. Cross section SEM image of a cermet membrane (top part) on a porous alumina support (bottom part) [96].

Myoung-Jin Lee et al. [97] reported a novel cermet membrane composed of $Ti_4Cr_3Nb_3O_2$ with 50 wt% of PdAg. Niobium oxide was added due to the catalytic properties for ionization of hydrogen molecules. The measured permeability of this mixture was $1 \cdot 10^{-4}$ mol m^{-1} s^{-1} Pa$^{-0.5}$ at 400 °C and 300 kPa of pressure difference using a planar membrane of 1.2 mm thick.

Cermet membranes are not only applied for the separation of hydrogen from gas mixtures such as syngas, but they can also be applied in membrane reactors for other applications such as water splitting, as reported in the literature [98].

2.1.5.2. *Pore-filled type membranes*

The principle of hydrogen permeation in pore-filled membranes is similar to that of cermet membranes: a mixed ceramic/metal membrane is produced and used for the separation. In cermet membranes powders of both materials are mixed and pressed before sintering. However, as the name implies, in pore-filled membranes the pores of a ceramic phase are filled with the metallic phase. The employed amount of metallic phase is only a fraction in comparison with cermet membranes and much less than conventional in thin film membranes. Moreover, the deposition of a porous ceramic layer on top of a filled mesoporous layer avoids exposure of the selective material to the external environment, such as in fluidized-bed membrane reactors.

The first reported pore-filled type membrane was for oxygen perm-selective separation, as discussed by Kim et al. [99]. Before the deposition of palladium, an YSZ layer was obtained with a dip-coating method on top of an α-Al$_2$O$_3$ porous support, having 5 μm thick layer after being dried at 40 °C and relative humidity of 40-50% followed by calcination at 1000 °C for 3 h. Palladium was introduced into the 100 nm pore-sized YSZ layer by a reservoir method. Palladium acetate was dissolved in a HCl-acetone mixture followed by one day drying and subsequent calcination at 500 °C for 2 h under hydrogen, in order to reduce Pd^{2+} into Pd^0. The remaining pores were filled with YSZ by CVD employing ZrCl$_4$ and YCl$_3$ as metal precursors. The deposition was performed in the presence of oxygen in order to form the desired metal oxide (Y$_2$O$_3$-ZrO$_2$) at 1000 °C. The prepared membrane was used for oxygen separation, but the presence of palladium suggested the possibility to use the same membrane as a hydrogen separation membrane.

Pacheco Tanaka and co-workers from AIST (National Institute of Advanced Industrial Science and Technology, Japan) [10] prepared pore-filled membranes for hydrogen separation introducing palladium in a thin nanoporous γ-Al$_2$O$_3$ layer deposited on top of a tubular porous α-alumina support by vacuum-assisted dip-coating of a boehmite sol containing PVA and PEG. The calcination was performed at 600 °C for 3 h. Palladium seeds were introduced in the 5 μm thick γ-Al$_2$O$_3$ layer by dipping into a palladium acetate dissolved in chloroform followed by reduction (Pd^{2+}→Pd^0) in hydrazine. Afterward, a ceramic protective layer (γ-Al$_2$O$_3$) was deposited on top of the previous Pd-activated ceramic layer using the same approach. During the cool-down step after calcination, a hydrogen stream was introduced to reduce possible oxidized palladium. Finally, the activated Pd seeds were grown by vacuum-assisted ELP. A schematic representation of this membrane configuration is

represented in Figure 2.7. Reduction of palladium grains to nm size suppresses α-β transition and the membrane can work at lower temperatures [100,101]. Indeed, these membranes were tested in the temperature range from 50-300 °C without failure of the membrane and the best results were obtained at 300 °C and a pressure difference of 400 kPa, yielding a hydrogen flux of ~0.55 mol m^{-2} s^{-1} and a H_2/N_2 perm-selectivity of 1000 [10]. Due to the difference in thermal expansion coefficient between alumina and Pd (Table 2.2) the permeation test at temperatures above 400 °C resulted in membrane failure. To avoid this problem, the mesoporous γ-Al$_2$O$_3$ layer was replaced by an YSZ/γ-Al$_2$O$_3$ layer in order to minimize the difference in thermal expansion with the metal [16]. The effect of the amount of YSZ was studied and it was observed that the nitrogen flux was increased when the amount of YSZ was increased. The measured hydrogen flux at 500 °C and a pressure difference of 400 kPa was ~0.616 mol m^{-2} s^{-1}, which was half of the flux achieved for a conventional supported thin film with the same membrane thickness (3.23 μm). The ideal H_2/N_2 perm-selectivity was 350. Since the amount of palladium is only a fraction of that employed for films and YSZ-Al$_2$O$_3$ does not transport hydrogen, the obtained results are as expected. Long-term tests were performed for 200 h in the temperature range of 500-600 °C. A gradual loss in the hydrogen flux was observed during the first 100 h at 500 °C, then the temperature was increased to 600° C, showing an initial hydrogen flux increases related to the temperature effect. Again, the hydrogen flux decreased during the first 20 h at 600 °C. Afterward a stable permeated hydrogen flux was maintained for longer times. The preparation of this type of membranes was patented in 2006 [102].
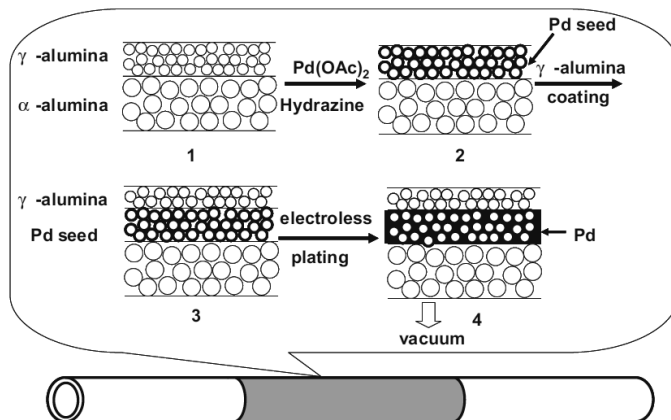
Figure 2.7. Schematic representation of pore-filled type membranes performed by Pacheco Tanaka et al. [107].

A pore-filled type membrane was integrated in a membrane reactor for hydrogen production by dehydrogenation of methyl cyclohexane producing toluene and hydrogen [103]. Platinum supported onto alumina particles was used as catalyst, mixed with sand and introduced into the inner part of the tube, where the palladium was located (see Figure 2.8). The reaction was

performed in the temperature range below the critical temperature for α-β phase transition, 150-325 °C without formation of coke onto the catalyst bed. The introduction of the membrane into the reactor improved the conversion of the reaction to 60-80% in a temperature range of 150-225 °C, while at higher temperatures complete conversion in both systems was achieved, where the effect of the membrane was only visible in the recovery of the hydrogen, which increased as the temperature increased. The stability of membrane was proven for 600 h confirming constant membrane efficiency (i.e. flux and selectivity).
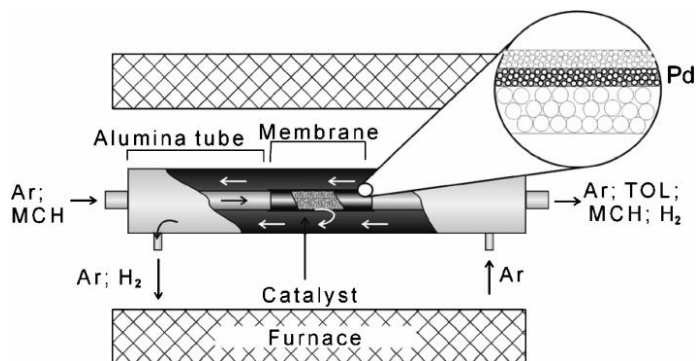
Figure 2.8. Schematic representation of a pore-filled type membrane integrated in a packed-bed membrane reactor for the dehydrogenation of methylcyclohexane into toluene and hydrogen.

The use of YSZ guarantees better thermal properties than palladium membranes as was reported for a pore-fill-type membrane prepared with an YSZ porous support and coated with a mesoporous layer of the same material [104]. The hydrogen selectivity was improved by adding a surfactant (Triton® X-100) to the plating solution in order to decrease the surface tension. The hydrogen flux at 600 °C and 50 kPa of pressure difference increased from 0.956 mol m^{-2} s^{-1} (without addition of the surfactant) to 1.368 mol m^{-2} s^{-1} when the concentration of the surfactant in the resulting plating solution was 0.05 wt%. The H$_2$/N$_2$ ideal perm-selectivity for a membrane prepared without addition of the surfactant was 1200, while for the membrane with 0.05 wt% of surfactant in the plating solution the resulting ideal perm-selectivity was 20000.

Some years later (2012) the research group of AIST reported a study where hydrogen permeation of thin-film and pore-filled type membranes were compared in the presence of steam and CO$_2$ [105]. A thin palladium membrane was deposited by chemical vapor deposition onto an α-Al$_2$O$_3$ porous support, while pore-filled type membranes were produced in a similar way as reported earlier [10]. The thickness of the deposited film by CVD was around 1-2 μm, while the embedded Pd on γ-Al$_2$O$_3$ layer was close to 10 μm thick. The filled pores presented a distribution in pore size of about 1-9 nm and a surface area of 213 m^2 g^{-1} after calcination at 600 °C, which means that the Pd particle size was in the nano-range. In the presence of pure hydrogen, the permeance of the conventional thin-film

membrane was a factor three larger than the pore-filled type membrane, $1.3 \cdot 10^{-3}$ mol m^{-2} s^{-1} Pa$^{-0.5}$ for the thin film and $4.1 \cdot 10^{-4}$ mol m^{-2} s^{-1} Pa$^{-0.5}$ for the pore-filled membrane at 300 °C and a pressure difference of 200 kPa. The hydrogen permeation rates decreased for both membranes when CO_2 was introduced into the gas stream at 300 °C. However, the CO_2 poisoning was more pronounced for the conventional thin-film membrane than for pore-filled membrane. Moreover, the hydrogen flux was completely recovered when CO_2 was removed for the pore-filled membrane, whereas only 80% of the initial hydrogen flux was recovered for the CVD membrane. The introduction of steam decreases the initial hydrogen flux for both membrane types, but the flux was successfully recovered after exposure to steam for both membranes. Concerning the perm-selectivity, for the conventional membrane the initial H_2/N_2 separation factor was ~883 (re-calculated values explained at Table 2.8), which was decreased to ~447 and ~409 after exposure to CO_2 and steam, respectively. For the pore-filled membrane, the hydrogen flux before and after exposure to CO_2 and H_2O remain the same, ~0,095 mol m^{-2} s^{-1} at 200 kPa ($4.75 \cdot 10^{-7}$ mol m^{-2} s^{-1} Pa^{-1}) and an initial selectivity of ~176. No changes were reported by the authors for the pore-filled membrane. However, re-calculated selectivities after exposure to CO_2 and steam were ~206 and ~12, respectively.

A similar concept was reported by Nair et al. [106] for a hollow fiber configuration. Three types of configurations were reported, the so-called "encapsulated Pd (M-E)", "Pd encapsulated nanopore (M-EN)" and "Pd nanopore (M-N)" membranes. All these types of membranes were supported on a α-Al$_2$O$_3$ hollow fiber followed by boehmite slip casting. For the Pd encapsulated case, the γ-alumina surface was activated with Pd followed by growth of a thin Pd layer by ELP. Subsequently, the surface was coated with another γ-alumina layer (Figure 2.9a). The second type of membrane, "Pd encapsulated nanopore", can be easily prepared by filling the resulted pores of the "encapsulated Pd membrane" with palladium using ELP, connected with the first deposited Pd layer as shown in Figure 2.9b. The equivalent palladium thickness was 1.6 μm, but the amount of deposited palladium was relatively low in comparison with convectional supported membranes.
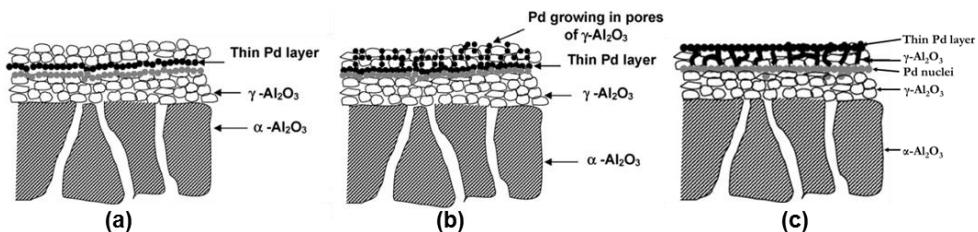

Figure 2.9. Schematic representation of encapsulated Pd (a), Pd encapsulated nanopore (b) and Pd nanopore (c) [106].

The other membrane configuration, "Pd-nanopore" (Figure 2.9c), differs from the other two configurations in that not only pores are filled, but also a 2 μm thick Pd layer is grown on top of the alumina layer. Permeation tests were performed at 370 °C and a feed side pressure of 300 kPa, observing a higher hydrogen flux and perm-selectivity for the encapsulated nanopore membranes. Indeed, the measured hydrogen flux (and selectivity) for Pd-encapsulated nanopore, Pd encapsulate and Pd-nanopore membranes were ~0.25 mol m^{-2} s^{-1} (H$_2$/N$_2$ = 8750), ~0.26 mol m^{-2} s^{-1} (H$_2$/N$_2$ = 3800), and ~0.13 mol m^{-2} s^{-1} (H$_2$/N$_2$ = 550), respectively. Thermal stability was confirmed at the same temperature (370 °C) for 150-200 h, resulting in an increase of the hydrogen flux at lower pressures for the encapsulated nanopore membrane, 0.67 mol m^{-2} s^{-1}, while the perm-selectivity decreased to 160. The selectivity of the nanopore membrane was reduced to half of the calculated value before thermal aging, while the hydrogen flux remained close to 0.1 mol m^{-2} s^{-1}. The largest decrease in terms of selectivity was for the encapsulated membrane, 10 times lower (380) with a hydrogen flux increase from 0.26 to 0.5 mol m^{-2} s^{-1}. The low selectivity of these membranes was associated to thermal stress caused by the discontinuities between alumina and palladium due to differences in thermal expansion, as for the pore-filled membranes prepared by Pacheco Tanaka and co-workers [10]. The same group also showed similar results for a nanopore type membrane [107], where the hydrogen flux and ideal perm-selectivity at 500 °C and a pressure difference of 4 bar were 0.56 mol m^{-2} s^{-1} and 6600, respectively.

Another way to prepare pore-filled type membranes was patented in 2009 by Wakuy et al [108]. The authors first deposited a thin mesoporous ceramic layer followed by activation of the surface by filling the pores with Pd particles. Afterward, the deposited ceramic layer with palladium seeds was removed leaving a portion of the deposited Pd into the original porous surface. Again, a ceramic layer was deposited as a protective layer followed by electroless plating to grow palladium and completely fill the pores.

The Ohio State University patented in 2010 a pore-filled type membrane employing ZrO$_2$ as an intermediate layer between the support and palladium layer [109]. They suggested deposition of ZrO$_2$/Pd nano-composite on top of a macroporous support, consisting of Al$_2$O$_3$ or ZrO$_2$, followed by deposition of a thin Pd (or Pd alloy) layer by ELP with a thickness ranging from 10 nm to 1 μm. The ZrO$_2$/Pd (30/70 vol%) and the macroporous layers were also deposited on top of the Pd or Pd-alloy layer to protect the hydrogen selective metals. There is no chemical adhesion between Pd and ZrO$_2$, but the adherence of ZrO$_2$ with the macroporous layer is easier due to their chemical affinity. A membrane supported on top of γ-alumina with a 120 nm Pd/ZrO$_2$ composite layer was covered with 215 nm Pd and tested in the presence of pure hydrogen at 200, 260 and 320 °C. The measured fluxes were 0.04, 0.1 and 0.25 mol m^{-2} s^{-1} respectively, with a pressure difference of 2 bar across the feed and permeate sides.

The most recent reported study on pore-filled type membranes was performed by Yogo and co-workers [110]. They deposited directly Pd into α-Al_2O_3 porous tubes by dip-coating with an average pore size of 100 nm using a Pd-gel containing $PdCl_2$ as palladium carrier in HCl and agarose L polymer as binder. An ice bath was used to cool the Pd-gel onto the porous support followed by reduction in the presence of hydrazine. After cleaning, 10 min of electroless plating was performed in order to grow the Pd seeds. Before carrying out a loner ELP, the Pd-gel was removed by calcination of the sample at 850 °C. The palladium layer obtained inside the porous support was around 8-10 μm at 10 μm depth. The amount of palladium used for the pore-filled membranes was 34% of that required for a supported thin-film membrane with the same thickness. The hydrogen permeance at 500 °C and 150 kPa of pressure difference was $1.2 \cdot 10^{-6}$ mol m^{-2} s^{-1} Pa^{-1}, and stable for 150 h at different temperatures (200-500 °C) in the presence of a gas mixture H_2/N_2. The ideal perm-selectivity of this membrane was above 10000.

In conclusion, pore-filled type membranes represent an interesting alternative when membranes are integrated in a fluidized bed membrane reactor to avoid abrasion problems of the membrane surface due to the scouring action of the fluidized catalyst particles.

Table 2.8. Permeation data of some conventional supported membranes, cermet membranes and pore-filled membranes.

Membrane materials										
Porous support/ Inter-diffusion layer	Selective layer	Preparation method	Selective layer thickness (μm)	T (°C)	H_2 flux (mol m^{-2} s^{-1})	Pressure difference (kPa)	n	Permeance H_2 (mol m^{-2} s^{-1} Pa^{-n})	H_2/N_2 Selectivity	Ref.
PSS	$Pd_{77}Ag_{23}$ (+ TT air)	PVD-MS	2.8	400	18.43	2500	0.5	$1.46 \cdot 10^{-2}$	2900	[26]
Self-supported	$V_{0.9}Fe_{0.05}Al_{0.05}$	Arc melting	400	400	0.170	700	0.5	$3 \cdot 10^{-4}$	-	[67]
Self-supported	Pd-V-Pd	ELP	2-100-2	400	1.12	600	0.5	$1.8 \cdot 10^{-3}$	∞	[68]
PSS	$(Ni_{0.6}Nb_{0.4})_{0.7}Zr_{0.3}$	Flow casting	50-90	450	0.155	627	0.5	$1.4 \cdot 10^{-8}$	-	[71]
Self-supported	60 vol% Ta-YSZ	Uniaxial Pressed	500	500	$8.93 \cdot 10^{-3}$	<200	-	-	-	[79]
Self-supported	50 vol% Pd-GDC	Isostatically pressed	282	900	0.041	<100	0.5	$1.74 \cdot 10^{-4}$	-	[80]
Self-supported	50 vol% Pd-CZY	Pressed	500	900	0.017	<100	0.5	$6.2 \cdot 10^{-5}$	-	[81]
Self-supported	50 vol% Pd-YSZ	Isostatically pressed	218	900	0.024	<100	-	-	-	[82]
Self-supported	40 vol% Ni-BZCY $(Ba(Zr_{0.1}Ce_{0.7}Y_{0.2})O_{3-\delta})$	Uniaxially pressed	1000	900	$4.2 \cdot 10^{-4}$	-	-	-	-	[86]
Self-supported	40 vol% Ni-BZCY $(Ba(Zr_{0.1}Ce_{0.7}Y_{0.2})O_{3-\delta})$	Uniaxially pressed	266	900	$6 \cdot 10^{-3}$	<100	0.5	$2.17 \cdot 10^{-5}$	-	[87]
BZCY	40 vol% Ni-BZCY $(Ba(Zr_{0.1}Ce_{0.7}Y_{0.2})O_{3-\delta})$	Co-pressed	30	900	$2.4 \cdot 10^{-3}$	-	-	-	-	[90]
Self-supported	40 vol% Ni-BCY $(Ba(Ce_{0.9}Y_{0.1})O_{3-\delta})$	Cold isostatic pressing	230	800	$5.88 \cdot 10^{-3}$	-	-	-	-	[91]
40 vol%Ni- BZCYYb	40 vol% Ni-BZCYYb $(Ba(Zr_{0.1}Ce_{0.7}Y_{0.1}Yb_{0.1})O_{3-\delta})$	Particle suspension coating	44	900	$8.33 \cdot 10^{-3}$	-	-	-	-	[92]
40 vol%Ni-BCTb	40 vol% Ni-BCTb $(BaCe_{0.95}Tb_{0.05}O_{3-\delta})$	Uniaxial pressing	90	850	0.068	<100	-	-	-	[94]
α-Al2O3	60 vol% Pd-YSZ	Paste-painting	18	900	0.387	<100	-	-	-	[96]
α-Al2O3	Pd/γ-Al2O3	Pore-filled	4-5	300	0.55	400	-	-	1000	[10]
α-Al2O3	Pd/YSZ-γ-Al2O3	Pore-filled	3.23	500	0.616	500	-	-	350	[16]
α-Al2O3	Pd/γ-Al2O3	CVD	1-2	300	0.265	200	0.5	$1.3 \cdot 10^{-3}$	883[a]	[105]
α-Al2O3	Pd/γ-Al2O3	Pore-filled	10	300	0.095	200	0.5	$4.05 \cdot 10^{-4}$	176[b]	[105]
α-Al2O3	Pd-encapsulated (M-E)	Pore-filled	1.1	370	0.26	275	-	-	3800	[106]
α-Al2O3	Pd-encapsulated nanopore(M-EN)	Pore-filled	1.6	370	0.25	275	-	-	8750	[106]

Pd-based membranes: State-of-art | 45

α-Al$_2$O$_3$	Pd-nanopore(M-N)	2.6	370	0.13	275	-	-	550	[106]
α-Al$_2$O$_3$	Pd-nanopore	4	500	0.56	410	-	-	6600	[107]
α-Al$_2$O$_3$	70%Pd-30%ZrO$_2$	~0.215	320	0.25	200	-	-	-	[109]
α-Al$_2$O$_3$	Pd/γ-Al$_2$O$_3$	8-10	500		50	1	$1.20 \cdot 10^{-6}$	10000	[110]

[a]Recalculated value. N$_2$ permeance $1.5 \cdot 10^{-9}$ mol m^{-2} s^{-1} Pa^{-1} (Table 1 of reference). Hydrogen flux at 200 kPa of pressure difference: ~0.265 mol m^{-2} s^{-1} (Figure 3a of reference). Then hydrogen permeance is $1.32 \cdot 10^{-6}$ mol m^{-2} s^{-1} Pa^{-1}; [b]Recalculated value. N$_2$ permeance: $2.7 \cdot 10^{-9}$ mol m^{-2} s^{-1} Pa^{-1} (Table 1 of reference). Hydrogen flux at 200 kPa of pressure difference: ~0.095 mol m^{-2} s^{-1}. Then hydrogen permeance is $4.75 \cdot 10^{-7}$ mol m^{-2} s^{-1} Pa^{-1}.

2.2.   Conclusions

An overview of the latest achievements in the development of different types of integrated H_2 perm-selective membranes for the production of H_2 has been given in this chapter. Requirements that need to be fulfilled by H_2 perm-selective membranes for its integration in packed or fluidized bed membrane reactors are discussed, as well as the selection of the materials for the support and interdiffusion layer. Depending on the operation conditions, stainless steel (316L) and ZrO_2/YSZ as a support and diffusion barrier are preferred for applications at around 400-500 °C. For applications at higher operating temperatures supports with higher stability are required, such as Hastelloy X and Ni-based alloys (Inconel).

Concerning the material for the selective layer, Pd-based membranes represent the best choice in comparison with non-palladium alloys (V, Nb, Ta), yielding higher permeabilities than pure Pd. However, their tendency to embrittlement is also high. PdAg membranes exhibit a high flux, PdAu membranes a high sulfur resistance, whereas PdAgAu membranes combine both properties. However, for high-temperature applications such as methane steam reforming, alloys like PdRu and PdPt are required for improved thermal stability at temperatures above 500 °C. Combination of all these elements to create a membrane which could work under extreme conditions is interesting. However, the possible techniques for their preparation is limited to PVD, due to the complexity to prepare these mixed membranes with ELP.

Integration of supported membranes in fluidized bed membrane reactors require membranes with improved abrasion resistance because of the scouring action of the catalyst particles which may deteriorate the membrane properties dramatically. Cermet membranes may represent an interesting option, since part of their surface do not suffer from erosion since they are much harder than the catalyst particles. However, the hydrogen selective material is not completely covered. For this reason, pore-filled membranes are suggested as the best alternative to avoid membrane abrasion. In Chapter 4 the preparation and experimental results of this type of membranes are presented. For their preparation, first the mesoporous layer where palladium is going to be incorporated (and the protective layer) have been studied in order to control the thickness and pore size of the layers, which is presented in Chapter 3. The diffusion mechanism of these layers and their physico-chemical properties have also been studied in detail.

Bibliography

[1]   Energy Efficiency and Renewable Energy Report of the DOE Workshop on Hydrogen Separations and Purification, Arlinton, VA, USA, 2004.

[2]   S. Yun, S. Ted Oyama, Correlations in palladium membranes for hydrogen separation: A review, J. Memb. Sci. 375 (2011) 28–45. doi:10.1016/j.memsci.2011.03.057.

[3]   A. Sieverts, W. Krumbhaar, Ülber die löslichkein von gasen in metallen und legierungen sieverts, Berichte Der Dtsch. Chem. Gesellschaft. 43 (1910) 893–900.

[4]   W.D. Callister, D.G. Rethwisch, Thermal Properties, in: Fundam. Mater. Sci. Eng. An Integr. Approach, 3rd ed., Jonh Wiley ans Sons, 2007: pp. 713–729.

[5]   S.-K. Ryi, H.-S. Ahn, J.-S. Park, D.-W. Kim, Pd–Cu alloy membrane deposited on CeO2 modified porous nickel support for hydrogen separation, Int. J. Hydrogen Energy. 39 (2014) 4698–4703. doi:10.1016/j.ijhydene.2013.11.031.

[6]   D.R. Lide, S.R. Data, E.A. Board, G. Baysinger, S. Chemistry, C.E. Library, L.I. Berger, R.N. Goldberg, B. Division, H. V Kehiaian, K. Kuchitsu, G. Rosenblatt, D.L. Roth, D. Zwillinger, CRC Handbook of Chemistry and Physics, (n.d.).

[7]   I.P. Mardilovich, E. Engwall, Y.H. Ma, Dependence of hydrogen flux on the pore size and plating surface topology of asymmetric Pd-porous stainless steel membranes, Desalination. 144 (2002) 85–89. doi:10.1016/S0011-9164(02)00293-X.

[8]   S. Uemiya, State-of-the-Art of Supported Metal Membranes for Gas Separation, Sep. Purif. Rev. 28 (1999) 51–85. doi:10.1080/03602549909351644.

[9]   B. McCool, G. Xomeritakis, Y.. Lin, Composition control and hydrogen permeation characteristics of sputter deposited palladium–silver membranes, J. Memb. Sci. 161 (1999) 67–76. doi:10.1016/S0376-7388(99)00087-3.

[10]   D.A. Pacheco Tanaka, M.A. Tanco Llosa, T. Nagase, J. Okazaki, Y. Wakui, F. Mizukami, T.M. Suzuki, Fabrication of Hydrogen-Permeable Composite Membranes Packed with Palladium Nanoparticles, Adv. Mater. 18 (2006) 630–632. doi:10.1002/adma.200501900.

[11]   P.M. Thoen, F. Roa, J.D. Way, High flux palladium–copper composite membranes for hydrogen separations, Desalination. 193 (2006) 224–229. doi:10.1016/j.desal.2005.09.025.

[12]   R. Checchetto, N. Patel, a. Miotello, R.S. Brusa, Nanolayers on nanochannels for hydrogen purification, J. Appl. Phys. 105 (2009) 34502. doi:10.1063/1.3072673.

[13]   X.L. Pan, G.X. Xiong, S.S. Sheng, N. Stroh, H. Brunner, Thin dense Pd membranes supported on α-Al2O3 hollow fibers, Chem. Commun. (2001) 2536–2537. doi:10.1039/b108395c.

[14]   L.-Q. Wu, N. Xu, J. Shi, Novel method for preparing palladium membranes by photocatalytic deposition, AIChE J. 46 (2000) 1075–1083.

doi:10.1002/aic.690460518.

[15]   X. Li, Y. Fan, W. Jin, Y. Huang, N. Xu, Improved photocatalytic deposition of palladium membranes, J. Memb. Sci. 282 (2006) 1–6. doi:10.1016/j.memsci.2006.03.024.

[16]   D.A. Pacheco Tanaka, M.A. Llosa Tanco, J. Okazaki, Y. Wakui, F. Mizukami, T.M. Suzuki, Preparation of "pore-fill" type Pd–YSZ–γ-Al2O3 composite membrane supported on α-Al2O3 tube for hydrogen separation, J. Memb. Sci. 320 (2008) 436–441. doi:10.1016/j.memsci.2008.04.044.

[17]   J. Okazaki, T. Ikeda, D. a. P. Tanaka, M. a. L. Tanco, Y. Wakui, K. Sato, F. Mizukami, T.M. Suzuki, Strong Interaction at the Palladium/Alumina Interface of Membrane during Hydrogen Permeation at Elevated Temperature, Chem. Lett. 37 (2008) 1004–1005. doi:10.1246/cl.2008.1004.

[18]   S.N. Paglieri, K.Y. Foo, J.D. Way, J.P. Collins, D.L. Harper-Nixon, A New Preparation Technique for Pd/Alumina Membranes with Enhanced High-Temperature Stability, Ind. Eng. Chem. Res. 38 (1999) 1925–1936.

[19]   Y. Huang, R. Dittmeyer, Preparation and characterization of composite palladium membranes on sinter-metal supports with a ceramic barrier against intermetallic diffusion, J. Memb. Sci. 282 (2006) 296–310. doi:10.1016/j.memsci.2006.05.032.

[20]   H. Gharibi, M. Saadatinasab, A. Zolfaghari, Hydrogen permeability and sulfur tolerance of a novel dual membrane of PdAg/PdCu layers deposited on porous stainless steel, J. Memb. Sci. 447 (2013) 355–361. doi:10.1016/j.memsci.2013.07.037.

[21]   A. Tardini, C. Gerboni, L. Cornaglia, PdAu membranes supported on top of vacuum-assisted ZrO2-modified porous stainless steel substrates, J. Memb. Sci. 428 (2013) 1–10. doi:10.1016/j.memsci.2012.10.029.

[22]   A. Calles, D. Alique, L. Furones, Thermal stability and effect of typical water gas shift reactant composition on H 2 permeability through a Pd-YSZ-PSS composite membrane, Int. J. Hydrogen Energy. 39 (2014) 1398–1409. doi:10.1016/j.ijhydene.2013.10.168.

[23]   R. Sanz, J.A. Calles, D. Alique, L. Furones, H2 production via water gas shift in a composite Pd membrane reactor prepared by the pore-plating method, Int. J. Hydrogen Energy. 39 (2014) 4739–4748. doi:10.1016/j.ijhydene.2013.12.145.

[24]   S.-K. Ryi, S.-W. Lee, D.-K. Oh, B.-S. Seo, J.-W. Park, J.-S. Park, D.-W. Lee, Electroless plating of Pd after shielding the bottom of planar porous stainless steel for a highly stable Hydrogen selective membrane, J. Memb. Sci. (2014). doi:10.1016/j.memsci.2014.04.058.

[25]   K. Zhang, H. Gao, Z. Rui, P. Liu, Y. Li, Y.S. Lin, High-Temperature Stability of Palladium Membranes on Porous Metal Supports with Different Intermediate Layers, Ind. Eng. Chem. Res. 48 (2009) 1880–1886. doi:10.1021/ie801417w.

[26]   T. a. Peters, M. Stange, R. Bredesen, On the high pressure performance of thin

supported Pd–23%Ag membranes—Evidence of ultrahigh hydrogen flux after air treatment, J. Memb. Sci. 378 (2011) 28–34.

[27]   A.E. Lewis, H. Zhao, H. Syed, C. a. Wolden, J.D. Way, PdAu and PdAuAg composite membranes for hydrogen separation from synthetic water-gas shift streams containing hydrogen sulfide, J. Memb. Sci. 465 (2014) 167–176. doi:10.1016/j.memsci.2014.04.022.

[28]   Ø. Hatlevik, S.K. Gade, M.K. Keeling, P.M. Thoen, a. P. Davidson, J.D. Way, Palladium and palladium alloy membranes for hydrogen separation and production: History, fabrication strategies, and current performance, Sep. Purif. Technol. 73 (2010) 59–64. doi:10.1016/j.seppur.2009.10.020.

[29]   H.W. Abu El Hawa, S.N. Paglieri, C.C. Morris, A. Harale, J. Douglas Way, Identification of thermally stable Pd-alloy composite membranes for high temperature applications, J. Memb. Sci. 466 (2014) 151–160. doi:10.1016/j.memsci.2014.04.029.

[30]   G. Straczewski, J. Völler-Blumenroth, H. Beyer, P. Pfeifer, M. Steffen, I. Felden, A. Heinzel, M. Wessling, R. Dittmeyer, Development of thin palladium membranes supported on large porous 310L tubes for a steam reformer operated with gas-to-liquid fuel, Chem. Eng. Process. Process Intensif. 81 (2014) 13–23. doi:10.1016/j.cep.2014.04.002.

[31]   C.-B. Lee, S.-W. Lee, J.-S. Park, S.-K. Ryi, D.-W. Lee, K.-R. Hwang, S.-H. Kim, Ceramics used as intermetallic diffusion barriers in Pd-based composite membranes sputtered on porous nickel supports, J. Alloys Compd. 578 (2013) 425–430. doi:10.1016/j.jallcom.2013.06.007.

[32]   E. Fernandez, J.A. Medrano, J. Melendez, M. Parco, J.L. Viviente, M. van Sint Annaland, F. Gallucci, D.A. Pacheco Tanaka, Preparation and characterization of metallic supported thin Pd-Ag membranes for hydrogen separation, Chem. Eng. J. 305 (2016) 182–190.

[33]   J.A. Medrano, E. Fernandez, J. Melendez, M. Parco, D.A.P. Tanaka, M. van Sint Annaland, F. Gallucci, Pd-based metallic supported membranes: High-temperature stability and fluidized bed reactor testing, Int. J. Hydrogen Energy. (2015) 1–13. doi:10.1016/j.ijhydene.2015.10.094.

[34]   H. Zhao, K. P, J. Gu, A. Li, N. Stroh, H. Brunner, G. Xiong, Preparation of palladium composite membranes by modified electroless plating procedure, 142 (1998) 147–157.

[35]   F. Roa, J.D. Way, The effect of air exposure on palladium–copper composite membranes, Appl. Surf. Sci. 240 (2005) 85–104. doi:10.1016/j.apsusc.2004.06.023.

[36]   K. Zhang, S.K. Gade, J.D. Way, Effects of heat treatment in air on hydrogen sorption over Pd–Ag and Pd–Au membrane surfaces, J. Memb. Sci. 403–404 (2012) 78–83. doi:10.1016/j.memsci.2012.02.025.

[37]   M.E. Ayturk, E.E. Engwall, Y.H. Ma, Microstructure Analysis of the Intermetallic

Diffusion-Induced Alloy Phases in Composite Pd/Ag/Porous Stainless Steel Membranes, Ind. Eng. Chem. Res. 46 (2007) 4295–4306. doi:10.1021/ie061677j.

[38]   S.-K. Ryi, J.-S. Park, K.-R. Hwang, C.-B. Lee, S.-W. Lee, Repair of Pd-based composite membrane by polishing treatment, Int. J. Hydrogen Energy. 36 (2011) 13776–13780. doi:10.1016/j.ijhydene.2011.07.120.

[39]   M. Broglia, P. Pinacci, M. Radaelli, a. Bottino, G. Capannelli, a. Comite, G. Vanacore, M. Zani, Synthesis and characterization of Pd membranes on alumina-modified porous stainless steel supports, Desalination. 245 (2009) 508–515. doi:10.1016/j.desal.2009.01.004.

[40]   A. Li, J. R.Grace, C.J. Lim, Preparation of thin Pd-based composite membrane on planar metallic substrate, J. Memb. Sci. 298 (2007) 175–181. doi:10.1016/j.memsci.2007.04.016.

[41]   Y.-H. Chi, P.-S. Yen, M.-S. Jeng, S.-T. Ko, T.-C. Lee, Preparation of thin Pd membrane on porous stainless steel tubes modified by a two-step method, Int. J. Hydrogen Energy. 35 (2010) 6303–6310. doi:10.1016/j.ijhydene.2010.03.066.

[42]   F. Braun, A.M. Tarditi, J.B. Miller, L.M. Cornaglia, Pd-based binary and ternary alloy membranes: Morphological and perm-selective characterization in the presence of H2S, J. Memb. Sci. 450 (2014) 299–307. doi:10.1016/j.memsci.2013.09.026.

[43]   M. Chotirach, S. Tantayanon, S. Tungasmita, K. Kriausakul, Zr-based intermetallic diffusion barriers for stainless steel supported palladium membranes, J. Memb. Sci. 405–406 (2012) 92–103. doi:10.1016/j.memsci.2012.02.055.

[44]   D. Wang, J. Tong, H. Xu, Y. Matsumura, Preparation of palladium membrane over porous stainless steel tube modified with zirconium oxide, Catal. Today. 93–95 (2004) 689–693. doi:10.1016/j.cattod.2004.06.060.

[45]   H. Gao, J. Slin, Y. Li, B. Zhang, Electroless plating synthesis, characterization and permeation properties of Pd–Cu membranes supported on ZrO2 modified porous stainless steel, J. Memb. Sci. 265 (2005) 142–152. doi:10.1016/j.memsci.2005.04.050.

[46]   J. Tong, C. Su, K. Kuraoka, H. Suda, Y. Matsumura, Preparation of thin Pd membrane on CeO2-modified porous metal by a combined method of electroless plating and chemical vapor deposition, J. Memb. Sci. 269 (2006) 101–108. doi:10.1016/j.memsci.2005.06.023.

[47]   S. Samingprai, S. Tantayanon, Y.H. Ma, Chromium oxide intermetallic diffusion barrier for palladium membrane supported on porous stainless steel, J. Memb. Sci. 347 (2010) 8–16. doi:10.1016/j.memsci.2009.09.058.

[48]   F. Gallucci, F. Chiaravalloti, S. Tosti, E. Drioli, A. Basile, The effect of mixture gas on hydrogen permeation through a palladium membrane: Experimental study and theoretical approach, Int. J. Hydrogen Energy. 32 (2007) 1837–1845.

[49]   F.D. Manchester, A. San-Martin, J.M. Pitre, The H-Pd (Hydrogen-Palladium) System, J. Phase Equilibria. 15 (1994) 62–83.

[50]   A. Maeland, T.B. Flanagan, The Hydrogen-Palladium System, Platin. Met. Rev. 10 (1966) 20–23.

[51]   J. Okazaki, D. Tanaka, M. Tanco, Y. Wakui, F. Mizukami, T. Suzuki, Hydrogen permeability study of the thin Pd–Ag alloy membranes in the temperature range across the α–β phase transition, J. Memb. Sci. 282 (2006) 370–374. doi:10.1016/j.memsci.2006.05.042.

[52]   B.A.G. Knapton, Palladium Alloys for Hydrogen Diffusion Membranes, Platin. Met. Rev. 21 (1977) 44–50.

[53]   S.J. Khatib, S. Yun, S.T. Oyama, Sulfur resistant Pd and Pd alloy membranes by phosphidation,   J.   Memb.   Sci.   455   (2014)   283–293. doi:10.1016/j.memsci.2013.12.074.

[54]   G. Barbieri, F. Scura, F. Lentini, G. De Luca, E. Drioli, A novel model equation for the permeation of hydrogen in mixture with carbon monoxide through Pd-Ag membranes, Sep. Purif. Technol. 61 (2008) 217–224.

[55]   N. a. Khan, a. Uhl, S. Shaikhutdinov, H.-J. Freund, Alumina supported model Pd–Ag catalysts: A combined STM, XPS, TPD and IRAS study, Surf. Sci. 600 (2006) 1849–1853. doi:10.1016/j.susc.2006.02.016.

[56]   Y. Sakamoto, F.L. Chen, Y. Kinari, F. Sakamoto, Effect of carbon monoxide on hydrogen permeation alloy membranes, Int. J. Hydrogen Energy. 210 (1996) 1017–1024.

[57]   A. Kulprathipanja, O. Alptekin, J.L. Falconer, J.D. Way, Pd and Pd – Cu membranes : inhibition of H2 permeation by H2S, 254 (2005) 49–62. doi:10.1016/j.memsci.2004.11.031.

[58]   H.W. Abu El Hawa, S.N. Paglieri, C.C. Morris, A. Harale, J. Douglas Way, Application of a Pd–Ru composite membrane to hydrogen production in a high temperature   membrane   reactor,   Sep.   Purif.   Technol.   (2015)   1–10. doi:10.1016/j.seppur.2015.02.005.

[59]   V. Gryaznov, Metal Containing Membranes for the Production of Ultrapure Hydrogen and the Recovery of Hydrogen Isotopes, Sep. Purif. Methods. 29 (2000) 171–187. doi:10.1081/SPM-100100008.

[60]   S.N. Tripathi, S.R. Bharadway, S.R. Dharwadkar, The Pd-Ru System (Palladium-Ruthenium), J. Phase Equilibria. 14 (1993) 638–642.

[61]   L.P. Didenko, V.I. Savchenko, L.A. Sementsova, L.A. Bikov, Hydrogen flux through the membrane based on the Pd–In–Ru foil, Int. J. Hydrogen Energy. 41 (2016) 307–315. doi:10.1016/j.ijhydene.2015.10.107.

[62]   M.D. Dolan, Non-Pd BCC alloy membranes for industrial hydrogen separation, J. Memb. Sci. 362 (2010) 12–28. doi:10.1016/j.memsci.2010.06.068.

[63]   A. Basile, F. Gallucci, S. Tosti, Synthesis, Characterization and Applications of Palladium Membranes, in: R. Mallada, M. Menendez (Eds.), Inorg. Membr. Synth.

Charact. Appl., Elsevier B.V, 2008.

[64]   T. Nambu, K. Shimizu, Y. Matsumoto, R. Rong, N. Watanabe, H. Yukawa, M. Morinaga, I. Yasuda, Enhanced hydrogen embrittlement of Pd-coated niobium metal membrane detected by in situ small punch test under hydrogen permeation, J. Alloys Compd. 446–447 (2007) 588–592. doi:10.1016/j.jallcom.2007.02.063.

[65]   S.N. Paglieri, J.D. Way, Innovations in Palladium Membrane Research, Sep. Purif. Rev. 31 (2002) 1–169. doi:10.1081/SPM-120006115.

[66]   V.N. Alimov, a. O. Busnyuk, M.. Notkin, a. I. Livshits, Pd–V–Pd composite membranes: Hydrogen transport in a wide pressure range and mechanical stability, J. Memb. Sci. 457 (2014) 103–112. doi:10.1016/j.memsci.2014.01.053.

[67]   K.H. Kim, H.C. Park, J. Lee, E. Cho, S.M. Lee, Vanadium alloy membranes for high hydrogen permeability and suppressed hydrogen embrittlement, Scr. Mater. 68 (2013) 905–908. doi:10.1016/j.scriptamat.2013.02.028.

[68]   D.M. Viano, M.D. Dolan, F. Weiss, A. Adibhatla, Asymmetric layered vanadium membranes for hydrogen separation, J. Memb. Sci. 487 (2015) 83–89. doi:10.1016/j.memsci.2015.03.048.

[69]   J.-Y. Oh, W.-S. Ko, J.-Y. Suh, Y.-S. Lee, B.-J. Lee, W.Y. Yoon, J.-H. Shim, Enhanced high temperature hydrogen permeation characteristics of V–Ni alloy membranes containing a trace amount of yttrium, Scr. Mater. 116 (2016) 122–126. doi:10.1016/j.scriptamat.2016.02.003.

[70]   N. Watanabe, H. Yukawa, T. Nambu, Y. Matsumoto, G.X. Zhang, M. Morinaga, Alloying effects of Ru and W on the resistance to hydrogen embrittlement and hydrogen permeability of niobium, J. Alloys Compd. 477 (2009) 851–854. doi:10.1016/j.jallcom.2008.10.164.

[71]   S.N. Paglieri, N.K. Pal, M.D. Dolan, S.-M. Kim, W.-M. Chien, J. Lamb, D. Chandra, K.M. Hubbard, D.P. Moore, Hydrogen permeability, thermal stability and hydrogen embrittlement of Ni–Nb–Zr and Ni–Nb–Ta–Zr amorphous alloy membranes, J. Memb. Sci. 378 (2011) 42–50. doi:10.1016/j.memsci.2011.04.049.

[72]   H. Iwahara, T. Yajima, H. Ushida, Effect of ionic radii of dopants on mixed ionic conduction (H+ + O2-) in BaCeO3- based electrolytes, Solid State Ionics. 1 (1994) 267–271.

[73]   H. Iwahara, Technological challenges in the application of proton conducting ceramics, Solid State Ionics. 77 (1995) 289–298.

[74]   J. Guan, S.E. Dorris, U. Balachardran, M. Liu, Transport properties of BaCe0.95Y0.05O3-α a mixed conductors hydrogen separation for, Solit State Ionics. 100 (1997) 45–52.

[75]   I. Guan, The Effects of Dopants and A:B Site Nonstoichiometry on Properties of Perovskite-Type Proton Conductors, J. Electrochem. Soc. 145 (1998) 1780–1786.

[76]   J. Guan, S.E. Dorris, U. Balachandran, M. Liu, Development of Mixed-Conducting

Ceramic Membranes for Hydrogen Separation, in: 1998: pp. 1–12.

[77]   U. Balachandran, T.H. Lee, S. Wang, G. Zhang, J.T. Dusek, S.E. Dorris, Recent advances in the development of dense ceramic membranes for hydrogen separation, Fuel Chem. Div. Prepr. 47 (2002) 820–821.

[78]   U. Balachandran, T.H. Lee, L. Chen, S.J. Song, J.J. Picciolo, S.E. Dorris, Hydrogen separation by dense cermet membranes, Fuel. 85 (2006) 150–155. doi:10.1016/j.fuel.2005.05.027.

[79]   J. Hoon, S. Il, W. Jong, I. Hyun, S. Hyun, Stability of Ta/YSZ cermet membrane for hydrogen separation, Energy Procedia. 4 (2011) 756–762. doi:10.1016/j.egypro.2011.01.116.

[80]   S. Jeon, M. Choi, C. Park, E.D. Wachsman, S. Song, High sulfur tolerance dual-functional cermet hydrogen separation membranes, J. Memb. Sci. 382 (2011) 323–327. doi:10.1016/j.memsci.2011.08.024.

[81]   S. Jeon, D. Lim, M. Choi, E.D. Wachsman, S. Song, Hydrogen separation by Pd–CaZr0.9Y0.1O3−δ cermet composite membranes, Sep. Purif. Technol. 79 (2011) 337–341. doi:10.1016/j.seppur.2011.03.018.

[82]   S. Jeon, M. Choi, B. Singh, S. Song, Hydrogen separation by dual functional cermet membranes with self-repairing capability against the damage by H2S, J. Memb. Sci. 428 (2013) 46–51. doi:10.1016/j.memsci.2012.11.009.

[83]   N. Bonanos, K.S. Knight, B. Ellis, Perovskite solid electrolytes : Structure , transport properties and fuel cell applications, Solid State Ionics. 79 (1995) 161–170.

[84]   N. Zakowsky, S. Williamson, J. Irvine, Elaboration of CO2 tolerance limits of BaCe0.9Y0.1O3-δ electrolytes for fuel cells and other applications, Solid State Ionics. 176 (2005) 3019–3026. doi:10.1016/j.ssi.2005.09.040.

[85]   K.D. Kreuer, Aspects of the formation and mobility of protonic charge carriers and the stability of perovskite-type oxides, Solid State Ionics. 125 (1999) 285–302.

[86]   L. Yan, W. Sun, L. Bi, S. Fang, Z. Tao, W. Liu, Influence of fabrication process of Ni-BaCe0.7Zr0.1Y0.2O3-d cermet on the hydrogen permeation performance, J. Alloys Compd. 508 (2010) L5–L8. doi:10.1016/j.jallcom.2010.08.040.

[87]   C. Zuo, T.H. Lee, S.E. Dorris, U. Balachandran, M. Liu, Composite Ni–Ba(Zr0.1Ce0.7Y0.2)O3 membrane for hydrogen separation, J. Power Sources. 159 (2006) 1291–1295. doi:10.1016/j.jpowsour.2005.12.042.

[88]   C. Zuo, S.E. Dorris, U. Balachandran, M. Liu, Effect of Zr-Doping on the Chemical Stability and Hydrogen Conductor, (2006) 4647–4650.

[89]   W.R. Kang, K.B. Lee, Development of rare earth element-doped Ni–Ba(Ce/Zr)O3 cermets for hydrogen-permeable membranes, J. Ind. Eng. Chem. 29 (2015) 194–198. doi:10.1016/j.jiec.2015.04.003.

[90]   Z. Zhu, W. Sun, L. Yan, W. Liu, W. Liu, Synthesis and hydrogen permeation of Ni-Ba(Zr0.1Ce0.7Y0.2)O3-δ metal e ceramic asymmetric membranes, Int. J. Hydrogen

Energy. 36 (2011) 6337–6342. doi:10.1016/j.ijhydene.2011.02.029.

[91]   H. Kim, B. Kim, J. Lee, K. Ahn, H. Kim, K. Joong, B. Kim, Y. Whan, H. Lee, J. Lee, Microstructural adjustment of Ni – BaCe0.9Y0.1O3-δ cermet membrane for improved hydrogen permeation, Ceram. Int. 40 (2014) 4117–4126. doi:10.1016/j.ceramint.2013.08.066.

[92]   M. Liu, W. Sun, X. Li, S. Feng, D. Ding, D. Chen, M. Liu, H. Cheol, High-performance Ni-BaZr0.1Ce0.7 Y0.1Yb0.1O3-d (BZCYYb) membranes for hydrogen separation, Int. J. Hydrogen Energy. 8 (2013) 3–9. doi:10.1016/j.ijhydene.2013.09.057.

[93]   Z. Zhu, W. Sun, Y. Dong, Z. Wang, Z. Shi, Q. Zhang, W. Liu, Evaluation of hydrogen permeation properties of Ni–Ba(Zr0.7Pr0.1Y0.2)O3−δ cermet membranes, Int. J. Hydrogen Energy. 39 (2014) 11683–11689. doi:10.1016/j.ijhydene.2014.05.163.

[94]   Y. Wei, J. Xue, W. Fang, Y. Chen, H. Wang, J. Caro, Enhanced stability of Zr-doped Ba(CeTb)O(3-δ)-Ni cermet membrane for hydrogen separation., Chem. Commun. 51 (2015) 11619–21. doi:10.1039/c5cc03391h.

[95]   Z. Zhu, W. Sun, Z. Wang, J. Cao, Y. Dong, W. Liu, A high stability Ni-La0.5Ce0.5O2-γ asymmetrical metal-ceramic membrane for hydrogen separation and generation, J. Power Sources. 281 (2015) 417–424. doi:10.1016/j.jpowsour.2015.02.005.

[96]   U.B. Balachandran, T.H. Lee, C.Y. Park, J.E. Emerson, J.J. Picciolo, S.E. Dorris, Dense cermet membranes for hydrogen separation, Sep. Purif. Technol. 121 (2014) 54–59. doi:10.1016/j.seppur.2013.10.001.

[97]   M.J. Lee, Y.S. Lee, M.H. Jang, T.W. Hong, Evaluations of hydrogen permeability on Ti4Cr3Nb3O2(TCN)-20wt.%Ni composite membrane by hot press sintering, J. Alloys Compd. 645 (2015) S325–S328. doi:10.1016/j.jallcom.2014.12.152.

[98]   U. Balachandran, Use of mixed conducting membranes to produce hydrogen by water dissociation, Int. J. Hydrogen Energy. 29 (2004) 291–296. doi:10.1016/S0360-3199(03)00134-4.

[99]   J. Kim, Y.S. Lin, Synthesis and oxygen-permeation properties of thin YSZ/Pd composite membranes, AIChE J. 46 (2000) 1521–1529. doi:10.1002/aic.690460805.

[100] T. Kuji, Y. Matsumura, H. Uchida, T. Aizawa, Hydrogen absorption of nanocrystalline palladium, J. Alloys Compd. 330–332 (2002) 718–722. doi:10.1016/S0925-8388(01)01597-3.

[101] A. Pundt, C. Sachs, M. Winter, M.. Reetz, D. Fritsch, R. Kirchheim, Hydrogen sorption in elastically soft stabilized Pd-clusters, J. Alloys Compd. 293–295 (1999) 480–483. doi:10.1016/S0925-8388(99)00469-7.

[102] T. Suzuki, D.A. Pacheco Tanaka, M. Llosa Tanco, Method for purifing/separating hydrogen, JP20056265076, 2006.

[103]   A. Gora, D. a. P. Tanaka, F. Mizukami, T.M. Suzuki, Lower Temperature Dehydrogenation of Methylcyclohexane by Membrane-assisted Equilibrium Shift, Chem. Lett. 35 (2006) 1372–1373. doi:10.1246/cl.2006.1372.

[104]   T. Zhao, J. Okazaki, D.A. Pacheco Tanaka, T.M. Suzuki, Y. Wakui, Hydrogen separation with "pore-fill" type palladium membrane, in: AIChE Annu. Meet. Conf. Proc., 2011.

[105]   K. Sato, M. Nishioka, H. Higashi, T. Inoue, Y. Hasegawa, Y. Wakui, T.M. Suzuki, S. Hamakawa, Influence of CO2 and H2O on the separation of hydrogen over two types of Pd membranes : Thin metal membrane and pore-filling-type membrane, J. Memb. Sci. 415–416 (2012) 85–92. doi:10.1016/j.memsci.2012.04.053.

[106]   B.K.R. Nair, M.P. Harold, Pd encapsulated and nanopore hollow fiber membranes: Synthesis and permeation studies, J. Memb. Sci. 290 (2007) 182–195. doi:10.1016/j.memsci.2006.12.028.

[107]   S.H. Israni, B.K.R. Nair, M.P. Harold, Hydrogen generation and purification in a composite Pd hollow fiber membrane reactor: Experiments and modeling, Catal. Today. 139 (2009) 299–311. doi:10.1016/j.cattod.2008.02.020.

[108]   Y. Wakui, D.A. Pacheco Tanaka, T. Suzuki, M. Fujio, High-durability hydrogen separation membrane and its manufacturing method, JP2009022843, 2009.

[109]   K. Shgau, H. Verweij, Stable supported Pd-Alloy membranes, US 2010/0071556, 2010.

[110]   K. Yogo, H. Takeyama, K. Nagata, Pore-fill-type Palladium Porous Alumina Composite Membrane for Hydrogen Separation, Energy Procedia. 37 (2013) 1104–1108. doi:10.1016/j.egypro.2013.05.207.

Chapter 3

Diffusion mechanism in mesoporous YSZ/γ-Al$_2$O$_3$ layers

In this chapter nanoporous ceramic supports for pore-filled membranes were prepared using ceramic supports (α-Al$_2$O$_3$) with a pore size of 100 nm and adding additional layers with different proportions of YSZ/γ-Al$_2$O$_3$ (ranging from 50% to 90% of YSZ) by dip-coating and the effect of different parameters in the preparation method have been investigated. The diffusion mechanisms of N$_2$, He and CO$_2$ in the supported nanoporous layers have been studied in detail with permeation measurements in the temperature range of 50-400 °C with pressure differences of 30-100 kPa. It was observed that as the amount of γ-Al$_2$O$_3$ in the nanoporous layers increases, the adsorption of CO$_2$ is favoured at low temperatures and pressures.

"Think like a proton and stay positive".
Unknown.

3.1.   Introduction

As reported in Chapter 1, fluidized-bed reactors can offer very good mass and heat transfer characteristics, while also allowing sufficient freedom to tune the installed membrane area and required catalyst volume [1]. One important concern possibly affecting fluidized bed membrane reactors is possible erosion or damage of the membrane surface by the scouring action of the moving and colliding fluidized particles. Indeed, the selective layer should be on the reaction side where the pressure is much higher, otherwise the membrane layer could be pealed-off due to the pressure difference. To solve this problem one should either use very thick membrane layers (which is not economically feasible because of their low flux and high costs) or somehow protect the membrane layer with an additional porous layer, where the pores have a smaller size compared to the fluidized catalyst particles (to avoid clogging of the porous structure).

This protection can be achieved with an interesting membrane concept previously reported by Pacheco Tanaka [2,3], the so-called pore-filled membrane concept. In these membranes the palladium selective layer is located in the pores of a mesoporous γ-Al₂O₃ or YSZ (yttria-stabilized zirconia)/γ-Al₂O₃ layer and protected by a top ceramic nano-porous layer. In this type of membranes, the palladium is filled into the pores of the support by vacuum-assisted electroless plating (see Chapter 2). Embrittlement of conventional supported membranes in the presence of hydrogen (α→β phase transition) is suppressed in pore-filled membranes due to the particle size of the palladium [13]. However, these types of membrane have not yet been tested for fluidized-bed membrane reactor (FBMR) concepts. Moreover, the observed thermal instability of the Pd/γ-Al₂O₃ system in long-term tests at 400 °C can be attributed to the mismatch of the thermal expansion coefficients of alumina and palladium. This can be circumvented by using a composite based on a mixed sol of γ-Al₂O₃ and YSZ with a similar thermal expansion as palladium. The presence of alumina into the matrix gives resistance to the fatigue and higher hardness values than YSZ alone [14]. Although the pore-filled membrane may promise to be an interesting concept [3,6,7], a more systematic study on the characteristics of the support modification and porous structure is required to be able to produce stable pore-filled membranes with reproducible results.

At high temperatures (more than 600 °C) under hydrogen, alumina can react with Pd membranes reducing the hydrogen permeation [8–10]. The focus of this chapter is the study of the deposition of YSZ/γ-Al₂O₃ nanoporous layers with more than 50 wt% of YSZ, where the Pd layer is located in pore-filled membranes. Additionally, the transport mechanism through this porous support is evaluated from gas permeation experiments for different gas components, viz. nitrogen, helium and carbon dioxide, at different temperatures and pressures. The surface area and pore size distribution of the composite layers have been measured and are discussed.

3.2. Experimental

3.2.1. Membrane preparation

3.2.1.1. Synthesis of YSZ sol

The YSZ nanoparticles were prepared by the hydrothermal synthesis method (8 mol% of Y_2O_3) [12]. An aqueous solution containing 0.92 M of $ZrO(NO_3)_3 \cdot 2H_2O$ and 0.16 M of $Y(NO_3)_3 \cdot 6H_2O$ was stirred for 4 hours and heated in an autoclave at 110 °C for 13 hours. Purification of YSZ was done after thermal treatment adding ammonia to adjust the solution at pH 9. The precipitate was filtered and washed with distilled water until pH 6. The dispersed sol obtained was acidified with nitric acid and peptized at 95 °C overnight. The final pH was around 1. The particle size of YSZ was measured by DLS. The distribution size of hydrodynamic particles was 7-15 nm. The final concentration of the ceramics in the sol was obtained by ICP measurement.

3.2.1.2. Preparation of YSZ/γ-Al₂O₃ mixed sol

Sol mixtures of various YSZ/γ-Al₂O₃ proportions were prepared from, commercial boehmite (γ-AlO(OH)), Kawaken Fine Chemical Co.) with a particle size range of 8-20 nm, the synthesized YSZ and PVA-PEG as drying controlling agents [3]. For the study of the dipping parameters on the thickness of the layer, the total concentration of ceramics was fixed at 1.6 wt% with a mass ratio of 50 wt% YSZ and 50 wt% boehmite; and the total amount of PVA was modified from 0.4 to 2.0 wt%. On the other hand, for the diffusion mechanism study, the PVA was fixed at 1.2 wt%, while the total concentration of ceramics was decreased from 1.6 to 1.2 wt% and the YSZ content was increased from 50% to 90%. In all cases a PEG concentration of 0.3 wt% was used.

3.2.1.3. Preparation of modified tubular substrates with YSZ/γ-Al₂O₃

As porous substrate α-Al₂O₃ tubes were used with an asymmetrical multilayer (pore size of the top layer of 100 nm) with an outer diameter of 10.0-10.3 mm and wall thickness of 1-1.5 mm, provided by Rauschert Kloster Veilsdorf. For proper handling of the membrane during the preparation, the porous tubes were joined to dense alumina tubes (provided by OMEGA with 6 mm OD and a wall thickness of 1 mm). The applied glass (ASF1761, Asahi Glass Co., Ltd) in the junction between porous and dense tube is cured at 1050 °C for 40 minutes in air. The heating ramps from room temperature to 200 °C was 3 °C min^{-1} and then to 1050 °C with 12 °C min^{-1} [11].

The nanoporous layers were prepared by the dip-coating, drying and calcination process. The composite solution was warmed up at 25 °C before the dipping under stirring. The dipping solutions prepared for the diffusion mechanism study are presented in Table 3.1. The parameters used to study the effect of the coating parameters on the thickness of the layer, viz. the dipping time, the amount of PVA and whether vacuum is applied or not during the dipping, are presented in Table 3.2. Subsequently, the tubes were slowly lifted and dried in a climatic chamber (40 °C and 60% RH) for 5 hours. The samples were turning during the drying process in order to obtain a homogeneous layer over the entire surface. Finally, the calcination of the coated layer was performed at 550 °C with a heating rate of 1 °C min^{-1} and 3 h dwelling in air.

Table 3.1. Parameters used for the dip-coating of samples used in the diffusion mechanism study*.

Dip-coating parameters			
Amount of ceramic (wt%)	Mass ratio YSZ/γ-Al₂O₃	PVA (wt%)	Dipping time (s)
1.6	50/50	1.2	12
1.5	60/40	1.2	12
1.4	70/30	1.2	12
1.3	80/20	1.2	12
1.2	90/10	1.2	12

*In all cases: concentration of PVA 1.2 wt%, dipping time 12 s, dipping using vacuum.

Table 3.2. Samples for the study of the dipping parameters on the membrane thickness*.

Sample	Parameters		
	PVA (wt%)	Dipping time (s)	Vacuum
PF-A72	1.2	48	Yes
PF-A73	1.2	48	No
PF-A74	1.2	12	Yes
PF-A75	1.2	12	No
PF-A76	1.2	3	Yes
PF-A77	1.2	3	No
PF-A78	0.6	12	Yes
PF-A79	0.6	12	No
PF-A80	1.0	12	Yes
PF-A81	1.0	12	No
PF-A82	1.4	12	Yes
PF-A83	1.4	12	No
PF-A84	2.0	12	Yes
PF-A85	2.0	12	No

*In all cases the prepared sol was 1.6 wt% of ceramic with the same mass ratio YSZ/γ-Al₂O₃ (50/50).

The prepared mixed sols were dropped on a Teflon petri dish and dried at the same conditions as the coated supports for 24-48 h and the films obtained were also calcined in air at 550 °C and 650 °C for 3 hours. The obtained powders were characterized by XRD and BET.

3.2.2.   Gas permeation measurements

A classical steady state permeation experiment was used for the determination of the composite parameters. The set up used for single gas measurements is illustrated in Figure 3.1. The driving force between the retentate and permeate zone (pressure difference) is regulated by a backpressure controller (Horiba Stec, UR-7340 model). The permeate side is maintained at atmospheric pressure. The permeated flux is measured by Horiba flow meters (STEC PV-2 and STEC PV-3).

The steady state permeation experiments were performed at temperatures between 50 and 400 °C and in the pressure difference range of 30-100 kPa using single gases helium, nitrogen and carbon dioxide.
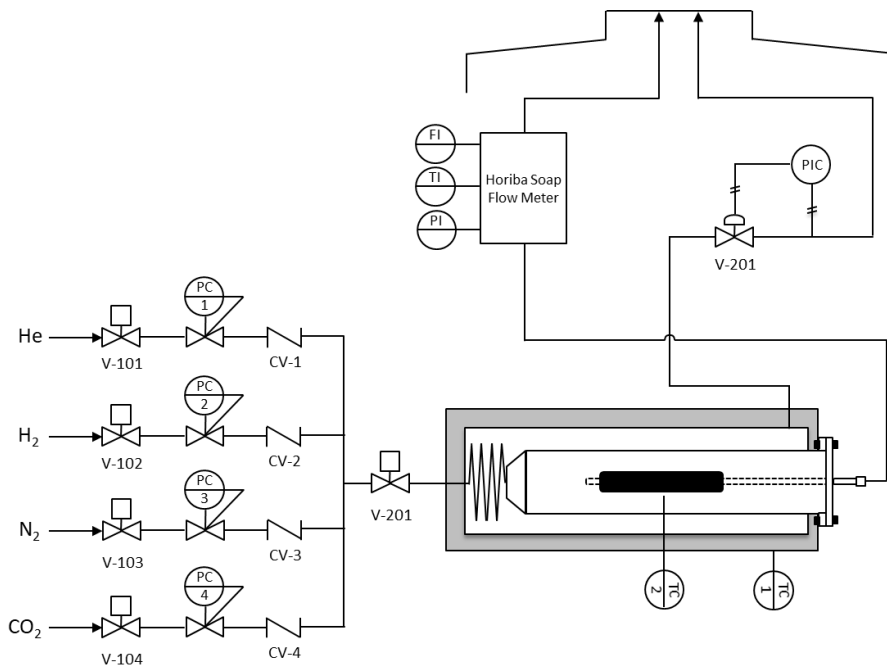

Figure 3.1. Set-up for the permeation measurements.

3.2.3. Characterization

A Zetasizer Nano SZ ZEN3600 (Malvern Instruments) was used for the determination of the particle size of the sols (YSZ and boehmite). Thickness measurements of the nanoporous layers were carried out using cross-sectional images with a SEM (FEI Quanta 250 FEG). A cross-section EDX study of pore-filled membranes was performed using a JEOL JSM-5910LV. The pore size and surface area of the unsupported and supported membranes were obtained from the BET nitrogen adsorption isotherm obtained with a ThermoScientific Surfer. The crystal structure of the nanoporous powders was obtained by powder X-ray diffraction (Rigaku MiniFlex 600) in the 2θ range of 20-90° with a step size of 0.02° 2θ, operating at 40 kV and 15 mA with CuKα radiation.

3.3 Results and discussion

3.3.1. Preparation of YSZ/γ-Al$_2$O$_3$ mesoporous membranes

The particle size distributions of the YSZ sol (7-15 nm) and boehmite (8-20 nm) measured by dynamic light scattering methods were practically the same with a mean diameter of 10 nm (hydrodynamic diameter). The measured particle size of YSZ and boehmite particle size are shown in Figure A.3 and Figure A.4 respectively in Appendix A. Supported YSZ/γ-Al$_2$O$_3$ mixed membranes were prepared by dip-coating deposition and after drying in a climatic chamber calcining in air. Addition of the boehmite sol to the YSZ, improves the adhesion with the surface of α-Al$_2$O$_3$, and decreases the thermal expansion of the mixture and improves the resistance to fatigue of YSZ [14].

3.3.2. Thickness measurements of the nanoporous YSZ/γ-Al$_2$O$_3$ layers

The effect of the following parameters in the preparation procedure of the nanoporous YSZ/γ-Al$_2$O$_3$ layers on the thickness of the obtained layers have been investigated:

a. Ceramic concentration in the solution.
b. Deposition time.
c. Polymer content.
d. Applying vacuum during deposition.

The thickness of the deposited layers using different concentrations of ceramics was measured with SEM (cross section) and the results are shown in Figure 3.2. The temperature of the solution was fixed at 25 °C, the deposition time to 12 s and vacuum was applied during the coating. Different mass ratios of YSZ and boehmite were used. As the amount of YSZ increases, thinner membranes without cracks should be prepared; the concentration and YSZ composition selected produced membranes without cracks. The coated porous support

is made of α-Al_2O_3, which has a lower expansion coefficient than the deposited mixed YSZ/γ-Al_2O_3. In order to avoid cracks formation at the surface due to this difference in expansion coefficients, the amount of YSZ was increased while the total content in ceramics was decreased. The average measured thickness and the errors (from at least 4 measurements) as a function of the concentration of the solutions is also presented in Figure 3.2. The thickness increases linearly with the concentration of the solution (R^2 = 0.985), which means that the thickness can be controlled by the concentration of the solution when the coating time is fixed to 12 s and vacuum is applied.
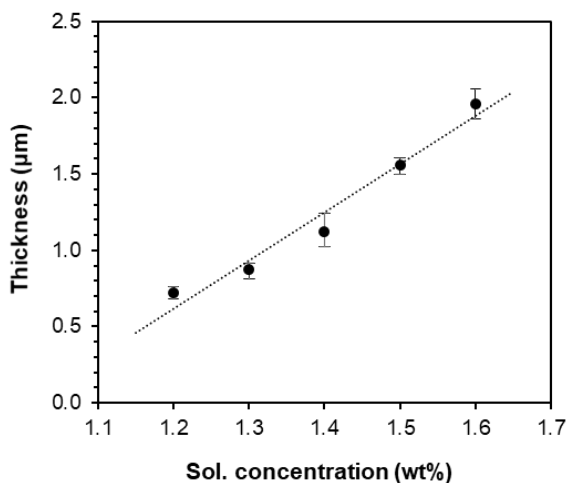

Figure 3.2. Measured thickness of the ceramic layers in cross section with SEM for solutions with different ceramics concentrations in the solution.

The second study was performed by fixing the concentration of the ceramics of the solution to 1.6 wt% with the same YSZ/γ-Al_2O_3 ratio (50/50) (Table 3.2). As can be observed in Figure 3.3 (top), when the coating time is increased, the thickness also increases. Better correlation is obtained when vacuum is applied. Samples deposited during 48 s show cracks on the surface. On the other hand, as the amount of polymer is increased in the solution, the thickness of the layer increases. However, a direct correlation for both samples (deposited with and without vacuum) was not obtained (Figure 3.3 bottom).
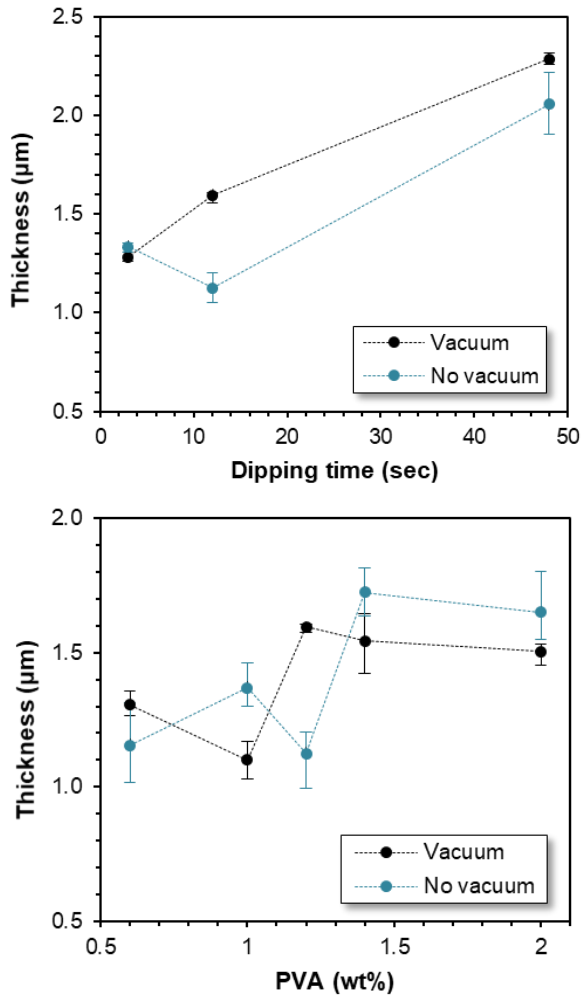
Figure 3.3. Measured thickness in cross section depending on dipping time (top) and PVA content in the solution (bottom). (● Applying vacuum; ● without applying vacuum).

Figure 3.4 shows the cross-section of a nanoporous layer with 60 wt% YSZ (top) and 70 wt% YSZ (botton) deposited on top of an α-alumina asymmetric support (with a mean pore size of 100 nm). The concentration of the ceramics in the solution was 1.4 wt%. The coating was performed while applying vacuum from the inner part for 12 s and the amount of PVA was 1.2 wt%. A relatively uniform and dense layer is created on the support structure.
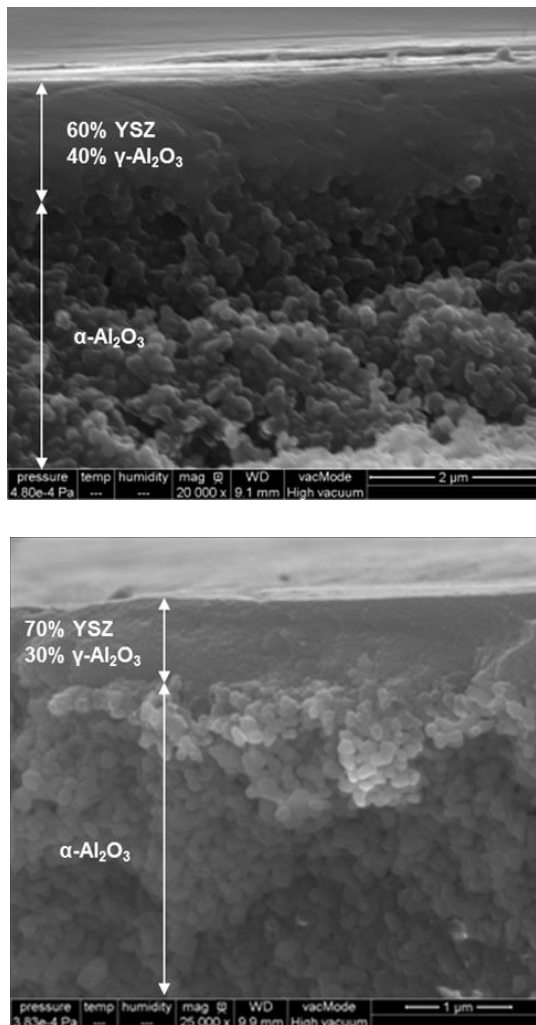
Figure 3.4. SEM cross section of nanoporous layer with 60 wt% YSZ (top) and 70 wt% YSZ (botton) on top of an α-alumina asymmetric support.

3.3.3.   Surface area and pore size distribution

Figure 3.5 shows the nitrogen adsorption/desorption isotherm of the YSZ/γ-Al$_2$O$_3$ (mass ratio 50:50) calcined at 550 °C. The isotherm profiles present a typical IV characteristic with a recognizable hysteresis loop typical of mesoporous materials [18]. The curve at low p/p$_0$ indicates that multilayer adsorption prevails, since the first monolayer was completed on the mesoporous walls. The calculated BET surface area was 309 m^2 g^{-1}. In Figure 3.6 (top) the surface area for all the mixtures of YSZ/γ-Al$_2$O$_3$ calcined at 550 °C is reported as a function of the YSZ concentration (pure YSZ was included in the graph for comparison). It can be

observed that as the amount of YSZ increases from 50 wt% to 100 wt%, the surface area decreases from 300 m^2 g^{-1} to 50 m^2 g^{-1}. This is related to the increased sintering behavior of YSZ particles compared to γ-Al$_2$O$_3$ particles. The pore size distribution of these mixtures increases when the amount of YSZ is increased. As shown in Figure 3.6 (bottom), the pore diameter of the mixtures containing 50 wt% of YSZ varies roughly from 1 to 5 nm, while for pure YSZ the distribution is much broader ranging from 2 nm to 9 nm. The results obtained from samples with 50 wt% of YSZ calcined at 550 °C and 650 °C are shown in Figure A.1 (in Appendix A).
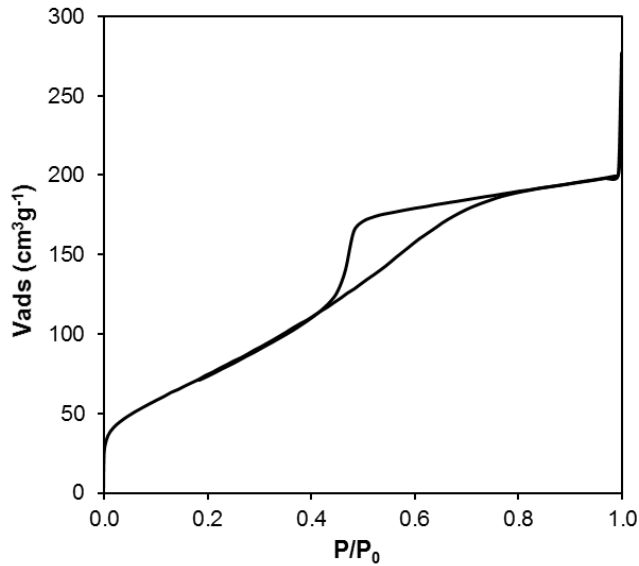
Figure 3.5. Nitrogen adsorption/desorption isotherm of YSZ-γ-Al$_2$O$_3$ (50:50) calcined at 550°C.
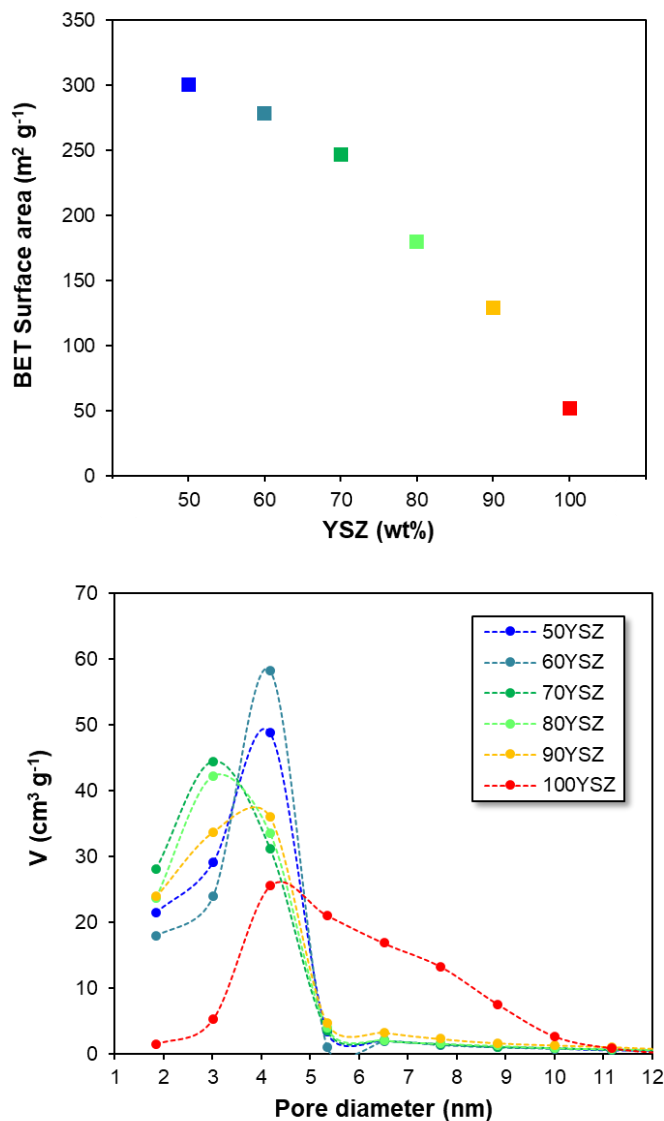
Figure 3.6. BET surface area (top) and pore diameter distribution (bottom) of different YSZ/γ-Al$_2$O$_3$ powders calcined at 550 °C in air for 3 h.

3.4.   Crystallite and particle size

According to the XRD patterns for the samples calcined at 550 °C shown in Figure 3.7 (top), the YSZ is related to the cubic phase. The peak broadening could be due to the presence of a tetragonal phase [19]. It is observed that as the amount of γ-Al$_2$O$_3$ increases, the intensity of the peaks related to the cubic YSZ crystals decreases and they become broader. This relates to

the presence of amorphous γ-Al₂O₃, which remains as such in the temperature range of 350-1000 °C [20, 21].

The crystallite size can be calculated from the XRD patterns using the Scherrer equation by measuring the FWHM (full width at half maximum) of the diffraction peaks. The relation between crystallite size and the FWHM reads as follows [22]:

$$L_{hkl} = \frac{K\lambda}{\beta_{hkl}\cos\theta} \qquad\qquad\qquad \text{(Eq. 3.1)}$$

where L_{hkl} is the mean crystallite size, λ is the X-ray wavelength of CuKα (1.5418 Å), β_{hkl} is the FWHM (in radians), K is the shape factor and θ is the Bragg angle. The value of K varies from 0.89 for spherical to 0.94 for cubic particles. Usually 0.9 is used assuming that the crystallites are spherical [19]. This relation is valid for crystallites smaller than 100 nm [23]. The crystalline size of the YSZ phase was determined for the peak (101) centered at ~30° and is shown in Figure 3.7 (bottom), showing the trend that the crystal size decreases for increased γ-Al₂O₃ content. The calculated crystal size for the samples with 70 and 80 wt% YSZ are somewhat smaller than expected, similar anomalous behavior is observed in the pore size distribution (Figure 3.6 bottom). As was explained before, the crystal growth of YSZ is hindered due to the presence of γ-Al₂O₃. According to Vegard's law, the solubility of Al₂O₃ in YSZ is only around 0.3 wt% because of the differences in their crystal structures. This means that they cannot form a solid solution and most of the Al₂O₃ is going to segregate at the grain boundary of YSZ, inhibiting the sintering process thereof. The diffractograms for samples calcined at 550 and 650 °C with 50 wt% of YSZ are shown in Figure A.2 (in Appendix A).

Before calcination at 550 °C, the hydrodynamic particle size of boehmite and YSZ was measured by DLS. Both solutions showed a peak centered at 10 nm. After calcination, the particle size was obtained by TEM images. As shown in Figure 3.8, the particle size of pure YSZ calcined at 550 °C is higher (10-20 nm) than the particle size obtained for the mixture with 50 wt% of γ-Al₂O₃ (< 7 nm). Thus, the particle size of YSZ/γ-Al₂O₃ mixtures decreases, as the amount of gamma-alumina increases. This effect can be explained with the same reasoning as for the crystal size: sintering of YSZ is blocked due to the presence of amorphous γ-Al₂O₃ [19].
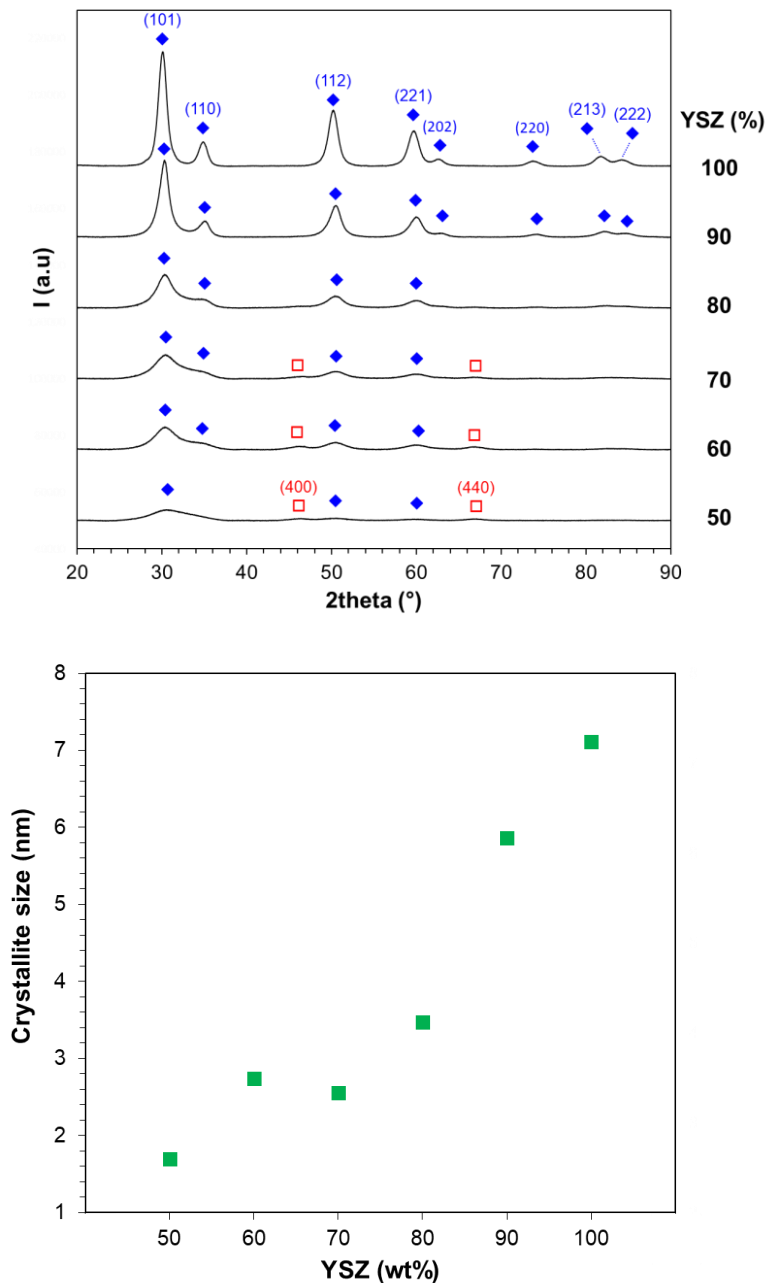
Figure 3.7. XRD patterns (top) and crystallite size (bottom) of different YSZ/γ-Al$_2$O$_3$ powders calcined in air at 550 °C for 3h. (◆): (ZrO$_2$)$_{0.92}$(Y$_2$O$_3$)$_{0.08}$ (JCPDS 01-070-4431); (□) Gamma-Al$_2$O$_3$ (JCPDS 00-002-1420).
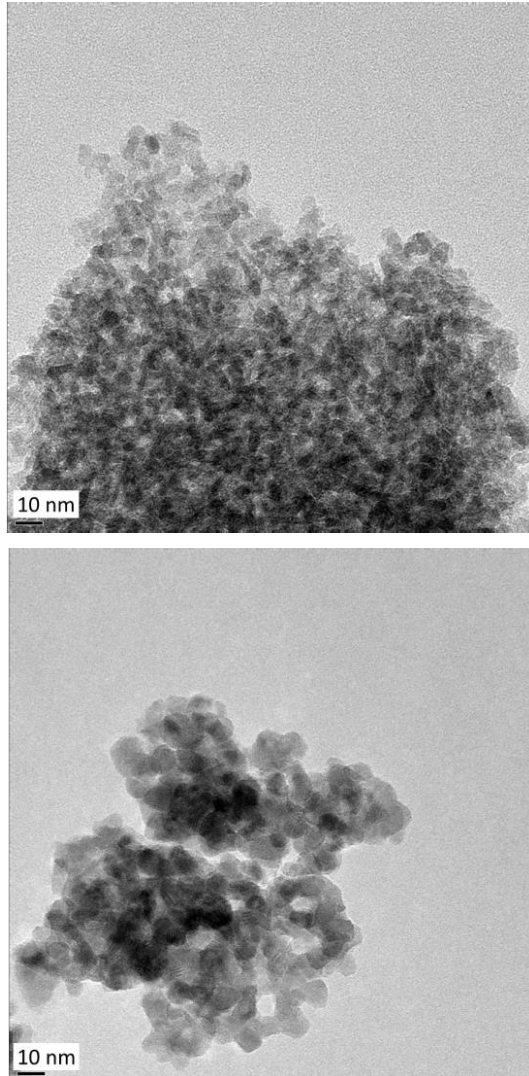
Figure 3.8. TEM images of samples calcined at 550 °C during 3 hours in air: 50 wt% YSZ/ 50 wt% Al$_2$O$_3$ (top) and YSZ (bottom).

3.3.5. Permeation measurements

The quality of the top layer was evaluated by N$_2$, He and CO$_2$ gas permeation experiments at different temperatures (ranging from 50 °C to 400 °C) with a pressure difference range of 30-100 kPa for the nanoporous YSZ/γ-Al$_2$O$_3$ membranes with different mass ratios (ranging from 50% to 90% of YSZ). All the permeation results obtained for all the porous membranes are included in Appendix A in Table A.2 to Table A.6.

The gas permeance (J_0) is related to the mean pressure (P_m) by Eq. (1), where C_1 and C_2 denotes the Knudsen and viscous (Poiseuille) flow respectively [3,18]:

$$J_0 = C_1 + C_2 P_{ave} \qquad \text{(Eq. 3.2)}$$

When the permeance (J_0) is independent of the average pressure (P_{ave}), Knudsen diffusion occurs as the transport mechanism. This means that the membrane is defect free. On the contrary, a large dependency on the average pressure indicates the presence of large pores or defects.

The permeances of three gases for a mesoporous layer with 60 wt% YSZ at 400 °C are reported in Figure 3.9 (top), showing that the permeance is almost constant or only slightly increases as a function of the pressure difference for the three different gases. In particular, for helium, the permeance slightly increases as the pressure difference increases. This effect is related to a slightly larger contribution of viscous flow at higher pressures, while Knudsen flow is independent of pressure. Since the kinetic diameters of nitrogen and carbon dioxide are larger than the kinetic diameter of helium, the viscous flow contribution is much less important for N_2 and CO_2. The ideal perm-selectivities of the binary gases used in this study are summarized in Table 3.3. Moreover, in Table 3.4 the slopes and intercepts obtained by plotting the measured permeance versus the average pressure for the three gases are given. For the three gases, the slope is in the order of 10^{-12} mol m^{-2} s^{-1} Pa^{-2}, which means that the Knudsen contribution is much larger than the viscous flow contribution. The graphs used for the calculation of the slopes and intercepts for all the membranes are shown in Figure A.5, and their values in Table A.7 to

Table A.9 (Appendix A).

Table 3.3. Ideal Knudsen perm-selectivities for different binary mixtures of gases.

Diffusing gases	Knudsen perm-selectivity
He/N_2	2.65
He/CO_2	3.32
N_2/CO_2	1.25
H_2/N_2	3.74

Table 3.4. Slopes and intercepts calculated for a porous membrane with 60 wt% YSZ at 400 °C.

Gas	Slope (mol m^{-2} s^{-1} Pa^{-2})	Intercept (mol m^{-2} s^{-1} Pa^{-1})
He	$9.03 \cdot 10^{-12}$	$1.00 \cdot 10^{-5}$
N_2	$1.89 \cdot 10^{-12}$	$4.91 \cdot 10^{-6}$
CO_2	$3.71 \cdot 10^{-12}$	$4.23 \cdot 10^{-6}$
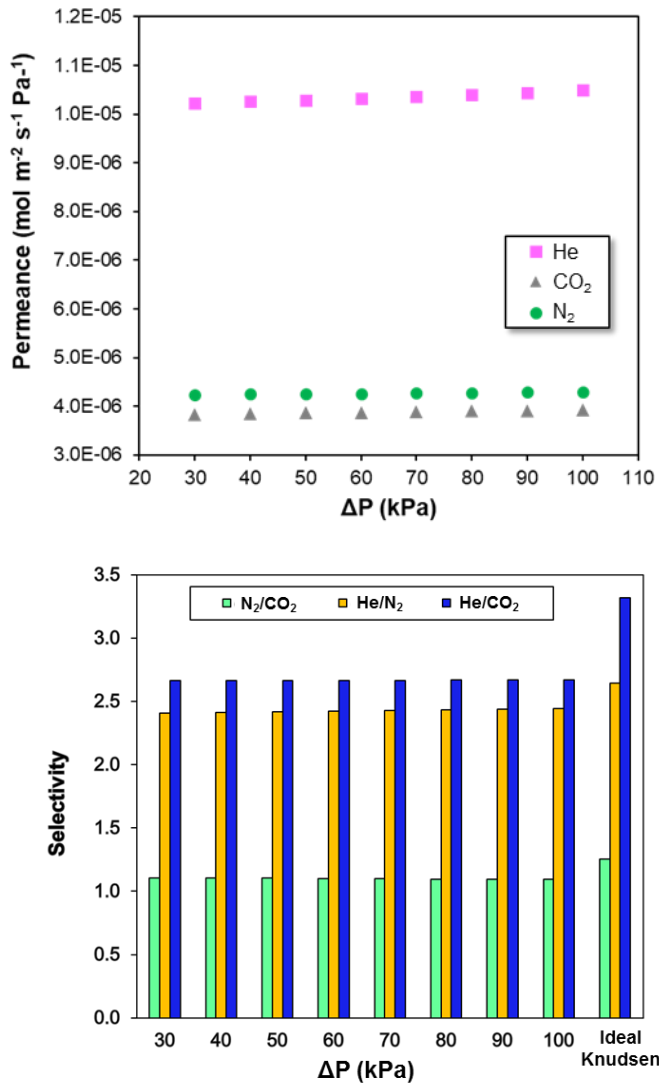
Figure 3.9. N_2, He and CO_2 permeance (top) and ideal perm-selectivities (bottom) of (60 wt%) YSZ/(40 wt%) γ-Al₂O₃ layer at 400 °C and different pressures.

3.3.5.1.   Composition dependence

Diffusion of gases through porous media depends on the internal configuration such as the porosity, tortuosity, mean pore size and the thickness of the layer. Addition of γ-Al₂O₃ influences the transport properties of the membrane. The permeance of N_2, He and CO_2

obtained at 400 °C and 100 kPa of pressure difference for various YSZ/γ-Al$_2$O$_3$ is reported in Figure 3.10 (top). It is clear that a larger presence of YSZ increases the total flux of the diffusing species; since YSZ is more easily sintered than γ-Al$_2$O$_3$, and the total surface of the membrane is the same, the growth of YSZ leaves larger spaces (bigger pores) between the alumina grains increasing the passage of gases. At the same time the ideal Knudsen perm-selectivities (Figure 3.10, bottom) are closer to the ideal values, when the amount of alumina in the mesoporous layer is increased.
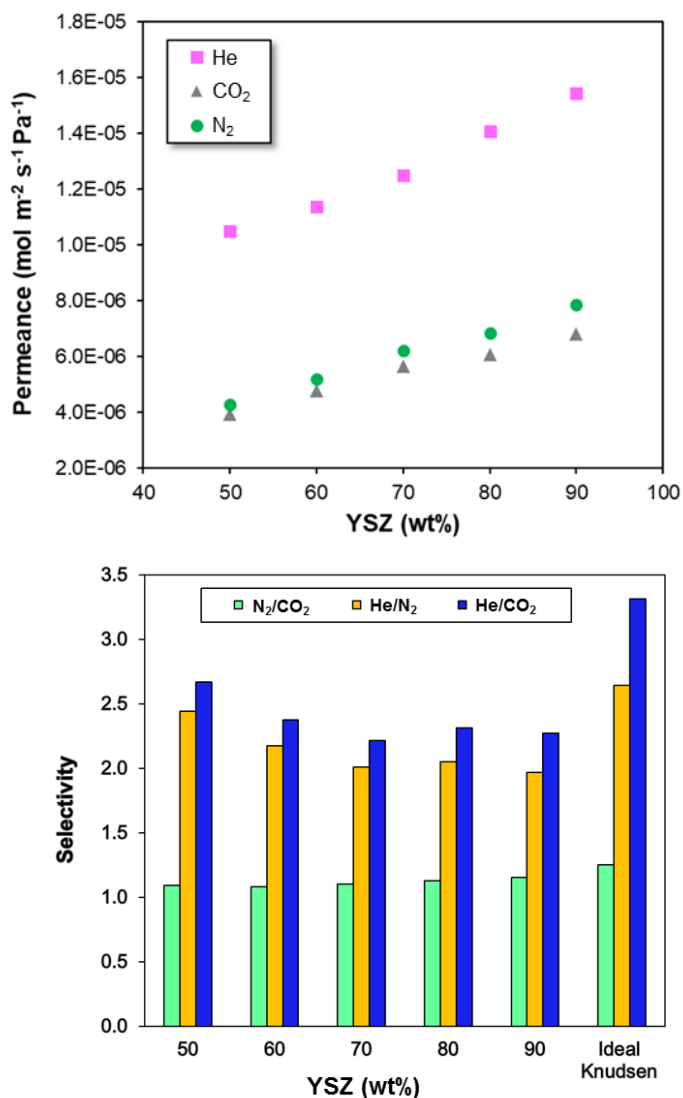

Figure 3.10. N$_2$, He and CO$_2$ permeance (top) and ideal perm-selectivities at 100 kPa of pressure difference (bottom) for different YSZ/γ-Al$_2$O$_3$ layers at 400 °C and 100 kPa pressure difference.

However, as will be explained in more detail below, the thickness of the mesoporous layer is larger for composites with a smaller amount of YSZ, since the prepared solutions for the coating contains a smaller total amount of ceramics when the composition of YSZ is higher.

In order to compare the effect of the composition on the permeation properties with the surface area, the permeability (thickness standardized) values were compared and can be observed in Figure 3.11, showing that a lower content of YSZ results in larger permeabilities for the case of a nanoporous layer based on 50 wt% γ-Al$_2$O$_3$, which represents the best alternative for their application as matrix phase in palladium-based pore-filled membranes.
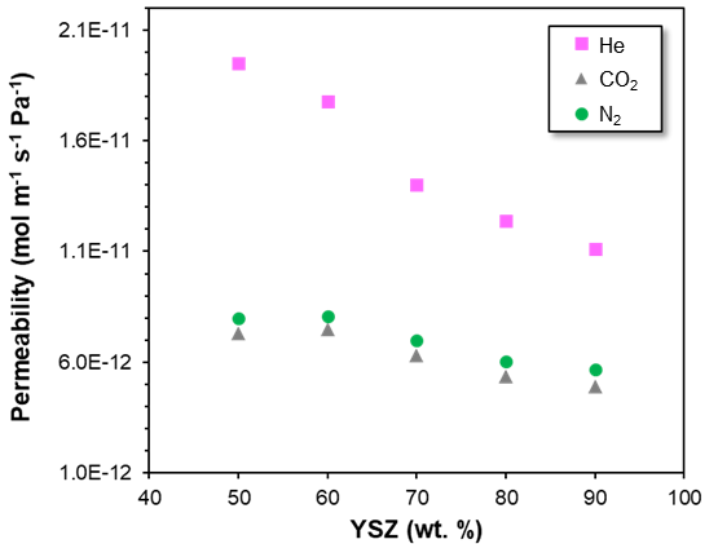
Figure 3.11. Permeabilities of N$_2$, He and CO$_2$ at 400 °C and 100 kPa pressure difference as a function of the amount of YSZ (wt%) of the mesoporous composites.

3.3.5.2. *Temperature dependence*

In order to analyze the temperature influence on the diffusion mechanism through the nanoporous layers, experiments were performed at different temperatures (from 50 °C to 400 °C). As an example, for a nanoporous layer with 50 wt% YSZ and 100 kPa pressure difference, when the temperature is increased, the permeance of the three gases strongly decreases (see Figure 3.12 top). The decrease in the permeance for different gases follows the expected trend (Figure 3.12 bottom), since at lower temperatures the viscous contribution is more significant than the Knudsen flow contribution. The viscosity of the permeated gases is higher when the operating temperature is increased, which entails an increase in the frictional resistance thereof, rendering the relative contribution of the Knudsen mechanism more important for non-adsorbable gases (helium and nitrogen). However, for CO$_2$

(adsorbable gas) at lower temperatures, the permeance is higher due to the contribution of surface diffusion.

Thus, one would expect that the Knudsen contribution increases for increasing temperatures, and the ideal perm-selectivity to approach the ideal Knudsen perm-selectivity. As shown in Figure 3.12 (bottom), this is not the case for all gases, probably because the separation factors are influenced by interactions between the gases and the walls of the pores. Inspecting the perm-selectivity for non-adsorbable pure gases (He/N_2) relative to the ideal selectivity, it shows a slight decrease when increasing the operating temperature, against all expectations. However, they are close to the ideal Knudsen perm-selectivity (2.65), which implies that adsorption does not take place significantly and that permeation takes place predominantly by Knudsen diffusion. In contrast, the observed ideal perm-selectivity for He/CO_2 and N_2/CO_2, exhibit a much more pronounced dependency on temperature, explained by the exothermic nature of the surface adsorption of CO_2, increasing the perm-selectivity at higher temperatures.

An Arrhenius like relationship can describe the change of permeation with temperature:

$$J = J_0 exp\left(-Ea/_{RT}\right) \qquad\qquad (Eq.\ 3.3)$$

where J is the permeability, J_0 is the pre-exponential permeability constant, Ea the apparent activation energy and T the temperature (in K). The activation energy, Ea, is the sum of two contributions: the heat of sorption of the molecules and the activation energy associated with the mobility of the molecules [25]. The activation energies evaluated (Eq. 3.3) in this study are shown in Figure 3.13. Negative values of activation energy are generally associated to an adsorption of the molecule on the surface of the pore as well as the contribution of viscous and Knudsen flow due to the inverse dependency with temperature. CO_2 adsorption occurs on the γ-Al_2O_3 layers since the gas molecules interact with the material at the pore wall. Thus, CO_2 is adsorbed at the surface of the pores and diffuse along the pores due to pressure difference, resulting in an additional flow [16].
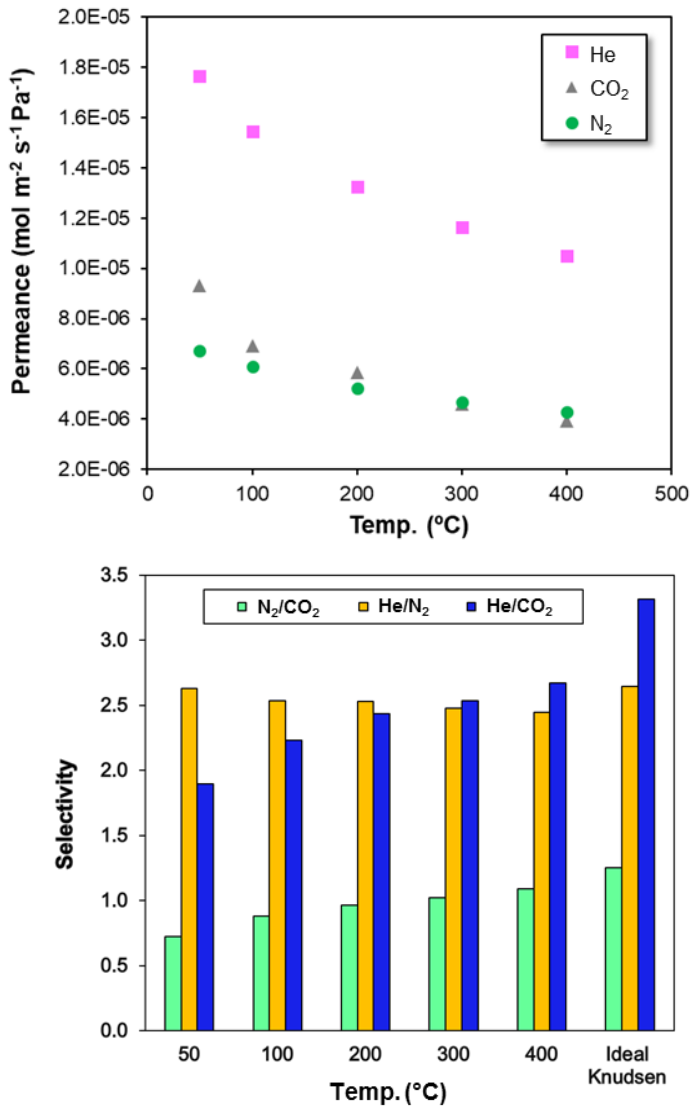
Figure 3.12. N_2, He and CO_2 permeance (top) and ideal Knudsen perm-selectivities (bottom) for a nanoporous layer with 50 wt% YSZ as a function of temperature (pressure difference was 100 kPa).

Regarding the structural properties of the studied layers, the activation energy provides an indication of the probability of the molecules to cross the channels of the porous structure. As the pores constrictions increase, the activation energy involved in the diffusion process is increased, related to a larger number of interactions between the permeating molecule and the pore wall, reducing the amount of permeated gas. At the same time, the transport resistance increases as the alumina content increases. However, the experimental results show for non-adsorbable gases (nitrogen and helium) a linear trend of Ea with the concentration

of alumina, while for the adsorbable CO_2 the same tendency is found until 30 wt% of γ-Al_2O_3 in content. For higher concentrations of gamma-alumina, the activation energy decreases dramatically, which indicates a change in the rate-limiting transport mechanism, i.e. the increased importance of surface diffusion, where CO_2 molecules are adsorbed on the pore surface of the membrane.
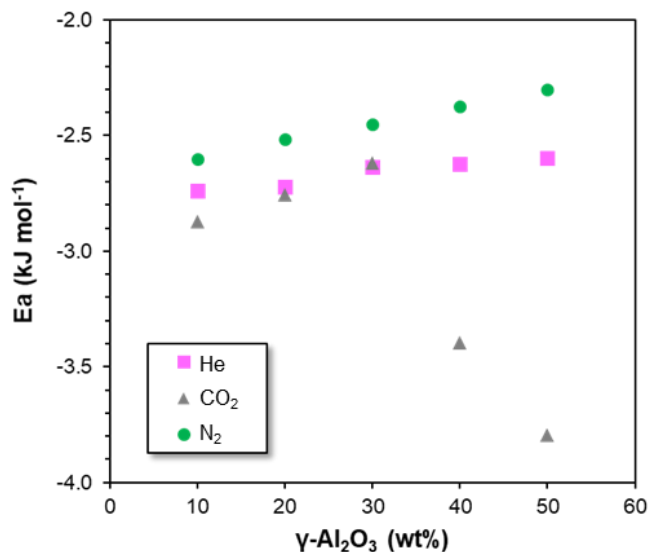
Figure 3.13. Calculated (lumped) activation energies for the permeation of different gases through the nanoporous layers as a function of the composition of the nanoporous layers.

3.4. Conclusions

Nanoporous YSZ/γ-Al_2O_3 membranes have been successfully prepared by a dip-coating technique onto α-Al_2O_3 supports. The parameters in the preparation of and the diffusion mechanisms of He, N_2 and CO_2 in the nano/mesoporous layers have been investigated in detail. The pore size of the nanoporous layers decreases when the amount of γ-Al_2O_3 increases, and consequently the viscous flow contribution decreases: at 400 °C the ideal perm-selectivity increases from ~2.2 with (10 wt% γ-Al_2O_3) to ~2.7 (50 wt% γ-Al_2O_3), whereas the ideal Knudsen perm-selectivity for He/CO_2 is 3.32. The He/CO_2 separation factor decreases for higher operating temperatures, which could be related to the increased contribution of surface diffusion of CO_2. Layers with a high content in γ-Al_2O_3 (40-50 wt%) have been employed for the preparation of pore-filled membranes onto α-Al_2O_3 supports, as is described in Chapter 4, and for double-skinned membranes (Chapter 5) due to the high surface area and small and narrow pore-size distribution.

Bibliography

[1]   F. Gallucci, M. van Sint Annaland, J.A.M. Kuipers, Theoretical comparison of packed bed and fluidized bed membrane reactors for methane reforming, Int. J. Hydrogen Energy. 35 (2010) 7142–7150.

[2]   D.A. Pacheco Tanaka, M.A. Tanco Llosa, T. Nagase, J. Okazaki, Y. Wakui, F. Mizukami, T.M. Suzuki, Fabrication of Hydrogen-Permeable Composite Membranes Packed with Palladium Nanoparticles, Adv. Mater. 18 (2006) 630–632. doi:10.1002/adma.200501900.

[3]   D.A. Pacheco Tanaka, M.A. Llosa Tanco, J. Okazaki, Y. Wakui, F. Mizukami, T.M. Suzuki, Preparation of "pore-fill" type Pd–YSZ–γ-Al2O3 composite membrane supported on α-Al2O3 tube for hydrogen separation, J. Memb. Sci. 320 (2008) 436–441. doi:10.1016/j.memsci.2008.04.044.

[4]   R.J. Wolf, M.W. Lee, J.R. Ray, Pressure-Composition Isotherms for Nanocrystalline Plladium Hydrode, Phys. Rev. Lett. 73 (1994) 557–560.

[5]   S. Tekeli, Influence of alumina addition on grain growth and room temperature mechanical properties of 8YSCZ/Al2O3 composites, Compos. Sci. Technol. 65 (2005) 967–972. doi:10.1016/j.compscitech.2004.10.024.

[6]   R. Sanz, J.A. Calles, D. Alique, L. Furones, S. Ordóñez, P. Marín, Hydrogen production in a Pore-Plated Pd-membrane reactor: Experimental analysis and model validation for the Water Gas Shift reaction, Int. J. Hydrogen Energy. 40 (2015) 3472–3484. doi:10.1016/j.ijhydene.2014.11.120.

[7]   T. Zhao, J. Okazaki, D.A. Pacheco Tanaka, T.M. Suzuki, Y. Wakui, Hydrogen separation with "pore-fill" type palladium membrane, in: AIChE Annu. Meet. Conf. Proc., 2011.

[8]   J. Okazaki, T. Ikeda, D. a. P. Tanaka, K. Sato, T.M. Suzuki, F. Mizukami, An investigation of thermal stability of thin palladium–silver alloy membranes for high temperature hydrogen separation, J. Memb. Sci. 366 (2011) 212–219.

[9]   J. Okazaki, T. Ikeda, D.A. Pacheco Tanaka, M.A. Llosa Tanco, Y. Wakui, K. Sato, F. Mizukami, T.M. Suzuki, Importance of the support material in thin palladium composite membranes for steady hydrogen permeation at elevated temperatures, Phys. Chem. Chem. Phys. 11 (2009) 8632–8638. doi:10.1039/B909401F.

[10]   J. Okazaki, T. Ikeda, D. a. P. Tanaka, M. a. L. Tanco, Y. Wakui, K. Sato, F. Mizukami, T.M. Suzuki, Strong Interaction at the Palladium/Alumina Interface of Membrane during Hydrogen Permeation at Elevated Temperature, Chem. Lett. 37 (2008) 1004–1005. doi:10.1246/cl.2008.1004.

[11]   E. Fernandez, A. Helmi, K. Coenen, J. Melendez, J.L. Viviente, D.A. Pacheco Tanaka, M. van Sint Annaland, F. Gallucci, Development of thin Pd–Ag supported membranes for fluidized bed membrane reactors including WGS related gases, Int. J. Hydrogen Energy. 40 (2015) 3506–3519.

[12]   Z. Ryu, J. Zheng, M. Wang, B. Zhang, Characterization of pore size distributions on carbonaceous adsorbents by DFT, Carbon N. Y. 37 (1999) 1257–1264. doi:10.1016/S0008-6223(98)00322-4.

[13]   Z.-H. Tan, X. Guo, Synthesis and characterization of highly dispersed YSZ particles with diameter ≤5nm, Ceram. Int. 41 (2015) 4953–4958. doi:10.1016/j.ceramint.2014.12.058.

[14]   M.I.F. Macedo, C.C. Osawa, C.A. Bertran, Sol-Gel Synthesis of Transparent Alumina Gel and Pure Gamma Alumina by Urea Hydrolysis of Aluminum Nitrate, J. Sol-Gel Sci. Technol. 30 (2004) 135–140.

[15]   G. Paglia, C. Buckley, A. Rohl, B. Hunter, R. Hart, J. Hanna, L. Byrne, Tetragonal structure model for boehmite-derived γ-alumina, Phys. Rev. B. 68 (2003) 144110. doi:10.1103/PhysRevB.68.144110.

[16]   A.W. Burton, K. Ong, T. Rea, I.Y. Chan, On the estimation of average crystallite size of zeolites from the Scherrer equation: A critical evaluation of its application to zeolites with one-dimensional pore systems, Microporous Mesoporous Mater. 117 (2009) 75–90. doi:10.1016/j.micromeso.2008.06.010.

[17]   R.E. Dinnebier, K. Friese, Modern XRD methods in mineralogy, Stuttgart, n.d.

[18]   R.J.R. Uhlhorn, M.H.B.J.H. In´t Veld, K. Keizer, A.J. Burggraaf, Synthesis if ceramic membranes. Part I: Synthesis of non-supported and supported γ-alumina membranes without defect, J. Mater. Sci. 27 (1992) 527–537.

[19]   R.M. De Vos, H. Verweij, Improved performance of silica membranes for gas separation, J. Memb. Sci. 143 (1998) 37–51.

[20]   E.S.P.B. V, K. Keizer, R.J.V.A.N. Vuren, A.J. Burggraaf, Gas separation mechanisms in microporous modified γ-Al2O3 membranes, J. Mebrane Sci. 39 (1988) 285–300.

[21]   K.S.W. Sing, D.H. Everett, R.A.W. Haul, L. Moscou, R.A. Pierotti, J. Rouquérol, T. Siemieniewska, Reporting physisortion data for gas/solid systems, Pure Appl. Chem. 57 (1985) 603–619.

Appendix A

The nitrogen adsorption/desorption isotherm of YSZ/γ-Al₂O₃ (50 wt./50 wt.%) samples calcined at 550 °C and 650 °C are shown in Figure A.1 (up). The isotherm profiles present a type IV shape according to IUPAC classification with a recognizable hysteresis loop typical for mesoporous materials [21]. The surface area decreased from 300 to 257 m² g⁻¹ as the calcination temperature was increased from 550 °C to 650 °C, both presenting similar pore size distributions (see Figure A.1, down).
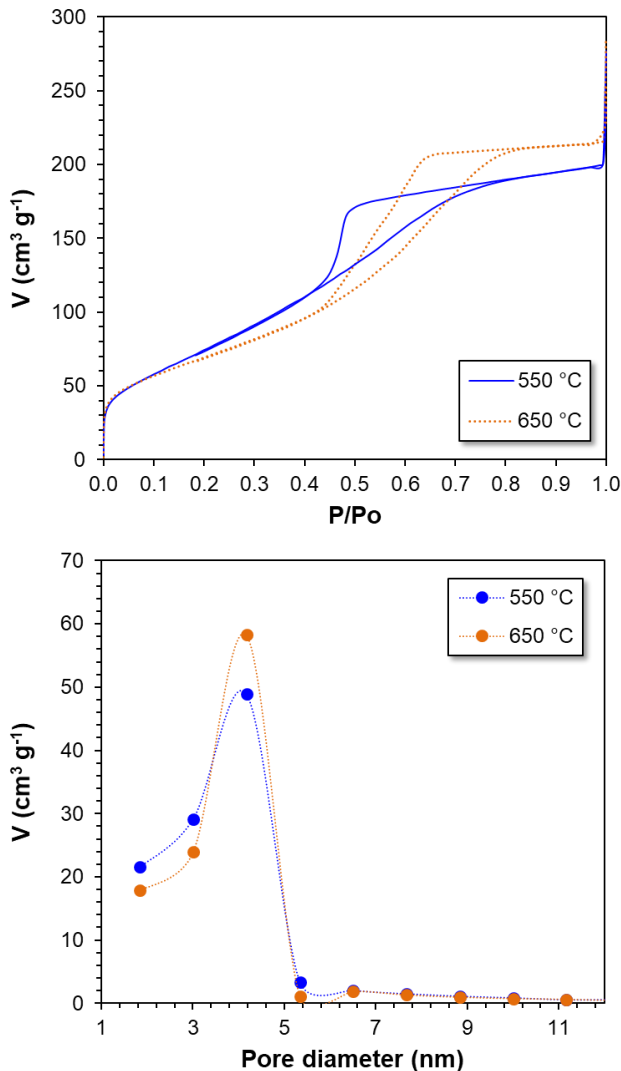
Figure A.1. Nitrogen isotherms and pore size distributions of YSZ/γ-Al₂O₃ powders (50 wt% YSZ) calcined in air at 550 °C and 650 °C for 3h.

According to the XRD patterns for samples (50 wt. % YSZ/50 wt. % γ-Al₂O₃) calcined at 550 °C or 650 °C, shown in Figure A.2, the peaks related to cubic YSZ become more intense and sharp when the calcination was carried out at 650 °C due to the crystal growth. It was calculated that the crystal size of YSZ increases from 1.7 nm to 3.5 nm as the calcination temperature increased from 550 °C to 650 °C. Peaks centered at ~45° and ~67° are related to amorphous γ-Al₂O₃ [14] and became also more intense when the sample was calcined at 650 °C.
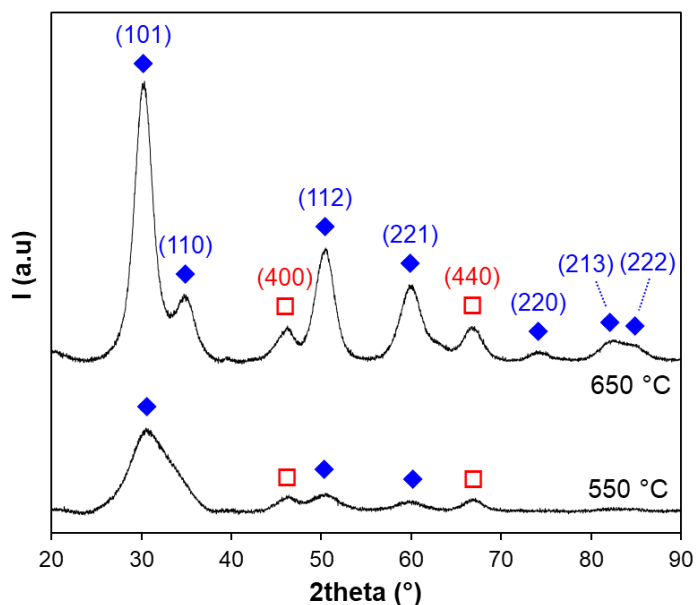
Figure A.2. XRD patterns of YSZ/γ-Al₂O₃ powders (50 wt% YSZ) calcined in air at 550 °C and 650 °C for 3h. (◆): $(ZrO_2)_{0.92}(Y_2O_3)_{0.08}$ (JCPDS 01-070-4431); (□) Gamma-Al₂O₃ (JCPDS 00-002-1420).
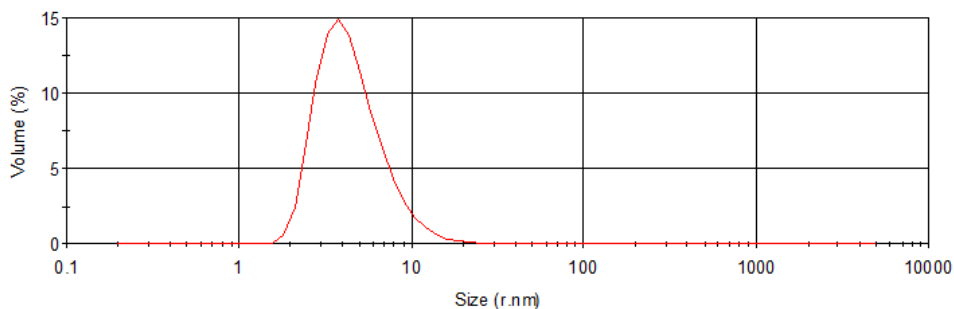
Figure A.3. Particle size distribution in volume of YSZ solution.
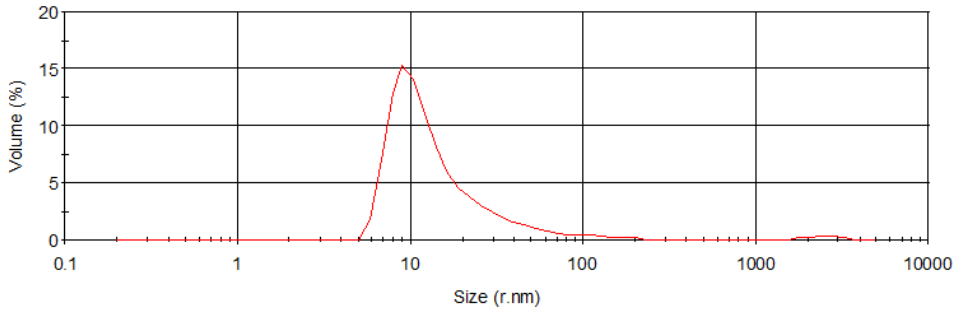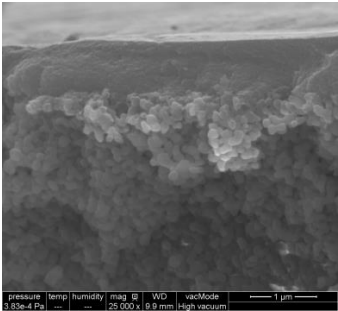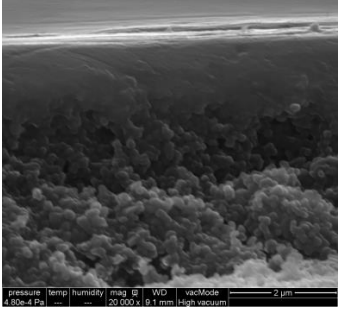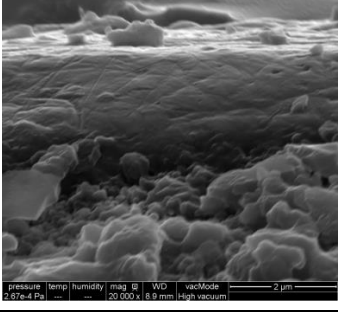
Figure A.4. Particle size distribution in volume of bohemite solution.

Table A.1. SEM cross section images of mesoporous layers with different proportions of YSZ (from 50 wt% to 90 wt%) deposited don top of α-Al₂O₃ support.

Mesoporous layer composition	SEM image (Cross section)	Amount of ceramics at sol. (wt. %)	Thickness (μm)
90%YSZ/10%γ-Al₂O₃		1.2	0.73
80%YSZ/20%γ-Al₂O₃		1.3	0.83

Table A.1. SEM cross section images of mesoporous layers with different proportions of YSZ (from 50 wt% to 90 wt%) deposited don top of α-Al2O3 support. (Continued)

Mesoporous layer composition	SEM image (Cross section)	Amount of ceramics at sol. (wt. %)	Thickness (μm)
70%YSZ/30%γ-Al$_2$O$_3$		1.4	1.29
60%YSZ/40%γ-Al$_2$O$_3$		1.5	1.57
50%YSZ/50%γ-Al$_2$O$_3$		1.6	1.92

Permeances of N_2, He and CO_2 are given at tables from Table A.2 to Table A.6 at different temperatures (50-400 °C) for all the mesoporous membranes.

Table A.2. PF-A111: 50 wt% YSZ-50 wt% γ-Al$_2$O$_3$ deposited on top of α-Al$_2$O$_3$ support (100 nm pore size). Deposited layer calcined at 550ᵒC during 3 h in air. Permeance values calculated at 100 kPa of pressure difference.

Gas	Permeance (10^{-6} mol m^{-2} s^{-1} Pa^{-1})				
	50 °C	100 °C	200 °C	300 °C	400 °C
He	17.66	15.47	13.26	11.64	10.49
N$_2$	6.71	6.10	5.24	4.69	4.29
CO$_2$	9.30	6.93	5.44	4.59	3.93

Table A.3. PF-A102: 60 wt% YSZ-40 wt% γ-Al$_2$O$_3$ deposited on top of α-Al$_2$O$_3$ support (100 nm pore size). Deposited layer calcined at 550ᵒC during 3 h in air. Permeance values calculated at 100 kPa of pressure difference.

Gas	Permeance (10^{-6} mol m^{-2} s^{-1} Pa^{-1})				
	50 °C	100 °C	200 °C	300 °C	400 °C
He	19.66	16.83	14.40	12.66	11.38
N$_2$	8.24	7.44	6.36	5.69	5.19
CO$_2$	8.93	7.39	6.00	5.27	4.79

Table A.4. PF-A62: 70 wt% YSZ-30 wt% γ-Al$_2$O$_3$ deposited on top of α-Al$_2$O$_3$ support (100 nm pore size). Deposited layer calcined at 550ᵒC during 3 h in air. Permeance values calculated at 100 kPa of pressure difference.

Gas	Permeance (10^{-6} mol m^{-2} s^{-1} Pa^{-1})				
	50 °C	100 °C	200 °C	300 °C	400 °C
He	21.43	18.63	15.91	13.91	12.50
N$_2$	10.02	9.02	7.67	6.83	6.22
CO$_2$	9.45	8.96	7.21	6.28	5.64

Table A.5. PF-A51: 80 wt% YSZ-20 wt% γ-Al$_2$O$_3$ deposited on top of α-Al$_2$O$_3$ support (100 nm pore size). Deposited layer calcined at 550ᵒC during 3 h in air. Permeance values calculated at 100 kPa of pressure difference.

Gas	Permeance (10^{-6} mol m^{-2} s^{-1} Pa^{-1})				
	50 °C	100 °C	200 °C	300 °C	400 °C
He	24.35	21.69	18.01	15.70	14.08
N$_2$	11.25	9.94	8.49	7.55	6.86
CO$_2$	10.31	9.49	7.81	6.80	6.08

Table A.6. PF-A65: 90 wt% YSZ-10 wt% γ-Al$_2$O$_3$ deposited on top of α-Al$_2$O$_3$ support (100 nm pore size). Deposited layer calcined at 550ᵒC during 3 h in air. Permeance values calculated at 100 kPa of pressure difference.

Gas	Permeance (10^{-6} mol m^{-2} s^{-1} Pa^{-1})				
	50 °C	100 °C	200 °C	300 °C	400 °C
He	25.59	24.03	19.84	17.26	15.46
N$_2$	13.11	11.45	9.77	8.65	7.85
CO$_2$	11.79	10.70	8.78	7.60	6.79

As an example, in Figure A.5 the permeance values of N_2, He and CO_2 versus average pressure (P_{ave}) are shown for one of the membranes (PF-A102: 60%YSZ-40% γ-Al_2O_3). From these graphs, slopes and intercepts are calculated. Tables from Table A.7 to

Table A.9 collect all the slopes and intercepts calculated for H_2, N_2 and CO_2 for all the membranes at different temperatures.
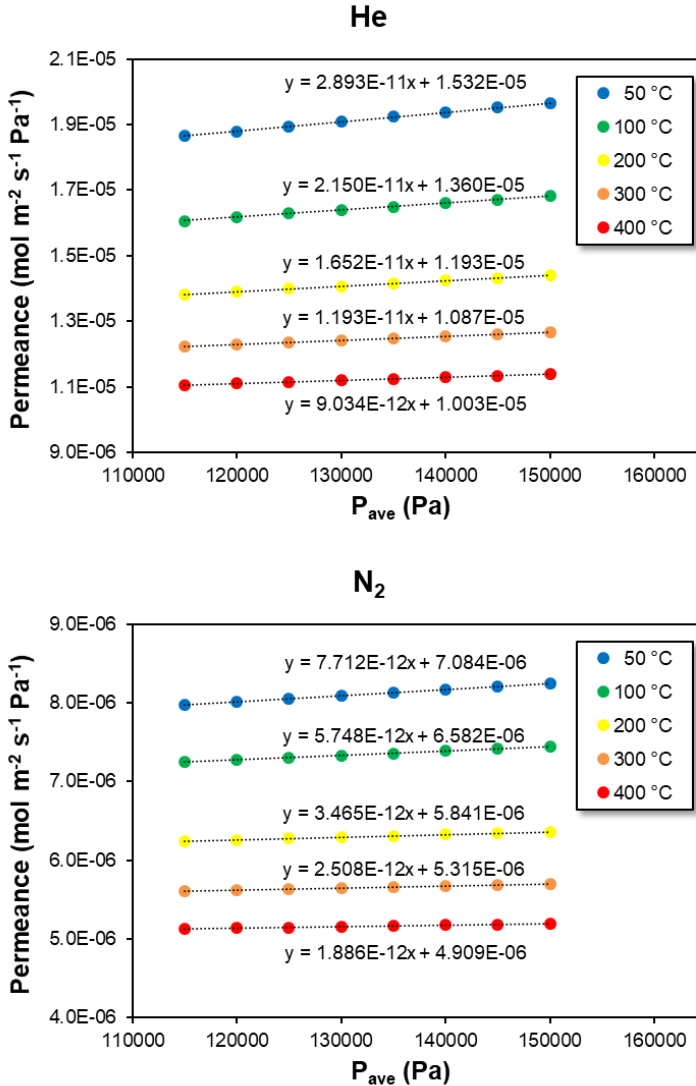
Figure A.5. He, N_2 and CO_2 permeances of PF-A102 (60%YSZ-40% γ-Al₂O₃) in the temperature range of 50-400 °C.

Table A.7. Calculates slopes and intercepts of mesoporous membranes with different proportions of YSZ at different temperatures for helium.

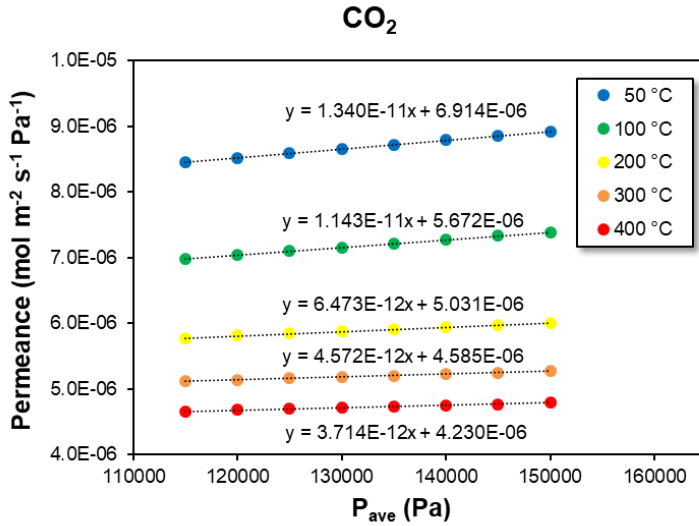| YSZ (wt%)	Slope (10^{-11} mol m^{-2} s^{-1} Pa^{-2})					Intercept (10^{-5} mol m^{-2} s^{-1} Pa^{-1})				
	50°C	100°C	200°C	300°C	400°C	50°C	100°C	200°C	300°C	400°C
50	2.785	1.966	1.423	1.024	0.767	1.348	1.252	1.112	1.011	0.933
60	2.895	2.150	1.652	1.193	0.903	1.532	1.360	1.193	1.087	1.003
70	3.819	2.698	1.937	1.427	1.068	1.571	1.460	1.300	1.178	1.089
80	4.594	5.597	2.345	1.694	1.282	1.746	1.630	1.449	1.316	1.216
90	4.332	4.227	2.766	2.000	1.512	1.912	1.769	1.569	1.426	1.319

Table A.8. Calculates slopes and intercepts of mesoporous membranes with different proportions of YSZ at different temperatures for nitrogen.

YSZ (wt%)	Slope (10^{-11} mol m^{-2} s^{-1} Pa^{-2})					Intercept (10^{-5} mol m^{-2} s^{-1} Pa^{-1})				
	50°C	100°C	200°C	300°C	400°C	50°C	100°C	200°C	300°C	400°C
50	0.525	0.396	0.242	0.177	0.135	0.593	0.550	0.488	0.443	0.409
60	0.771	0.575	0.347	0.251	0.189	0.708	0.658	0.584	0.532	0.491
70	1.090	0.807	0.487	0.346	0.262	0.839	0.781	0.694	0.631	0.583
80	1.428	0.972	0.631	0.456	0.350	0.910	0.847	0.755	0.687	0.633
90	1.620	1.229	0.822	0.595	0.457	1.064	0.961	0.854	0.776	0.716

Table A.9. Calculates slopes and intercepts of mesoporous membranes with different proportions of YSZ at different temperatures for carbon dioxide.

YSZ (wt%)	Slope (10^{-11} mol m^{-2} s^{-1} Pa^{-2})					Intercept (10^{-5} mol m^{-2} s^{-1} Pa^{-1})				
	50°C	100°C	200°C	300°C	400°C	50°C	100°C	200°C	300°C	400°C
50	1.404	0.930	0.547	0.357	0.267	0.720	0.553	0.462	0.406	0.353
60	1.340	1.143	0.647	0.457	0.371	0.691	0.567	0.503	0.459	0.423
70	1.556	1.558	0.882	0.617	0.461	0.712	0.663	0.589	0.536	0.495
80	1.843	1.638	1.038	0.731	0.556	0.755	0.703	0.626	0.571	0.525
90	1.921	1.975	1.270	0.897	0.674	0.889	0.774	0.688	0.625	0.578

Chapter 4

Pd-based pore-filled membranes for hydrogen separation

The permeation characteristics of palladium-based pore-filled (PF) membranes have been investigated with gas permeation and structural characterization of the membranes. PF membranes have been prepared by filling the nanoporous γ-Al$_2$O$_3$/YSZ (or pure YSZ) layer supported onto porous α-Al$_2$O$_3$ and ZrO$_2$ with Pd. The number of nanoporous layers and the applied vacuum level during the electroless plating process have been studied. Gas permeation properties of the PF membranes have been determined in a temperature range of 300-550 °C. The measured hydrogen permeances have been found to be lower than previously reported for similar membranes. It has been found that the hydrogen fluxes do not depend on the thickness of the nanoporous layers (γ-Al$_2$O$_3$/YSZ or pure YSZ) or on the vacuum pump employed for filling with Pd. The physicochemical characterization performed showed that the palladium deposited does not form a percolated network across the mesoporous layer(s), leading to low hydrogen permeances and thus low H$_2$/N$_2$ perm-selectivities.

"I have not failed. I've found 10000 ways that won't work".
Thomas Alva Edison.

4.1. Introduction

Several reports on the use of Pd-based membranes for hydrogen separation in fluidized bed membrane reactors have been published in the last few years [1–5]. When particles are in continuous contact with the (thin) hydrogen selective layer, depending on the gas velocity, particles can erode the membrane surface by creating pinholes, leading to a decrease in the membrane perm-selectivity. Pore-filled (PF) type membranes avoid direct contact of fluidized particles with the hydrogen selective material, since the Pd is located inside the nano-pores of the substrate [6], protected by a mesoporous layer composed of γ-Al_2O_3/YSZ or pure YSZ. Another advantage of this membrane configuration is that the embrittlement due to α-β phase transition is prevented due to the nanometric size of the palladium clusters, where the hydrogen loading preferentially occurs on the surface rather than on the interior of the particles [7].

It has been reported that, when Pd is filled in the nanopores composed of only γ-Al_2O_3 the membranes are not stable at temperatures above 400 °C due to the large difference in the thermal expansion coefficient of Pd and alumina; in addition, the hydrogen permeance of conventional Pd alloy membranes supported on alumina showed a decay when they were exposed to hydrogen at high temperature (650 °C) [8]. Inclusion of YSZ into the mesoporous layer diminishes the probability of alloying of Pd with alumina, while the thermal expansion is closer to that of palladium [9]. For these reasons, in Chapter 3 the study was focused on the preparation of nanoporous membranes made out of γ-Al_2O_3/YSZ with more than 50 wt% of YSZ for their use for pore-filled membranes.

In this chapter, the permeation properties of pore-filled membranes have been studied by varying the porous support material, thickness and composition of the nanoporous layers and the vacuum level applied during VA-ELP (vacuum-assisted electroless plating), among other parameters. The permeation properties of many membranes have been studied with single gas tests, while also a long-term test has been performed. Hydrogen fluxes were found to be lower than expected. Thus, a physicochemical characterization has been performed on a pore-filled membrane by electron tomography in order to understand why the hydrogen flux is so low.

4.2. Experimental

4.2.1. Membrane preparation

For the preparation of Pd pore-filled membranes, first the γ-Al_2O_3/YSZ layers were deposited onto porous α-Al_2O_3 (OD/ID 10/7 and 10/4 mm) with a pore size of 100 nm, provided by Rauschert Kloster Veilsdorf, according to the procedure reported in Chapter 3. After

modification with the mesoporous composite of YSZ/γ-Al$_2$O$_3$ (see step 1 in Figure 4.1), the tubular support was activated with nano-palladium nuclei by dipping it into a chloroform solution of palladium acetate (0.4 wt%) and applying vacuum from the inner part of the tube in order to fill the pores with the solution containing Pd^{2+}. The impregnated support was dried at 105 °C and subsequently reduced with a hydrazine solution (2M) at room temperature for 1-2 minutes (step 2 in Figure 4.1). The sample was afterwards cleaned with distilled water and dried for 1 h at 105 °C. This cycle was repeated until the surface of the modified support became black. Depending on the mass ratio of YSZ/γ-Al$_2$O$_3$ the number of cycles was varied between 6 to 8 times. This is clearly a procedure to be further optimized in a second stage of the work.
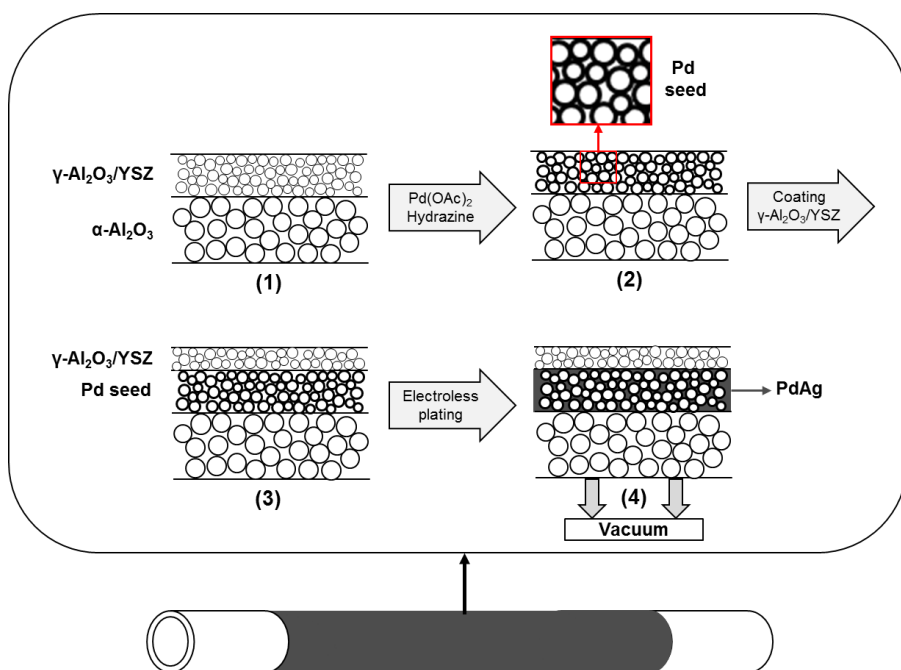
Figure 4.1. Schematic description of the preparation of Pd pore-filled membranes.

Once the activation was completed, the support was again coated with the composite as a protecting layer (third step in Figure 4.1), calcined and cooled down under 10 vol. % H$_2$/N$_2$ atmosphere. Afterward, the nano-palladium particles in the first mesoporous layer were forced to grow by vacuum-assisted electroless plating using a rotatory (Edwards RV3) and a turbomolecular pump (Edwards T-Station 75), where the maximum vacuum measured was $2 \cdot 10^{-2}$ mbar and $1 \cdot 10^{-6}$ mbar, respectively. Finally, the membrane was annealed at 550 °C for 4 hours under 10 vol. % H$_2$/90 vol. % N$_2$. The VA-ELP and annealing processes were repeated until the nitrogen leakage at room temperature of the membrane was below $8 \cdot 10^{-9}$

mol m^{-2} s^{-1} Pa^{-1} (this value is considered as the maximum acceptable value for preparing a good membrane). The composition of the electroless-plating bath is reported in Table 4.1.

Table 4.1. Composition of the electroless plating bath for pore-filled membranes.

Chemical	Concentration (M)
Palladium acetate	0.02
Ammonia	2
Phosphinic acid	0.004
Formic acid	0.1

The nanoporous layer was also deposited onto porous supports composed of asymmetric α-Al_2O_3 (OD/ID 10/7 mm) with an intermediate TiO_2 layer and a ZrO_2 top layer with 3 nm pore size (see Figure 4.2). In this case, the top porous support layer was first activated with palladium nuclei and then a protective layer of YSZ was deposited, which is possible owing to the similar thermal expansion coefficient with the top layer of the support (ZrO_2). Then, Pd nano-seeds were forced to grow by VA-ELP as in the case of the α-Al_2O_3 support, followed by the annealing process. As described for α-Al_2O_3 supports, the cycle (VA-ELP and annealing steps) was repeated until the nitrogen permeance was below 8·10^{-9} mol m^{-2} s^{-1} Pa^{-1}.
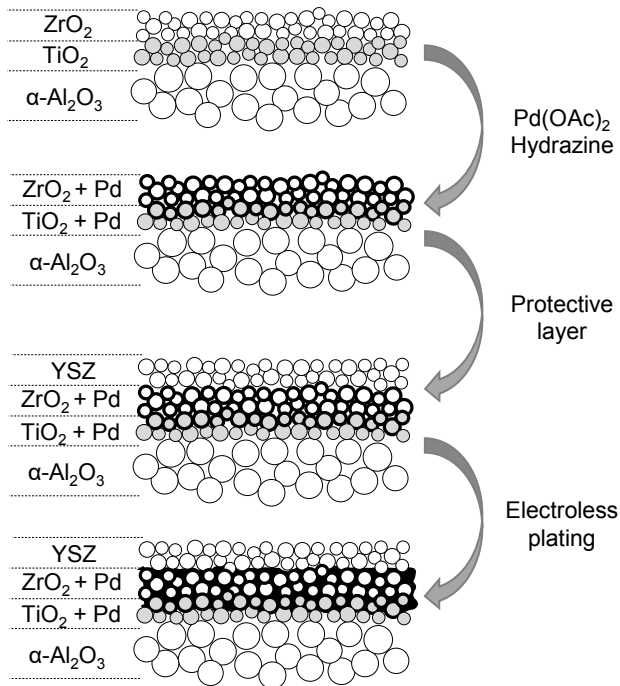

Figure 4.2. Schematic representation of the preparation of Pd pore-filled membranes using a porous α-Al_2O_3 support with an intermediate TiO_2 layer and a ZrO_2 top layer with a pore size of 3 nm.

Various vacuum levels were applied during the vacuum-assisted electroless plating (VA-ELP) step. A vacuum was applied at the inner side of the tubes in order to force the Pd^{2+} ions present in the plating solution to pass through the pores; therefore, the plating is carried out inside the pores where Pd (catalyst for the reaction) is present. As the vacuum level increased, the number of cycles (VA-ELP and annealing) needed to fill the pores decreased (see Table 4.2), so that the plating time can be increased while still avoiding growth of palladium on the surface.

Table 4.2. Capabilities of the vacuum pump during VA-ELP of pore-filled membranes.

Parameter	Rotatory pump	Turbomolecular pump
Measured pressure during ELP (mbar)	$2 \cdot 10^{-2}$	$1 \cdot 10^{-6}$
Number of VA-ELP steps	4-15	2-6
Plating time (min)	4-12	8-60

4.2.2. Gas permeation measurements

The membranes have been tested with pure gases (hydrogen or nitrogen) in an empty reactor in the temperature range of 300-550 °C and with a transmembrane pressure difference of 30-400 kPa. The setup used for single gas measurements was described in Chapter 3. The same set-up was used for the case of a long-term test (single gas test with H_2 or N_2) performed at 500 °C and 550 °C for up to 900 h. The pressure difference between the retentate and permeated sides (at atmospheric pressure) was regulated by a back-pressure regulator (Horiba Stec. UR-7340 model) at the retentate side. Permeated fluxes were measured with an automated soap film flow meter (Horiba STEC VP-1, VP-2 and VP-3).

4.2.3. Characterization

The membrane thickness was measured using cross-sectional images with a SEM (FEI Quanta 250 FEG). The carbon content has been determined by the infrared absorption method after combustion in an induction furnace using a CS400 LECO analyzer, where the produced CO_2 volume was measured.

Preparation of a sample for the transmission electron microscope (TEM) was undertaken using a Thermo Scientific Helios 660 focused ion beam (FIB) dual-beam instrument. A cross-sectional sample was taken from the surface of a cut sample, using a 30 kV Ga ion beam to prepare an approximately 150 nm thick lamella.

Characterization of the Pd distribution was carried out with a Thermo Scientific Talos F200A scanning transmission electron microscope (STEM), possessing a high brightness X-FEG electron source and Super-X energy dispersive X-ray (EDX) silicon drift detectors (SDDs). The microscope was operated at an accelerating voltage of 200 kV with a beam

current of 260 pA, a convergence angle of 12 mrad and a HAADF acceptance inner angle of 50 mrad. EDX spectrum images were acquired with the Thermo Scientific Velox software (version 1.6.0), with a total per pixel dwell time of approximately 2.5 ms and an image size of 387 × 439 pixels. A tilt series for HAADF-STEM tomography was acquired using Xplore3D acquisition software at angular increments of 1° from −75° to +75°. Image alignment was performed using patch tracking in the IMOD software package, followed by the use of a simultaneous reconstruction technique (SIRT) to perform the reconstruction with 20 iterations. Segmentation of Au and Pd voxels was performed using an auto threshold in Avizo. Visualization of the 3D reconstructions was also performed in the Avizo software package.

4.3. Results and discussion

4.3.1. Nanoporous membrane characterization

The thickness of the supported nanoporous membranes prepared with just the protective layer, and membranes with three mesoporous layers (the first two layers with palladium seeding and the third one as a protective layer), have been characterized with cross-section SEM (see Figure 4.3). Table 4.3 summarizes the configuration and thickness of some nanoporous membranes that have been prepared with different support materials (α-Al$_2$O$_3$ and ZrO$_2$). As has been in explained in Chapter 3, relatively thick (> 3 µm) γ-Al$_2$O$_3$/YSZ nanoporous layers that possess a high content of YSZ but without cracks are very difficult to be obtained. Therefore, for layers with a high YSZ content, thinner membranes should be prepared. For this reason, the thickness of a single layer made of pure YSZ (PF-Z2) was only 0.31 µm, while membranes with three layers made of 50 wt% YSZ possess thicker layers (2.47-3.27 µm). The difference in the thickness of samples with three layers could be related to a non-uniform layer formed during the drying process. The tubes have to turn horizontally in order to get a homogenous layer. A small curvature in the support (junction between porous and dense ceramic tubes, see preparation section in Chapter 3) can lead to variations in the thickness of the layers.
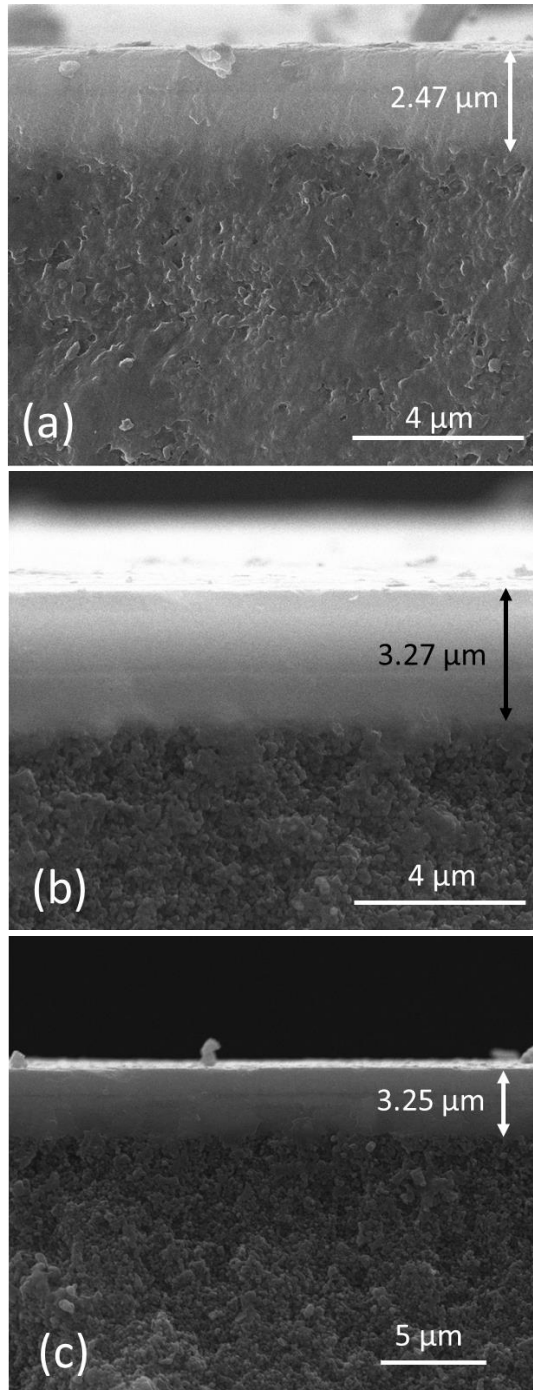
Figure 4.3. SEM cross section images of PF-A133 (a), PF-145 (b) and PF-155 (c).

Table 4.3. YSZ/γ-Al$_2$O$_3$ nanoporous layers prepared on α-alumina (100 nm pore size) and zirconia (3 nm pore size) supports.

Membrane	Mesoporous layer(s)			
	Number of layers*	YSZ content (wt%)	Calcination temperature (°C)	Thickness (μm)
PF-A45	2	60	550	2.04 ± 0.10
PF-A133	3	50	550	2.47 ± 0.12
PF-A145	3	50	550	3.27 ± 0.04
PF-A155	3	50	550	3.25 ± 0.12
PF-A172	3	50	550	2.94 ± 0.12
PF-Z2	1	100	550	0.31 ± 0.02

* Membranes with two or three layers means that resp. one and two layers were prepared before seeding and then the protective layer was deposited. For membranes with one layer, the supports were seeded and the protective layer was deposited on top.

Pacheco Tanaka et al. reported the preparation of Pd-PF membranes with a γ-Al$_2$O$_3$/YSZ (50 wt% YSZ) nanoporous layer supported using symmetric alumina capillary tubes (OD: 2 mm) with 150 nm pore size; using this support, a 3 μm thick γ-Al$_2$O$_3$/YSZ layer was obtained in only one dipping calcination process [6]. In the current study, asymmetric alumina tubes were used and several attempts were carried out to prepare γ-Al$_2$O$_3$/YSZ layers with a similar thickness to those reported by Pacheco Tanaka without defects, however, without success. This indicates the importance of the support in the preparation of the Pd pore-filled membranes.

4.3.2. Pd pore-filled membrane

The nitrogen permeation of the PF-membranes has been measured at room temperature after each VA-ELP and annealing step. The gas permeation properties (H$_2$ and N$_2$) of the PF-membranes with a nitrogen permeance lower than $8 \cdot 10^{-9}$ mol m^{-2} s^{-1} Pa^{-1} at room temperature were tested in the temperature range of 300-550 °C. In Table 4.4 the characteristics of the prepared membranes, their permeation properties and the number of VA-ELP cycles required to reach the desired maximum N$_2$ permeance are listed. Membranes prepared using α-Al$_2$O$_3$ as a support need a larger number of cycles when a rotatory pump was employed (from 8 to 12), while with turbomolecular pump lower nitrogen permeances was obtained with fewer cycles (from 2 to 6). Some membranes have been prepared using both types of pumps, where the required number of cycles was in between what was required when using the same pump (from 6 to 10). This is related to the suction level of each pump. The turbomolecular pump allows performing the electroless plating for longer periods compared to the rotatory pump, while still avoiding the growth of palladium on the surface. On the other hand, the number of VA-ELP cycles does not depend on the number of mesoporous layers, composition or calcination temperature, as can be concluded from Table 4.4.

The measured hydrogen permeance and ideal H_2/N_2 perm-selectivity of the membranes summarized in Table 4.4 are also plotted in Figure 4.4. The ideal perm-selectivity is defined as the radio of the permeability of two gas species, $\alpha_{ab}=Pe_{(a)}/Pe_{(b)}$, measured separately under identical conditions. It can be observed that the performance of the membranes is not directly related to the thickness of the mesoporous layers or the number of platings performed before the permeation test. The best performance (in terms of hydrogen permeance) was obtained for a membrane prepared onto an Al_2O_3 support, viz. PF-A135, containing three mesoporous layers (where the third layer acts as a protective layer), with a hydrogen permeance of $\sim 3.63 \cdot 10^{-6}$ mol m^{-2} s^{-1} Pa^{-1} at 550 °C and an ideal perm-selectivity of ~ 478. However, this value is too low for the implementation of these membranes for reactors/separators for hydrogen production with high purity. In addition, the number of VA-ELP steps performed to reach this selectivity (low N_2 leakage) was 8, which is not feasible for industrial scale production because of the thermal treatment (annealing) that has to be repeated after each VA-ELP step. Moreover, other membranes showed lower hydrogen permeances, reaching values around 10^{-8}-10^{-9} mol m^{-2} s^{-1} Pa^{-1}, which are much lower than those obtained by Pacheco Tanaka et al. [6,10].

Table 4.4. Summary of tested membranes with nitrogen permeance below $8 \cdot 10^{-9}$ m^{-2} s^{-1} Pa^{-1}.

Membrane	Support			Nano-porous layer(s)			VA-ELP		Permeation properties			
	Material	Pore size (nm)	OD/ID (mm)	Number of layers[a]	YSZ content (wt%)	Calcination temp. (°C)	Pump[b]	Number of cycles[c]	Temp. (°C)	ΔP (bar)	H$_2$ permeance (mol m^{-2} s^{-1} Pa^{-1})	H$_2$/N$_2$
PF-A15	α-Al$_2$O$_3$	100	10/7	2	60	550	R	8	400	1	$8.27 \cdot 10^{-8}$	20
PF-A41	α-Al$_2$O$_3$	100	10/7	2	50	550	R	7	400	1	$7.02 \cdot 10^{-8}$	72
PF-A45	α-Al$_2$O$_3$	100	10/7	2	60	550	R	9	400	1	$1.95 \cdot 10^{-7}$	27
PF-A135	α-Al$_2$O$_3$	100	10/7	3	50	650	R	8	550	0.3	$3.63 \cdot 10^{-6}$	478
PF-A137	α-Al$_2$O$_3$	100	10/7	2	50	550	R	12	550	1	$8.87 \cdot 10^{-7}$	552
PF-A144	α-Al$_2$O$_3$	100	10/7	3	50	550	R+T	6	300	1	$2.50 \cdot 10^{-7}$	777
PF-A146	α-Al$_2$O$_3$	100	10/7	3	50	550	R+T	10	550	3	$7.72 \cdot 10^{-8}$	56
PF-A157	α-Al$_2$O$_3$	100	10/7	1	50	550	T	6	300	3	$6.06 \cdot 10^{-8}$	246
PF-A170	α-Al$_2$O$_3$	100	10/4	3	50	550	T	4	300	1	$4.23 \cdot 10^{-8}$	20
PF-A172	α-Al$_2$O$_3$	100	10/4	3	50	550	T	2	300	2	$6.28 \cdot 10^{-9}$	12
PF-Z2	ZrO$_2$	3	10/7	1	100	650	R	15	400	1	$8.00 \cdot 10^{-8}$	62
PF-Z13	ZrO$_2$	3	10/7	1	100	650	R	4	300	1	$1.60 \cdot 10^{-7}$	90
PF-Z16	ZrO$_2$	3	10/7	1	100	650	R	4	400	1	$1.64 \cdot 10^{-7}$	850
PF-Z16 (2)[d]	ZrO$_2$	3	10/7	1	100	650	R	4	400	1	$1.29 \cdot 10^{-7}$	375

[a] Membranes with 2 and 3 layers means that 1 and 2 layers were prepared before seeded and then the protective layer was deposited. For membranes with one layers, the supports were seeded and the protective layers was deposited on top.

[b] R: Rotatory pump. T: turbomolecular pump.

[c] Each cycle is referred to the VA-ELP process and the annealing treatment.

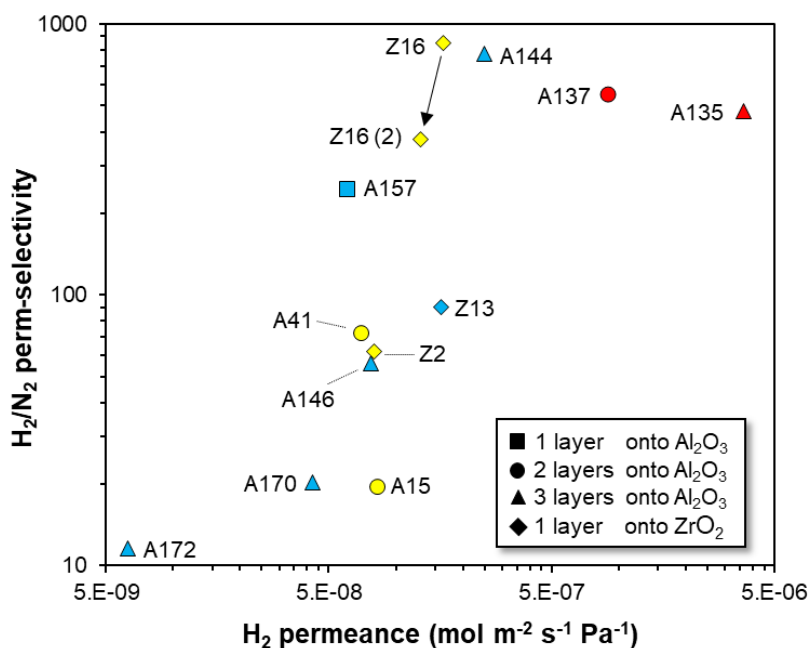[d] Permeation after keeping membrane Z16 under N$_2$ at 400 °C overnight.

Figure 4.4. Hydrogen permeance and ideal H_2/N_2 perm-selectivity of tested pore-filled membranes with different numbers of mesoporous layers and different support materials. Symbol colors refer to the testing temperature: 300 °C (blue), 400 °C (yellow) and 550 °C (red).

For the case of ZrO_2 supports with a top layer pore size of 3 nm, a single mesoporous layer of pure YSZ was deposited thanks to the thermal stability of ZrO_2 and YSZ in the presence of H_2 at high temperature in comparison with alumina [8]. In this case, the membranes tested have been prepared using the rotary pump (using 4 to 15 cycles). Membranes PF-Z2, PF-Z13 and PF-Z16 showed H_2 permeances around $\sim 1 \cdot 10^{-7}$ mol m^{-2} s^{-1} Pa^{-1} at 300-400 °C (see Table 4.4). The best results were observed for PF-Z16 with an ideal H_2/N_2 perm-selectivity of 850. However, after keeping the membrane under nitrogen overnight, the H_2 permeance decreased to 40% of the initial value, indicated in Figure 4.4 as Z16(2). This decay is attributed to the presence of a TiO_2 layer between the ZrO_2 top layer and the α-Al_2O_3 of the support (see Figure 4.2). During the preparation of the pore-filled membranes, palladium can come into contact with the TiO_2 and fill the pores of the TiO_2 layer. Strong interaction between Pd and TiO_2 was observed before by Fernandez et al. [3], when a conventional Pd-based membrane was brought into contact with TiO_2 particles during the water-gas-shift reaction in a fluidized bed Pd membrane reactor. Under H_2 and at high temperature in the presence of Pd, TiO_2 can be reduced to Ti metal, forming a Pd-Ti alloy with a low H_2 permeation [11].

A PF-membrane prepared onto an alumina support (100 nm pore size) with two mesoporous layers of 60 wt% YSZ was tested in a long-term test for 900 h. The measured thickness was about 2 µm in total. The palladium is located in between the mesoporous layers. However, most of the palladium is at the first micrometer of the mesoporous layer as can be observed in Figure 4.5, indicated with the purple line. The blue line refers to zirconium and it can be seen that the presence of this element decreases as the amount of palladium is larger. At the mesoporous layer, the presence of alumina is increasing, as the analysis line goes to the support (α-Al$_2$O$_3$).

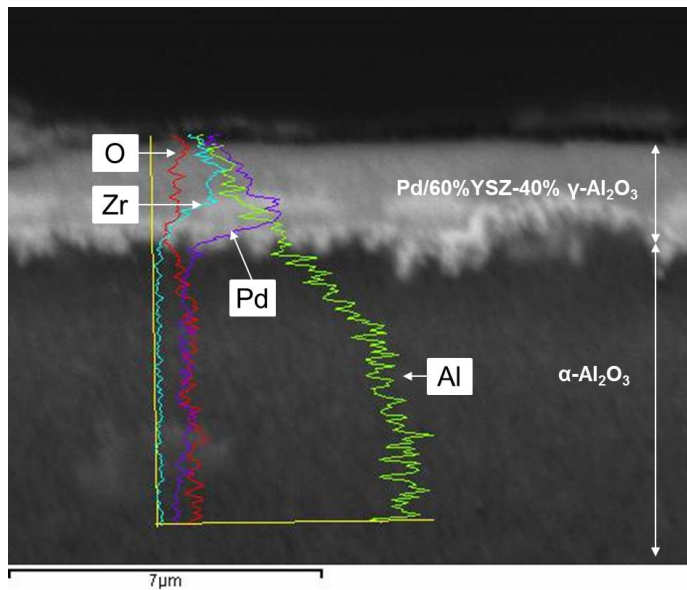Figure 4.5. Cross-sectional SEM images of the pore-filled Pd/YSZ/γ-Al$_2$O$_3$ (60 wt.% YSZ) membrane with EDX line profiles of different elements present in the membrane (post-mortem).

The hydrogen and nitrogen permeation was monitored at 500 °C and 550 °C under 50 kPa of trans-membrane pressure difference (Figure 4.6). For a period of 340 hours, single gas tests were performed at 500 °C. During this period, both hydrogen and nitrogen permeation rates were increasing while the selectivity decreased. Then, the operating temperature was increased to 550 °C. Since that moment the performance of the membrane was the same as before at 500 °C; the hydrogen and nitrogen permeance increased while the perm-selectivity decreased until about 20. However, after 600 hours a sudden increase in the H$_2$ permeation rate was observed (due to higher purity in the hydrogen used for the test). After that, the hydrogen flux continued increasing while the nitrogen permeance decreased. At the end of the experiment the hydrogen and nitrogen permeance at 550 °C and 50 kPa of pressure difference were $1.76 \cdot 10^{-7}$ and $3.5 \cdot 10^{-9}$ mol m^{-2} s^{-1} Pa^{-1}, respectively, corresponding to an increase in the ideal perm-selectivity to approximately 50. Although these values are very low

for Pd-based membranes, it can be concluded that the pore-filled type membrane is stable at the investigated operating temperatures for 900 hours.
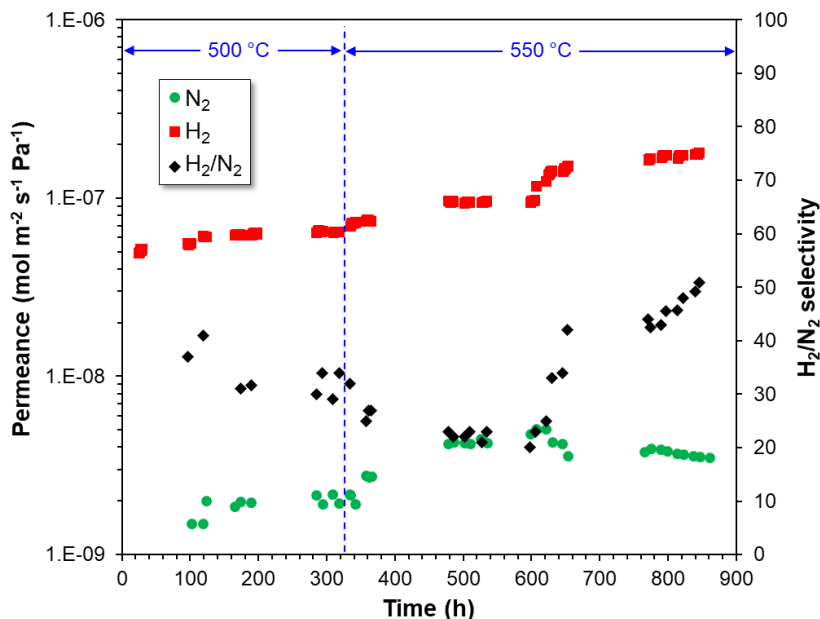

Figure 4.6. Long-term permeation test of the pore-filled Pd/YSZ/γ-Al$_2$O$_3$ (60 wt% YSZ) type membrane performed during 900 h at 500 °C and 550 °C in pure hydrogen and nitrogen.

In order to understand why the hydrogen flux is so low, the permeation properties of two membranes, PF-A137 and PF-A146, prepared with the rotary pump and both the rotatory and turbomolecular pumps respectively, have been measured as a function of the number of VA-ELP and annealing cycles. As shown in Figure 4.7, after a number of cycles the N$_2$ and H$_2$ fluxes decrease. After several cycles, the nitrogen leakage decreases to $1 \cdot 10^{-9}$ mol m^{-2} s^{-1} Pa^{-1}, while the hydrogen permeation continues to decrease, resulting in ideal perm-selectivities of ~552 (PF-A137) and ~56 (PF-A146). Lower H$_2$ fluxes are expected if more cycles are repeated in order to decrease the N$_2$ flux. To answer why the hydrogen permeances are so low (in many cases even in the order of 10^{-8}-10^{-9} mol m^{-2} s^{-1} Pa^{-1} as shown in (Table 4.4), a physicochemical characterization of the PF-membranes has been performed.
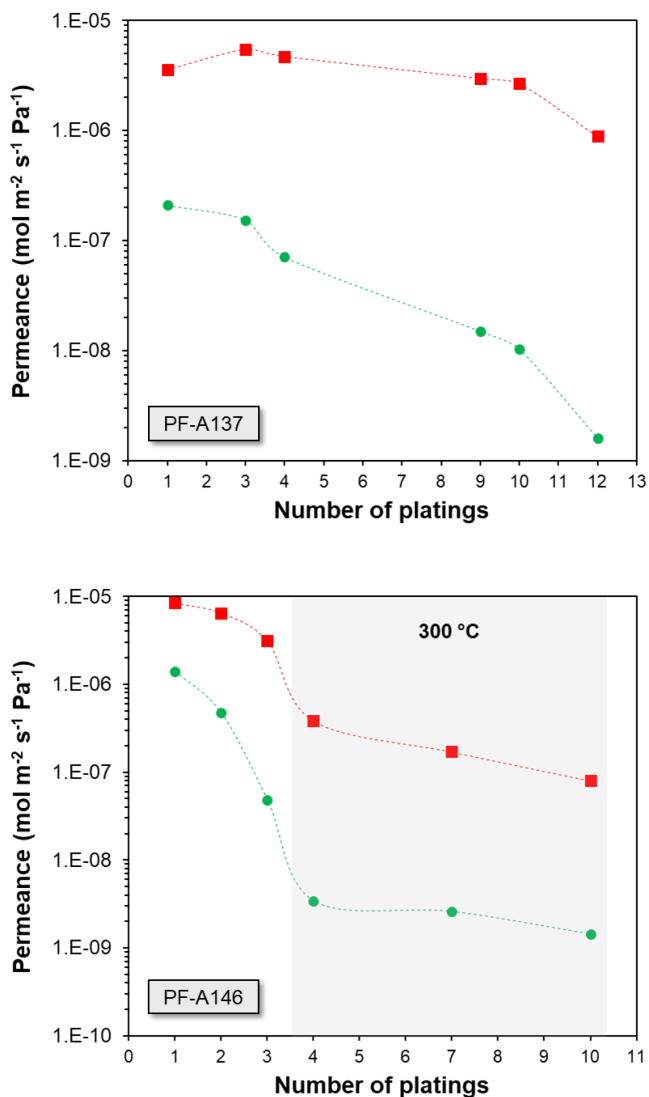
Figure 4.7. H_2 (squares) and N_2 (circles) permeances of pore-filled membranes PF-A137 (up) and PF-A146 (down) measured at 550 °C.

One reason for the low H_2 flux could be the formation of carbon (which blocks the hydrogen transport through the membrane) during the annealing process due to the chemicals employed during the preparation of the membranes. The carbon content of a membrane was investigated by carbon analysis undertaken by CO_2 infrared detection. The amount of carbon measured was 0.013 wt%, which is sufficiently low to exclude carbon formation as cause for the low H_2 permeance of the membranes.

The microstructure of the PF membranes has been characterized in more detail by TEM electron tomography. The three nano-porous layers deposited in the membrane PF-A172 have been observed by HAADF-STEM (high-angle annular dark-field scanning transmission electron microscope) imaging (see Figure 4.8a). According to STEM-EDX analysis, the top layer contains almost no Pd, which is expected in the protective layer as the Pd seeds were not deposited in this layer. The second layer contains a small number of discrete particles and the bottom layer contains a large number of discrete Pd particles (see Figure 4.8b). There are interfaces of approximately 10-20 nm between each layer and the one between the second and bottom layers is rich in Pd, which is due to the presence of a higher concentration of Pd seeds in the pores of the interphases. The Al (Figure 4.8c) and Zr (Figure 4.8d) concentrations were approximately constant through the membrane. These results are fairly clear from the 2D images. In addition, the non-percolated palladium network along the mesoporous layers has been confirmed by STEM tomography (Figure 4.9). The 3D reconstruction validates that although small clusters of Pd particles are interconnected at the interface between the two layers, they are in general discrete and do not form an interconnected network. However, the resolution of the STEM tomography in this case is approximately 5-10 nm and therefore it could be possible that the interconnections smaller than 5 nm are not resolved. Higher resolution imaging in 2D at thin regions of the sample confirms that the larger Pd nanoparticles are not connected and supports the tomography data (Figure 4.10). The results of STEM imaging suggest that hydrogen molecules need to split and recombine several times before passing through the membrane, thus resulting in a low hydrogen transport, much lower than expected.

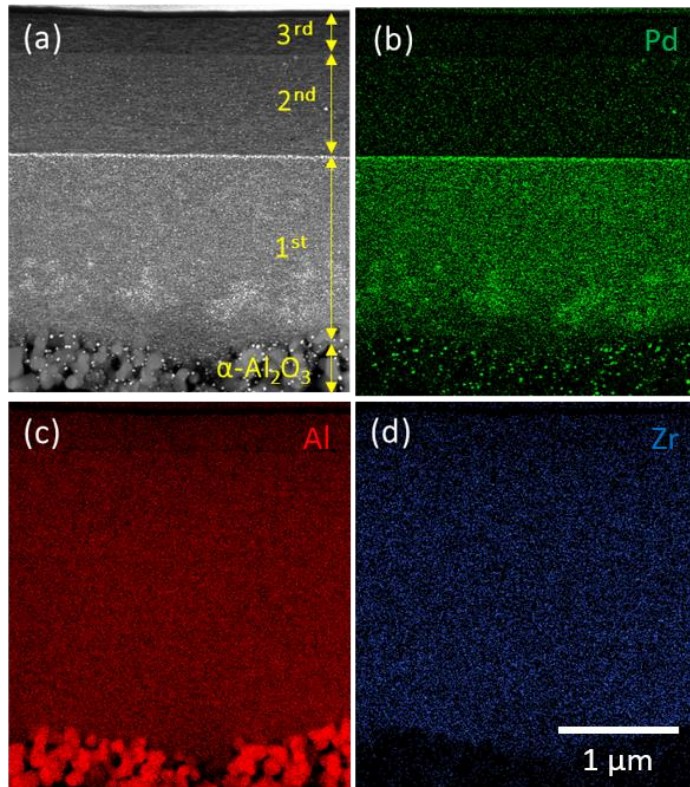Figure 4.8. HAADF STEM cross section image of PF-A172 (a) and STEM-EDX mapping of Pd (b), Al (c) and Zr (d).
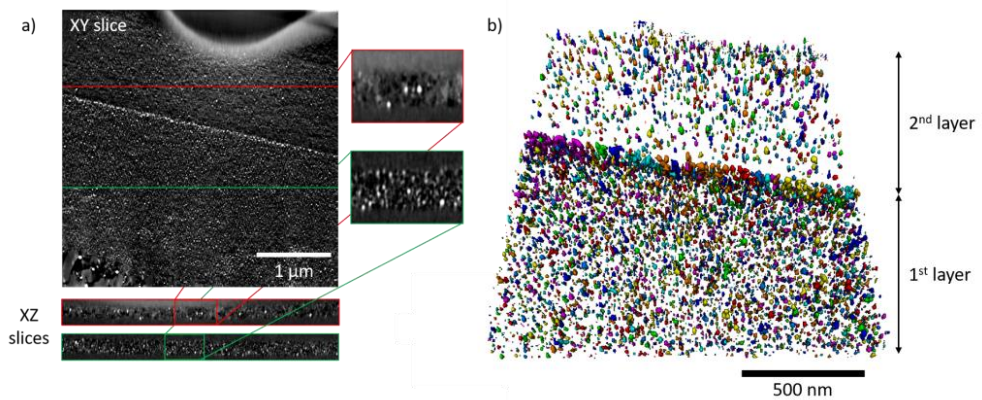

Figure 4.9. A 3D reconstruction of Pd obtained by STEM tomography. a) Slices through the reconstruction (in both the XY and XZ directions) showing the discrete nature of the Pd nanoparticles with magnified regions of the XZ slices. b) Volume rendering of the segmented Pd nanoparticles.
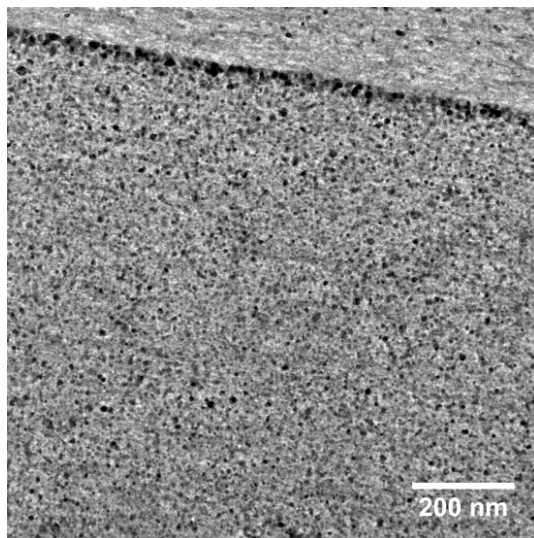
Figure 4.10. TEM image showing two distinct layers and the isolated Pd nanoparticles within these layers.

The observed microstructure does not yet explain why the palladium grains do not grow to an interconnected structure. This requires additional research efforts, as the PF membranes are still very interesting, considering that the amount of palladium used in the pore-filled membrane is a small fraction of that used for conventional supported membranes. In order to maintain the protective characteristics of the mesoporous layer, another membrane concept was developed, the so-called double-skinned (DS) membrane, where a conventional supported Pd-based membrane is protected with a mesoporous ceramic layer (see Chapter 5 and 6).

4.4. Conclusions

The permeation properties of several pore-filled membranes for hydrogen separation have been studied in detail in order to understand why the hydrogen flux and thus the ideal perm-selectivity are much lower than expected. Membranes with different support materials and different numbers of nanoporous layers have been prepared using different vacuum levels for the VA-ELP. It has been observed that the permeation properties of the membranes are not directly related to the number of nanoporous layers and the applied vacuum level for ELP. It has been concluded by electron tomography analysis that the main reason for the low hydrogen flux through the membranes is that the Pd does not form an interconnected network across the mesoporous layers. Hence, the hydrogen needs to split and recombine several times along the palladium clusters created throughout the porous media. Further studies need to be carried out to investigate why the palladium grains grow without connection to each other.

Bibliography

[1]   A. Helmi, E. Fernandez, J. Melendez, D. Pacheco Tanaka, F. Gallucci, M. van Sint Annaland, Fluidized Bed Membrane Reactors for Ultra Pure H2 Production—A Step forward towards Commercialization, Molecules. 21 (2016) 376. doi:10.3390/molecules21030376.

[2]   J.A. Medrano, E. Fernandez, J. Melendez, M. Parco, D.A.P. Tanaka, M. van Sint Annaland, F. Gallucci, Pd-based metallic supported membranes: High-temperature stability and fluidized bed reactor testing, Int. J. Hydrogen Energy. (2015) 1–13. doi:10.1016/j.ijhydene.2015.10.094.

[3]   E. Fernandez, A. Helmi, K. Coenen, J. Melendez, J.L. Viviente, D.A. Pacheco Tanaka, M. van Sint Annaland, F. Gallucci, Development of thin Pd–Ag supported membranes for fluidized bed membrane reactors including WGS related gases, Int. J. Hydrogen Energy. 40 (2015) 3506–3519.

[4]   E. Fernandez, A. Helmi, J.A. Medrano, K. Coenen, A. Arratibel, J. Melendez, N.C.A. de Nooijer, V. Spallina, J.L. Viviente, J. Zuñiga, M. van Sint Annaland, D.A. Pacheco Tanaka, F. Gallucci, Palladium based membranes and membrane reactors for hydrogen production and purification: An overview of research activities at Tecnalia and TU/e, Int. J. Hydrogen Energy. 42 (2017) 13763–13776. doi:10.1016/j.ijhydene.2017.03.067.

[5]   E. Fernandez, K. Coenen, A. Helmi, J. Melendez, J. Zu??iga, D.A. Pacheco Tanaka, M. Van Sint Annaland, F. Gallucci, Preparation and characterization of thin-film Pd-Ag supported membranes for high-temperature applications, Int. J. Hydrogen Energy. 40 (2015) 13463–13478. doi:10.1016/j.ijhydene.2015.08.050.

[6]   D.A. Pacheco Tanaka, M.A. Llosa Tanco, J. Okazaki, Y. Wakui, F. Mizukami, T.M. Suzuki, Preparation of "pore-fill" type Pd–YSZ–γ-Al2O3 composite membrane supported on α-Al2O3 tube for hydrogen separation, J. Memb. Sci. 320 (2008) 436–441. doi:10.1016/j.memsci.2008.04.044.

[7]   R.J. Wolf, M.W. Lee, J.R. Ray, Pressure-composition isotherms for nanocrystalline palladium hydride, Phys. Rev. Lett. 73 (1994) 557–562.

[8]   J. Okazaki, T. Ikeda, D.A. Pacheco Tanaka, M.A. Llosa Tanco, Y. Wakui, K. Sato, F. Mizukami, T.M. Suzuki, Importance of the support material in thin palladium composite membranes for steady hydrogen permeation at elevated temperatures., Phys. Chem. Chem. Phys. 11 (2009) 8632–8638. doi:10.1039/b909401f.

[9]   S. Tekeli, Influence of alumina addition on grain growth and room temperature mechanical properties of 8YSCZ/Al2O3 composites, Compos. Sci. Technol. 65 (2005) 967–972. doi:10.1016/j.compscitech.2004.10.024.

[10]   D.A. Pacheco Tanaka, M.A. Tanco Llosa, T. Nagase, J. Okazaki, Y. Wakui, F. Mizukami, T.M. Suzuki, Fabrication of Hydrogen-Permeable Composite Membranes Packed with Palladium Nanoparticles, Adv. Mater. 18 (2006) 630–632. doi:10.1002/adma.200501900.

[11]   Y. Huang, R. Dittmeyer, Preparation and characterization of composite palladium membranes on sinter-metal supports with a ceramic barrier against intermetallic diffusion, J. Memb. Sci. 282 (2006) 296–310. doi:10.1016/j.memsci.2006.05.032.

Chapter 5

Development of double-skin membranes for H$_2$ production in a FBMR

The preparation and performance characterization of new PdAg supported membranes with a porous protecting layer are presented in this chapter. Supported membranes with a selective layer of 1 μm and a protective mesoporous layer have been prepared. Outstanding H$_2$ permeance (5·10^{-6} mol m^{-2} s^{-1} Pa^{-1}) and H$_2$/N$_2$ perm-selectivity (over 25000) were measured at 400 °C and 1 bar of pressure difference. One membrane has been tested for more than 750 h in the presence of fluidized glass beads showing a decay in the perm-selectivity to approximately 5000, mainly due to the sealing leakages. However, the protective layer was removed during this long-term test. Another membrane has been tested for more than 2000 h in a fluidized bed membrane reactor with a Rh reforming catalyst supported on promoted alumina in the bubbling fluidization regime. During tests with binary mixtures mass transfer limitations toward the membrane were observed as a result of the large H$_2$ permeance of the membranes.

"There is a driving force more powerful than steam, electricity and nuclear power: the will".
Albert Einstein.

5.1. Introduction

Industrial exploitation of membrane-assisted fluidized bed membrane reactors is affected by the hydrogen production capacity and the required number of membranes, which depends on the thickness of the selective layer. Self-supported membranes would require an enormous number of membranes, whereas thin-film supported membranes seem to be the most interesting option. The thinner the layer, the larger the permeated H_2 flux and thus the smaller the required membrane area (thus having a double benefit in terms of Pd costs). Nevertheless, thin layers (< 4-5 µm) generally are not perfectly dense and often present a few small pores where other gases could pass through, decreasing the purity of the permeated hydrogen. Even if the membranes exhibit a high perm-selectivity, once they are integrated into a fluidized bed membrane reactor, they must resist erosion from the scouring action of the fluidized catalyst.

As pore-filled membranes have failed because the Pd layer was not interconnected (see Chapter 4), the main objective of this chapter is to produce a hydrogen permeable membrane by depositing a protective layer on top of a very thin selective Pd-based layer. As the membrane function is given by the two layers, we named this new kind of membranes double-skinned membranes. The experimental procedure for the membrane preparation and the subsequent permeation tests is first described. The Pd-Ag layers were prepared by simultaneous ELP (electroless plating) and the protective layer by dip-coating. Permeation characteristics of the membranes were studied by single gas tests and by tests with binary gas mixtures. The membranes showed a high hydrogen permeance and H_2/N_2 perm-selectivity. Furthermore, the resistance of the membrane under fluidization conditions for two types of particles during long-term tests is investigated and discussed.

5.2. Experimental

5.2.1. Preparation

Porous tubular substrates (10/4 mm o.d./i.d.) made by α-Al_2O_3 with an asymmetrical geometry were provided by Rauschert Kloster Veilsdorf and used as porous support with a top layer of 100 nm pore size. The porous substrates were joined with dense ceramic tubes using a glass sealant, following a procedure reported in Chapter 3.

Prior to the simultaneous deposition of the Pd-Ag layer, the porous substrates were activated with palladium nuclei by dipping the supports into a chloroform solution of palladium acetate, followed by reduction with hydrazine, as reported Chapter 4. The tubular supports with palladium seeds were immersed into a plating bath for co-deposition of the Pd-Ag layer. The composition of bath used is summarized in Table 5.1. The co-deposition was carried out

at 64 °C for 1 hour. For the last 45 minutes of deposition vacuum was applied from inside the tube to close the pores of the support.

Table 5.1. Chemical composition of electroless plating bath.

Chemicals	Concentration (M)
Palladium acetate	0.01
Silver nitrate	$3.23 \cdot 10^{-4}$
EDTA	0.15
Ammonia	5
Hydrazine	0.013

After the Pd-Ag layer deposition, the samples were washed with distilled water and dried overnight and annealed at 550 °C for 4 h in a reducing atmosphere (10 vol% H_2/90 vol% N_2). Nitrogen was fed during heating (3 °C min^{-1}) and cooling steps. Finally, a thin (< 1 μm) mesoporous ceramic layer (50% YSZ/50% γ-Al_2O_3) was deposited on top of the Pd-Ag layer by a dip-coating technique, as reported in Chapter 3.

5.2.2. Physico-chemical characterization of double-skinned membranes

The cross-section of the double-skinned (DS) membranes was analysed with a Scanning Electron Microscope (FEI Quanta 250 FEG). For each membrane at least four measurements were carried out to determine the layer thickness. The Pd-Ag composition in the selective layer was calculated by measuring by ICP-OES (Varian Vista MPX Inductively Coupled Plasma Optical Emission Spectrometer) the concentration of silver and palladium in the plating bath before and after the deposition of the layer.

5.2.3. Permeation measurements

One end of the supported membranes was connected to a dense metallic tube and the other end was closed with a metallic tap using graphite ferules following the procedure reported by Fernandez et al. [5]. The connectors were tightened to the membrane with a torque wrench applying 7 Nm. The total length of the membranes with the connector was 150 mm (see Figure 5.1). Once the sealings were tightened, a leak test was performed by feeding helium from the inside of the membrane while the membrane was submerged in ethanol. No bubbles were detected from the sealing parts, indicating that the sealings were properly tightened. Finally, the membranes were dried to remove ethanol and integrated into the reactor. The permeation setup used for the gas permeation measurements (single gas test and gas mixtures) is illustrated in Figure 5.2. A shell and tube module was made from stainless steel with an inner diameter of 42.7 mm. The gas pressure in the shell side was controlled with a back-pressure controller connected to the retentate side. The permeate side of the membrane was kept at atmospheric pressure. No sweep gas was applied during the

experiments, while the hydrogen flux was measured with an automated mass flow meter (Defender 220) and nitrogen with an automated soap film flow meter for flow rates > 0.2 mL min^{-1} (Horiba, model VP1) and another soap bubble flow meter for flow rates < 0.2 mL min^{-1}. Single gas tests were carried out at temperatures between 300-500 °C with nitrogen and hydrogen. Mixed gas permeation tests with H_2-N_2 and H_2-CO_2 mixtures were performed at 400 °C.

Figure 5.1. A Pd-Ag double-skinned membrane (150 mm long) with a ceramic protective layer supported onto an α-Al_2O_3 porous support and sealed with graphite-based seals.

5.3. Results and discussion

5.3.1. Thickness measurement of double-skinned membranes

The thickness of the selective and protective layers has been determined by SEM images of the cross section of DS-2 (Figure 5.3a) and DS-3 (Figure 5.3b) membranes. The thickness of the selective layer was determined at ~1 μm (± 0.26) and ~1.8 (± 0.23) μm for DS-2 and DS-3, respectively. The thickness of the DS-2 protective layer was ~0.5 μm (± 0.06) and for the case of DS-3 slightly thicker, ~0.67 μm (± 0.10). An EDS mapping of the cross-section of the DS-3 membrane has been performed for palladium, silver, aluminium and oxygen (Figure 5.4). From these images it was confirmed that the Pd-Ag selective layer is placed between the alumina support and the protective ceramic layer. The surface area (300 $m^2 g^{-1}$) and pore size (1-5 nm) of the protective layer were characterized by BET, as reported in Chapter 3.
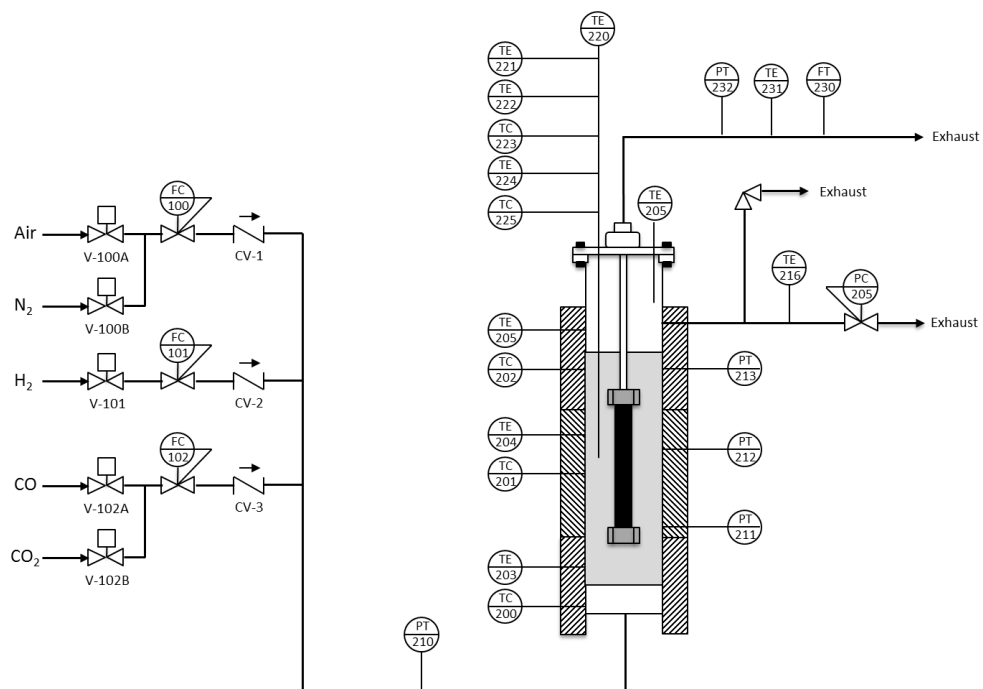
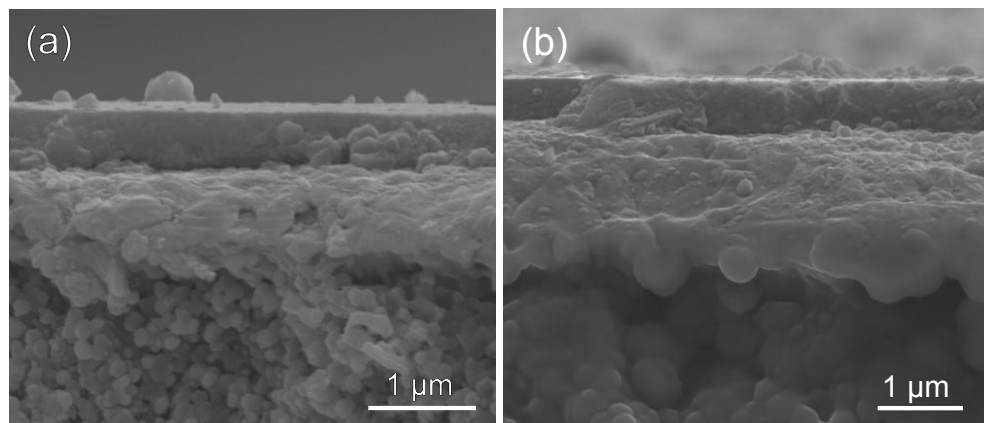Figure 5.2. PID of the setup for the permeation measurements.

Figure 5.3. SEM cross-section images of double-skinned membranes. DS-2 (a) and DS-3 (b).
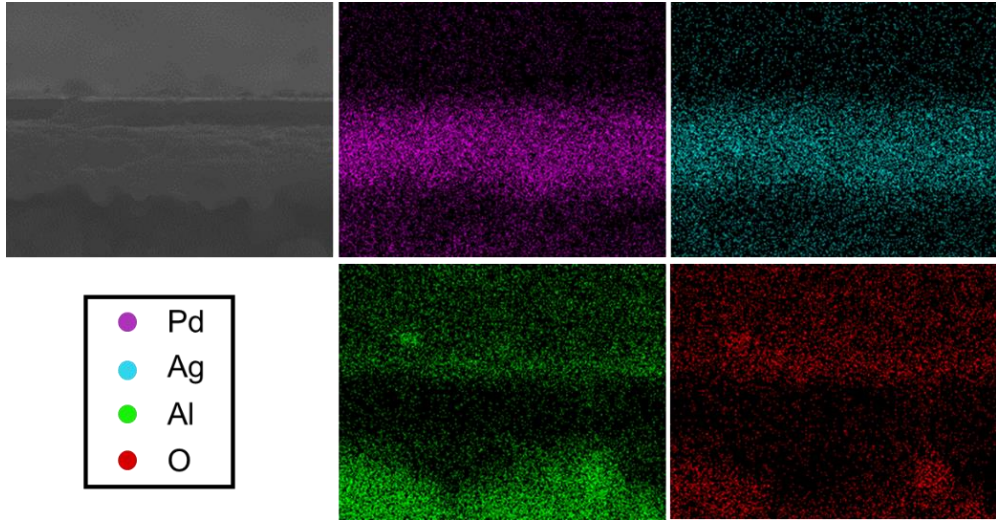
Figure 5.4. EDS mapping results from fresh DS-3 membrane in cross section.

5.3.2. Membrane preparation properties

The equation describing the hydrogen flux through Pd-based membranes is written in terms of a Sieverts' type law as follows:

$$J = \frac{Pe}{t}\left(p_{H2,ret}^{n} - p_{H2,perm}^{n}\right)$$ (Eq. 5.1)

where J is the hydrogen flux, Pe is the permeability, t the thickness of the selective layer, p_{H2} is the hydrogen partial pressure at the permeate and retentate side respectively and n the pressure exponent.

Figure 5.5 shows the hydrogen fluxes through the DS-2 membrane at different temperatures (300-500 °C) and different transmembrane pressures differences. The best fit for the hydrogen fluxes (J) and $\left(p_{H2,ret}^{n} - p_{H2,perm}^{n}\right)$ was found for a pressure exponent value n of 0.783 (after activation by flowing air at 400 °C for 2 min). For Pd-based membranes, the pressure exponent should equal 0.5 in case the rate limiting step is diffusion through the bulk of the palladium. Since the determined n-value deviates from 0.5, this may indicate the influence of Knudsen diffusion in the mesoporous protecting layer (1-5 nm pore size) and/or viscous flow in the porous support (100 nm pore size) [6] on the overall hydrogen permeation rate; if both these cases were rate limiting, the n-value would be unity. Moreover, the rate-limiting step in thin membranes are surface reactions rather than bulk-diffusion, also causing an n-value above 0.5. This is in agreement with the study reported by Melendez et al. [7], who

have shown that for ultra-thin membranes (< 1 µm) higher *n*-values are measured as a consequence of partially rate-limiting surface reactions.
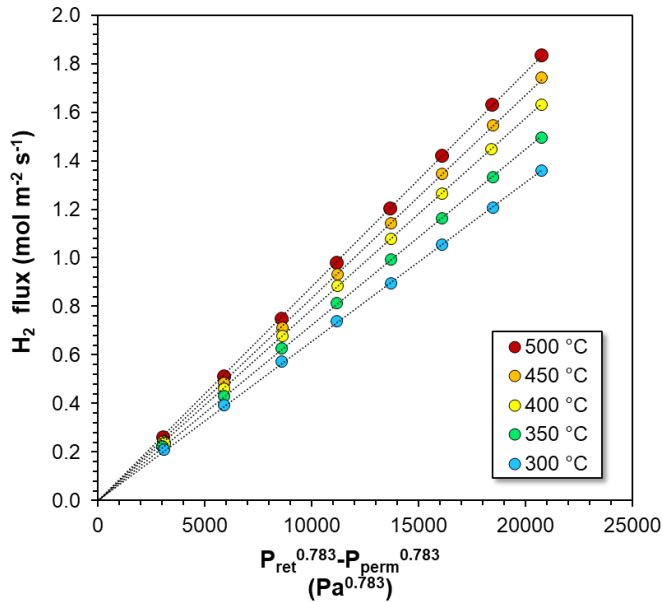
Figure 5.5. Measured hydrogen flux from 300 °C to 500 °C after activation in air at 400 °C as a function of the hydrogen pressure difference.

Fluxes measured in the temperature range 300-500 °C were used to estimate the activation energy for hydrogen permeation through the membrane. The permeance depends on the temperature according to the Arrhenius relation given by [8],

$$Q = Q_0 e^{-\frac{Ea}{RT}} \xrightarrow{\ln} \ln Q = \ln Q_0 - \frac{Ea}{RT} \qquad \text{(Eq. 5.2)}$$

where Q is the permeance of the membrane, Q_o the pre-exponential factor, Ea the activation energy, R the universal gas constant, and T the absolute temperature. One of the assumptions of this equation is that the pressure exponent n does not vary with temperature.

By plotting the natural logarithm of the calculated permeances as a function of 1/RT (see Figure 5.6) the activation energy was determined at 5.11 kJ mol^{-1}. This activation energy is a lumped value including the permeation through the mesoporous protective layer, the dense metal layer and the support. This value is similar to values reported by Melendez et al. [7] who reported activation energies ranging from 5.47 to 7.81 kJ mol^{-1} for membranes with a similar content of silver (5.7 to 9 wt%) and with the same range of thicknesses of the selective

layer (0.46 to 1.29 µm). Many parameters can affect the activation energy, such as the thickness of the selective layer, the grain microstructure of the layer and the preparation method [9,10].
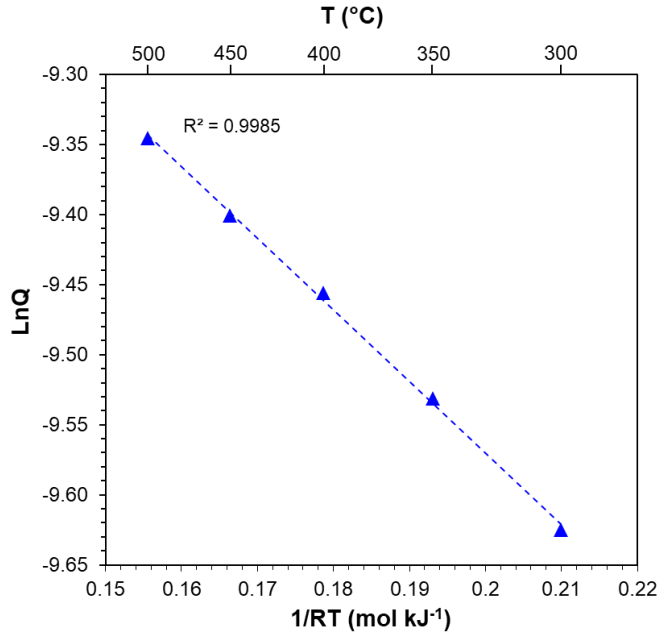
Figure 5.6. Arrhenius plot based on the H₂ permeance after activation in air at 400 °C.

The measured hydrogen and nitrogen fluxes during single gas tests were used to calculate the H_2/N_2 ideal perm-selectivity of the membrane. The hydrogen permeances and H_2/N_2 perm-selectivities at different temperatures (300-500 °C) and 1 bar of pressure difference are shown in Figure 5.7. The nitrogen leakage at 1 bar of pressure difference was $2 \cdot 10^{-10}$ mol m^{-2} s^{-1} Pa^{-1} and $1.7 \cdot 10^{-10}$ mol m^{-2} s^{-1} Pa^{-1} at 300 °C and 500 °C, respectively showing a Knudsen permeation mechanism probably due to the permeation through the mesoporous protective layer where the Pd-Ag layer is not present.
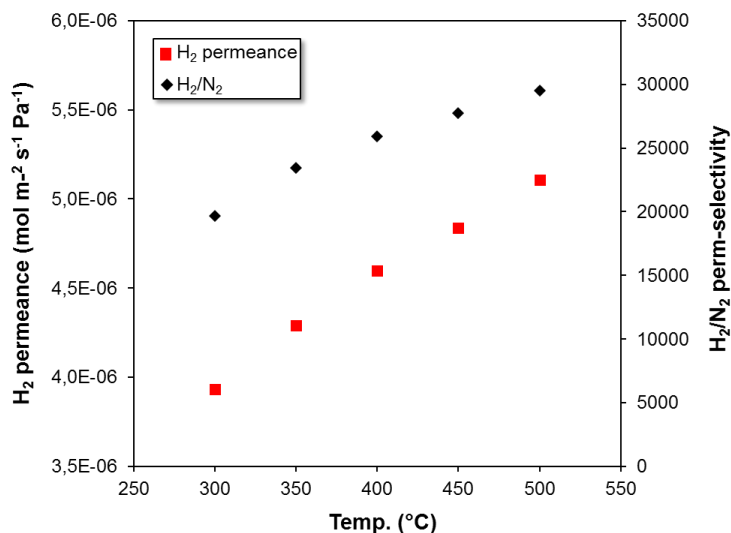
Figure 5.7. H_2 permeance and H_2/N_2 perm-selectivity in the temperature range of 300-500 °C and 1 bar of pressure difference for the DS-2 membrane.

In Table 5.2 the permeation properties of reported supported Pd-based membranes thinner than 3 µm are listed. Mejdell et al. [11] reported a 1.4 µm thick $Pd_{77}Ag_{23}$ layer supported into a microchannel reactor with a hydrogen flux of $22.5 \cdot 10^{-6}$ mol m^{-2} s^{-1} Pa^{-1} at 300 °C and 1 bar of pressure difference. The selectivity of this membrane was 5700 at the beginning of the test. However, after 7 days of testing this value decreased to 390. Concerning the tubular supported Pd-based membranes, the largest hydrogen flux was reported by Peters et al. [12] with a ~1.9-3.9 µm-thick $Pd_{77}Ag_{23}$ film prepared by PVD-MS and transferred to a PSS tube. At 400 °C, the H_2 flux at 1 bar of pressure difference was $14.9 \cdot 10^{-6}$ mol m^{-2} s^{-1} Pa^{-1}, while the selectivity was 7700. A similar flux was reported by Melendez et al. [7] for a very thin (0.49 µm) $Pd_{91}Ag_9$ membrane supported onto a ceramic porous substrate. However, this high flux was achieved at the expense of a low perm-selectivity (48). Membranes with different thicknesses were tested and the best selectivity (3500) was measured for the membrane with the larger thickness, with a high H_2 permeance at 400 °C of $9.2 \cdot 10^{-6}$ mol m^{-2} s^{-1} Pa^{-1}. The best combination of flux and selectivity at 400 °C was reported by Catalano et al. [13], who measured a H_2 flux at 1 bar pressure difference of $5.1 \cdot 10^{-6}$ mol m^{-2} s^{-1} Pa^{-1} for a 2.5 µm-thick $Pd_{80}Ag_{20}$ membrane with a selectivity over 10000. In the present work a membrane (DS-2 with 5 wt% Ag) has been produced with a selective layer of ~1 µm with a similar flux ($4.6 \cdot 10^{-6}$ mol m^{-2} s^{-1} Pa^{-1}) and a H_2/N_2 perm-selectivity of ~26000. The results reported in this work are one of the best reported in terms of the combination of a high permeability and selectivity.

Table 5.2. Permeation properties of Pd-based supported membranes reported in the literature.

Selective layer/ support	Preparation method	Thickness (μm)	Temp. (°C)	Pressure difference (kPa)	H$_2$ Flux (mol m^{-2} s^{-1})	H$_2$ permeance (10^{-6} mol m^{-2} s^{-1} Pa^{-1})	H$_2$/N$_2$	Ea (kJmol^{-1})	n	Ref.
Metallic porous support										
Pd$_{77}$Ag$_{23}$/PSS	PVD-MS[a]	>2	350	500	1.5	3.0	500	-	-	[14]
Pd$_{77}$Ag$_{23}$/microchannel	PVD-MS[a]	1.4	300	80	1.8	22.5	5700	-	-	[11]
Pd$_{77}$Ag$_{23}$/PSS	PVD-MS[a]	1.9-3.8	400	100	1.49	14.9	≈7700	-	0.631	[12]
Ceramic porous support										
Pd$_{91}$Ag$_9$/Al$_2$O$_3$	ELP	0.46	400	100	1.57	15.7	48	5.47	0.81	[7]
Pd$_{95}$Cu$_5$/ZrO$_2$-Al$_2$O$_3$	ELP	1.3	365	145	0.718	4.95	127	-	0.553	[6]
Pd$_{77}$Ag$_{23}$/YSZ-Al$_2$O$_3$(HF)	S-ELP[b]	0.4	450	100	0.87	8.7	416	8.76	1.09	[15]
PdAg/ZrO$_2$	PVD-ELP	0.7-0.8	400	100	0.8	8.0	500	-	0.5	[16]
Pd$_{91}$Ag$_9$/Al$_2$O$_3$	ELP	0.78	400	100	1.06	10.6	636	6.60	0.67	[7]
Pd$_{90}$Ag$_{10}$/Al$_2$O$_3$[17]	ELP	2.1	400	400	1.00	2.5	>1000	5.77	0.5	[17]
Pd$_{80}$Ag$_{20}$/Al$_2$O$_3$	ELP	2.2	400	400	1.64	4.1	>1000	2.93	0.5	[17]
Pd$_{77}$Ag$_{23}$/YSZ-Al$_2$O$_3$(HF)	S-ELP[b]	0.8	450	100	0.8	8.0	1212	14.2	1.09	[15]
Pd$_{92.8}$Ag$_{7.2}$/Al$_2$O$_3$	ELP	1.17	400	100	0.92	9.2	1270	7.81	0.62	[7]
Pd$_{77}$Ag$_{23}$/YSZ-Al$_2$O$_3$(HF)	S-ELP[b]	1.2	450	100	0.57	5.7	1583	13.64	1.09	[15]
Pd/YSZ-Al$_2$O$_3$(HF)	ELP	1.2	450	100	0.39	3.9	2600	20.48	1.09	[15]
Pd/α-Al$_2$O$_3$(HF)	ELP	1.5	450	100	0.237	2.37	3115	13.3	1	[18]
Pd$_{94.3}$Ag$_{5.7}$/Al$_2$O$_3$	ELP	1.29	400	100	0.92	9.2	3500	7.67	0.64	[18]
Pd/Al$_2$O$_3$(HF)	ELP	0.9	460	105	0.42	4.0	9200	15.0	1	[7]
Pd$_{80}$Ag$_{20}$/Al$_2$O$_3$	ELP	2.5	400	100	0.51	5.1	>10000	17.8	0.5	[19]
Pd$_{80}$Ag$_{20}$/Al$_2$O$_3$	ELP	2.5	400	100	0.34	3.4	>10000	17	0.5	[19]
Pd$_{95}$Ag$_5$/Al$_2$O$_3$	S-ELP[b]	1	400	100	0.46	4.6	25938	5.11	0.783	This Chapter

[1]Physical vapour deposition–magnetron sputtering. [2]Simultaneous electroless plating.

5.3.3. Long-term membrane performance under catalyst fluidization

Once the membrane (DS-2) properties were studied with tests with single gas and binary gas mixtures in absence of fluidized particles, shown in Figure 5.8 for the first 250 h with the grey background, the reactor was cooled down to room temperature in order to introduce glass beads with a particle size of 250-350 μm. The volume of the particles was enough to completely cover the membranes. Subsequently, the reactor was heated again to 350 °C and the particles were fluidized (U/U_{mf} = 2) for 100 h. Then, the fluidization velocity was increased to U/U_{mf} = 3 and the temperature to 400 °C (1 bar of transmembrane pressure). The same binary gas mixture tests as performed before the introduction of the particles were repeated to evaluate the effect of the presence of fluidized particles on the bed-to-membrane mass transfer limitations. The total flow rate was varied from 10 to 20 L min^{-1}. Thus, the membrane surface suffers more attrition since the fluidization velocity and particle mixing increase. The H_2/N_2 perm-selectivity was around 25000, while after the introduction of the particles the selectivity started decreasing until the end of the long-term test (after 975 h the selectivity decreased to 5500). During the fluidization tests with glass beads, the filter downstream of the retentate side was clogged twice. The temperature was decreased to 300 °C to be able to clean the filter (see the peaks in the temperature and pressure in Figure 5.8). A grey powder was found and this was characterized by XRD. The diffractogram obtained corresponds to glass beads (composed mainly of SiO_2). This indicates that particles were breaking during the tests probably due to erosion with reactor walls and the membrane surface. Once the long-term test was concluded and the module was cooled down, it was observed that the protective layer was removed from the surface of the membrane. As the selectivity had decreased, a leak test was performed to localize the position of the leakage. As described above, the membrane was pressurized to 1 bar with helium from the inner side of the membrane while it was submerged into ethanol. The membrane was dipped slowly to assess which part of the membrane was responsible for the gas leakage. It was found that the sealing (both top and bottom sealing) were responsible for the leakage and not the membrane surface. Thus, even though the protective layer was removed, the selective layer was still intact. It could be expected that the protective layer was removed due to the collisions of the hard glass particles with the membrane surface. To assess this, other tests were performed with actual catalyst particles with a higher hardness compared to glass.
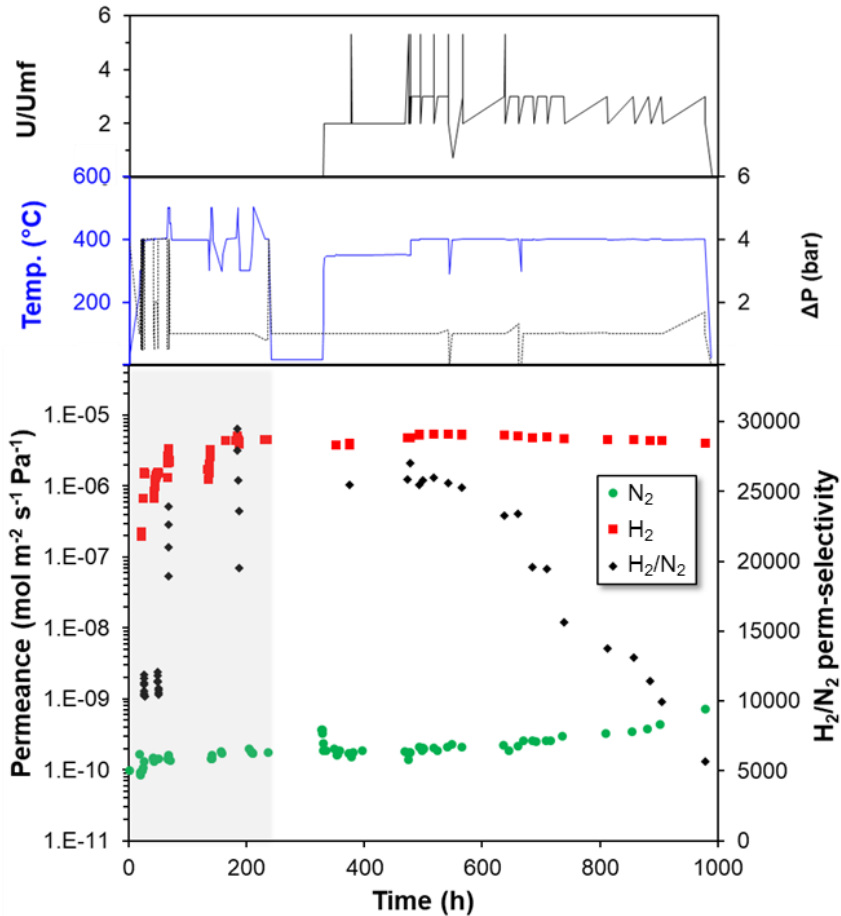
Figure 5.8. Hydrogen and nitrogen permeances and ideal perm-selectivity of membrane DS-2 during a long-term test. First 250 h in absence of glass beads. Rest of test was performed in presence of particles under bubbling fluidization regime. Temperature, pressure and U/U_{mf} profiles during the test are represented above the figure.

Another membrane (DS-1) with 4 wt% of silver in the selective layer was tested under fluidization conditions for longer time with a catalyst provided by Johnson Matthey®. The catalyst consisted of modified alumina particles (100-300 μm size) loaded with 0.5 wt% of rhodium. Unlike the glass particles, the promoted alumina supported Rh particles were non-spherical and harder. Consequently, attrition with the membrane surface is expected to be more severe anticipating a faster decrease in the selectivity in comparison with the glass beads experiments. The nitrogen permeance at 400 °C was $4.15 \cdot 10^{-10}$ mol m^{-2} s^{-1} Pa^{-1} before the integration of the membrane into the reactor and a defect on the membrane surface was already identified during the leak test of the sealings. This value increased during the first 350 hours (see Figure 5.9). Hydrogen and nitrogen permeation tests were carried out until the permeance was constant (350 h). During this time, single gas test and binary gas mixture

tests were performed (those results are not included in this paper). At this point, the ideal perm-selectivity of the membrane at 1 bar of pressure difference was ~2800 and ~3700 at 300 °C and 500 °C respectively and the N_2 permeance increased to ~$1.4 \cdot 10^{-9}$ mol m^{-2} s^{-1} Pa^{-1}. Subsequently, the reactor was cooled down to 200 °C and the catalyst was introduced immersing the membrane completely. The bed was fluidized in the freely bubbling regime (U/U_{mf} = 3) at 400 °C and 1 bar of pressure difference. The H_2 and N_2 permeation was monitored for more than 1500 hours. During this period the ideal perm-selectivity was maintained at around 2000 and the H_2 permeance at $3.35 \cdot 10^{-6}$ mol m^{-2} s^{-1} Pa^{-1}. Then, the temperature was increased to 450 °C and maintained for 7 days. Finally, the temperature was increased to 500 °C. As can be clearly observed in Figure 5.9, the nitrogen leakage starts rising dramatically when the temperature was raised to 450 °C. At the end of the experiment, the nitrogen leakage was $3 \cdot 10^{-8}$ mol m^{-2} s^{-1} Pa^{-1} at 500 °C.

The membrane surface and sealing were studied in more detail at room temperature. After this long-term test, it was observed that the protective layer remained at the surface of the membrane, indicating that the abrasion of the surface was not the primary cause of the layer removal of the previous membranes. A helium leak test was carried out by immersing the membrane in ethanol and introducing 1 atm pressure of gas. Leaks were observed at both end sealings, but more extensive at the top sealing. In order to quantify the contribution of the membrane surface to the total nitrogen leakage, both sealings were covered with a gas tight resin. It was calculated that the nitrogen leakage contribution of the membrane surface was only 8% of total leakage. This is probably due to rearrangement of the Pd(Ag) metal as previously reported by Ma and co-workers [20]. Thus, it can be concluded that the membrane performance has been affected after this long-term test (~2500 h) for only 8% and the main leaks were found at the sealings.
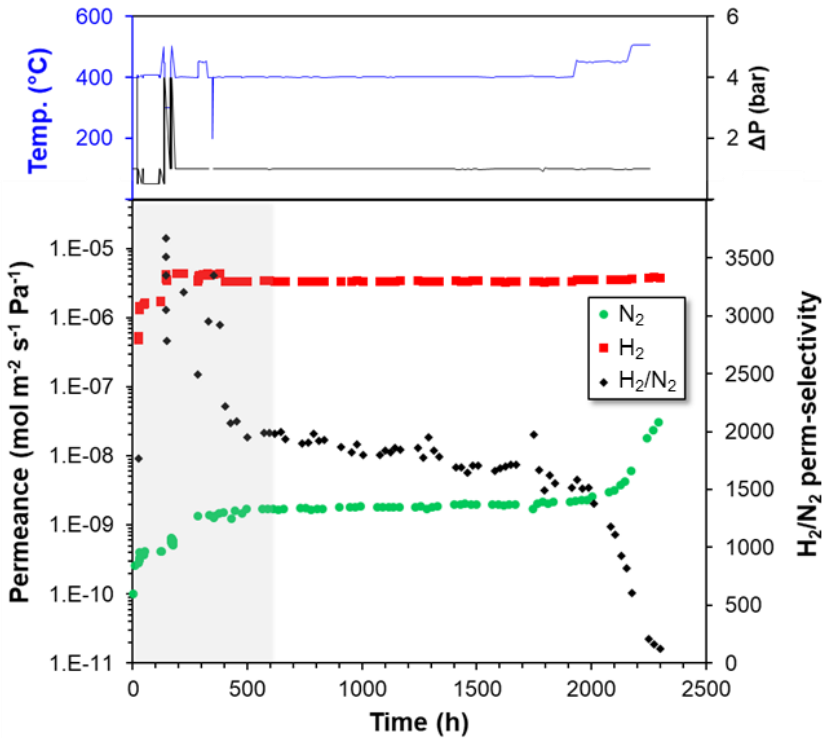
Figure 5.9. Long-term test DS-1 membrane with 4 wt% of silver in the selective layer. Rh supported on promoted alumina particles were introduced after 400 hours. Temperature and pressure profiles are represented above. The U/U_{mf} = 3 was kept constant during the test.

A third membrane (DS-3) with 4 wt% of silver has been tested at 550 °C and 1 bar of pressure difference under fluidization conditions for ~700 hours with the same catalyst as the previous membrane DS-1 (alumina based, see Figure 5.10). The hydrogen permeance of DS-3 at 550 °C is lower ($1.3 \cdot 10^{-6}$ mol m^{-2} s^{-1} Pa^{-1}) than the DS-2 at 500 °C ($3.2 \cdot 10^{-6}$ mol m^{-2} s^{-1} Pa^{-1}). This could be partly related to the thicker selective layer of DS-3 (~1.86 μm) in comparison with the DS-2 (~1 μm), but also differences in the thickness of the protective layers (~0.5 μm and ~0.67 μm for DS-2 and DS-3, respectively) could play a role.

As shown in Figure 5.10, the ideal H$_2$/N$_2$ perm-selectivity was not as high as for DS-2. This is not only related to the lower hydrogen permeance of DS-3, but rather to a large defect found on the surface of the membrane that contributed to the nitrogen leakage. The increase in the N$_2$ leakage was extremely fast during the first 250 hours. The experiment was stopped when the ideal perm-selectivity had decreased to almost 50. As was been done for the DS-1 membrane, the leakage contribution was quantified at room temperature by pressurizing the inner side with helium before and after covering the sealings with a gas-tight resin. For the case of DS-3 with a defect since the beginning of the test, the total contribution of the

membrane to the leakage was 20%. Further studies should be done in order to improve the sealing of the supported membranes onto ceramic supports.

These tests also showed that the protective layer was still in place after the tests. One can speculate that the removal of the protective layer of the first membrane could be attributed to softening of the glass beads which subsequently got adhered to the protective layer. Collisions with other particles could then tear off part of the porous layer as schematically depicted in Figure 5.11. Fluidized particles can exhibit a tendency to agglomerate at elevated temperatures, and this agglomeration can already occur well below the melting point or softening point. It was found by Guo et al. [21] that glass beads starts to become sticky at 450 °C in the bubbling fluidization regime, which even led to defluidization.
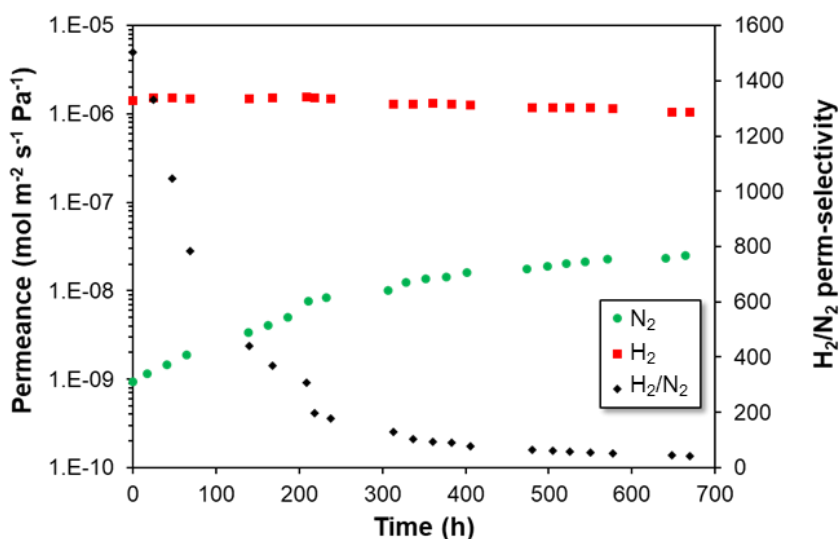

Figure 5.10. Long-term test at 550 °C of DS-3 membrane with 4 wt% of silver at the selective layer. Rh supported on promoted alumina particles were introduced at the beginning of the test.
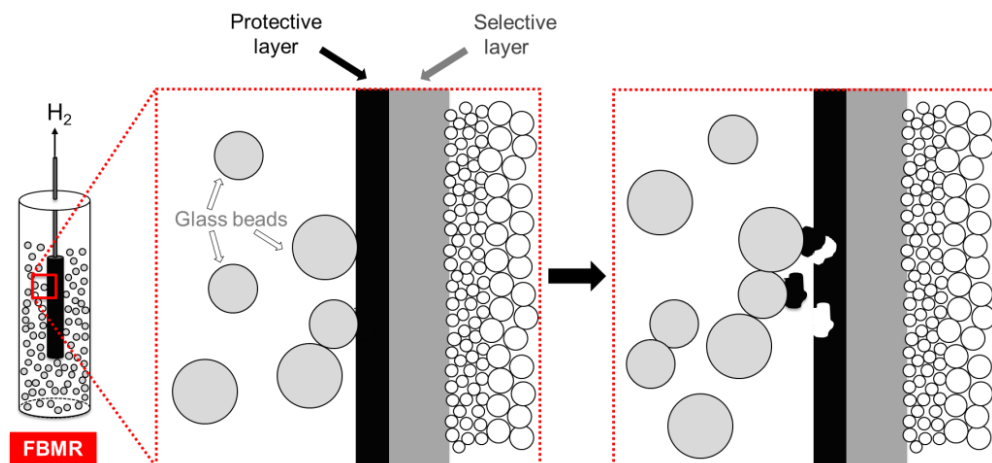
Figure 5.11. Schematic representation of removal of the protective layer with glass beads under fluidization at 400 °C.

5.3.4. Permeation tests with binary mixtures

The membrane DS-2 (with 5 wt% of silver) was tested with binary mixtures of H$_2$-N$_2$ and H$_2$-CO$_2$ varying the hydrogen feed content from 50 to 100 vol%. Permeation tests were carried out at 400 °C with a total feed flow rate fixed at 10 L min^{-1}. Those experiments were repeated in the presence of fluidized glass beads. In this case, different feed flow rates were studied (10, 15 and 20 L min^{-1}). In all cases the permeate side was maintained at atmospheric pressure.

Figure 5.12a and c show that the hydrogen flux decreased significantly in the presence of N$_2$ or CO$_2$, even if only 10 vol% of N$_2$ or CO$_2$ was mixed with H$_2$. The decrease in the H$_2$ flux is very similar for all the studied mixtures, so that no interaction of CO$_2$ with the membrane (nor reverse water gas shift) was observed. These results suggest the formation of a concentration mass transfer boundary layer in the gas phase which reduces the H$_2$ concentration in the proximity of the membrane surface. This phenomenon, referred to as concentration polarization, becomes prominent for membranes with a high H$_2$ permeance, even if the H$_2$ volume fraction in the retentate side is still high [5,7,16,22].

Once glass beads were introduced into the reactor (Figure 5.12b and d), the same binary gas mixture tests were carried out. The results show that the H$_2$ permeation flux for the case of the fluidized bed tests was slightly higher compared with the experiments in the empty tube, which demonstrates that the fluidized bed, due to particle movement, increases the gas mixing and thus reduces the extent of external mass transfer limitations (i.e. the thickness of concentration profile near the membrane surface is reduced). However, this improvement

was observed only at low transmembrane pressures for each mixture. As an example, for a H_2-N_2 mixture with 50 vol% H_2, the H_2 flux is larger in presence of glass beads, when the partial pressure of hydrogen is lower than 1.4 bar (Figure 5.13a). While for a feed with 90 vol% H_2, this value increased to 1.7 bar (Figure 5.13b). Above these pressures, the hydrogen flux in fluidized beds is lower than the one measured in the empty tube. This could be related to the appearance of another phenomenon. At high fluxes the particles are dragged towards the membrane surface with the formation of densified zones close to the membranes [23] that will induce an additional mass transfer resistance decreasing the flux.

The total feed flow rate also influences the hydrogen flux as shown in Figure 5.13. In the presence of glass beads, as the total feed flow rate increases, the permeated H_2 flux also increases. However, the hydrogen recovery at the permeate side decreases and the membrane surface area to feed flow rate decreases, thus the effect of the membrane on the hydrogen recovery decreases [24]. The same trend was observed for mixtures of H_2-CO_2 (see Figure 5.13c).
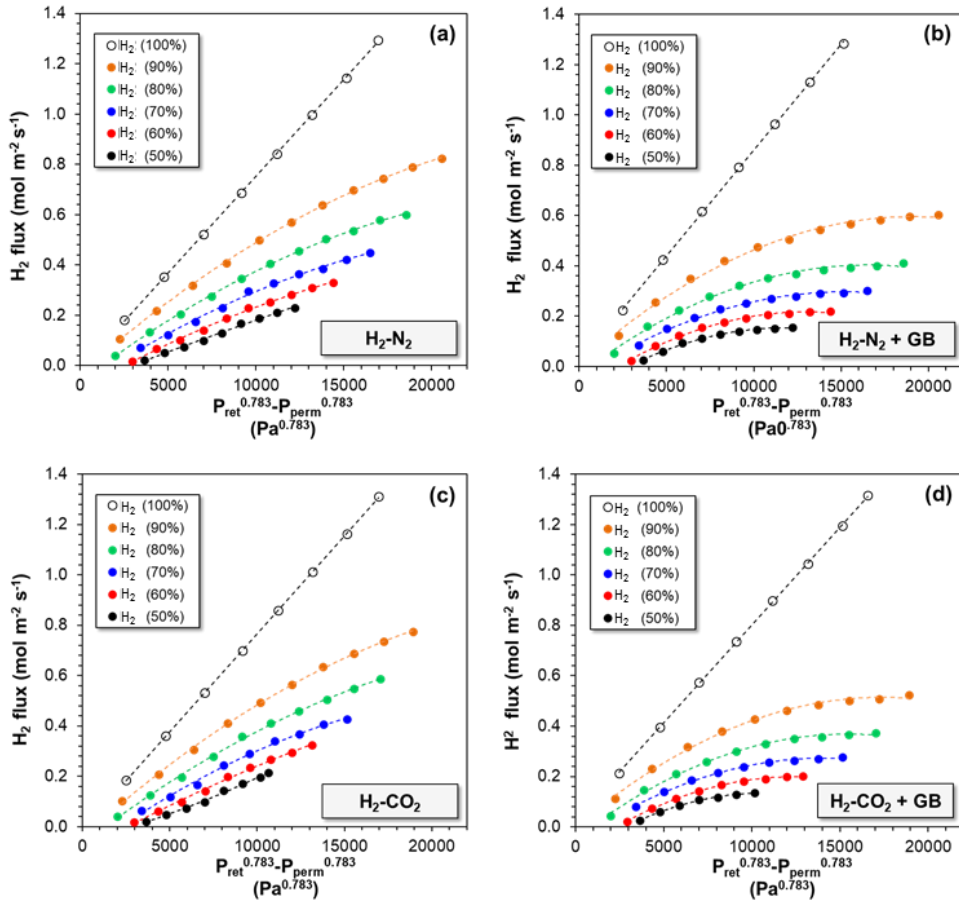
Figure 5.12. Hydrogen transmembrane flux of DS-2 at 400 °C vs driving force over calculated n-value (0.783) of binary mixtures: (a) H_2-N_2, (b) H_2-N_2 with glass beads, (c) H_2-CO_2 and (d) H_2-CO_2 with glass beads from 50 to 100% of H_2 purity in volume. Total feed flow: 10 L min^{-1}.
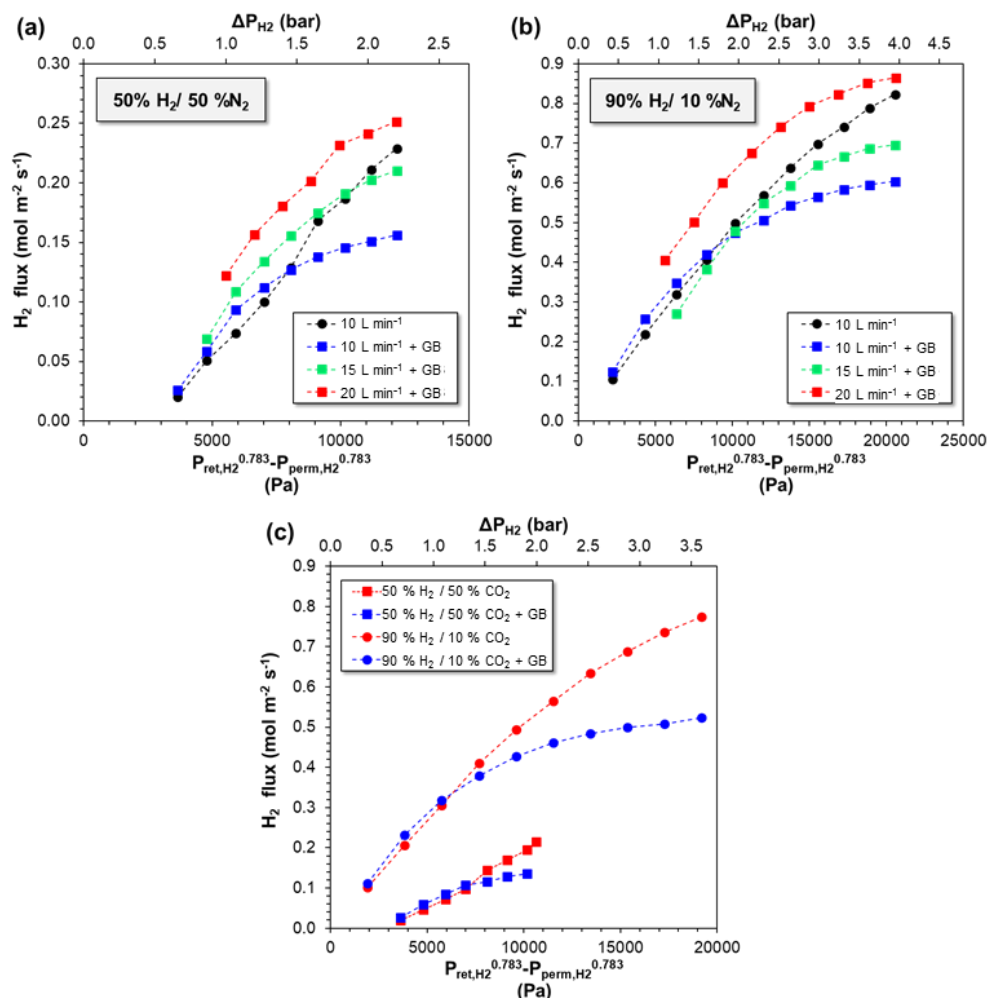
Figure 5.13. H_2 transmembrane flux of DS-2 at 400 °C of binary mixtures at different total flow rates in absence and presence of glass beads. (a) H_2-N_2 mixture with 50% vol. H_2, (b) H_2-N_2 mixture with 90% vol. H_2 and (c) H_2-CO_2 mixture with 50% and 90% vol. H_2.

5.4. Conclusions

We have reported the preparation and characterization of PdAg ceramic-supported membranes with a porous ceramic protective layer. Supported membranes with a selective layer of 1 μm ($Pd_{95}Ag_5$) showed a H_2 permeance of $5·10^{-6}$ mol m^{-2} s^{-1} Pa^{-1} and a H_2/N_2 perm-selectivity over 25000 at 400 °C and 1 bar of pressure difference. In a fluidized bed membrane reactor with a bed of glass beads operated in the freely-bubbling fluidization regime, the H_2/N_2 perm-selectivity decreased to about 5000 after 750 h of fluidization. The protective layer was removed during this long-term experiment and this might be attributed

to the softening of the glass beads that end up adhering to the porous layer finally removing the layer as a results of vigorous particle collisions.

Another membrane was tested for 2500 h in the fluidized bed membrane reactor with a commercial reforming catalyst (Rh supported on promoted alumina) in the bubbling fluidization regime. Even with a defect in the membrane surface prior to the reactor tests, the ideal perm-selectivity of the membrane remained almost constant (at around 2000) over more than 1500 h of fluidization at 400 °C and 1 bar of pressure difference. Only when the temperature was raised, the selectivity started decaying rapidly and this could be attributed to leakages in the sealings.

As expected, mass transfer limitations (concentration polarization) were observed due to the large H_2 permeance of the membranes. For the fluidized bed membrane reactor two different effects have been observed: at low permeation velocities (low partial pressure differences) the particle mixing enhances the bed-to-membrane mass transfer rate, thereby diminishing the concentration polarization. On the other hand, at higher pressure differences, the particles induce more mass transfer resistances, probably due to the formation of densified zones around the membranes. Possibilities to reduce the formation of densified zones need to be further explored.

Despite the very promising results of the double-skinned membranes, this research has also demonstrated that the sealing of these membrane needs to be further improved. The issue with the fittings can be solved/avoided by employing metallic porous supports welded to a metallic dense tube for their proper integration into a reactor. In Chapter 6 the performance of a conventional and double-skinned membranes supported onto a metallic support is investigated.

Bibliography

[1]   C.S. Patil, M. van Sint Annaland, J.A.M. Kuipers, Fluidised bed membrane reactor for ultrapure hydrogen production via methane steam reforming: Experimental demonstration and model validation, Chem. Eng. Sci. 62 (2007) 2989–3007.

[2]   F. Gallucci, L. Paturzo, A. Basile, A simulation study of the steam reforming of methane in a dense tubular membrane reactor, Int. J. Hydrogen Energy. 29 (2004) 611–617.

[3]   A. Arratibel, D.A. Pacheco Tanaka, M. van Sint Annaland, F. Gallucci, 3 – Membrane reactors for autothermal reforming of methane, methanol, and ethanol, in: Membr. React. Energy Appl. Basic Chem. Prod., 2015: pp. 61–98.

[4]   F. Gallucci, M. van Sint Annaland, J.A.M. Kuipers, Theoretical comparison of packed bed and fluidized bed membrane reactors for methane reforming, Int. J. Hydrogen Energy. 35 (2010) 7142–7150.

[5]   E. Fernandez, A. Helmi, K. Coenen, J. Melendez, J.L. Viviente, D.A. Pacheco Tanaka, M. van Sint Annaland, F. Gallucci, Development of thin Pd–Ag supported membranes for fluidized bed membrane reactors including WGS related gases, Int. J. Hydrogen Energy. 40 (2015) 3506–3519.

[6]   P.M. Thoen, F. Roa, J.D. Way, High flux palladium-copper composite membranes for hydrogen separations, Desalination. 193 (2006) 224–229.

[7]   J. Melendez, E. Fernandez, F. Gallucci, M. van sint Annaland, P.L. Arias, D.A. Pacheco Tanaka, Preparation and characterization of ceramic supported ultra-thin (~1 µm) Pd-Ag membranes, J. Memb. Sci. 528 (2017) 12–23.

[8]   P.P. Mardilovich, Y. She, Y.H. Ma, M.-H. Rei, Defect-free palladium membranes on porous stainless-steel support, AIChE J. 44 (1998) 310–322.

[9]   S.N. Paglieri, K.Y. Foo, J.D. Way, J.P. Collins, D.L. Harper-Nixon, A New Preparation Technique for Pd/Alumina Membranes with Enhanced High-Temperature Stability, Ind. Eng. Chem. Res. 38 (1999) 1925–1936.

[10]   F.C. Gielens, H.D. Tong, M.A.G. Vorstman, J.T.F. Keurentjes, Measurement and modeling of hydrogen transport through high-flux Pd membranes, J. Memb. Sci. 289 (2007) 15–25.

[11]   A.L. Mejdell, M. Jøndahl, T.A. Peters, R. Bredesen, H.J. Venvik, Experimental investigation of a microchannel membrane configuration with a 1.4 µm Pd/Ag23 wt.% membrane–Effects of flow and pressure, J. Memb. Sci. 327 (2009) 6–10.

[12]   T. a. Peters, M. Stange, R. Bredesen, On the high pressure performance of thin supported Pd–23%Ag membranes—Evidence of ultrahigh hydrogen flux after air treatment, J. Memb. Sci. 378 (2011) 28–34.

[13]   J. Catalano, M. Giacinti Baschetti, G.C. Sarti, Influence of the gas phase resistance on hydrogen flux through thin palladium–silver membranes, J. Memb. Sci. 339

(2009) 57–67.

[14]   T.A. Peters, W.M. Tucho, A. Ramachandran, M. Stange, J.C. Walmsley, R. Holmestad, A. Borg, R. Bredesen, Thin Pd-23%Ag/stainless steel composite membranes: Long-term stability, life-time estimation and post-process characterisation, J. Memb. Sci. 326 (2009) 572–581.

[15]   T. Maneerung, K. Hidajat, S. Kawi, Ultra-thin (1µm) internally-coated Pd-Ag alloy hollow fiber membrane with superior thermal stability and durability for high temperature H2 separation, J. Memb. Sci. 452 (2014) 127–142.

[16]   E. Fernandez, J.A. Sanchez-Garcia, J. Melendez, V. Spallina, M. van Sint Annaland, F. Gallucci, D. a. Pacheco Tanaka, R. Prema, Development of highly permeable ultra-thin Pd-based supported membranes, Chem. Eng. J. 305 (2016) 149–155.

[17]   J. Okazaki, T. Ikeda, D. a. P. Tanaka, K. Sato, T.M. Suzuki, F. Mizukami, An investigation of thermal stability of thin palladium–silver alloy membranes for high temperature hydrogen separation, J. Memb. Sci. 366 (2011) 212–219.

[18]   G.B. Sun, K. Hidajat, S. Kawi, Ultra thin Pd membrane on α-Al2O3 hollow fiber by electroless plating: High permeance and selectivity, J. Memb. Sci. 284 (2006) 110–119.

[19]   S. Yun, J.H. Ko, S.T. Oyama, Ultrathin palladium membranes prepared by a novel electric field assisted activation, J. Memb. Sci. 369 (2011) 482–489.

[20]   F. Guazzone, Y.H. Ma, Leak growth mechanism in composite Pd membranes prepared by the electroless deposition method, AIChE J. 54 (2008) 487–494. doi:10.1002/aic.11397.

[21]   Q. Guo, T. Suda, J.C.H.I. Sato, G. Yue, Agglomeration behavior in a bubbling fluidized bed at high temperature, Chem. Eng. Commun. 191 (2004) 1329–1342.

[22]   D. Pizzi, R. Worth, M. Giacinti Baschetti, G.C. Sarti, K. ichi Noda, Hydrogen permeability of 2.5 µm palladium-silver membranes deposited on ceramic supports, J. Memb. Sci. 325 (2008) 446–453.

[23]   N.T.Y. Dang, F. Gallucci, M. van Sint Annaland, Micro-structured fluidized bed membrane reactors: Solids circulation and densified zones distribution, Chem. Eng. J. 239 (2014) 42–52.

[24]   F. Gallucci, M. Van Sint Annaland, J.A.M. Kuipers, Autothermal reforming of methane with integrated CO2 capture in novel fluidized bed membrane reactors, Asia-Pacific J. Chem. Eng. 4 (2009).

Chapter 6

Metallic supported membranes for FBMR: Comparison between conventional and double-skin membranes

Pd-Ag supported membranes have been prepared by coating a ceramic interdiffusion barrier onto a Hastelloy X (0.2 μm media grade) porous support followed by deposition of the hydrogen selective Pd-Ag (4-5 μm) layer by electroless plating. To one of the membranes an additional porous Al_2O_3YSZ layer (protective layer with 50 wt% of YSZ) was deposited by dip-coating followed by calcination at 550 °C on top of the Pd-Ag layer, and this membrane is referred to as a double-skin membrane. Both membranes were integrated at the same time in a single reactor in order to assess and compare the performance of both membranes under identical conditions. The membranes have first been tested in an empty reactor with pure gases (H_2 and N_2) and afterwards in the presence of a catalyst (rhodium onto promoted alumina) fluidized in the bubbling regime. The membranes immersed in the bubbling bed were tested at 400 °C and 500 °C for 115 and 500 hours, respectively. The effect of the protective layer on the permeation properties and stability of the membranes were studied. The double-skin membrane showed a H_2 permeance of $1.55 \cdot 10^{-6}$ mol m^{-2} s^{-1} Pa^{-1} at 500 °C and 4 bar of pressure difference with an ideal perm-selectivity virtually infinite before incorporation of particles. This selectivity did not decay during the long-term test under fluidization with catalyst particles.

"Our greatest glory is not in never falling, but in rising everything we fall".
Confucius.

6.1. Introduction

When ceramic supports are employed for the preparation of double-skin membranes good results in terms of flux and stability have been observed, as described in Chapter 5. Nonetheless, the fittings (graphite sealing) employed for the integration of the membrane into the reactor started failing with time and high temperature, thus contributing to an increase in the nitrogen leakage thereby decreasing the ideal perm-selectivity. This issue can be solved by employing metallic porous supports. As explained in the previous chapter, to achieve defect-free thin layers on top of porous substrates, a low surface roughness and small pore sizes (with a narrow pore distribution) of the support materials are required. On the one hand, ceramic supports (Al_2O_3, ZrO_2, YSZ, etc.) are the most exploited so far, due to their high chemical stability, low cost and high surface quality. However, their mechanical strength is lower compared to metallic supports and the sealing of such supports in membrane modules is more challenging [1]. On the other hand, metallic supports provide a much higher mechanical strength and relatively easy integration into a reactor. However, their surface quality is generally lower. The relatively large roughness and pore size (2-20 µm) of metallic supports can be reduced by the deposition of a ceramic porous layer, which also helps avoiding inter-metallic diffusion of elements present in the metallic support and the Pd-based selective layer, when the membranes are employed at high temperatures under reducing environments. Ceramic barriers have been successfully deposited onto metallic supports by dip-coating [2–6], sputtering [7–9] and atmospheric plasma deposition (APS) [7,10,11]. Prior to the deposition of the ceramic barrier, a heat treatment of the metallic stainless steel porous supports in air is necessary in order to create a Cr_2O_3 layer. This layer allows a better adhesion between the support and the ceramic layer, thus reducing at the same time the possibilities of inter-metallic diffusion of Pd [6,12]. Finally, the main techniques for the deposition of a Pd-based layer are electroless plating (ELP), electroplating, physical vapor deposition (PVD) and chemical vapor deposition (CVD) [13].

The use of Pd-based supported membranes in FBMRs has received a growing interest in the last decade [14–18]. However, the long-term stability of the membranes in fluidized bed membrane reactors at high temperatures (> 400 °C) is limited, since defects can appear due to the mobility of the atoms present in the selective layer or as consequence of the attrition by the fluidized particles. To overcome the stability problems of membranes in fluidized beds, this chapter focuses on the development of novel double-skin membranes, which offer attrition resistance under fluidization conditions thanks to the addition of a very thin porous ceramic protective layer on top of the Pd-based H_2 perm-selective layer.

In particular, a conventional metallic-supported membrane and a counterpart double-skin (DS) membrane have been tested under fluidization conditions and their performance has been compared to investigate the long-term stability of the novel DS membranes. It was

found that in the temperature range of 400-500 °C, conventional supported membranes suffer from a pronounced decay in the initial ideal H_2/N_2 perm-selectivity in the presence of the fluidized catalyst, whereas the novel DS-membranes maintain much higher selectivities at the same conditions. In the first part, the preparation of the membranes, and the characterization techniques and experimental setup used for the tests are described. Subsequently, the main findings are presented and discussed in the results section.

6.2. Experimental

6.2.1. Membrane preparation

Porous Hastelloy X tubes with media grade of 0.2 µm, welded to non-porous Inconel tubes at both ends (having one side as dead-end) from Mott Metallurgical Corporation have been used in this study as membrane support material. The supports have an outer diameter of 3/8" and an active (porous) length of 139 mm.

Before the deposition of the ceramic barriers, the metallic supports were oxidized at 750 °C for 1 hour with a heating rate of 3 °C min^{-1}. In order to decrease the pore size and roughness at the surface, the supports were graded with α-Al_2O_3/YSZ and YSZ slurries before the deposition of the Pd-Ag layer. The slurry of the ceramic barrier consisted of α-Al_2O_3 particles (AKP-30, Sumitomo) and YSZ (TZ-8Y, Tosoh Corp.) particles dispersed in deionized water. Then, a polyvinyl alcohol (PVA, MW 78000 g mol^{-1}, Polyscience Europe Gmbh) solution and polyethylene glycol (PEG 400 g mol^{-1} synthesis grade, Scharlau) were added to the slurries. The composition of the slurries used in this study are summarized in Table 6.1.

Table 6.1. Components of the interdiffusion barrier slurries.

Material	Concentration at the slurry (wt%)	
	Slurry A	Slurry B
α-Al_2O_3	2.1	0
YSZ	0.9	1.5
PVA	3	1.5
PEG	0.6	0.3

The metallic porous supports were dipped into the slurry for 3 minutes at 25 °C, and were subsequently dried in a climatic chamber under continuous rotation for 5 h at 40 °C and 60 % relative humidity. Finally, the samples were calcined in air at 400 °C for 30 minutes in order to decompose the organics present in the slurry and then sintered at 750 °C for 4 hours in a 10 vol% H_2 in He atmosphere. After each sintering process, and prior to the next coating, the roughness and the nitrogen permeance of the supports were measured. In total five coatings were performed (3 of slurry A followed by 2 coatings of slurry B) for membrane

M15 and three coatings for M33 (2 of slurry A followed by a single coating of slurry B). A final sintering treatment has been performed during 6 hours at 800 °C under the H_2/He atmosphere.

The deposition of the Pd-Ag layer was carried out by a simultaneous electroless plating technique (ELP). First, the surface of the porous substrate was activated with palladium seeds by dipping the membrane into a chloroform solution of palladium acetate. This step has been repeated 6 times. Subsequently, the membranes were dried at 110 °C and the palladium seeds were reduced in a hydrazine solution at room temperature. Finally, the tubes were cleaned with water and dried again. This cycle was repeated until the surface turned to a homogeneous black color. The Pd-Ag co-deposition has been performed at 64 °C for 5 hours. During the first 2 hours, the membranes were rotating inside the bath and in the last 3 hours vacuum was applied from inside the tube. The deposition time and the composition of the bath used for the preparation of the two membranes (M15 and M33) are summarized in Table 6.2. As the last step of the process, the membranes were cleaned, dried and annealed at 650 °C for 4 hours in a reducing atmosphere.

Table 6.2. Chemical composition of electroless plating bath and deposition time for membranes M15 and M33.

Parameter	M15	M33
Palladium acetate (M)	0.0103	0.0122
Silver nitrate (M)	$7.5 \cdot 10^{-4}$	$3 \cdot 10^{-4}$
EDTA (M)	0.15	0.15
Ammonia (M)	5	5
Hydrazine (M)	0.015	0.015
Deposition time (min)	309	323

The membrane M15 has first been investigated as prepared, and subsequently it has been turned into a double-skin membrane. To do so, a mesoporous YSZ/γ-Al_2O_3 protecting layer has been deposited on top of the Pd-Ag layer of membrane M15 by a vacuum-assisted dip-coating technique at room temperature, followed by calcination at 550 °C for 4 hours (Chapter 3). The protective layer containing 50 wt% of YSZ is expected to be ~1 μm-thick, as reported in Chapter 5. The membrane M15 with the protective layer is henceforth named as M15-DS. The colors present at the surface of the membrane (see Figure 6.1) is associated with the scattered visible light by the YSZ particles present in the mesoporous protective layer.
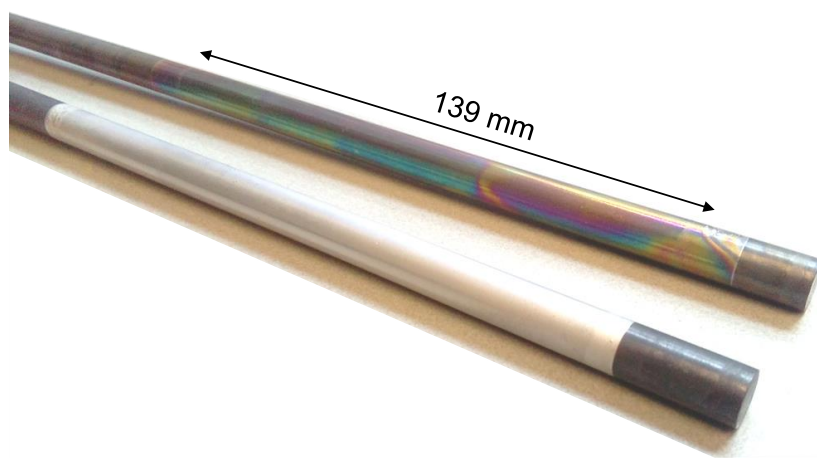
Figure 6.1. A Pd-Ag double-skin membrane with a ceramic protective layer supported onto a Hastelloy X porous support (up) and a conventional supported membrane (down).

6.2.2. Membrane characterization

Prior to the deposition of the selective Pd-Ag layer, the surface roughness (R_a and R_t) and the nitrogen permeance of the metallic porous supports have been determined after each deposition step in the membrane preparation process. The surface roughness was analyzed with a Vecco Dektak 150 contact profilometer, and the measurement has been done using a 2 μm radius stylus tip. After each deposition step, the measurement has been performed at five different locations with a spot length of 4 mm long. The R_t is the total height of the roughness profile (highest peak to valley distance) and R_a is the arithmetical mean roughness.

The composition of the selective layer was determined by measuring the concentration of both metals (Pd and Ag) in the plating bath before and after the deposition of the layer with an ICP-OES technique in a Varian Vista MPX Inductively Coupled Plasma Optical Emission Spectrometer.

The thickness of the deposited ceramic layer and the perm-selective layers has been determined by scanning electron microscope (SEM) techniques in a FEI Quanta 250 FEG equipment. These measurements were carried out using a metallic supported membrane prepared using exactly the same conditions as M15.

6.2.3. Gas permeation measurements

The membranes were installed in a reactor made of stainless steel (AISI310) with an inner diameter of 102 mm and 100 cm in height, with a porous plate distributor (40 μm pore size)

welded at the bottom. A more detailed description of the setup used for the permeation tests can be found in the work of Helmi et al. [16]. First, the permeation properties of membrane M15 (without the protective layer) were determined at 500 °C in an empty reactor. Then, the protective layer was deposited onto this membrane and finally both membranes (M15-DS and M33) were installed in the reactor. The system was heated under a nitrogen atmosphere up to 400 °C at a heating rate of 2 °C min^{-1}. Before the investigation into the performance of the membranes, they were activated in air at 400 °C for two minutes in order to remove organic impurities from the surface. Afterward, the nitrogen and hydrogen single gas permeation measurements were carried out at temperatures between 400 and 500 °C. The activation energy for hydrogen permeation was calculated from the hydrogen permeation values at various temperatures by fitting Sieverts' law, as reported in Chapter 5. Subsequently, the module was cooled down to room temperature in order to integrate the catalyst particles inside the reactor. The particles used consisted of modified alumina particles with 0.5 wt% of rhodium with a particle size ranging between 100 and 300 µm provided by Johnson Matthey® (typical catalyst for methane reforming in fluidized beds). The performance of the membranes was monitored for 615 h in the presence of the catalyst in the continuous bubbling fluidization regime at 400-500 °C.

6.3.   Results and discussion

6.3.1.   Membrane characterization

As described in the previous section, α-Al$_2$O$_3$/YSZ and YSZ layers have been deposited onto the metallic porous substrates prior to the deposition of the Pd-Ag layer to avoid a possible interaction between metallic elements present in the supports and the selective layer at high temperatures. After each deposition of ceramic barrier, the roughness (R_a and R_t) of the supports has been determined and the values measured are listed in Table 6.3. The initial R_t of the porous supports ($\sim$ 8.1 µm) decreases for both membranes, M15 and M33, after each deposition. After the deposition of a layer with slurry A (α-Al$_2$O$_3$, YSZ), the R_t of M15 decreases to almost half of the initial R_t ($\sim$ 4.15 µm), while membrane M33 required the deposition of 5 layers to reach similar values. A similar trend is observed for the R_a parameter, which largely decreased after the first deposition for M15, but decreased much less pronounced after subsequent depositions.

The nitrogen permeance has been measured after each deposition of a ceramic layer. The decay in the nitrogen permeance after the first layer deposition, $1.02 \cdot 10^{-5}$ mol m^{-2} s^{-1} Pa^{-1} for M15 and $2.46 \cdot 10^{-5}$ mol m^{-2} s^{-1} Pa^{-1} for M33 corresponds to the decrease in surface roughness. Before the deposition of the Pd-Ag layer, the nitrogen permeances are around 5.7 (M15) and 3.7 (M33) times smaller than the nitrogen permeance of the bare tubes.

Finally, the ELP deposition of the Pd-Ag layer was carried out for 303 min and 328 min onto M15 and M33 respectively and the determined nitrogen permeances were for both lower than $7 \cdot 10^{-10}$ mol m^{-2} s^{-1} Pa^{-1} after annealing at 550 °C for 4 h.

Table 6.3. Surface roughness and nitrogen permeances of membranes M15 and M33 after deposition of each ceramic layer and the Pd-Ag layer.

Step	Ra (µm)		Rt (µm)		N_2 permeance[b] (mol m^{-2} s^{-1} Pa^{-1})	
	M15	M33	M15	M33	M15	M33
Support[a]	0.86 ± 0.14		8.10 ± 2.14		4.71·10^{-5}	
Oxidized[a]	0.88 ± 0.13		8.49 ± 1.32		3.34·10^{-5}	
Slurry A (1st)	0.56 ± 0.01	0.84 ± 0.13	4.15 ± 0.45	6.46 ± 1.08	1.02·10^{-5}	2.46·10^{-5}
Slurry A (2nd)	0.48 ± 0.02	0.72 ± 0.13	4.08 ± 0.76	5.67 ± 1.78	9.68·10^{-6}	2.03·10^{-5}
Slurry A (3rd)	-	0.67 ± 0.12	-	4.35 ± 0.66	-	1.82·10^{-5}
Slurry B (1st)	0.44 ± 0.05	0.61 ± 0.06	4.19 ± 0.95	5.71 ± 2.44	8.22·10^{-6}	1.86·10^{-5}
Slurry B (2nd)	-	0.63 ± 0.14	-	4.70 ± 1.49	-	1.42·10^{-5}
Final sintering	NA	0.59 ± 0.08	NA	4.09 ± 0.58	NA	1.27·10^{-5}
ELP[c]	-	-	-	-	6.55·10^{-10}	1.70·10^{-11}

N/A: not available data
[a] Average values from other five bare supports
[b] Measured at room temperature.
[c] after annealing at 650 °C for 4 hours.

SEM cross section images were obtained from another metallic supported membrane prepared under the same conditions as M15. As can be observed in Figure 6.2 (a and b), the pores of the support (very irregular) ranges between 10 and 20 µm. Furthermore, it has also been observed that the thickness of the ceramic inter-diffusion barrier is not homogeneous along the membrane. In some regions, the ceramic layer creates a barrier between the selective layer and the support pores (Figure 6.2c), while in other regions this ceramic barrier is not observed (i.e. is very thin) and the selective Pd-Ag layer seems to be deposited directly onto the support surface (Figure 6.2d). Therefore, inter-diffusion of metallic species from the support towards the selective layer could be expected when working at high temperatures. From Figure 6.2b and Figure 6.2c, it can also be confirmed that the pores in the surface of the metallic support are well covered by ceramic particles. The measured average thickness of the Pd-Ag layer from 5 different cross section images was 4.02 µm (± 0.24 µm), and a similar thickness could also be expected for M33. The measured silver content in the selective layer of membrane M33 is lower (~ 6.9% wt%) than in M15 (~ 16.8 wt%). This is expected since the amount of silver nitrate added for the electroless plating for M15-DS was 2.5 times larger than for M33, and this is in agreement with the determined silver content measured for both membranes, being 2.43 times larger for M15-DS.
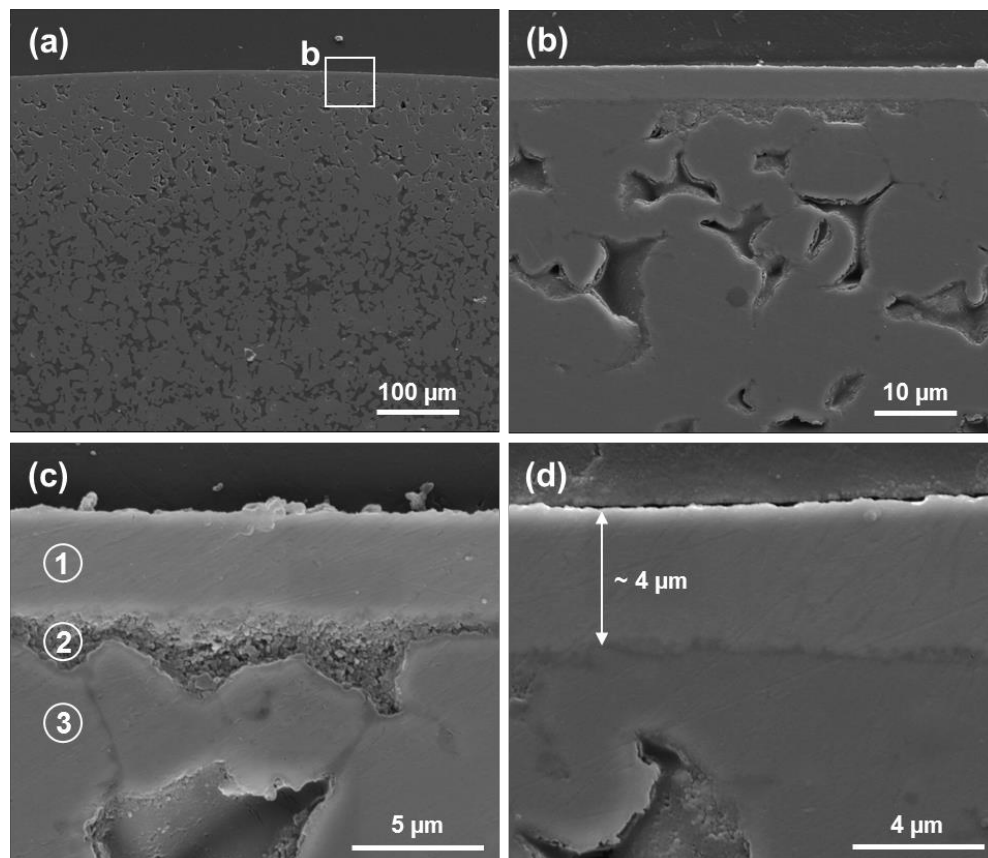
Figure 6.2. SEM cross section image of a conventional Pd-Ag metallic supported membrane. Images with different magnifications: 250x (a), 2500x (b), 8000x (c) and 10000x (d). Numbered points in (c) are related to the Pd-Ag layer (1), YSZ-Al$_2$O$_3$ interdiffusion layer (2) and Hastelloy X porous support (3).

6.3.2. Membrane permeation properties

The main goal of this test is to compare the permeation properties of a conventional supported Pd-Ag membrane with the new double-skin (DS) membrane before and during fluidization conditions. The metallic supports allow an easier installation of the membranes into the reactor, since they can be easily connected to the metallic reactor using standard Swagelok fittings (or, in a real reactor, by welding of the tube to the reactor flange).

Before the deposition of the mesoporous protective layer onto M15, its permeation properties have been measured in pure hydrogen and nitrogen at 500 °C and 3 bar of pressure difference for about 500 h (after activation by flowing diluted air at 500 °C for 1 min). As reported in Figure 6.3, the hydrogen permeance of the membrane (1.92·10^{-6} mol m^{-}

^{2} s^{-1} Pa^{-1}) remains stable during the whole duration of the experiment, while the ideal H$_2$/N$_2$ perm-selectivity decays from 3300 to 1700. The nitrogen leakage at 500 °C increased from $5.89 \cdot 10^{-10}$ to $1.19 \cdot 10^{-9}$ mol m^{-2} s^{-1} Pa^{-1} (with a pressure difference of 3 bar). After this test, the leakages of the membrane have been checked by introducing the membrane in ethanol and pressurizing with helium from the inner side of the tube (1 bar of pressure difference). During this test, bubbles coming out from the membrane surface were observed.
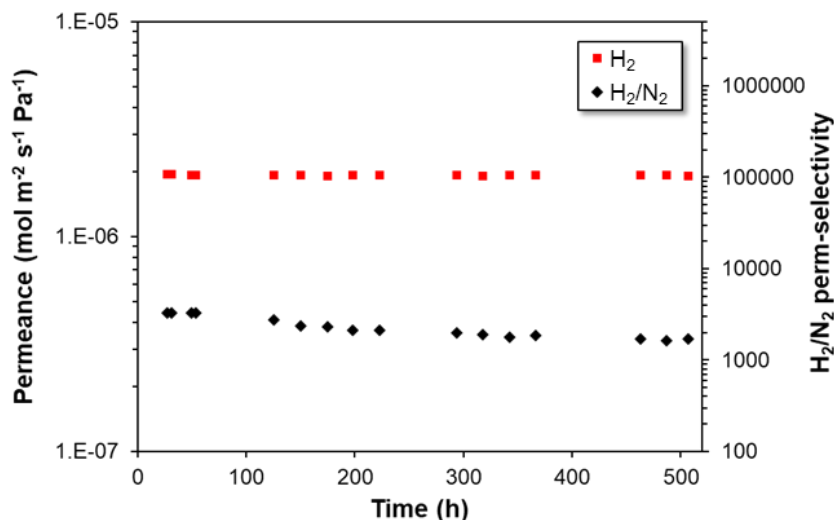

Figure 6.3. H$_2$ permeance and ideal H$_2$/N$_2$ perm-selectivity of the M15 membrane at 500 °C and 3 bar of pressure difference.

Once the mesoporous layer was deposited onto M15 (from now on referred to as M15-DS) these bubbles were not observed (i.e. the small pores on the membrane surface were covered by ceramic particles, effectively improving the perm selectivity of the membrane). The hydrogen permeation for both membranes (M15-DS and M33) was measured at different transmembrane pressures and at temperatures in the range of 400-500 °C (see Figure 6.4) after being exposed to air for 2 minutes at 400 °C for their activation. The membranes showed a linear trend with a pressure exponential factor, n, of 0.62 and 0.72 for M33 and M15-DS respectively. It is well accepted that the deviation from Sieverts' law (n=0.5) can be attributed to the influence of the support or to external mass transfer limitations [19,20]. The addition of the mesoporous protective layer leads to an increase in the n-value, which could be related to the effects of Knudsen diffusion and viscous flow in the porous protective layer, as reported in Chapter 5.

The activation energies determined for the temperature range of 400-500 °C are 6.26 and 7.17 kJ mol^{-1} for M15-DS and M33, respectively. An activation energy and n-value of 5.8 kJ mol^{-1} and 0.738, respectively, was reported by Fernandez et al. [21] for a membrane with 4-5

μm-thick Pd-Ag layer supported onto a Hastelloy-X porous substrate using the same ceramic interdiffusion barrier as reported in this chapter. The lower activation energy of M15-DS in comparison with M33 can be attributed to the effect of the Knudsen diffusion-viscous flow through the mesoporous protective layer, where this diffusion mechanism is characterized by a lower activation energy than the solution-diffusion mechanism in the Pd-Ag selective layer [22].
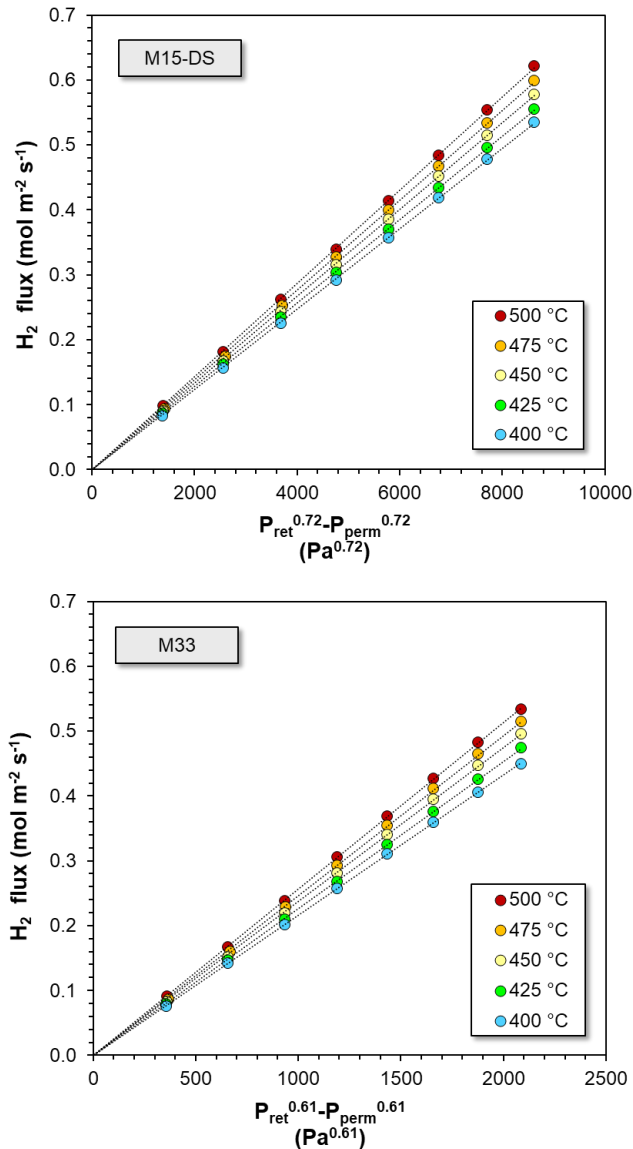

Figure 6.4. Measured hydrogen flux from 400 °C to 500 °C after activation in air at 400 °C as a function of the hydrogen pressure difference.

The main parameters obtained during the single gas permeation test for the conventional and double-skin membranes are summarized in Table 6.4. The results show that the hydrogen permeance of M15-DS at 500 °C ($1.55 \cdot 10^{-6}$ mol m^{-2} s^{-1} Pa^{-1}) is somewhat lower than for M15 ($1.92 \cdot 10^{-6}$ mol m^{-2} s^{-1} Pa^{-1}), which was expected due to the presence of the mesoporous protective layer that increases the mass transfer resistance. A slightly lower permeance ($1.34 \cdot 10^{-6}$ mol m^{-2} s^{-1} Pa^{-1}) was measured for the metallic supported membrane M33, which could be related to the lower content in silver in comparison with M15-DS, as mentioned previously. It is indeed already reported in the literature that the addition of Ag to Pd improves the hydrogen permeability, resulting in a 1.7 times larger permeation rate when 23 wt% of silver is added compared to pure palladium [23]. On the other hand, no nitrogen flow was detected using a Bronkhorst flow meter (0.001 mL min^{-1}) through the double-skin membrane, resulting in a virtually infinite perm-selectivity. For graphical purposes, the nitrogen permeation selected is that of the detection limit of the flow meter, leading to a N$_2$ permeance of $4.47 \cdot 10^{-13}$ mol m^{-2} s^{-1} Pa^{-1} at 4 bar of transmembrane pressure and to an ideal perm-selectivity of 3500000. For membrane M33, the ideal selectivity measured was 93300, corresponding to a nitrogen leakage of $1.43 \cdot 10^{-11}$ mol m^{-2} s^{-1} Pa^{-1}.

Table 6.4. Main parameters of conventional metallic supported (M33) and double-skin membrane (M15-DS) in an empty reactor.

Parameters	M15-DS	M33
H$_2$ permeance (mol m^{-2} s^{-1} Pa^{-1})*	$1.55 \cdot 10^{-6}$	$1.34 \cdot 10^{-6}$
Ideal H$_2$/N$_2$ perm-selectivity*	> 3500000	93300
Ea (kJ mol^{-1})	6.26	7.17
n-value	0.72	0.61

*Measured at 500 °C and ΔP = 4 bar.

6.3.3. Long-term membrane performance under catalyst fluidization

After 200 hours of the preliminary test (single gas test in an empty reactor), the system was cooled down to room temperature for the addition of the catalyst particles into the reactor (first peak in the temperature profile in Figure 6.5). Once more, the system was heated to 400 °C while catalyst particles were kept under continuous bubbling fluidization. The membrane stability under fluidization conditions has been evaluated between 400 and 500 °C for a total time of 615 hours (115 at 400 °C and 500 hours at 500 °C). The main objective of this test was to compare the performance and long-term stability of the two membranes under fluidization conditions. As shown in Figure 6.5, once the catalyst was filled in the reactor, the ideal perm-selectivity of the conventional supported membrane (M33) decreased during the first hours to ~14000. This value further decreased until ~ 1000 after 615 hours, caused by an increase in the nitrogen leakage from $8.76 \cdot 10^{-11}$ to $1.4 \cdot 10^{-9}$ mol m^{-2} s^{-1} Pa^{-1} at 4 bar of pressure difference. On the other hand, the DS-membrane (M15-DS) did not show any nitrogen leakage under the same conditions, demonstrating indeed a much

higher attrition resistance than the conventional metallic supported membrane. In terms of H_2 permeance stability, the H_2 permeance of membrane M33 has been progressively increasing during the test, while the double-skin membrane suffered from a small decrease in time, which can be associated with some sintering of the protective layer and/or an interaction between the gamma-alumina and palladium layers. Densification of the protective layer can occur during the fluidization test at 500 °C, decreasing the pore size and thus H_2 permeance of the overall membrane. Interaction between the support and palladium was also observed by Pacheco Tanaka et al. at 650 °C were the hydrogen flux decreased about 50 % after 130 hours, while no decay was observed at 550 °C. However, the support consisted of α-Al_2O_3 instead of γ-Al_2O_3 (as in this work) which may interact with palladium at lower temperatures than α-Al_2O_3. The sintering of the ceramic interdiffusion barrier does not seem to be responsible of this decrease in the permeance, since M15 was tested at 500 °C for ~ 500 hours without showing any flux decay (Figure 6.3). Nonetheless, it was observed that during the last 200 hours at 500 °C the hydrogen permeance of both membranes reached a plateau with values of $1.20 \cdot 10^{-6}$ and $1.43 \cdot 10^{-6}$ mol m^{-2} s^{-1} Pa^{-1} for M15-DS and M33, respectively. During the test in the bubbling fluidization regime, the setup was cooled down twice as can be observed in the temperature profile of Figure 6.5. No effect on the H_2 permeance was observed, concluding that the leakage of both membranes did not increase as a result of these temperature changes.
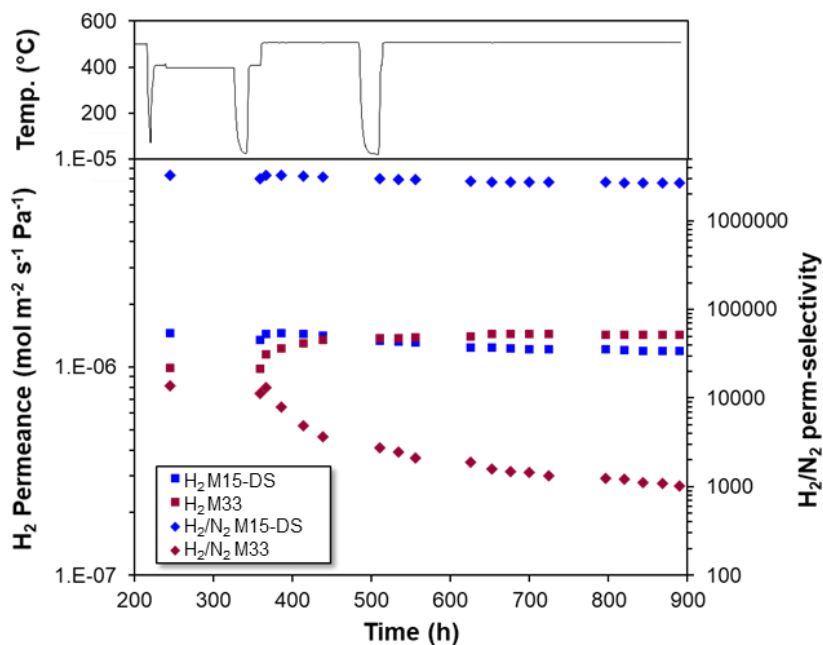

Figure 6.5. Hydrogen and ideal perm-selectivity at 4 bar of pressure difference for M33 and M15-DS in presence of Rh based catalyst under bubbling fluidization conditions.

Only a few reports on the long-term stability of Pd membranes under fluidization conditions have been published so far. The characteristic of the membranes, particles, operating conditions and their permeation properties (permeance and ideal selectivity) reported so far in the literature are summarized in Table 6. **5**.

The initial ideal perm-selectivity of membranes prepared onto alumina supports is, in general, lower than for metallic supported membranes. For alumina-supported membranes, the largest selectivity was found to be around 27000, which decreased down to 10000 after 48 hours at 400 °C under continuous fluidization with alumina-based particles [24]. A better performance was observed after 600 h at 400 °C by Helmi et al. [16]. These authors observed a drop in the ideal perm-selectivity (from 20000 to 13000), which was caused by a thermal shock that the membrane module suffered due to an oven failure during the test. A ceramic supported double-skin membrane showed a decrease in the selectivity from 25000 to 5000 after 750 hours of fluidization with glass beads at 350-400 °C (Chapter 5). After the test, it was found that the protective layer was pealed off, which was attributed to the softening of the glass beads and subsequent adhesion to the protective layer, which was then finally removed due to the collision of these particles with other particles of the fluidized bed. A similar membrane (showing a defect prior to the test) was tested at 400 °C with alumina particles, and the selectivity remained constant (~ 2000) over 1500 hours. Only when the temperature was increased, a decrease in the selectivity was observed and this was attributed to a sealing failure. A faster sealing failure was observed for another ceramic-supported DS membrane also referred to in Chapter 5 and tested at higher temperatures (550 °C) for 700 hours. Similar sealing problems were also observed by other authors when employing ceramic supports for the preparation of the H_2 selective membranes [25].

On the other hand, when metallic supports are used, sealing problems are avoided and the performance of the membrane alone can be evaluated under fluidization conditions. Roses et al. [18] reported the performance of a Pd-Ag membrane supported onto an Inconel porous tube (one selective layer on the outer surface and another one on the inner surface of the tube), and no leakages were observed during 260 hours of continuous fluidization. A membrane prepared in the same way as M33 was tested by Medrano et al. [15] and showed an ideal selectivity of >200000 for about 800 h in an empty reactor, while this selectivity decreased to 2850 at 600 °C. The authors attributed the increased leakage to a defect formation in the surface of the membrane. Later, the membrane was tested under reactive conditions in a fluidized bed membrane reactor in the temperature range of 500-600 °C. However, the performance in terms of perm-selectivity was quite low (< 600) in comparison to M33. Finally, as mentioned previously, the addition of the protective layer allows preventing attrition and a high ideal perm-selectivity was maintained. The M15-DS did not show any leakages and the calculated perm-selectivity remained close to 3 million. The selectivity decrease suffered during the 615 hours test, is related to the previously mentioned

H$_2$ flux reduction. Two other works have been published that use a similar type of membrane as M33 [26,27]. Medrano et al. [26] reported on the demonstration of the MA-CLR (membrane assisted chemical looping reforming) using three metallic-supported membranes and found that the ideal perm-selectivity decreased from 5400 to 4850 after 100 hours of operation at 500-600 °C. A longer test was reported by Wassie et al. [27] for a different concept, viz. MA-GSR (membrane assisted gas switching reforming), where four membranes were tested for about 240 hours at temperatures ranging from 400 to 550 °C. However, their initial perm-selectivity (11000) decreased down to merely 150, which was attributed to defect formation at the membrane surface due to the formation of PdO, resulting in the formation of pores in the selective layer.

These results demonstrate that the double-skin membranes exhibit a much better performance under fluidization conditions than other supported membranes. Future work will be focused on the evaluation of the performance of the double skin membranes under reactive conditions.

Table 6. 5. Permeation properties of Pd-based supported membranes in a fluidized bed membrane reactor reported in the literature.

Selective layer/ support	Thickness selective layer (µm)	Particles	Temp. (°C)	ΔP (bar)	H_2 permeance (10^{-6} mol m^{-2} s^{-1} Pa^{-1})	Test duration (h)	H_2/N_2		Ref.
							t=0	t=end	
PdAg/Al$_2$O$_3$	3-4	Pt-Ni/CeO$_2$/SiO$_2$	450-550	1.5-3	1.25[f]	~500	~1290[f]	N/A	[25]
PdAg/Al$_2$O$_3$	1.29	Pt/Al$_2$O$_3$	400	1	9	1000	1800	1600	[14]
YSZ-Al$_2$O$_3$/PdAg/Al$_2$O$_3$	1	Glass beads	350-400	1	4.6	750	~25000	~5000	Chapter 5
YSZ-Al$_2$O$_3$/PdAg/Al$_2$O$_3$	1-2	Rh/Al$_2$O$_3$	400-500	1	3.35	2000	2000	100	Chapter 5
YSZ-Al$_2$O$_3$/PdAg/Al$_2$O$_3$	1.86	Rh/Al$_2$O$_3$	550	1	1.3	700	1500	50	Chapter 5
PdAg/Al$_2$O$_3$	3.6	Al$_2$O$_3$[b]	400	1-4	5	48	27000	10000	[24]
PdAg/Al$_2$O$_3$	4-5	Pt/Al$_2$O$_3$	400	1	4	600	20000	13000	[16]
PdAg/PSS	25	NiO/Al$_2$O$_3$	550	6.5-9.7	0.4-0.8[e]	178	~3000[d]	~1700[d]	[17]
PdAg/Inconel/PdAg	4.5[a]	Al$_2$O$_3$[b]	500-630	5.2	N/A	260	∞	∞	[18]
PdAg/Hast. X	4-5	NiO/CaAl$_2$O$_4$	500-600	1-4	1.3	-	574	132	[15]
PdAg/Hast. X	4-5	NiO/CaAl$_2$O$_4$	500-600	1	1.3	100	5400	4890	[26]
PdAg/Hast. X	4-5	NiO/Al$_2$O$_3$	400-550	1-2	0.8	240	10000	150	[27]
PdAg/Hast. X	4	Rh/Al$_2$O$_3$	400-500	4	1.2	615	14000	1000	This chapter
YSZ-Al$_2$O$_3$/PdAg/Hast. X	4	Rh/Al$_2$O$_3$	400-500	4	1.43	615	3500000	2700000[c]	This chapter

N/A: Not available or not reported by authors.

[a] 2 layers of PdAg, the one in the outer surface has a thickness of 3 µm and the one in the inner side of 1.5 µm.

[b] Alumina particles as a filler together with a noble metal-based CPO catalyst

[c] The used nitrogen permeance for the calculation of ideal permselectivity was based in the detection limit of the flow meter (0.001 mL min^{-1}).

[d] The real selectivity has been calculated Taking into account the measured H_2 purity at the permeate under reactive conditions for the experiment number 4 (99.995 %) and experiment number 16. (99.94 %)

[e] Permeated hydrogen for experiment 4 and 6. H_2 permeance was calculated while taken into account the installed membrane area and pressure difference between retentate and permeate sides.

[f] Average value for 5 membranes.

6.4.   Conclusions

In this chapter, two different Pd-Ag membranes supported on porous metallic supports have been prepared, tested and characterized. The objective of this study was to investigate the performance of these membranes against attrition when they are immersed in fluidized beds. Porous metallic supports have been employed due to their higher mechanical strength in comparison to porous ceramic supports. The addition of a porous protective layer to a Pd-Ag layer largely enhanced the stability of the performance of membranes under fluidization conditions, paving the way for their application in fluidized bed membrane reactors. In fact, it was observed that the membrane without the protective layer suffered from significant erosion leading to an increase in the nitrogen leakage under fluidization conditions, while the performance of the double-skin membrane remained stable for more than 615 hours at temperatures of 400-500 °C and at 4 bar of pressure difference. The high ideal perm-selectivity measured with the double-skin membrane achieves the H_2 purity needed for its use in fuel cells, which could promote the further development of membrane reactors for small-scale hydrogen production. The results also clearly show that the protective layer can be used to improve the perm-selectivities of membranes that have small defects on their surface.

Bibliography

[1]   A. Arratibel Plazaola, D.A. Pacheco Tanaka, M. van Sint Annaland, F. Gallucci, Recent advances in Pd-based membranes for membrane reactors, Molecules. 22 (2017) 1–53. doi:10.3390/molecules22010051.

[2]   A. Tardini, C. Gerboni, L. Cornaglia, PdAu membranes supported on top of vacuum-assisted ZrO2-modified porous stainless steel substrates, J. Memb. Sci. 428 (2013) 1–10. doi:10.1016/j.memsci.2012.10.029.

[3]   S.-K. Ryi, S.-W. Lee, D.-K. Oh, B.-S. Seo, J.-W. Park, J.-S. Park, D.-W. Lee, Electroless plating of Pd after shielding the bottom of planar porous stainless steel for a highly stable Hydrogen selective membrane, J. Memb. Sci. (2014). doi:10.1016/j.memsci.2014.04.058.

[4]   F. Braun, A.M. Tarditi, J.B. Miller, L.M. Cornaglia, Pd-based binary and ternary alloy membranes: Morphological and perm-selective characterization in the presence of H2S, J. Memb. Sci. 450 (2014) 299–307. doi:10.1016/j.memsci.2013.09.026.

[5]   H. Gao, J. Slin, Y. Li, B. Zhang, Electroless plating synthesis, characterization and permeation properties of Pd–Cu membranes supported on ZrO2 modified porous stainless steel, J. Memb. Sci. 265 (2005) 142–152. doi:10.1016/j.memsci.2005.04.050.

[6]   K. Zhang, H. Gao, Z. Rui, P. Liu, Y. Li, Y.S. Lin, High-Temperature Stability of Palladium Membranes on Porous Metal Supports with Different Intermediate Layers, Ind. Eng. Chem. Res. 48 (2009) 1880–1886. doi:10.1021/ie801417w.

[7]   Y. Huang, R. Dittmeyer, Preparation and characterization of composite palladium membranes on sinter-metal supports with a ceramic barrier against intermetallic diffusion, J. Memb. Sci. 282 (2006) 296–310. doi:10.1016/j.memsci.2006.05.032.

[8]   C.-B. Lee, S.-W. Lee, J.-S. Park, S.-K. Ryi, D.-W. Lee, K.-R. Hwang, S.-H. Kim, Ceramics used as intermetallic diffusion barriers in Pd-based composite membranes sputtered on porous nickel supports, J. Alloys Compd. 578 (2013) 425–430. doi:10.1016/j.jallcom.2013.06.007.

[9]   M. Chotirach, S. Tantayanon, S. Tungasmita, K. Kriausakul, Zr-based intermetallic diffusion barriers for stainless steel supported palladium membranes, J. Memb. Sci. 405–406 (2012) 92–103. doi:10.1016/j.memsci.2012.02.055.

[10]   A. Calles, D. Alique, L. Furones, Thermal stability and effect of typical water gas shift reactant composition on H2 permeability through a Pd-YSZ-PSS composite membrane, Int. J. Hydrogen Energy. 39 (2014) 1398–1409. doi:10.1016/j.ijhydene.2013.10.168.

[11]   G. Straczewski, J. Völler-Blumenroth, H. Beyer, P. Pfeifer, M. Steffen, I. Felden, A. Heinzel, M. Wessling, R. Dittmeyer, Development of thin palladium membranes supported on large porous 310L tubes for a steam reformer operated with gas-to-liquid fuel, Chem. Eng. Process. Process Intensif. 81 (2014) 13–23.

doi:10.1016/j.cep.2014.04.002.

[12]   S. Samingprai, S. Tantayanon, Y.H. Ma, Chromium oxide intermetallic diffusion barrier for palladium membrane supported on porous stainless steel, J. Memb. Sci. 347 (2010) 8–16. doi:10.1016/j.memsci.2009.09.058.

[13]   S. Yun, S. Ted Oyama, Correlations in palladium membranes for hydrogen separation: A review, J. Memb. Sci. 375 (2011) 28–45. doi:10.1016/j.memsci.2011.03.057.

[14]   J. Melendez, E. Fernandez, F. Gallucci, M. van sint Annaland, P.L. Arias, D.A. Pacheco Tanaka, Preparation and characterization of ceramic supported ultra-thin (~1 μm) Pd-Ag membranes, J. Memb. Sci. 528 (2017) 12–23.

[15]   J.A. Medrano, E. Fernandez, J. Melendez, M. Parco, D.A.P. Tanaka, M. van Sint Annaland, F. Gallucci, Pd-based metallic supported membranes: High-temperature stability and fluidized bed reactor testing, Int. J. Hydrogen Energy. (2015) 1–13. doi:10.1016/j.ijhydene.2015.10.094.

[16]   A. Helmi, E. Fernandez, J. Melendez, D. Pacheco Tanaka, F. Gallucci, M. van Sint Annaland, Fluidized Bed Membrane Reactors for Ultra Pure H2 Production—A Step forward towards Commercialization, Molecules. 21 (2016) 376. doi:10.3390/molecules21030376.

[17]   A. Mahecha-Botero, T. Boyd, A. Gulamhusein, N. Comyn, C.J. Lim, J.R. Grace, Y. Shirasaki, I. Yasuda, Pure hydrogen generation in a fluidized-bed membrane reactor: Experimental findings, Chem. Eng. Sci. 63 (2008) 2752–2762.

[18]   L. Roses, F. Gallucci, G. Manzolini, M. van Sint Annaland, Experimental study of steam methane reforming in a Pd-based fluidized bed membrane reactor, Chem. Eng. J. 222 (2013) 307–320. doi:10.1016/j.cej.2013.02.069.

[19]   T. a. Peters, M. Stange, R. Bredesen, On the high pressure performance of thin supported Pd–23%Ag membranes—Evidence of ultrahigh hydrogen flux after air treatment, J. Memb. Sci. 378 (2011) 28–34.

[20]   S.K. Ryi, J.S. Park, S.H. Kim, S.H. Cho, D.W. Kim, The effect of support resistance on the hydrogen permeation behavior in Pd-Cu-Ni ternary alloy membrane deposited on a porous nickel support, J. Memb. Sci. 280 (2006) 883–888. doi:10.1016/j.memsci.2006.03.007.

[21]   E. Fernandez, J.A. Medrano, J. Melendez, M. Parco, J.L. Viviente, M. van Sint Annaland, F. Gallucci, D.A. Pacheco Tanaka, Preparation and characterization of metallic supported thin Pd-Ag membranes for hydrogen separation, Chem. Eng. J. 305 (2016) 182–190.

[22]   X. Tan, K. Li, Dense Metallic Membrane Reactors, in: Inorg. Membr. React. Fundam. Appl., John Wiley and Sons, 2015: pp. 1–290. doi:10.1002/9781118672839.

[23]   A. Basile, A. Iulianelli, T. Longo, S. Liguori, M. De Falco, Chapter 2 Pd-based

Selective Membrane State-of-the Art, in: M. De Falco, L. Marrelli, G. Iaquaniello (Eds.), Membr. React. Hydrog. Prod. Process., Springer London, London, 2011. doi:10.1007/978-0-85729-151-6.

[24]   E. Fernandez, A. Helmi, K. Coenen, J. Melendez, J.L. Viviente, D.A. Pacheco Tanaka, M. van Sint Annaland, F. Gallucci, Development of thin Pd–Ag supported membranes for fluidized bed membrane reactors including WGS related gases, Int. J. Hydrogen Energy. 40 (2015) 3506–3519.

[25]   V. Spallina, G. Matturro, C. Ruocco, E. Meloni, V. Palma, E. Fernandez, J. Melendez, A.D. Pacheco Tanaka, J.L. Viviente Sole, M. van Sint Annaland, F. Gallucci, Direct route from ethanol to pure hydrogen through autothermal reforming in a membrane reactor: Experimental demonstration, reactor modelling and design, Energy. 143 (2018) 666–681. doi:10.1016/j.energy.2017.11.031.

[26]   J.A. Medrano, I. Potdar, J. Melendez, V. Spallina, D.A. Pacheco-Tanaka, M. van Sint Annaland, F. Gallucci, The membrane-assisted chemical looping reforming concept for efficient H2 production with inherent CO2 capture: Experimental demonstration and model validation, Appl. Energy. 215 (2018) 75–86. doi:10.1016/j.apenergy.2018.01.087.

[27]   S.A. Wassie, J.A. Medrano, A. Zaabout, S. Cloete, J. Melendez, D.A.P. Tanaka, S. Amini, M. van Sint Annaland, F. Gallucci, Hydrogen production with integrated CO2 capture in a membrane assisted gas switching reforming reactor: Proof-of-Concept, Int. J. Hydrogen Energy. 43 (2018) 6177–6190. doi:10.1016/j.ijhydene.2018.02.040.

Chapter 7

Epilogue

"The idea is to die young as late as possible".
Ashley Montagu.

7.1. Conclusions

The interest in the production of ultra-pure hydrogen at small scale has increased steadily in the past decades. Pd-based membranes have been employed as standalone hydrogen separation from gas mixtures or have been directly integrated into the reactor (membrane reactors) where the hydrogen is produced, so that the in-situ separation shifts the equilibrium reactions thereby increasing the conversion of the reactants. Thin (supported) membranes are preferred to extract as much hydrogen as possible from the reaction zone. Membranes can be integrated into different reactor configurations, where fluidized bed membrane reactors are preferred due to the advantages shown in comparison to packed-bed membrane reactors for highly permeable membranes (decreased concentration-polarization effects and isothermal conditions). However, problems regarding the erosion of the membrane surface due to persistent collisions of catalyst particles need to be solved, since they can lead to a strong decay of the membrane performance.

In this thesis two types of attrition resistant membranes have been developed for their integration into a fluidized bed membrane reactor for hydrogen separation. The so-called Pd-based pore-filled membranes (Chapter 4) have been prepared by dip-coating and an electroless plating technique onto ceramic porous supports (alumina and zirconia). The diffusion mechanism in the different mesoporous layers have been studied (chapter 3) prior to their use as a support, as well as in the protective layer for the preparation of pore-filled membranes. The prepared membranes showed, however, a low H_2/N_2 ideal perm-selectivity (<1000) due to the low hydrogen permeance. It has been observed by TEM electron tomography that the palladium did not form a percolative network along the mesoporous layer, leading to the necessity for a H_2 molecule to split and recombine many times, resulting in a very low hydrogen permeation through the membrane.

Another type of membrane, called here double-skin (DS), have been developed (and patented) during this thesis work to increase the hydrogen permeance while keeping the surface of the membrane protected from direct contact of particles (catalyst) and avoid the erosion of the hydrogen-selective layer (PdAg). Ceramic and metallic supports have been employed for their preparation. Ceramic supported DS membranes (Chapter 5) with 1 μm-thick PdAg layer showed an exceptionally high H_2 permeance ($5 \cdot 10^{-6}$ mol m^{-2} s^{-1} Pa^{-1}) and ideal H_2/N_2 perm-selectivity (>25000) at 400 °C and 1 bar of transmembrane pressure difference. Integration of membranes into a fluidized bed membrane reactor demonstrated (with an alumina-based catalyst) that the membrane module (membrane + sealing) suffered from a strong decay in the H_2/N_2 perm-selectivity mainly due to sealing failure (graphite ferrules). After 2000 h of testing at 400-500 °C, 92% of the N_2 leakage was observed through the sealings. This decay was more pronounced when the membrane module was tested at 550 °C. Employment of metallic supported membranes avoid this key issue, since the porous

support is welded to a metallic dense tube. A conventional membrane with a 4-5 µm-thick PdAg layer has been deposited onto Al_2O_3-YSZ modified Hastelloy X support (Chapter 6). This membrane has been compared with a metallic-supported DS membrane, and both membranes showed a high H_2 permeance (1.3-$1.5 \cdot 10^{-6}$ mol m^{-2} s^{-1} Pa^{-1}) at 500 °C and 4 bar of pressure difference. Both membranes also showed a high ideal H_2/N_2 perm-selectivity without the presence of particles in the reactor, over 3500000 for the DS membrane and <100000 the conventional membrane. The performance of the conventional membrane decayed when catalyst particles (Rhodium onto promoted alumina) were integrated into the membrane reactor. After 615 hours under fluidization conditions at 400-500 °C the conventional membrane showed an ideal H_2/N_2 permselectivity of only ~1000 (nitrogen leakage increased two orders of magnitude), while the DS membrane did not exhibit any increase in nitrogen leakage. These promising results demonstrate the great possibilities of the double-skin membranes in fluidized bed membrane reactors for production of ultra-pure hydrogen at small scale.

7.2. Recommendations

The results from this research suggest that the lifetime of the membranes can be enhanced when the DS concept is employed. However, their integration in a membrane reactor at high temperatures (>500 °C) need to be further studied. The stability of the H_2 selective layer (PdAg) may be compromised at high temperatures due to the increased mobility of atoms along the surface and in the bulk. Surface diffusion prevails at temperatures below the Tamman temperature (T_{tm}= 0.5 of the melting point), while above this temperature, also bulk diffusion occurs. Diffusion of atoms can lead to the creation of defects. The Tamman temperature of palladium and silver are 641 °C and ~344 °C, respectively. When membranes operate at temperature above 400 °C, silver atoms possess high energy to move along the crystal structure of the alloy. The stability of the H_2 selective layer can be enhanced by alloying palladium with other metals with a higher melting point than silver, such as gold, copper, ruthenium, platinum (Chapter 2).

The commercialization of Pd-based membranes does not depend only on their performance and life-time, but also on their price. Many aspects have an impact on the final price:

Porous supports: most of the ceramic supports are cheaper than metallic ones (depending on the material and surface quality). However, special fittings are required for their integration, while metallic-supported membranes do not need them. The surface quality of metallic supports are often, however, inferior, but can be improved by mechanical and/or chemical processes. Depending on their final application, metallic-supported membranes may also require an inter-diffusion barrier. Moreover, the selection of the material for the supports depends enormously on the final application. Nickel-based alloys are preferred for high-

temperature applications and stainless steel 316L for milder conditions. Ni-based alloys are extremely expensive and other alternatives need to be further explored. Furthermore, the recyclability of the support and palladium is an interesting option under study (for which a patent has been submitted) due to the price of both, supports and palladium.

Preparation method: The scaling up of the manufacturing method has to be studied in detail. Minimization of the number of steps (seedings, depositions of selective, interdiffusion and protective layers, apart from thermal treatments) are relevant for the minimization of the final price of the membranes. In this research electroless plating and dip-coating techniques have been employed for their reproducibility and simplicity. However, other alternatives such a physical and chemical vapor deposition are interesting due to the production capacity that already exists for other applications.

Membrane failure: In case of membrane or membrane module failure during operation, their substitution is required. The replacement of a membrane or module for a new one, while the "old" membrane/module is repaired or recycled, needs to be easy and as fast as possible, which requires a good reactor design., Both cases, the performance of the repaired and the new membranes has to be as close as possible to the initial properties.

7.3. Outlook

The WGS (water gas-shift) (CO + H_2O ⇔ CO_2 + H_2, ΔH = -41 kJ mol^{-1}) is an important reaction used for the production of hydrogen. The WGS reaction is commonly carried out in two consecutive fixed bed reactors: First a HTS (high temperature shift) step in the presence of an Fe-Cr based catalyst, followed by a second LTS (low temperature shift) step in the presence of a CuO-ZnO-based catalyst at lower temperatures (210-240 °C) [1]. Due to the complexity of the technology, a large effort has been devoted to develop catalysts to perform the WGS in a single stage. Since noble metals such as Au [1–4], Pt [5–7], Pt-Re [5,7–11], Pd [6,12], Pd-Re [10] showed a high activity at low temperatures, they are intensively studied. The choice of appropriate porous supports is a very important issue in the preparation of very efficient catalysts. The WGS reaction is thought to occur mainly through two reaction mechanisms: the regenerative (red-ox) mechanism, which involves successive oxidation and reduction of the surface, and the associative mechanism through an adsorbed surface intermediate [10]. Different porous oxides have been reported to be effective for WGS. Most common oxides employed as catalyst support are Al_2O_3 [1], ZrO_2 [7,9,11], CeO_2 [2,6,7,12], TiO_2 [1,2,4,7–11], CeO_2-TiO_2 [3,5]; however, supports with some oxygen vacancies such as ceria and titania are preferable [13]. Mesoporous supports as titania (TiO_2) has been widely studied, since they would give rise to well-dispersed metal particles on the surface, reducing the sintering effect [1,4]. Modified titania with nanoparticles of CeO_x shows a higher WGS activity than TiO_2 alone, because the interaction between the nanoparticles and the surface

of TiO_2 is very high, so that the geometry and electronic properties of the CeO_x are strongly modified increasing the reducibility of Ce; in addition, the TiO_2 surface increases the metal catalyst dispersion inducing a higher metal-support interaction [14,15]. It has been reported that the addition of Rhenium has a positive effect on the activity and stability and the use of a bimetallic Re-Pt formulation improved the stability and activity of Pt onto TiO_2 [9,10] and CeO_2-TiO_2 [5].

Fernandez et al. [16] studied the production of hydrogen using a Pd-Ag membrane fluidized bed reactor using RePtCe supported on TiO_2 at 400 °C. During the first hours of reaction, it was observed that the hydrogen permeation flux decreased dramatically attributed to the reaction between the TiO_2 support with the Pd based membrane forming a TiPd alloy with a low hydrogen permeability, similar to the strong interaction between the Pd and the support explained above.

Herein, we report the use of a Pd-based double-skin (DS) membrane, for WGS fluidized bed membrane reactors using the same catalyst (RePtCe supported on TiO_2) under similar conditions of fluidization as described above [16].

As reported previously in Chapter 5, the PdAg DS-membrane consists of a supported conventional Pd membrane, onto which a mesoporous YSZ/γ-Al_2O_3 is deposited by dip-coating technique followed by drying and calcination at 550 °C. Addition of this protective layer avoids direct contact of the catalyst with the membrane in fixed and fluidized bed membrane reactors. In Figure 7.1 one can observe the three different parts of the DS membrane: (1) mesoporous YSZ/γ-Al_2O_3 layer (protective layer), (2) hydrogen selective PdAg layer and (3) 100 nm pore size α-Al_2O_3 porous support. The thickness of the selective layer was measured to be approximately 1 µm, thus a high hydrogen flux is expected through the membrane. The mesoporous protective layer is also ultra-thin, around 500 nm thick. In Table 7.1 the main characteristics of the tested double-skin membrane and the conventional membrane tested by Fernandez et al. [16] have been summarized.
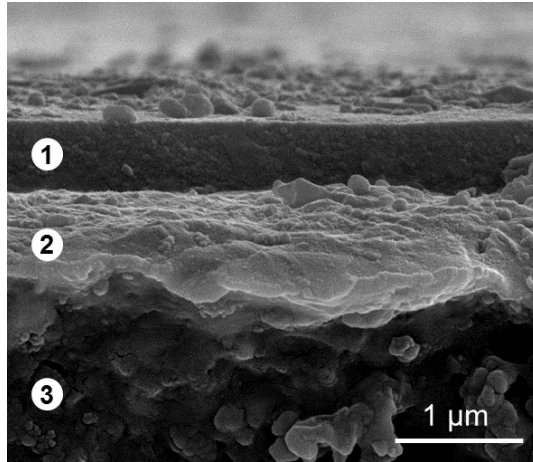
Figure 7.1. Cross section SEM image of a double-skin membrane. (1) Mesoporous YSZ-Al$_2$O$_3$ layer, (2) PdAg layer, (3) alumina asymmetric support.

The DS membrane permeation properties have first been studied at 400 °C with pure gases (H$_2$ and N$_2$) without the presence of catalyst particles. The system has been heated up to 400 °C under a nitrogen stream with a heating rate of 3 °C min^{-1}. Once the desired temperature was reached, the membrane was activated by addition of air for 2 minutes and then the air was purged with nitrogen; this cycle was repeated twice. As can be observed in Figure 7.2, the hydrogen flux increased from $4.22 \cdot 10^{-7}$ to $4.08 \cdot 10^{-6}$ mol m^{-2} s^{-1} Pa^{-1} after the first activation cycle. After the second activation, the hydrogen flux increased slightly and kept constant for about 150 minutes. The hydrogen permeance and H$_2$/N$_2$ permselectivity at 400 °C and 1 bar of transmembrane pressure was $4.70 \cdot 10^{-6}$ mol m^{-2} s^{-1} Pa^{-1} and ~13000. Once the hydrogen flux was stable, the catalyst with a particle size ranging from 100 to 305 μm (bed A) was introduced into the reactor for fluidization experiments. The permeation setup used for this test was reported previously in Chapter 5. The membranes were tested in the bubbling fluidization regime. Nitrogen and hydrogen fluxes through the membrane were monitored for about 145 hours without observing any decay in the hydrogen flux, as shown in Figure 7.3 (black dots). On the other side, Fernandez et al. [16] observed a strong decay in the hydrogen flux in the first hours (open dots in Figure 7.3) when a conventional Pd membrane (E54) was exposed to RePtCe/TiO$_2$ particles in a fluidized bed membrane reactor. The hydrogen flux decreased to 45% of the initial flux. In this case, the authors employed smaller particles (bed C: 76-105 μm). To assess the effect of the particles size, catalyst particles below 105 μm were introduced into the reactor together with the previous one (bed A) to obtain bed B; the hydrogen flux in the presence of the catalyst mixture remained constant for about 115 hours. The hydrogen flux did not show a decay thanks to the protective layer which avoids direct contact between catalyst particles and the H$_2$ selective layer. The properties of the employed catalytic beds are summarized in Table 7.2. For all cases (bed A,

bed B and bed C) the catalyst particles (30 wt.% of total bed) was mixed with TiO_2 filler (70 wt% of total bed) with a particle size ranging from 100 μm to 125 μm.

Table 7.1. Main characteristics of double skinned and conventional supported membranes tested under fluidization conditions in presence of TiO_2 based catalyst.

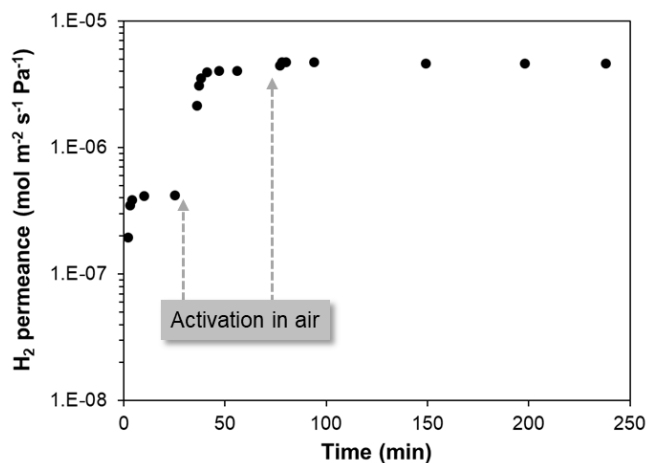| Membrane section	Parameter	Membrane	
		Double-skin (DS)	Conventional (ref. [16])
Support	Material	α-Al_2O_3	α-Al_2O_3
	Pore size (nm)	100	100
	OD/ID (mm)	10/4	10/7
Selective layer	Composition	PdAg (5.6 wt.% Ag)	PdAg (13.4 wt.% Ag)
	Thickness (μm)	~ 1	3.6
Protective layer	Composition	YSZ/γ-Al_2O_3 (50 wt. % YSZ)	-
	Thickness (μm)	~ 0.5	-

Figure 7.2. Evolution of hydrogen flux of the DS at 400 °C and 1 bar of ΔP during its activation with air in an empty reactor.
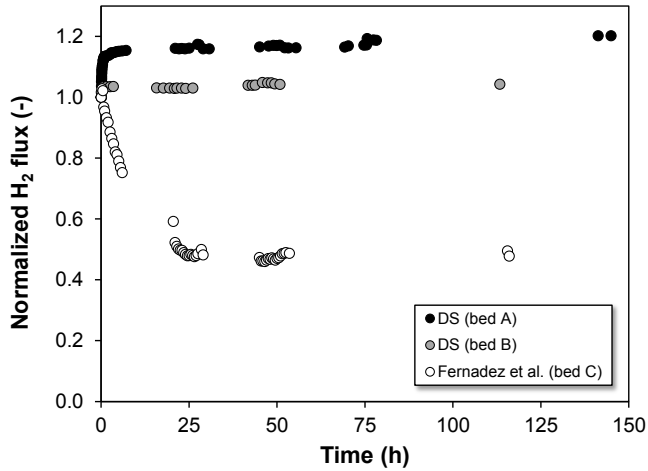
Figure 7.3. Normalized hydrogen flux of DS membrane with two different beds (A and B) and a conventional membrane (bed C).

Table 7.2. Characteristic of the catalyst bed (RePtCe/TiO$_2$) and filler (TiO$_2$) used for the fluidization test in presence of hydrogen at 400 °C and 1 bar of pressure difference.

Parameter		Membrane		
		DS	DS	E54 [16]
Catalytic bed	Bed type	A	B	C
	Particle size (μm)	100-305	< 305	75-106
Filler	Particle size (μm)	100-125	100-125	100-125

The initial H$_2$ permeance of the conventional membrane in an empty reactor was $2.2 \cdot 10^{-6}$ mol m^{-2} s^{-1} Pa^{-1}. Once the membrane was in contact with TiO$_2$ particles in H$_2$ at 400 °C, the measured initial permeance decreased to $2.0 \cdot 10^{-7}$ mol m^{-2} s^{-1} Pa^{-1} after 25 h and even down to $9.3 \cdot 10^{-8}$ mol m^{-2} s^{-1} Pa^{-1} after 50 h. Then, the H$_2$ permeance remained constant for another ~65 hours. From Figure 7.4 it is clear that the hydrogen permeance of the DS was not compromised by the presence of TiO$_2$ particles, while the conventional membrane (E54) suffered severely from interactions between the membrane and the TiO$_2$ particles.
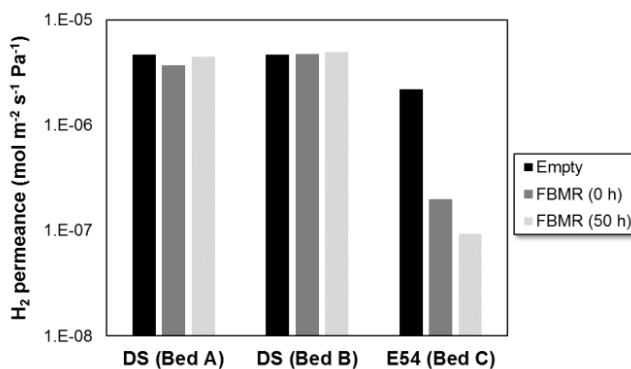
Figure 7.4. Hydrogen permeance of the double-skinned and conventional (E54) membrane in an empty reactor (without presence of particles) and fluidized bed membrane reactor at 400 °C.

Fernandez et al. [16] observed the presence of a high amount of Ti and O by XPS on the membrane surface after the fluidization test at 400 °C, but Pt, Re or Ce were not detected. As mentioned previously, interdiffusion between titania and Pd was also found by Huang et al. [17]; These authors attributed this behaviour to the partial reduction of titania; however, they did not report any H_2 flux decay during their test. We have reported in Chapter 3 the decay in hydrogen flux in a Pd-based pore-fill type membrane when a $ZrO_2/TiO_2/Al_2O_3$ support was employed. Since in a pore-fill type membrane the palladium is forced to be deposited (and grown) inside the pores, the palladium is in intimate contact with titania. This effect has not been found with alumina supports. On the other hand, a hydrogen flux reduction was observed in a Pt/TiO_2 membrane tested during 160 h at 400 °C [18]. After 80 h, the flux decreased down to 80% of the initial value; however, the authors attributed this decay to a possible decrease in the effective porosity of the support due to a rearrangement of the palladium layer decreasing the effective membrane area. The hydrogen flux decay in Pd/TiO_2 systems could be related to the reducibility of titania in the presence of hydrogen and the formation of an alloy with palladium. It was shown that the addition of Ti to the Pd crystal structure produces a progressive contraction of the lattice parameter [19], leading to the reduction of the octahedral interstitial distances decreasing the movement of hydrogen, which is exactly the opposite effect of adding silver to palladium [20]; it is well-known that the addition of Ag increases the H_2 permeation while simultaneously reducing the hydrogen embrittlement at low temperatures. Hydrogenation studies of different PdTi alloys showed a decrease in the hydrogen content with increasing titanium [19]. Moreover, the strong metal-support interaction (SMSI) between noble metals from group VIII when supported onto titanium oxide was also found when it is employed as catalyst support [21].

Summarizing, the use of titania as a catalyst support (or membrane support) with palladium, can lead to a chemical interaction in the presence of hydrogen at high temperatures (> 400 °C) decreasing the permeability of the Pd-based membrane. This chemical interaction can be

avoided by the deposition of a mesoporous protective ceramic layer onto the dense Pd layer, as in the double-skin membranes. In this study we have reported experimental results of permeation tests of these membranes in a fluidized bed membrane reactor, showing that the DS membrane not only avoids the chemical interactions of TiO_2 particles with the Pd layer, but also offers attrition resistance against fluidized particles. However, these membranes can also offer advantages for their application in packed-bed membrane reactors employing TiO_2 or other metal oxide supports that are sensitive to reduction when in contact with a Pd layer.

We have validated the use of double-skin membranes in the presence of TiO_2-based catalyst particles in a fluidized bed membrane reactor to prevent chemical interaction and provide attrition resistance. The protection by the deposited mesoporous layer allows avoiding direct contact between catalyst particles and the hydrogen selective PdAg layer. The hydrogen flux of a DS membrane did not decrease during the experiments at 400 °C, whereas a conventional supported membrane (without the protective layer) suffered severely from a hydrogen flux decay of 60 % due to chemical interaction with the catalyst particles.

Bibliography

[1] H. Sakurai, A. Ueda, T. Kobayashi, M. Haruta, Low-temperature water–gas shift reaction over gold deposited on TiO2, Chem. Commun. (1997) 271–272. doi:10.1039/a606192c.

[2] D. Mendes, H. Garcia, V.B. Silva, A. Mendes, L.M. Madeira, Comparison of nanosized gold-based and copper-based catalysts for the low-temperature water-gas shift reaction, Ind. Eng. Chem. Res. 48 (2009) 430–439. doi:10.1021/ie8010676.

[3] V. Idakiev, T. Tabakova, K. Tenchev, Z.Y. Yuan, T.Z. Ren, B.L. Su, Gold nanoparticles supported on ceria-modified mesoporous titania as highly active catalysts for low-temperature water-gas shift reaction, Catal. Today. 128 (2007) 223–229. doi:10.1016/j.cattod.2007.07.016.

[4] V. Idakiev, T. Tabakova, Z.Y. Yuan, B.L. Su, Gold catalysts supported on mesoporous titania for low-temperature water-gas shift reaction, Appl. Catal. A Gen. 270 (2004) 135–141. doi:10.1016/j.apcata.2004.04.030.

[5] V. Del Villar, L. Barrio, A. Helmi, M.V.S. Annaland, F. Gallucci, J.L.G. Fierro, R.M. Navarro, Effect of Re addition on the WGS activity and stability of Pt/CeO2-TiO2catalyst for membrane reactor applications, Catal. Today. 268 (2016) 95–102. doi:10.1016/j.cattod.2015.11.013.

[6] T. Bunluesin, R.J. Gorte, G.W. Graham, Studies of the water-gas-shift reaction on ceria-supported Pt, Pd, and Rh: Implications for oxygen-storage properties, Appl. Catal. B Environ. 15 (1998) 107–114. doi:10.1016/S0926-3373(97)00040-4.

[7] K.G. Azzam, I. V. Babich, K. Seshan, L. Lefferts, A bifunctional catalyst for the single-stage water-gas shift reaction in fuel cell applications. Part 2. Roles of the support and promoter on catalyst activity and stability, J. Catal. 251 (2007) 163–171. doi:10.1016/j.jcat.2007.07.011.

[8] K.G. Azzam, I. V. Babich, K. Seshan, L. Lefferts, Role of Re in Pt-Re/TiO2catalyst for water gas shift reaction: A mechanistic and kinetic study, Appl. Catal. B Environ. 80 (2008) 129–140. doi:10.1016/j.apcatb.2007.11.015.

[9] H. Iida, A. Igarashi, Structure characterization of Pt-Re/TiO2(rutile) and Pt-Re/ZrO2catalysts for water gas shift reaction at low-temperature, Appl. Catal. A Gen. 303 (2006) 192–198. doi:10.1016/j.apcata.2006.01.040.

[10] Y. Sato, K. Terada, S. Hasegawa, T. Miyao, S. Naito, Mechanistic study of water-gas-shift reaction over TiO2 supported Pt-Re and Pd-Re catalysts, Appl. Catal. A Gen. 296 (2005) 80–89. doi:10.1016/j.apcata.2005.08.009.

[11] H. Iida, A. Igarashi, Difference in the reaction behavior between Pt-Re/TiO2(Rutile) and Pt-Re/ZrO2catalysts for low-temperature water gas shift reactions, Appl. Catal. A Gen. 303 (2006) 48–55. doi:10.1016/j.apcata.2006.01.029.

[12] X. Wang, R.J. Gorte, The effect of Fe and other promoters on the activity of Pd/ceria for the water-gas shift reaction, Appl. Catal. A Gen. 247 (2003) 157–162.

doi:10.1016/S0926-860X(03)00095-4.

[13]   L. Li, L. Song, L. Zhu, Z. Yan, X. Cao, Black TiO2-x with stable surface oxygen vacancies as the support of efficient gold catalysts for water-gas shift reaction, Catal. Sci. Technol. 8 (2018) 1277–1287. doi:10.1039/C7CY02429K.

[14]   J.J. Plata, J. Graciani, J. Evans, J.A. Rodriguez, J.F. Sanz, Cu Deposited on CeOx-Modified TiO2(110): Synergistic Effects at the Metal-Oxide Interface and the Mechanism of the WGS Reaction, ACS Catal. 6 (2016) 4608–4615. doi:10.1021/acscatal.6b00948.

[15]   J.A. Rodriguez, D.C. Grinter, Z. Liu, R.M. Palomino, S.D. Senanayake, Ceria-based model catalysts: fundamental studies on the importance of the metal–ceria interface in CO oxidation, the water–gas shift, CO_2 hydrogenation, and methane and alcohol reforming, Chem. Soc. Rev. 46 (2017) 1824–1841. doi:10.1039/C6CS00863A.

[16]   E. Fernandez, A. Helmi, K. Coenen, J. Melendez, J.L. Viviente, D.A. Pacheco Tanaka, M. van Sint Annaland, F. Gallucci, Development of thin Pd–Ag supported membranes for fluidized bed membrane reactors including WGS related gases, Int. J. Hydrogen Energy. 40 (2015) 3506–3519.

[17]   Y. Huang, R. Dittmeyer, Preparation and characterization of composite palladium membranes on sinter-metal supports with a ceramic barrier against intermetallic diffusion, J. Memb. Sci. 282 (2006) 296–310. doi:10.1016/j.memsci.2006.05.032.

[18]   L.Q. Wu, N. Xu, J. Shi, Preparation of a palladium composite membrane by an improved electroless plating technique, Ind. Eng. Chem. Res. 39 (2000) 342–348. doi:10.1021/ie9904697.

[19]   M.M. Khader, F.M.N. Kheiri, B.E. El-Anadouli, B.G. Ateya, Mechanism of reduction of rutile with hydrogen, J. Phys. Chem. 97 (1993) 6074–6077. doi:10.1021/j100124a048.

[20]   S.N. Paglieri, J.D. Way, Innovations in Palladium Membrane Research, Sep. Purif. Rev. 31 (2002) 1–169. doi:10.1081/SPM-120006115.

[21]   S.J. Tauster, Strong Metal-Support Interactions, Acc. Chem. Res. 20 (1987) 389–394.

Publications and Contributions

List of publications

A. Arratibel, U. Astobieta, D. A. Pacheco Tanaka, M. van Sint Annaland, F. Gallucci *"N$_2$, He and CO$_2$ diffusion mechanism through nanoporous YSZ/γ–Al$_2$O$_3$ layers and their use in a pore–filled membrane for hydrogen membrane reactor"*, International Journal of Hydrogen Energy 41 (2016) 8732–8744.

G. Di Marcoberardino, M. Binotti, G. Manzolini, J.L. Viviente, **A. Arratibel**, L. Roses, F. Gallucci. *"Achievements of European projects on membrane reactor for hydrogen production"*, Journal of Cleaner Production 161 (2017) 1442–1450

E. Fernandez, A. Helmi, J.A. Medrano, K. Coenen, **A. Arratibel**, J. Melendez, N.C.A. de Nooijer, V. Spallina, J.L. Viviente, J. Zuñiga, M. van Sint Annaland, D.A. Pacheco Tanaka, F. Gallucci. *"Palladium based membranes and membrane reactor for hydrogen production and purification: An overview of research activities at Tecnalia and TU/e"*, International Journal of Hydrogen Energy 42 (2017) 13763–13776.

A. Arratibel, D. A. Pacheco Tanaka, M. van Sint Annaland, F. Gallucci. "Unravelling the transport mechanism of pore–filled membranes for hydrogen separation" Separation and Purification Technology 203 (2018) 41–47.

A. Arratibel, A. Pacheco Tanaka, I. Laso, M. van Sint Annaland, F. Gallucci. *"Development of Pd–based double–skinned membranes for hydrogen production in fluidized bed membrane reactors"*, Journal of Membrane Science 550 (2018) 536–544.

A. Arratibel, J. A. Medrano, J. Melendez, D. A. Pacheco Tanaka, M. van Sint Annaland, F. Gallucci. *"Attrition–resistant membranes for fluidized–bed membrane reactors: double–skin membranes"*, Journal of Membrane Science 563 (2018) 419–426.

Review papers

A. Arratibel, D.A. Pacheco Tanaka, M. van Sint Annaland, F. Gallucci. *"Recent Advances in Pd–based Membranes for Membrane Reactors"*, Molecules (2017), 22, 51.

A. Arratibel, A. Cruellas, Y. Liu, N. Badiola, D.A. Pacheco Tanaka, M. van Sint annaland, F. Gallucci. *"Oxygen transporting membranes for their application in membrane reactors: A review"* submitted to Energy Technology (2018).

A. Arratibel, D.A. Pacheco Tanaka, M. van Sint Annaland, F. Gallucci. *"On the use of double-skin membranes to prevent chemical interaction between membranes and catalysts"*, will be submitted to International Journal of Hydrogen Energy.

Book chapters

A. Arratibel, D.A. Pacheco Tanaka, M. van Sint Annaland, F. Gallucci. *"Membrane reactors for autothermal reforming of methane, methanol and ethanol"* in Membrane Reactor for Energy Applications and Basic Chemical Production (2015) 61–98.

F. Gallucci, **A. Arratibel**, J.A. Medrano, E. Fernandez, M. van Sint Annaland, D.A. Pacheco Tanaka. *"Hydrogen production with membrane systems"*, in Hydrogen Generation Technologies (2017) 131–151.

J.L. Viviente, J. Melendez, E. Fernandez, **A. Arratibel**, F. Gallucci, J. Zuñiga, D.A. Pacheco Tanaka. *"Ultrathin and thin film Pd–Ag membranes for hydrogen production"* in Membrane Engineering for the Treatment of Gases: Volume 2: Gas–separation Issues Combined with Membrane Reactors (2018) 95–138.

Conference contribution

A. Arratibel, E. Fernandez, J. Melendez, M.A. Llosa Tanco, F. Gallucci, D. A. Pacheco Tanaka. *"Preparation of Pd–Ag pore filled membranes for hydrogen separation"*, in European Hydrogen Energy Conference 2014 (EHEC2014), 12-14 March 2014, Sevilla, Spain. Poster presentation.

A. Arratibel, D. A. Pacheco Tanaka, F. Gallucci, M. van Sint Annaland. *"Preparation of Pd–Ag pore filled membranes for hydrogen separation"*, in 12th International Conference on Catalysis in Membrane Reactors (ICCMR12), 22–25 June 2015, Szczecin, Poland. Poster presentation. **Selected as best poster presentation.**

E. Fernandez, A. Helmi, J.A. Medrano, **A. Arratibel**, J. Melendez, J.L. Vivente, J. Zuñiga, M. van Sint Annaland, D.A. Pacheco Tanaka, F. Gallucci. *"Palladium based membrane reactors for hydrogen production"*, in 12th International Conference in Membrane Science and Technology (MST2015), 1-3 November 2015, Teheran, Iran. Oral presentation.

A. Arratibel, I. Laso, D. A. Pacheco Tanaka, M. van Sint Annaland, F. Gallucci. *"Preparation and characterization of Pd–based double–skinned membranes for hydrogen production in fluidized bed membrane reactors"*, in 13th International Conference on Catalysis in Membrane Reactors (ICCMR13), 10–13 July 2017, Houston, USA. Oral presentation.

A. Arratibel, J. A. Medrano, J. Melendez, D. A. Pacheco Tanaka, M. van Sint Annaland, F. Gallucci. *"Attrition–resistant membranes for fluidized–bed membrane reactors: double–skin membranes",* in European Hydrogen Energy Conference 2018 (EHEC2018), 14–16 May 2018, Malaga, Spain. Oral presentation.

D. A. Pacheco Tanaka, N.C.A. de Nooijer, E. Fernandez, J. Melendez, J.L. Viviente, J. A. Medrano, **A. Arratibel**, M. van Sint Annaland, F. Gallucci. *"Palladium membrane reactors for hydrogen production",* in European Hydrogen Energy Conference 2018 (EHEC2018), 14–16 May 2018, Malaga, Spain. Oral presentation.

Acknowledgments

Finally, the end of this long trip has been reached. More than four years working and travelling between Eindhoven and San Sebastian. Four years in which I have learnt more than ever about science and life. Support from every single person that I know has been relevant to conclude my PhD and I would like to thank to all of you for your support.

First of all I would like to thank to my promotor, Prof. Martin van Sint Annaland for giving me the opportunity to carry out my PhD between TU/e and Tecnalia under your supervision at the SPI group. We have discussed a lot during our meetings at TU/e and via skype when I was at Tecnalia. You gave me plenty of ideas (sometimes to many) and very critical points. Always trying to force me to perform simulations while I was trying to escape from them ;-).

Prof. Fausto Gallucci, my co-promotor and daily supervisor, it has been an amazing pleasure to be working under your supervision. Always there to advise and support me when I needed it. You have an incredible capacity to motivate a student (and also how to push him when required). I really enjoy all the discussion during meetings. Even every single time you came to the office asking for papers (every single day). Summarizing, thank you for being a great leader. See you in the future!

Dr. Alfredo, my membrane mentor, I would like to express my sincere gratitude for giving me the opportunity to continue with part of your work done in Japan and transfer part of your awesome knowledge on membranes and chemistry in general. Now that I´m in Tecnalia as researcher, we can continue this journey to explore more and new things!

Thank you to all the people that I met during this period in SMR for sharing such amount of great moments, eeeeespecially during coffe breaks, lunch time, FORT, dinners. Maria Nordio, Giulia, Alessandro, Alvaro, Wendy, Sol(i)mon, Michela, Ildefonso, Vincenzo, Mohammed, Milan, Paul, Francesco (Arancesco), Arash, Kai, Marian, Ramon, Maxim (and Poly), Gaopan, Feifei, Xiao, Krushna, Lizzy, Ivan, Tim, Evan, Dario, Kun, Aditya, Stefan. Thank you so much for all the nice moments I had with all of you! Thank you to Joost, Joris, Thijs and Herbert for their work in the setups. Without you, it would not have been possible to carry out all the test in the lab. Judith and Ada, thank you for your help during these years.

Thank you to all the membrane technology group at Tecnalia for their daily support. To be surrounded for such a great people, has no price. I always receive help when I needed it. Jon Melendez (ese pamplonica), Iker, Sara (my heroine), Margot, Miren, Oana, Nerea, Ekain, Jose Luis and to the "new" members, Jorge, Iñigo and Mari Mar. Special mention to my "now"

boss and friend, Jon Zuñiga. You bet for me and I can neveri thank you enough. Perhaps yes, with good membranes ;-).

What can I said about my officemates at STW 0.34... starting with Maria Ortiz (winter will come soon), Tommasso and José. Short period together, but incredible at the same time. Last 2 years and a half I shared the office ("best office ever") with three amazing guys to create the Spanish office (Jose and Aitor) +1 (Niek). Amazing team!! Even when the Dutch law wanted us to be separated. I don´t have words to express the great moments passed together and for holding me, the most complicated task. Aitor and José, my paranymphs, thank you for all the good vibes and great moments in and out of the office. You also made fan of me thousands of times... I´m to "short to catch" (as Juana Mari´s dictionary says) your jokes. Brom brom!! Os adoro mis pequeños! Niek, the Dutch Californian, thank you for being so enthusiastic with everything you do. I will never forget the experiment with the sausages.

I would like to acknowledge people from the faculty that I met during my PhD. Nerea (Rodriguez^2), best neighbour ever! Soy Duvel adicta gracias a ti! Thank you to Alexei and Andrey for all the laugh that we shared during our coffe breaks with a cigarette, crazy people are always welcome!! Ligning coins!

Dar las gracias a mi "pequeña" Elisa por cuidarme tanto desde el día 1 en que nos conocimos. Gora Donostia, Donostiarrak ta Donosti eguna! A Luis e Isabel (de Áragon), sois todo amor. No se puede ser más noble que vosotros. Viva Ainzón! En el 2019, más y major. Maria, my "daughter", this time you will be there together with a bottle of moscatel and a haaaaalf.

Ama, gracias por darme la oportunidad de estudiar todo lo que he querido y más. Gracias a tu apoyo, pude dejar el trabajo e irme a Barcelona a estudiar más. No contenta con ello, volví a Donosti y me meti a otro master. Has aguantado lloros, alegrias, frustraciones de tu hija durante tantos años y más aún durante el doctorado. Todo llega a buen puerto si se trabaja y como buena luchadora que soy (no se de quien lo he aprendido), he llegado a terminar todo con buena letra. Milesker Ama!

Quagteros!!! Mis pequeñarros (Mimis, Kuki, Jonasio, Patri y Gonzagius), que os voy a decir que no sepáis ya... apoyo incondicional y cariño siempre que me ha hecho falta. No sé como podéis aguantar al terremoto de emociones que soy. Me habéis ayudado a levantarme cada vez me caía. Parte de este trabajo es vuestro! VIDRIO!!!!!

Dar las gracias a todos los amig@s de todos los rincones de eeeeeSpain que me han apoyado incondicionalmente. Nahikkiki, Natasha, Natalia, Victor, Txiki, Lucia, Leyre (mi

nanoscientific girl favorita, Marina(–ius)) todos juntos me habeis dado mucho apoyo en distintas etapas del doctorado. Cada gesto cuenta! Contemos juntos!

Gracias por aparecer en mi vida Fer. Eres todo lo que puedo necesitar y más. Primera lección que me diste, "amor y passion". Con ello todo se puede conseguir! Sigamos cumpliendo con nuestra "palabrita".

Thank you to my little king, Poker. Me has dado tanto cariño… Te extraño mucho bola de pelo!

Biography

Alba Arratibel was born on the 27th August in 1985 in Donostia-San Sebastián, Spain. After finishing high-school in 2003 in Donostia-San Sebastián, she studied Industrial Technical Engineering with the specialization in Industrial Chemistry at Polytechnic School of San Sebastian-University of the Basque Country. On March 2008 she graduated with a dissertation entitled "recovery of steel and tin from tinplate".

In 2007 she has started working at Inasmet (Donostia-San Sebastian) for the recovery of aluminium from solid urban waste. Simultaneously, in 2008 she has started a master in Chemical Science and Technology in the National University of Distance Education and obtained the master degree in 2011. In 2009, she has moved to Barcelona to study Material Science Engineering at Polytechnic University of Catalonia after a dissertation entitlted "Synthesis and characterization of DLC (Diamond‿ like carbon) coating by chemical vapor deposition assisted by plasma (PECVD)". After her graduation in 2012 she returned to Donostia - San Sebastina to start with a master degree in Nanoscience. In 2013 she has obtained a master degree in Nanoscience in the Physical center of Materials - University of the Basque Country. After her master thesis on synthesis of inorganic nanoparticles.

In 2014 she started her PhD at the Eindhoven University of Technology in the Multiphase reactor group (Chemical process intensification, SPI) under the supervision of Prof. Martin van Sint Annaland and Prof. Fausto Gallucci. The PhD was performed in collaboration with Tecnalia within the Materials for Energy and Environment Area under the supervision of Dr. David Alfredo Pacheco Tanaka for membrane preparation. Two types of Palladium based membranes were prepared and tested for hydrogen separation in fluidized bed membrane reactors. She has developed a membrane called double-skin to prevent attrition of membrane which has been patented. During her PhD she was awarded as best poster presentation in the International Conference on Catalysis in Membrane Reactors celebrated in Szczecin (Poland) in 2015.